Shape and topology optimization of enzymatic microreactors

Pereira Rosinha Grundtvig, Ines; Woodley, John; Gernaey, Krist V.; Krühne, Ulrich

Publication date:
2015

Document Version
Publisher's PDF, also known as Version of record

SHAPE AND TOPOLOGY OPTIMIZATION OF ENZYMATIC MICROREACTORS

Inês Pereira Rosinha

PhD Thesis

November 2015

DTU Chemical Engineering
Department of Chemical and Biochemical Engineering

Danmarks Tekniske Universitet DTU

Shape and topology optimization of enzymatic microreactors

PhD Thesis

Inês Pereira Rosinha

CAPEC-PROCESS Research Center

Department of Chemical and Biochemical Engineering

Technical University of Denmark

November 2015

Address: Process and Systems Engineering Center (PROSYS)

Department of Chemical and Biochemical Engineering

Technical University of Denmark

Building 229

Dk-2800 Kgs. Lyngby

Denmark

Phone: +45 4525 2800

Web: www.kt.dtu.dk/forskning/prosys

Print: STEP

DTU Chemical Engineering
Department of Chemical and Biochemical Engineering

Abstract

Structural optimization methods have been used by mechanical and civil engineers over the years to find the optimal structures. Structural optimization is a series of computational techniques which include shape and topology optimization. Shape optimization is directly applied to the boundaries of a structure and results in the deformation of the configuration. Topology optimization contributes to the improvement of the layout of the material in a domain. The mechanical performance of a structure is evaluated by an objective function which can be for example maximizing its stiffness.

The need for effective and cost efficient reactors for pharmaceutical processes forces the industry to search for better technologies. In biochemical engineering, the used reactor design in a given process is usually limited to a range of well-established configurations and layouts. Usually the implemented reactors in a chemical process do not always yield in the best reaction conditions. This thesis develops an innovative application of topology and shape optimization methods to a chemical engineering problem. The main goal is to design a reactor according to the limitations of the reaction system by modifying the reactor configuration.

In this thesis structural optimization methods were exclusively applied to enzymatic microreactors. The case studies were chosen such that they can be experimentally tested afterwards. In this way, the design of the reactor is customized to the reaction system and it contributes to the reduction of extensive experimental work to find the best reactor configuration.

Shape optimization has been applied to an YY-microreactor with a rectangular cross-section with the intention to investigate the shape influence on the active mixing of substances and consequently in the reaction yield. The inlet and the outlet are located at the respective ends of the reactor. Both inlet and outlet have a Y shape where two streams meet at the entrance of the reaction chamber and two streams are split again at the exit. The optimization routine focuses on the modification of the microreactor shape parameters such as height and width. This is achieved by a computational fluid dynamic (CFD) simulation study, which investigates a biocatalytic reaction for the production of optically pure chiral amines in the reactor system. The routine implements kinetic models into a CFD framework (ANSYS CFX®), which is coupled with a self-programmed MATLAB® code. ANSYS CFX® performs the discretization of the microreactor into finite volume elements and calculates the main reactor outputs. The MATLAB® routine performs the optimization by changing the geometry. Furthermore, it includes the evaluation of the objective function, the new definition and execution of the next simulation for each new microreactor shape. Afterwards, the performance of the system is evaluated by comparing the objective function (reaction yield) with the previous best configuration. If the geometry changes

result in a better reaction yield, this geometry is selected as the best and the old configuration is discarded. The optimization routine continues until a constraint is fulfilled or the optimization converges. The changes of the geometry are performed by a gradient-free method named random search. The random search modifies the design variables by sampling in an arbitrary manner from a vector which sets the variation limits.

Subsequently, the same coupled routine between ANSYS CFX® and MATLAB® is applied to topology optimization. The method was used as a novel technique to computationally discover the best spatial distribution of an enzyme inside microreactors. Usually, the enzyme is uniformly distributed inside a reactor, which can mean either at a wall surface or in a packed bed reactor or free in solution. Therefore, these three applications are studied.

The aim is to improve the product formation per same amount of enzyme in the reactor. The Evolutionary Structural Optimization (ESO) method is adapted to perform the optimization. The ESO method removes inefficient elements from a structure by a gradual and iterative procedure according to a rejection criterion which determines the elements that should be removed every iteration.

The MATLAB® routine is featuring the adaptation of the ESO method to the biocatalytic reactor. The two-dimensional topology optimization is applied to a microreactor with immobilized enzyme on the wall surface. The selected reactor geometry is an adaptation of a previously scientific documented shape used in topology optimization of microreactors. The three-dimensional topology is computationally applied to the distribution of enzyme in a miniaturized packed bed reactor as well as to a microreactor with free enzyme in the volume.

In the last part of the thesis, the topology of microreactors is the experimentally studied. This is achieved by using the peroxidase-catalyzed oxidation of 2,2'-azino-bis(3-ethylbenzthiazoline-6-sulfonic acid) (ABTS) to its radical form by reduction of hydrogen peroxide. The determination of the kinetic mechanism is required in order to validate the optimized microreactors. Two microreactor shapes are topology optimized for posterior experimental validation. The first shape corresponds to the shape with immobilized peroxidase on the wall surface. The experimental validation was attempted by using a photochemical reaction. The reaction attaches linkage molecules to a masked surface, which has an immobilization pattern. The linkage molecules will thereafter react with the enzyme molecules binding them covalently to the surface.

The second microreactor configuration corresponds to a square shaped cross section microchannel with free enzyme in solution. For this case study, a well-mixed solution of enzyme and substrate is considered to enter the microreactor. The experimental comparison is performed by comparing an improved inlet configuration with a reference system. The configurations were selected and fabricated as a compromise considering the outcome of the topology optimization and the limitations of the fabrication process.

Resume

Metoder til optimering af strukturer er et hyppigt brugt værktøj af bygningsingeniører og maskiningeniører til finde optimale strukturer. Optimeringen er baseret på brugen af en række beregningsteknikker der beregner optimal form og topologi af et givent objekt. Formoptimering anvendes direkte på begrænsende overflader af en struktur og resulterer i deformation af objektet. Topologioptimering anvendes til at forbedre strukturen af objektet. Den mekaniske ydeevne af strukturen evalueres baseret på en funktion, der for eksempel maksimerer stivheden af den givne struktur.

I den farmaceutiske industri er der et massivt behov for at reducere omkostninger og øge effektiviteten af reaktorer, hvilket øger efterspørgslen på bedre teknologier og metoder. Hyppigt i kemiske og biokemiske processer er reaktorkonfigurationen begrænset til en række veletablerede design og konstruktioner. I mange tilfælde forårsager disse veletablerede design og konstruktioner dog en forringelse i effektiviteten af den kemiske/biokemiske proces. Dette skyldes at det tit er svært at sikre optimale reaktionsbetingelser i disse veletablerede reaktorkonfigurationer og geometrier. Formålet med denne ph.d. afhandling er derfor at udvikle anvendelsen af form- og topologioptimerings metoder til at løse disse problemstillinger. Mere specifikt er målet at optimere reaktionens betingelser ved at designe optimerede reaktorgeometrier indenfor begrænsningerne for et givent reaktionssystem.

I denne ph.d. afhandling er optimeringsmetoderne udelukkende blevet benyttet på casestudies der fokuserer på at optimere enzymatiske mikroreaktorer. Disse casestudies er valgt således, at resultatet af optimeringen kan valideres eksperimentelt. Optimeringsmetoderne gør det muligt at undgå omfattende eksperimentelt arbejde i bestræbelserne efter optimale reaktordesign.

Mere præcist er formoptimeringsmetoderne blevet brugt til at optimere formen af en YY-mikroreaktor, med et rektangulært tværsnit, for at forbedre blandingen af komponenter i systemet. Indløbet til og udløbet fra reaktoren har begge en Y form og er placeret i de respektive ender af reaktoren. Y-formen gør det muligt at sammenføre to strømme ved indgangen af reaktoren og splitte dem igen ved udgangen. Den benyttede optimeringsrutine varierer formparametre, som højde og bredde. Optimeringen foretages ved brug af Computational Fluid Dynamics (CFD) simuleringer, der beregner indflydelsen af de optimerede reaktorformer på den undersøgte enzymatiske reaktion. Beregningsrutinen implementerer modeller der beskriver enzymkinetikken i CFD (ANSYS CFX®) simuleringerne, koblet med MATLAB® kode der varierer formparametrene. ANSYS CFX® diskretiserer automatisk for miniaturereaktoren i begrænsede volumenelementer og beregner de opnåede udgangskoncentrationer fra reaktoren. MATLAB® beregningsrutinen optimerer derefter udbyttet ved at ændre geometrien, så udgangskoncentrationerne bliver optimeret. Ydeevnen af det optimerede system evalueres ved at

sammenligne reaktionsudbytte fra hver af de testede geometrier for miniaturereaktoren. Hvis de indførte ændringer i reaktorgeometrien resulterer i et bedre reaktionsudbytte, vælges denne nye geometri som den bedste og den gamle konfiguration kasseres. Optimeringens rutinen fortsætter indtil en manuelt defineret forudsætning for reaktionsudbytte er opfyldt, eller optimeringen konvergerer. Ændringerne af geometrien udføres af en gradient-fri metode kaldet *Random search*. *Random search* ændrer designparametrene ved vilkårligt at opsamle nye parameterværdier fra en vektor der beskriver systembegrænsningerne.

Efterfølgende er koblingen mellem ANSYS CFX® og MATLAB® og beregningsrutinen blevet benyttet til at foretage topologioptimering. Metoden blev anvendt som en ny teknik til at beregne den bedste rumlige fordeling af et enzym inde i en miniaturereaktor. Normalt er enzymet ligeligt fordelt inde i en reaktor, hvilket kan betyde enzymet enten er på reaktoroverfladen, på partikler der er pakket i en packed bed reaktor eller frit i reaktionsmediet. Derfor er disse tre forskellige måder at bruge enzymer i en reaktor undersøgt.

Målet med topologioptimeringen er at forbedre reaktionsudbyttet for en given mængde enzym i reaktoren. ESO (Evolutionary Structural Optimization) metoden benyttes til optimeringen. ESO metoden fjerner ineffektive elementer fra en struktur med en gradvis og iterativ procedure.

En todimensionel topologioptimering blev testet på en miniaturereaktor med immobiliseret enzym på reaktoroverfladen. Den valgte reaktorgeometri til denne del af topologioptimeringen er inspireret af en tidligere videnskabeligt dokumenteret reaktorgeometri. En tredimensionel topologioptimering blev anvendt til at beregne den optimale placering af enzymer i/på partikler i en miniaturiseret reaktor, samt for en miniaturereaktor hvor enzymet befandt sig frit i opløsningen.

I den sidste del af denne afhandling er topologioptimering af miniaturereaktorer undersøgt eksperimentelt. Valideringen blev påvist ved oxidering af 2,2'-azino-bis(3-ethylbenzthiazolin-6-sulfonsyre) (ABTS) ved at reducere hydrogenperoxid katalyseret af en peroxidase. I alt er to miniaturereaktorgeometrier topologioptimeret med det specifikke formål at eksperimentelt validere optimeringen. Den første geometri fokuserer på immobilisering af peroxidase på reaktoroverfladen, hvor valideringen blev forsøgt baseret på en fotokemisk reaktion. Den fotokemiske reaktion gør det muligt at binde peroxidase enzymet til overfladen i et ønsket mønster, som er påkrævet for at påvise topologioptimeringen.

Den anden miniature reaktorgeometri fokuserer på en firkantet reaktor kanal geometri, hvor enzymet er frit i opløsningen. I dette studie er det antaget at enzym og substrat er perfekt opblandet når de fødes til reaktoren. Optimeringen blev eksperimentelt valideret ved at sammenligne et optimeret system med et reference system. Valget af geometrier til valideringen af topologioptimeringen blev baseret på systemer, som ikke var begrænset af produktionsprocessen af reaktoren.

Preface

This thesis was prepared at the Department of Chemical and Biochemical Engineering at the Technical university of Denmark (DTU) as partial fulfilment of the requirements for acquiring a the Ph.D. degree in Chemical Engineering.

The work presented in this thesis was developed at the CAPEC-PROCESS Center in the period from November 2012 until October 2015. Associate Professor Ulrich Krühne was the main supervisor and was supported by the co-supervisors Professor John M. Woodley, Professor Krist V. Gernaey and Associate Professor Anders E. Daugaard.

The project was funded by the Project BIOINTENSE – Mastering Bioprocess integration and intensification across scales financed by the European Union through the 7th Framework Cooperation Programme (Grant agreement number: 312148).

An external research was held at the University of California in Berkeley, in the Department of Chemical and Biomolecular Engineering, under supervision of Professor Douglas Clark during the period September and December 2014.

Kgs. Lyngby, October 2015

Inês Pereira Rosinha

Acknowledgments

First and foremost I would like to express my sincere gratitude to my supervisor Associate Professor Ulrich Krühne for the continuous support of my Ph.D study and related research, for his patience, motivation, and immense knowledge. These past years have been a great experience; I would like to thank you for encouraging my research and allowing me to grow as research scientist and as a person.

I would like to thank my co-supervisors, Professor John M. Woodley, Professor Krist V. Gernaey and Associate Professor Anders E. Daugaard for providing invaluable perspective on my research project when most needed.

To my colleagues from CAPEC-PROCESS Center thank you very much for your support and great discussions over these three years. A special thanks to my friends and closest colleagues in the group (Carina, Ana Carolina, Dasha, Catarina, Mafalda, Teresa, Ricardo, Lisa, Hilde and Francesco) who supported me through the most difficult times by listening to me, giving me their advice and even bringing me coffee or tea.

I am grateful for the help of Professor Douglas Clark from the Department of Chemical and Biomolecular Engineering at the University of California in Berkeley, who made my external research, stay possible. I would like to thank him for helping me on setting up the topology optimization procedure and for his professional advices and point of views which made me look at my project in from other perspectives. My gratitude is also send to to Hannah Reese, my officemate in Berkeley, for the great moments during my external stay.

Quero agradecer aos meus pais por todas as vezes que me disseram para a acreditar em mim e que mesmo estando longe sempre me apoiaram. Obrigada por estarem do outro lado do telefone com uma palavra de conforto nos momentos mais difíceis e por festejarem comigo todas as minhas conquistas ao longo do doutoramento. Quero também agradecer à minha melhor amiga Ana Paias, que sempre me apoiou e me ouviu sobre as minhas dúvidas em relação à concretização do meu projecto e me deu sempre a sua perpectiva científica. Obrigada por teres lido alguns artigos científicos de forma a ajudares-me a clarificar as minhas ideias, apesar de nunca teres ouvido falar de optimização topológica.

Tusind tak til min dejlige forlovede, som var meget tålmodig og talte med mig i både gode og dårlige stunder. Tusind tak for din konstante og betingelsesløse støtte og al din kærlighed. Tak fordi du prøvede at forstå mit projekt og for at læse min afhandling. Tak fordi du ringede til mig hver dag fra USA eller Kina, det var dejligt at vide at du altid er der for at hjælpe mig.

Tusind tak til min danske familie for al jeres støtte og forståelse for at mit PhD projekt var meget vigtig for mig og at der var tider, hvor jeg ikke kunne være sammen med jer.

Abbreviations

ACE	Acetone
APH	Acetophenone
ATA	Amine transaminase
CCL	CFX Command Language
CFD	Computational fluid dynamic
ESO	Evolutionary Structural Optimization
FEA	Finite Element Analysis
FEM	Finite element method
FVM	Finite volume method
IPA	Isopropylamine
ISE	Isotropic Solid and Empty
MMA	Method of Moving Asymptotes
OC	Optimal Criteria
PDE	Partial differential equations
PEA	(*S*)-1-Phenylethylamine
RMS	Root mean square
RTD	Residence time distribution
SIMP	Solid Isotropic Material with Penalization
SLP	Sequential Linear Programming

Nomenclature

C	Concentration
D_f	Diffusion coefficient
d_i	Specified direction
$E(x)$	Property of the isotropic material of element x
ER	Evolutionary rate
J	Objective function
K_{EQ}	Equilibrium constant
K_i	Core inhibition constant
K_M	Michaelis-Menten constant
K_{Si}	Substrate inhibition constant
k_{cat}	Turnover number
k_i	Step length
L	Length
N	Governing equation
Pe	Peclet number
p	Pressure
$\bar{p}$	Vector of design variables
$\bar{q}$	Vector of candidate design variables
q	Flow variable
Re	Reynolds number
RR	Rejection criterion
R	Radius
Res	Residual
r	Reaction rate
S	Substrate
S_c	Source
S^n	n-Sphere
S_e	External source applied to the fluid
Sh	Sherwood number
T	Temperature
t	Time
t_{op}	Characteristic time

V	Volume
v	Velocity
γ_i	Design variable
λ	Lagrange multiplier
μ	Viscosity
ρ	Density
τ	Residence time
σ^{VM}	von Mises stress
Ψ	Geometry function

Contents

Chapter 1

Introduction

In biochemical engineering, only certain well-defined configurations are used as reactors in a process. The stirred tank reactor is the most common design used in biochemical processes such as in the pharmaceutical industry. Usually, the reactor operating conditions (e.g. pH, temperature, flowrate, inlet concentration) are optimized after the configuration has been defined. This project's main goal is to perform the intensification of the reactor differently and to optimize the reactor layout or configuration. Therefore, instead of adapting the reactor operation conditions, the reactor configuration is tailor-suited to the limitations of the reaction system.

This thesis presents a series of investigations for application of structural optimization methods to enzymatic microreactors. These techniques are usually used in mechanical engineering for improving the layout of structures. Structural optimization is a set of computational methods such as shape optimization and topology optimization. Shape optimization involves the deformation of the boundaries of an object. Topology optimization finds the optimal structure by changing the layout of the material in a domain. Both shape and topology optimization methods can be applied to several reaction systems in chemical engineering. In this thesis, they are applied to enzymatic microreactors. Figure 1.1 shows a comparison of the actual process intensification strategy and the novel strategy proposed in this thesis. Additionally, it also shows the link between the optimization methods from mechanical engineering and the new process intensification strategy.

This project covers a broad range of research areas such as structural optimization methods, computational fluid dynamics, programming, microreactor fabrication and biocatalysis. Moreover, the learning of the structural optimization methods required studying the basic concepts from physics and mechanics in order to understand how the methods work and how they could be applied to chemical engineering.

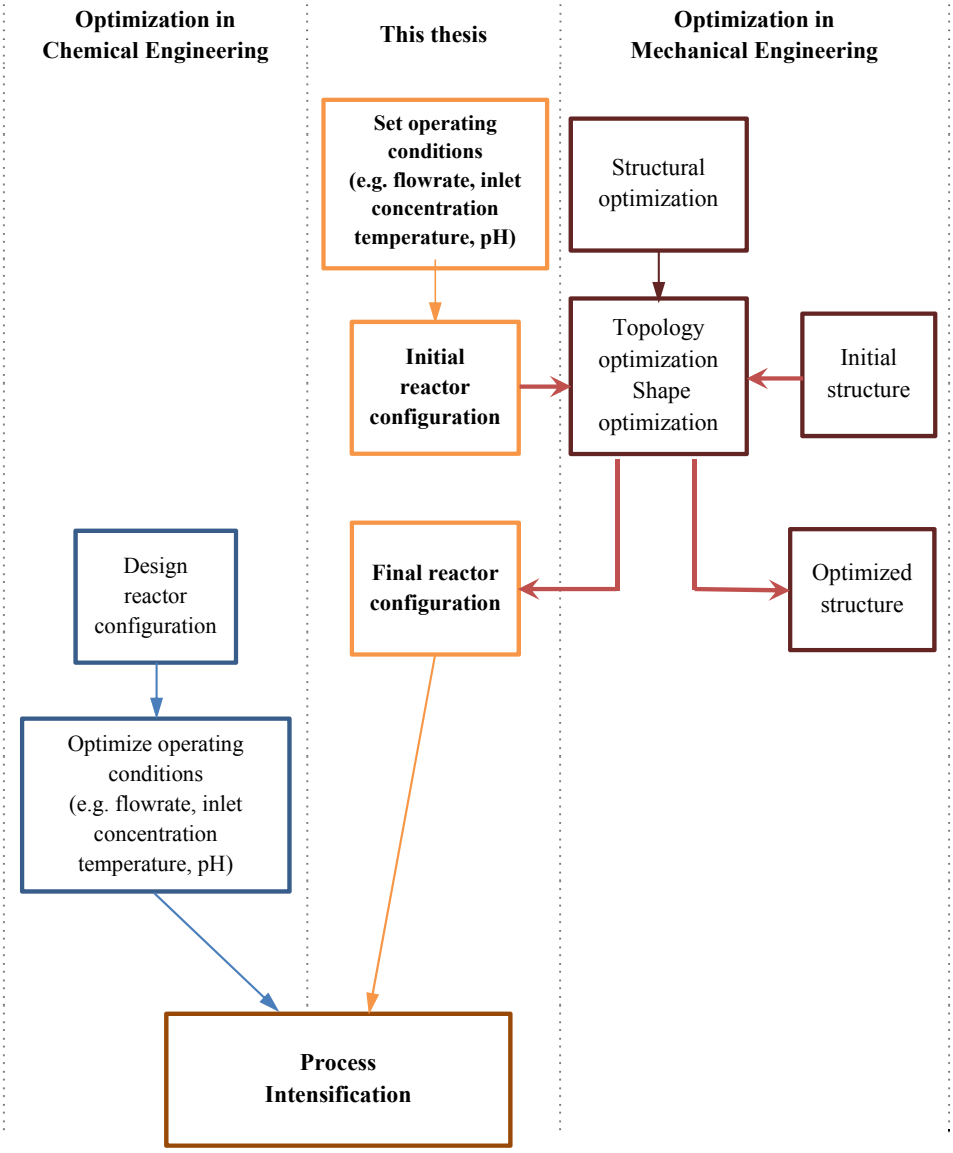

Figure 1.1 – Overview of project objective. Comparison between the general process intensification method and the innovative technique presented in this thesis using topology and shape optimization.

1.1 Motivation and specific research goals

In the pharmaceutical industry, numerous enzymes are used in the production of medicinal products and intermediates. Enzymatic reactions are usually characterized by complex kinetic mechanisms which might be associated to two or more substrates as well as substrate or product inhibition.

The design of a reactor usually does not take into account the different characteristics of the enzymatic reaction systems. Thus, the implemented reactor in a biochemical process does not yield the best reaction conditions. All reactors are characterized by their flow regime; it can be either laminar or turbulent. The flow in microreactors is laminar which is characterized by a parabolic flow profile, significant difference in radial residence times and mass transport by diffusion which results in large concentration profiles.

The non-uniform fluidic conditions and complex kinetics for an enzymatic reaction give a clear motivation to investigate the shape of microreactors and the topology optimization of the enzyme in microreactors in order to improve the product formation yield. The application of both shape and topology optimization methods gives the opportunity for developing an innovative strategy for reactor design and a new method for process intensification. These methods will be used to find the reactor with best performance regarding the reaction system properties. Moreover, many microreactor fabrication techniques are currently available which give the opportunity for possible experimental validation of these optimization methods.

Therefore the specific goals for this project are:

- The development of the interface between the computational fluid dynamics software (ANSYS CFX®), which evaluates the microreactors fluid dynamics and yields, and the optimization cycle implemented in the numerical software (MATLAB®).
- The investigation of the application of structural optimization methods used in mechanical engineering for optimizing a chemical engineering problem, specifically enzymatic microreactors. The development of a new process intensification strategy for reactor design. Instead of optimizing the operating conditions to a well-known design, the reactor configuration will be optimized in terms of layout in order to satisfy certain operating conditions.
- The application of shape optimization to a microreactor to evaluate how the variation of the geometry influences the reaction yield by keeping a constant the residence time of the compunds.
- The verification of using topology optimization methods for finding new microreactor configurations, which can produce more products from the same amount of enzyme and

substrates. In this way it is possible to find the best or at least an improved design before testing the microreactor in laboratory.

- The experimental work for the verification of computational results by comparing intensified microreactors with reference reactors.

1.2 Thesis outline

This thesis is divided in three parts: theoretical background, computational investigations and experimental investigation. All the computational investigations were performed considering that the microreactors operate under steady-state conditions.

Chapter 2 provides an introduction and background of the main aspects regarding shape and topology optimization. An overview about the important applications and the most commonly used methods for these two types of optimization are presented. This chapter includes also a brief description of the main aspects behind computational fluid dynamics and an insight into the setup of a CFD simulation using ANSYS CFX®. An overview about process intensification using microfluidics and main aspects regarding mixing inside a microsystem is presented. Finally, the application of shape and topology optimization to microreactors is reviewed.

Chapter 3 includes an investigation of shape optimization of a specific microbioreactor. For implementation of the shape optimization method, the interface between ANSYS CFX® and MATLAB® was established. This chapter includes a detailed description of the implementation of the shape optimization method and the interface of the two software tools. The enzymatic reaction chosen for this investigation is the synthesis of the chiral amine (*S*)-1-phenylethylamine and acetone from acetophenone and isopropylamine using amine transaminase as biocatalyst. This enzymatic reaction is characterized by both substrate and product inhibition and an unfavorable thermodynamic equilibrium, which drives the reaction towards the substrates.

Therefore, this computational study investigates the influence of the reactor shape on the mixing of enzyme and substrates streams, possible *in situ* product removal (ISPR) for the improvement of product yield.

Chapter 4 focuses on the adaptation of one of the topology optimization methods from the scientific literature and on the development of the interface between ANSYS CFX® and MATLAB® for applying the chosen method. Moreover this chapter includes two computational case studies of topology optimization. One of the case studies is the application of a two-dimensional optimization of immobilized enzyme distribution on the wall surface of the microreactor. The other case study investigates a three-dimensional topology optimization of immobilized enzyme in a packed bed microreactor. In this chapter, the computational studies were made in order to investigate how the flow conditions, mass transport phenomena, substrate and the reaction rate influence the product yield. The study does not include an evaluation of

strategies such as ISPR and therefore a simpler reaction mechanism is chosen. The chosen enzymatic reaction system follows Michaelis-Menten kinetics ($k_{cat} = 100\ s^{-1}, K_M = 25\ mM$).

Chapter 5 presents a series of experiments for verification of the computational results. These experiments are the initial stage for the validation of the topology optimization method. It includes the characterization and determination of the kinetic parameters for the chosen reaction system. The reaction system corresponds to peroxidase-catalyzed reduction of hydrogen peroxide by oxidation of 2,2'-azino-bis(3-ethylbenzthiazoline-6-sulfonic acid) (ABTS) to its radical form. The subsequent sections present the experimental work for investigation of topology influence on microreactors for both two-dimensional and three-dimensional case studies, respectively. Each case study includes the computational optimization of a microreactor with the determined kinetic mechanism and the experimental work for verification of the simulations outcome.

Chapter 6 presents an overall conclusion with the most important findings from this thesis and proposes possible future work for further research on process intensification using shape and topology optimization.

1.3 Publications included in the thesis

The following publications have resulted from the work presented in this thesis. The published manuscript is provided in Appendix A.

> *Pereira Rosinha, I., Woodley, J., Gernaey, K., Krühne, U. (2015) Topology optimization for biocatalytic microreactor configurations. 25th European Symposium on Computer Aided Process Engineering, Conference Proceedings*

Parts of this publication have been included in Chapter 4 in order to explain the adaptation of the Evolutionary Structural Optimization method and the topology optimization routine.

Chapter 2

Theoretical background and literature review

2.1 Introduction

This chapter includes a presentation of the main aspects regarding shape and topology optimization. An introduction of the shape and topology optimization concepts will be made and it will be complemented with an overview of applications and frequently applied methods to these types of optimization studies. Furthermore, a comparison between gradient-based and gradient-free methods will be made. Both categories will be described and one method for each class will be presented. Subsequently it will be possible to highlight the main differences between gradient-based and gradient-free methods, and to present their strengths and weaknesses.

This chapter will also give a brief insight into the theoretical aspects behind Computational Fluid Dynamics (CFD) such as the history, the concept and the discretization and calculation methods. Moreover the reader will be able to understand how the software used in this thesis (ANSYS CFX®) works.

This chapter also presents an overview of microfluidics and process intensification applied to microfluidics, since shape and topology optimization will be applied to microreactors in this project.

Finally, the cases of shape optimization and topology optimization applied to microfluidics will be reviewed.

2.2 Topology and shape optimization

Topology and shape optimization are computational techniques often used in mechanical and civil engineering with the purpose of finding an optimal structure. The evaluation of the structure performance is made by an objective function which can be maximizing stiffness or a minimal amount of material used in the structure.

Topology derives from the Greek words place (topos) and study (-logy) which corresponds to the field in mathematics which studies the spatial properties. Topology optimization is defined as a mathematical methodology which optimizes the layout or distribution of the material in a defined domain, by satisfying given constraints and minimizing (or maximizing) an objective function[1,2].

In turn, shape optimization is defined as a mathematical method which identifies the optimal shape by the deformation of the shape of the object by minimizing (or maximizing) an objective function and fulfilling a series of restrictions[1].

The shape optimization procedure is directed to the boundaries of the object. This means that no material is added or removed from the object; there is instead a deformation of the shell of the object. The deformation of the shape during the optimization procedure also involves the constant alteration of the domain which can be a complex process and problematic for the numerical solution.

On the other hand, in topology optimization the material can vary between no material or solid material within the domain, allowing also the material with densities between zero and solid material. Therefore, in topology optimization it is possible to remove material and generate structures with low or reduced amounts of material.

Shape and topology optimization procedures combine optimization methods and numerical methods, such as finite element method (FEM) or finite volume method (FVM), which will be explained further in this chapter.

The basic terms in a general optimization problem are[3]:

- Objective function: represents an equation in continuous problems or an amount in discrete problems which is optimized (minimized or maximized) according to changes of the design variables and following previously defined constraints.
- Design domain: is the allowable volume or area within which the design can exist.
- Design variables: are numerical parameters which make changes to the system during the optimization. Design variables can be continuous or discrete.
- Constraints: are the limits imposed to the system which will be optimized.
- Governing equations: are the equations which describe the physics or fluidics of the structure to be built.

2.2.1 Historical background

Structural optimization was first introduced at the end of the 19th century by Maxwell (1890)[4] who established the first theorems regarding the design of structures based on compression and tension elements[3]. His work was continued by Michell[5] in 1904 which is more recognized and well-known by the experts in this field due to his demonstration on obtaining unique configurations by minimizing their weight. His work corresponds to the basis for the development of direct design methods.

In the 1960s and 1970s, structural optimization research has experienced intense activity due to the affordable development of computers. In this period, the first structural optimization methods and numerical methods were presented and the researchers focused on discrete methods to solve structural optimization problems. Schmit[6] is considered widely to be the pioneer of the modern structural optimization methods by his work published in 1960. His work introduces the idea of combining the finite element analysis and non-linear programming mathematical methods in order to create automated methods to find the best configuration of a structure. Although the work developed during the 1960's decade revolutionized the way to design structures, the methods demonstrated to be highly computationally expensive [7]. For instance, a simple problem would often need hundreds of analyses of the structure which means that for large structures the computational cost of the optimization would be prohibitive. Computational cost is here defined as the amount of time necessary to solve an optimization problem computationally.

In the late 1960s, Prager[8] and Venkayya[9] have presented a new numerical method to apply to structural optimization known as Optimality Criteria[10]. This approach does not minimize directly the objective function, instead it specifies a criterion subjected to constraints and the design which satisfies it is considered to be the optimum. The main idea is to define a criterion which characterizes the optimal structure as a recursive formula which leads iteratively to the solution. This technique is considered to be intuitive and more efficient than the previous methods. Moreover, it also revealed to be an effective tool since it often provided a near-optimum design independently of the problem size[10].

In the 1980s, along with the exponential development of the computing technologies, the theoretical work on structural optimization was continued with further focus on numerical methods and application to larger-scale and realistic structures. In this period, structural optimization methods were continuously studied and the continuum structural optimization was introduced and widely developed.

The modification of the layout of the material revealed to be complex by using the shape optimization methods due to the fact that every iteration implied the modification of the model of the finite elements[11]. This challenge resulted in the search of methods which did not involve the modification of the domain but focused only on the distribution or layout of the material.

Therefore, in the end of the 1980s, Bendsøe and Kikuchi[12] have developed an alternative to the shape optimization named topology optimization. In this alternative method, the initial domain of the structure is fixed and therefore the finite element analysis used in the optimization process is unaltered.

The most well-known Isotropic Solid and Empty (ISE) methods in topology optimization are Solid Isotropic Material with Penalization (SIMP) and Evolutionary Structural Optimization (ESO). These gradient-based methods were the first methods to be developed for isotropic structures[13]. In an ISE method, the elements of the domain are either filled by a particular isotropic material or they are empty. An isotropic solid is a solid for which its physical properties do not depend on its orientation. Gradient-free methods have also been proposed for topology optimization[14–16], however these methods have the disadvantage of becoming excessively computationally expensive[17].

The basic idea behind the SIMP method was proposed by Bendsøe in 1989[18], but it was first introduced by Rozvany *et al*.[11]. This method is nowadays the most commonly used by the experts in the field. The ESO method was developed by Xie and Steven[19] and it has also been applied in various structural optimization problems. These two methods revolutionized the field of structural optimization by simplifying the implementation of structural optimization and enabling its application to more realistic problems. Further in this chapter, these two methods will be described in more detail.

2.2.2 Shape optimization methods – gradient-based and gradient-free methods

In shape optimization, several algorithms have been used over the years to solve structural optimization problems. These methods can be divided essentially in two categories: direct search methods often called gradient-free and gradient-based methods or sequential approximation methods.

Gradient-based methods are defined as deterministic algorithms which convergence to the optimum solution driven by the gradient of the objective function. Gradient-free optimization methods do not use derivatives in order to determine the optimum. Gradient-free methods are procedures which use heuristics like finding optimal solutions by trial and error or mimic the process of natural selection like evolutionary or genetic algorithms.

2.2.2.1 Gradient based methods

In the scientific literature, the majority of shape optimization studies is performed using gradient-based optimization procedures (e.g. Jakobsson and Amoignon (2007), Allaire *et al*. (2009), Mader and Martins (2014), Giannakoglou *et al.*(2012) [20–23]). The two most frequently used gradient-based methods are the adjoint method and the level-set method. In this section, only the adjoint

method will be described in detail to give the general idea of how the gradient-based methods work, and will be afterwards compared with the gradient-free methods. The level-set method has been described in detail by Osher [24] and Sethian[25]

The adjoint method is often used in problems related to fluid dynamics cases such as aerodynamic shapes [26–28] and is characterized by the discretization of the governing equations. The adjoint method was described well by Giannakoglou and Papadimitrious [29]. The adjoint method can be presented by two approaches: continuous or discrete. In continuous adjoint methods, the adjoint partial differential equations are built from the partial differential equations (PDE's) which define the flow. Afterwards, the adjoint PDE's are discretized and numerically solved. In contrast, in the discrete approach the adjoint equations are obtained directly from discretized PDE's describing the flow.

The discrete adjoint method is characterized by transforming a constrained optimization problem into an unconstrained problem by introducing Lagrange multipliers as adjoint variables [29]. Lagrange multipliers are used to find minima or maxima of a function, subject to equality constraints without the need of solving explicitly the constraints or use them as extra variables [30]. The discrete adjoint method can be formulated by the following problem representation:

$$\begin{aligned} &min\, J(q, \Psi(\gamma_i)) \\ &subject\ to\ N(q, \Psi(\gamma_i)) = 0 \end{aligned} \tag{2.1}$$

where J is the objective function, γ_i corresponds to a design variable (i=1,…,m) , Ψ represents the geometry function and q is the flow variable and N corresponds to a governing equation.

The total variation of the objective function with respect to a design change is given as follows:

$$\frac{\partial J}{\partial \gamma_i} = \frac{\partial J}{\partial \Psi}\frac{\partial \Psi}{\partial \gamma_i} + \frac{\partial J}{\partial q}\frac{\partial q}{\partial \gamma_i} \tag{2.2}$$

or

$$\delta J = \frac{\partial J}{\partial \Psi}\delta\Psi + \frac{\partial J}{\partial q}\delta q \tag{2.3}$$

Where $\frac{\partial \Psi}{\partial \gamma_i}$ is the geometric sensitivity and $\frac{\partial q}{\partial \gamma_i}$ is the flow sensitivity. The variation of the governing equation is given by:

$$\delta N = \frac{\partial N}{\partial \Psi}\delta\Psi + \frac{\partial N}{\partial q}\delta q \tag{2.4}$$

The variation of the governing equation can be added to the variation of the objective function and in this way the flow field can be eliminated from this expression. The variation of the flow field is not always generally available and therefore it is necessary to find an efficient method to handle it.

The addition of the flow variation to the objective function variation results in the so-called augmented objective function [31]:

$$\delta L = \delta J + \lambda\, \delta N \tag{2.5}$$

or

$$\begin{aligned} \delta L &= \left[\frac{\partial J}{\partial \Psi}\delta\Psi + \frac{\partial J}{\partial q}\delta q\right] + \lambda\left[\frac{\partial N}{\partial \Psi}\delta\Psi + \frac{\partial N}{\partial q}\delta q\right] \\ &= \left[\frac{\partial J}{\partial q} + \lambda\frac{\partial N}{\partial q}\right]\delta q + \left[\frac{\partial J}{\partial \Psi} + \lambda\frac{\partial N}{\partial \Psi}\right]\delta\Psi \end{aligned} \tag{2.6}$$

So choosing a Lagrange multiplier λ which satisfies

$$-\left(\frac{\partial J}{\partial q}\right)^{T} = \lambda\left(\frac{\partial N}{\partial q}\right)^{T} \tag{2.7}$$

eliminates the flow sensitivity δq from the augmented objective function,

$$\delta L = \left[\frac{\partial J}{\partial \Psi} + \lambda\frac{\partial N}{\partial \Psi}\right]\delta\Psi \tag{2.8}$$

The previous equation shows that the gradient of the objective function can be obtained from the geometric variations and from the solution of the adjoint field resulting from equation 0. According to these equations, the objective function is independent of the flow field variables.

The adjoint method is the only gradient-based method in the literature which is independent from the number of design variables. Therefore, it has a low computational cost when performing sensitivity analysis [27]. In most of the gradient-based methods, sensitivity analysis is performed by varying each design variable by a small amount and then, objective function is recomputed according to the sensitivity results. Thus, for each iteration, it is necessary to find $n + 1$ CFD solutions to solve an iteration of a problem with n design variables. In contrast, the adjoint method only requires performing one CFD solution per iteration.

2.2.2.2 Gradient-free methods

Despite the common application of gradient-based methods in shape optimization, there are some cases in which the optimization procedure consists of a gradient-free optimization method [32–34].

Genetic algorithms, pattern search and random search are some of the gradient-free optimization methods which can be applied to shape optimization[35–38].

Random search is a simple gradient-free optimization method and it has been occasionally applied to shape optimization in mechanical engineering [36,39]. In contrast to deterministic methodologies which characteristically guarantee convergence asymptotically, the random search method ensures the convergence through randomness and probability. Random search methods can be applied to both continuous and discrete optimization problems.

One advantage of random search methods compared with deterministic methods is that they can be applied to problems where the objective function is non-differentiable, discontinuous, discrete, or they can even be applied to a continuous-discrete domain.

Another advantage of the random search method is the possibility to implement the method in complex problems with discontinuous functions. Since this method only relies on function evaluations instead of gradient information as the deterministic methods, the random search method does not require that the objective function is a continuous expression [40]. Furthermore, the random search method is characterized as "robust" and is also known by its good performance since it generates quickly useful information in optimization problems.

The generic random search algorithm is defined by the following optimization problem[41]:

$$\text{Objective function:} \qquad J = \min_{\bar{x} \in S} f(\bar{p}) \tag{2.9}$$

where $\bar{p}$ is the vector of n design variables, S is an n-dimensional non-empty region and J is the objective function. The objective function for random search may be a "black-box" function, i.e. the objective function does not need to be defined by a mathematical expression and can be a numerical value of f which is returned for an input of $\bar{p}$.

The general random search algorithm is described by a sequence of iterates $\bar{p}_i$ on the iteration $i = 0,1, \ldots$ which may depend on the previous points and algorithmic parameters. The vector x_i may represent a single point or a collection of points. The generic random search algorithm is given by [41]:

Step 0: Initialization of the random search with the initial vector $\bar{p}_0 \subset S$ and iteration index $i = 0$.

Step 1: Generate a collection of candidate points $\bar{q}_{i+1} \subset S$ according to a specific generator.

Step 2: If $f(\bar{q}_i) < f(\bar{p}_i)$ a new local optimum set of points has been found. Update the vector $\bar{p}_i$ based on the optimum set of points $\bar{q}_{i+1}$.

Step 3: If a stopping criterion is met, stop the optimization routine. Otherwise increase i and return to Step 1.

The generic random search algorithm is dependent on the generator procedure of the candidate points at Step 1 and on the update procedure in Step 2. Two examples of generator procedures are the single-point generator and the multiple-point generator. For the single-point generators, the candidate $\bar{q}_{i+1}$ is generated based on the current point. A common method to generate a candidate point is to take a step size in a vector direction. Therefore, the Step 1 of the generic routine can be described by:

$$\bar{q}_{i+1} = \bar{p}_i + k_i \bar{d}_i \tag{2.10}$$

where the candidate point is taking a step from the current point p_i of length k_i in a specified direction d_i on iteration i.

In continuous problems the direction vector d_i may follow the gradient information of the direction of the previous iterations and the step length may be the result of a line search. However, if the step direction is closely related to the gradient, as in stochastic gradient searches, the problem might converge to a local optima convergence [41]. Therefore, the application of procedures to escape the local minima and find the global minimum must be introduced.

An alternative to generate the direction d_i that does not use any local information is to obtain the direction vector by sampling from a uniform distribution on an *n*-sphere. The *n*-sphere is the generalization of the ordinary sphere to spaces of arbitrary dimension [42]. The radius of an *n*-sphere is defined by a set of points in an *(n+1)*-dimensional Euclidean space which are at an equal distance r (radius) from the central point. Hence, the n-sphere centred at the origin is defined by:

$$S^n = \{p \in \mathbb{R}^{n+1} : \|p\| = r\} \tag{2.11}$$

where S^n is an *n*-dimensional manifold in an Euclidean *(n+1)*-dimensional space.

Specifically, a 0-sphere is the pair of points at the ends of a line segment, a 1-sphere corresponds to the circumference of the intersection of a disk and a plane and a 2-sphere corresponds to the two-dimensional surface which defines a three-dimensional ball. Spheres of dimension n>2 are called hyperspheres [42] and are difficult for human beings to imagine.

The step size can be generated through random generation and it may expand or shrink according to the success of the previously sample points.

Another method to generate the candidate points is the multiple point generator [41]. This method is using the current collection of points to generate the candidate points. This method is used by population-based random searches, which resemble biological processes such as genetic algorithms, evolutionary programming and ant colony optimization. Without the gradient information, most of the random search methods employ more than one solution for each

iteration. The generation of new candidate points is applied to the points, which revealed to give the best solutions at this point.

Similarly to the dependence of the method to find candidate points, the random search algorithm is also dependent on an update procedure of the new points. After a set of candidate points is generated and it has been verified that it generates a better system, the random search algorithm specifies an updated version of the current set of points. The current set of points will take on the value of the set of candidate points. The update procedure can be described by:

$$\bar{p}_{i+1} = \begin{cases} \bar{q}_{i+1}, & f(\bar{q}_{i+1}) < f(\bar{p}_i) \\ \bar{p}_i, & otherwise \end{cases} \tag{2.12}$$

This type of algorithm might get trapped in a local minimum if the neighbourhood or the method of generating candidate points is very restricted.

Gradient-free and gradient-based methods differ in many aspects such as the approach to gradually find the optimum using a gradient or not and the type of objective function and domain they can be applied to.

The gradient-based optimization methods are described as efficient to determine the local minima for nonlinearly-constrained and convex problems. However, these methods cannot be used when solving discrete design variables or discontinuous functions and domains since for these cases it is not possible to calculate a gradient[43]. Moreover, gradient-based methods have difficulties solving problems with several local minima since the gradient of these methods might evolve towards a local minimum of the system and present it as an optimal solution[43]. A potential way to overcome such challenges is to use a gradient-free optimizer, or to start at different initial conditions in the searched parameter space. Gradient-free methods are considered to have an increased chance to find the global optimum or a solution near the global optimum.

In fact, in gradient-based methods, when the number of design variables is large, it may be prohibitive to make all objective function evaluations for a sensitivity analysis in order to obtain a gradient[44]. However, gradient-free methods might also be computationally expensive in cases of problems with many design variables, since such a method does not make use of any domain information to guide the search[45].

2.2.3 Methods in topology optimization – Isotropic Solid or Empty methods

The main idea behind the ISE methods in topology optimization is to determine the optimal placement of an isotropic material and which locations should be empty.

As mentioned above gradient-based or gradient-free methods can be both applied to topology optimization. The most commonly used are the gradient-based methods. The implementation of topology optimization through gradient-free methods has been less frequently reported. However,

in the scientific literature, it is possible to find some applications of genetic algorithms to topology optimization (e.g. Kane and Schoenauer (1996) and Aydın and Ayvaz (2009)[46,47]).
The two most common gradient-based optimization methods are Solid Isotropic Microstructure with Penalization (SIMP) and Evolutionary Structural Optimization (ESO)[17].

2.2.3.1 Solid Isotropic Microstructure with Penalization (SIMP) method

The SIMP method uses the strategy of varying the density of the elements of the domain, assuming that the "density" (ρ) of the isotropic material may vary between zero (no material) or one (with material) [18]. The term density in this case does not correspond to the density of the material but to a pseudo-density which defines the fraction of the volume of the structure that is filled with the material:

$$V = \int_{\Omega} \rho(x) d\Omega \tag{2.13}$$

where V is the volume of the structure, x is an element of the domain and Ω corresponds to the domain.
The first step of this method is to distribute the material uniformly with density $\rho = 1$ over the domain (Ω). A material property is used as the basis for the problem definition and as the objective function. The material property is a function of the density of each element of the domain [2,12,48]. This material property depends on the type of problem; in mechanical engineering it is common to use properties such as material compliance (inverse of material stiffness) or Young modulus (also known as the modulus of elasticity which measures an object /substance resistance while being deformed elastically). The objective function can then be represented by the following equation:

$$E(x) = \rho(x)\, E_0 \tag{2.14}$$

where ρ corresponds to the design variable, in this type of problems considered to be the density of the material, x is the position of the element on the domain, $E(x)$ is the property of the material of element x and E_0 is the property basis of the isotropic material [2]. The vector of densities $\rho(x)$ can be defined by the following interval of values: $0 < \rho_{min} \leq \rho(x) \leq 1$. The value ρ_{min} is inserted in the model in order to avoid the mathematical singularity. Mathematical singularity can be defined as a point that fails for example in differentiability.
This method has as main goal to obtain a discrete solution with elements with density 1 and elements with density 0. A possibility to approximate each iteration solution to a discrete solution

is to introduce a form of penalization to the continuous variable, in this case the pseudo-density, in order to direct the result into a discrete solution (0-1 values)[2,48].

The SIMP introduces this penalization by adding an exponent to the design variable, and the objective function becomes:

$$E(x) = \rho(x)^n E_0 \tag{2.15}$$

where n is the penalization factor. When the exponent is higher than 3, the number of intermediate values of the design variable is low [48]. Figure 2.1 presents the effect of raising the design variable to an exponent. When the penalization factor n is equal to one the relation is linear. However, when the exponent is higher than one, the values of the objective function approximate the discrete solution [49]. As a rule of thumb, it is advisable to choose values higher than 3 for the penalization factor in order to avoid intermediate density values [49,50].

The optimization problem can be solved using one of the following approaches: Optimality Criteria (OC), Sequential Linear Programming (SLP) or the Method of Moving Asymptotes (MMA). These optimization methods are out of the scope of this thesis and therefore the reader is advised to read more about Optimality Criteria in Prager[8], Rozvany[51] and Rozvany[52], about Sequential Linear Programming (SQL) in Kikuchi[53] and Nishiwaki[54] and about the Method of Moving Asymptotes (MMA) in Svanberg[55].

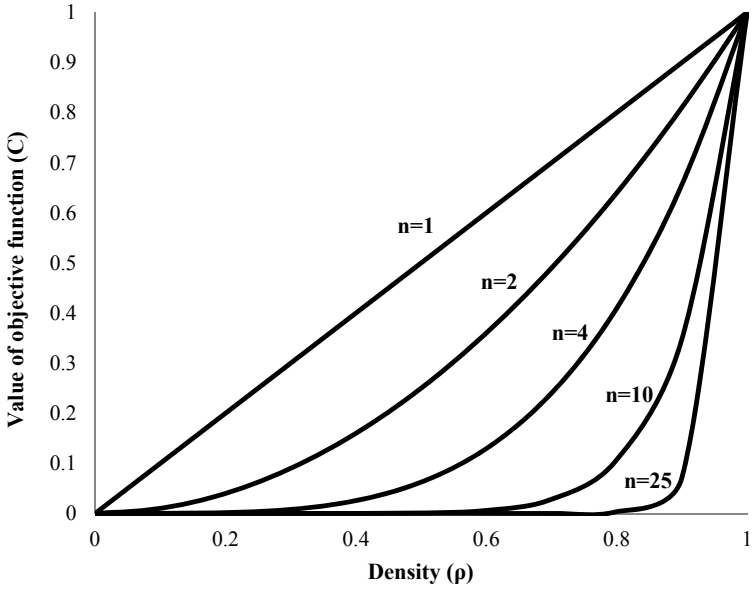

Figure 2.1 – Penalization factor (*n*) effect on the objective function for obtaining discrete solutions (adapted from Rietz[49]).

Checkerboard effect

The refining of the discretization of the domain of the problem (the domain is represented by more elements) allows the better contour of the optimized configuration as a discrete solution. However, the refining of the discretized domain results in the formation of a checkerboard pattern. The checkerboard pattern is a collection of elements whose densities alternate between solid and void material, resembling a checkerboard. The checkerboard pattern is caused by bad numerical modelling that overestimates parameters such as the stiffness of the checkerboards [56].

A solution to overcome this limitation is the use of a filtering method. Sigmund[57] has proposed a filtering method which is applied to the gradients of the densities which avoids the steep variations between the pseudo-densities. This method implies a filtering on determination of the stiffness of an element x which depends on the density in all eight points of the neighborhood of x. This results in a smoothing of the stiffness, and consequently in a filtering of the image. In Figure 2.2, it is possible to visualize the effect of refinement of the discretized domain on the appearance of the checkerboard.

Figure 2.2– Example of a topology optimization applied to a beam: a) coarse discretized domain; b) refined discretized domain and checkerboard appearance.

2.2.3.2 Evolutionary Structural Optimization (ESO) method

Similar to the SIMP method, the Evolutionary Structural Optimization (ESO) method has as main goal to optimize the distribution of material within a fixed domain, fulfilling specific restrictions. The distribution of the material is modified, by following the alterations of the mechanical structure.

The ESO method has been presented by Xie and Steven in 1993 [19]. The idea behind this method is very simple; the structure configuration evolves towards the optimum by slowly removing (hard-killing) inefficient elements in the structure. For example, elements with the lowest stresses are removed in order to maximize the structure stiffness. The selection of the objective function is very important for the optimization process and must be a function of the design variables.

This method presents some advantages due to its straightforward implementation. Moreover, it allows optimizing the topology with a faster convergence than stochastic algorithms (e.g. Genetic Algorithm), due to the sensitivity analysis of the elements that is performed in between iterations. The randomness of stochastic algorithms generates a larger number of iterations in order to find the optimal structure.

The ESO method is based on the removal of inefficient elements from a structure by a gradual and iterative procedure, which involves the creation of a rejection criterion. The rejection criterion is a way to evaluate the contribution of each element in the structure and to determine which elements should be removed in each iteration.

The explanation of this method in this section will be done by considering the optimization criterion as the maximum stress of a structure as presented by Xie and Steven. The stress criterion was chosen because it is a good indicator of inefficient material[58]. Low inefficient elements are characterized by low values of stress. The stress on each element should ideally be close to the same in every part of the structure. The stress of each element is evaluated by using the von Mises stress. The von Mises stress (σ^{VM}) is a parameter which determines whether an isotropic material will lose stability when a loading is applied to the structure.

The stress level of each element is determined by comparing the von Mises stress of the element (σ_x^{VM}) with the von Mises stress of the structure (σ_{max}^{VM}).

After the finite element analysis, the elements which satisfy the following condition are removed:

$$\frac{\sigma^{VM}}{\sigma_{max}^{VM}} < RR_k \tag{2.16}$$

Where RR_k corresponds to the current rejection criterion[58]. The rejection criterion is maintained constant until the process of removing elements reaches steady state. Steady state in this case means that no more elements can be removed with the current rejection criterion. In order to continue the removal of elements it is necessary to update the rejection criterion by introducing an evolutionary rate. The evolutionary rate (ER) is added to the rejection criterion[58]:

$$RR_{k+1} = RR_k + ER \tag{2.17}$$

The removal of the elements proceeds again until a new steady state is achieved and it is necessary to update the rejection criterion.

The optimization procedure continues until one of the constraints is fulfilled, for example until a requested structure volume is achieved or there is no more material which has a stress level less than a certain percentage of the maximum stress.

The evolutionary structural optimization can be summarized in the following procedure [58]:

1 – Discretize the domain in a mesh of fine elements;

2 – Perform finite element analysis to the domain;

3 – Eliminate the elements which satisfy the condition of the rejection criterion (equation (2.16));

4 – Update the rejection criterion using the evolutionary rate (ER);

5 – Repeat the steps 2 to 4 until an optimal structure is found or one of the constraints has been met.

2.3 Computational fluid dynamics

2.3.1 CFD History and concept

Computational fluid dynamics (CFD) is a branch of fluid mechanics that uses numerical algorithms and analysis to solve and analyze the behavior of fluid flows and the effects of fluid motion computationally. Therefore, CFD integrates three important disciplines: mathematics, fluid mechanics and computer science (See Figure 2.3). Computational fluid dynamics has become a widely used method to solve fluid-dynamic problems in addition to experimental and theoretical analytical methods [59].

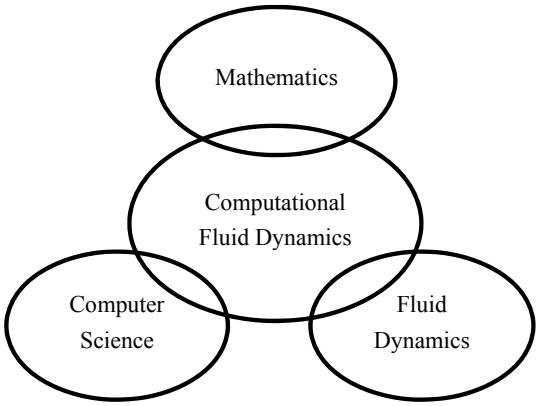

Figure 2.3 – Three important disciplines applied in Computational fluid dynamics.

An advantage of this numerical method is that it allows the study and better understanding of fluid dynamics phenomena, which are not possible to analyze through experiments.

CFD makes use of a fundamental set of partial differential equations which are based on three principles: conservation of momentum, conservation of mass and conservation of energy for a fluid. In many software programs these mathematical governing equations have been converted by computer scientists using high-level computer programming languages into computer programs or software packages.

The amount of computational fluid dynamics (CFD) application areas have been expanded in the past decades. Computational fluid dynamics has been developed in the early 1970's. The evolution of computer technology triggered the interest into simulating fluid flows and consequently, the development of CFD. However, only in the 1980's the solution of two-dimensional (2-D) and later three-dimensional (3-D) Euler equations was possible. With the development of supercomputers in the mid-80's, it became possible to run more demanding simulations such as viscous fluids governed by the Navier-Stokes equations.

The number of computational fluid dynamics application areas has been expanded tremendously in the past decades. Nowadays, computational fluid dynamics is applied both in industry and in academia research. Furthermore, CFD modelling has been used in a broader range of applications, besides astronautics and aeronautics, such as process, chemical, civil and environmental engineering.

In fact, the development of new and improved systems computationally and the computational optimization of existing equipment became very interesting since it resulted in enhanced efficiency and consequently costs reduction.

2.3.2 CFD applied to chemical reactor design

CFD has been successfully used as computational tool on numerous areas of application such as automotive, aerospace and wind power industry. More recently there has been an increasing interest into using CFD within a broader range of applications such as process or equipment development, medical studies, power generation, civil and environmental engineering and sports.

In this relation, the modelling of fluids encounters several adversities for the definition of the flow such as multi-phasic fluids, phase changes, the kinetics of chemical and biological conversion and thermodynamic properties[60]. The understanding of the fluid dynamics of multi-phasic systems for reaction and separation has not been fully developed. The lack of information is caused by the numerous interacting phenomena which determine the system behavior. Although the modelling of equipment for process engineering is common, accurate models are essential to understand in detail the fundamental phenomena.

In the past, engineers have investigated these phenomena through experimental work in order to quantify the fluid dynamics inside reactors. However, experiments at laboratory and pilot scale of reactors can be a time-consuming and expensive process. Moreover, many phenomena can be difficult to quantify experimentally. Therefore, CFD is a powerful tool that can be applied to process engineering for improving the design and operation of equipment in chemical and manufacturing processes.

A suitable implementation of CFD in processing engineering could be its application in scale up of equipment. Without the ability of simulating systems, a company has to build many prototypes to find the systems which keep the same conditions across scales [61]. The high costs associated to experimental development can be avoided by simulating the systems using CFD. Through CFD simulations it would be possible to determine the best conditions of operation before building the first prototype.

2.3.3 Advantages and limitations of CFD

The theoretical studies of fluid dynamics involve the approximation and simplification of the governing equations. CFD is a method which can help to study specific terms in these equations in more detail and therefore, it allows new paths for theoretical development and understanding.

In addition, CFD software solutions have been confirmed as useful tools for development of new equipment, since they reduce the time and cost involved with generating new designs when compared with a purely experimental approach[59]. CFD has also the advantage of being applied to any scale while experimental work is in general performed in bench or pilot plant scale. Moreover, the computational approach allows the collection of information at all points of the simulated structures while experimental approaches allow frequently only point measurements [59].

Furthermore, CFD enables the user to simulate flow conditions which are not feasible to investigate through experimental investigations such as nuclear reactor accidents or catastrophe scenarios. In nuclear accidents prevention, CFD simulations have been used in reactor safety for evaluating safety issues such as containment behavior under normal and abnormal operating conditions, and during accident situations[62]. Regarding catastrophe scenarios, CFD has been used in urban fire situations to investigate the performance of the fire extinguishing equipment [63] and in simulation of natural catastrophes by modelling a city for identifying the response of a structure to the disaster.

Nonetheless, the increasing application of CFD does not suggest thus far that it will substitute experimental testing when used for gathering information for design purposes. Although CFD is a useful tool which can help the user to understand and develop systems, it also has its limitations. A CFD user must be fully aware of the fundamental limitations.

In terms of solving the problem, CFD is subject to truncation errors and non-convergence. Moreover, CFD is based on the knowledge of physics and in certain aspects it is limited due to lack of knowledge. The areas with lack of knowledge are turbulent flow, multi-phase flows, boiling/condensation phenomena, chemistry and nanoscale physics [64,65].

The confidence in predictions is another limitation of CFD. CFD solutions are based on theoretical models which might still have severe deficiencies. Therefore, the prediction with such models might be questionable and differ from experimental results. In fact, the visualization of numerical solutions using vector plots, contour plots or animated videos of steady state or transient flows may be a useful way to analyze the obtained data. However, there is the risk that an erroneous solution looks good but in fact does not correspond to the expected flow behavior. Therefore, the results from a CFD solution should be properly analyzed and validated and the CFD users need to make a critical judgment of the computed results [65].

Finally, in some cases CFD is limited to simple applications due to the great amount of computer power (and time) required to run the multiple iterations that the technique requires. Although,

many companies are setting up parallel processing units, in which the CFD simulation is partitioned and run on several computers simultaneously, this limitation has not been overcome.

2.3.4 Setup of a computational fluid dynamic (CFD) simulation

The setup of a CFD simulation consists of the following steps: design the geometry, mesh generation, setup of all physical and boundary conditions and models for the system, simulation solution and post-processing of the simulation. The different steps for setting a CFD simulation are described in detail in Table 2.1.

Table 2.1– Detailed description of a CFD simulation procedure

Procedure	Description
Step 1 - Design the geometry	Design the geometry of the body of the flow problem that is analyzed.
Step 2 - Mesh generation	Discretization of the geometry into finite elements. Essentially, it divides the domain into many finite elements which will be used then to approximate the partial differential equations. The mesh can be structured in which all the elements are quadrilateral in 2D and hexahedral in 3D, or it can be established as an unstructured mesh in which the elements are triangles in 2D or tetrahedral in 3D.
Step 3 - Setup of all conditions and models for the system	Setup of boundary and initial conditions, fluid and turbulence models, chemical reaction model and definition of steady state or transient analysis.
Step 4 – Simulation solution	A solution is obtained by iterative convergence. Iterative convergence indicates that as discrete equations are repeated, then the simulation results approach a constant value.
Step 5 - Post-processing	Post-processing is extracting and visualizing the desired flow properties.

2.3.5 Governing equations

The numerical method in CFD uses algorithms for solving the governing equations of fluid dynamics. The governing equations of fluid dynamics are represented by the mathematical expressions of the conservation laws of physics[66]:

- Law of conservation of momentum – the rate of change of momentum corresponds to the sum of all the forces applied to the fluid element, they can be body forces and surface forces
- Law of conservation of mass – the rate of change of mass is equal to the sum of the rate of mass transfer and production and consumption of mass by reaction

– Law of energy conservation – the rate of change of energy is equal to the sum of the rate of heat transfer and the rate of work done on a fluidic system

A hexahedral fluid element is presented in Figure 2.4 to which the conservation of mass is applied as an example.

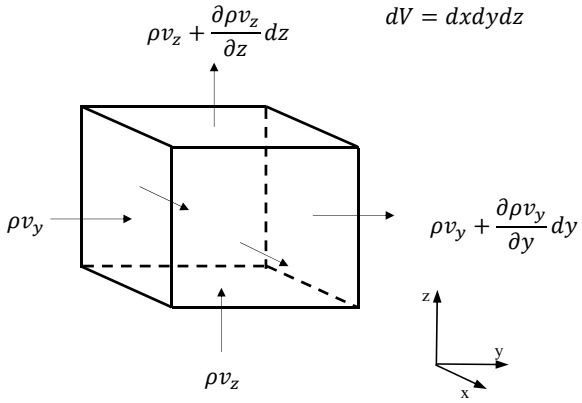

Figure 2.4– Representation of a hexahedral fluid element and the mass flux through its surfaces.

Variations of mass, momentum and energy of the fluid across its boundaries lead to the phenomena represented mathematically by the governing equations. All fluid properties are function of space and time and the density, pressure, temperature and velocity vectors are written as $p(x, y, z, t)$, $\rho(x, y, z, t)$, $T(x, y, z, t)$ and $v(x, y, z, t)$, respectively.

2.3.5.1 Momentum conservation equation

Newton's second law of motion corresponds to the momentum conservation principle and is the basis for the dynamics of fluid motion. Newton's second law of motion states that the rate of change of momentum equals the total sum of forces applied to a fluid element. There are two types of forces which act on a fluid element: surface forces which include pressure, viscous, shear and normal forces and body forces which include gravitational, centrifugal and electromagnetic forces.

The rate of increase of momentum per unit of volume of a fluid particle in the three coordinate directions (x, y, z) is given by:

$$\frac{\partial}{\partial t}\rho v_x, \qquad \frac{\partial}{\partial t}\rho v_y, \qquad \frac{\partial}{\partial t}\rho v_z \tag{2.18}$$

The x-component of the momentum equation is given by setting the rate of change of x-momentum of the fluid element equal to the total force in the x-direction on the element due to

surface forces and due to external sources. The momentum equation for the direction x is given by:

$$\frac{\partial}{\partial t}\rho v_x = -\left(\frac{\partial}{\partial x}\Phi_{xx} + \frac{\partial}{\partial x}\Phi_{yx} + \frac{\partial}{\partial x}\Phi_{zx}\right) + S_{Mx} \tag{2.19}$$

Where

- Φ_{xx} is the combined flux of x-momentum across the surface perpendicular to the x direction by molecular and convective mechanisms and is given by:

$$\Phi_{xx} = \pi_{xx} + \rho v_x v_x = p + \tau_{xx} + \rho v_x v_x \tag{2.20}$$

- Φ_{xy} is the combined flux of y-momentum across the surface perpendicular to the x direction by molecular and convective mechanisms and is given by:

$$\Phi_{xy} = \pi_{xy} + \rho v_x v_y = p + \tau_{xy} + \rho v_x v_y \tag{2.21}$$

- Φ_{xz} is the combined flux of z-momentum across the surface perpendicular to the x direction by molecular and convective mechanisms and is given by:

$$\Phi_{xz} = \pi_{xz} + \rho v_x v_z = p + \tau_{xz} + \rho v_x v_z \tag{2.22}$$

The momentum equations for the y and z directions are respectively:

$$\frac{\partial}{\partial t}\rho v_y = -\left(\frac{\partial}{\partial x}\Phi_{yx} + \frac{\partial}{\partial x}\Phi_{yy} + \frac{\partial}{\partial x}\Phi_{yz}\right) + S_{My} \tag{2.23}$$

$$\frac{\partial}{\partial t}\rho v_z = -\left(\frac{\partial}{\partial x}\Phi_{zx} + \frac{\partial}{\partial x}\Phi_{zy} + \frac{\partial}{\partial x}\Phi_{zz}\right) + S_{Mz} \tag{2.24}$$

When each of the components x, y and z are multiplied by the unit vector of their respective direction and the three components are added together vectorially, the momentum equation is in its general form [66]:

$$\frac{\partial}{\partial t}\rho \boldsymbol{v} = -(\boldsymbol{\nabla}\cdot\rho\boldsymbol{vv}) - \boldsymbol{\nabla}\cdot p - (\boldsymbol{\nabla}\cdot\boldsymbol{\tau}) + S_M \quad (2.25)$$

Rate of change of momentum	Momentum component by convection	Momentum component by molecular transport	External force applied to the fluid

The momentum component by molecular transport is characterized by two components: pressure force and viscous forces. The pressure force is always perpendicular to the exposed surface of the considered direction,x, y or z. The viscous forces are usually applied in an angle and are a function of three components, for example $\boldsymbol{\tau_x}$ is given by τ_{xx}, τ_{xy} and τ_{xz}.

The convective momentum component corresponds to the contribution of momentum increase by the velocity of the bulk flow. The velocity of the fluid may vary in all three directions, x, y and z. The convection components of the three directions are given by the following vector: $\rho v_x \boldsymbol{v}$, $\rho v_y \boldsymbol{v}$ and $\rho v_x \boldsymbol{v}$. Each of these components has an x-, y- and z-component. For instance for the x direction the convection component is given by $\rho v_x v_x$, $\rho v_x v_y$ and $\rho v_x v_y$.

2.3.5.2 Mass conservation and continuity equation

The mass conservation law is described by the continuity equation. The law of mass conservation states that the mass of control volume remains constant regardless any phenomena occurring inside the system. It also states that the mass is neither created nor destroyed in chemical reactions. This means that mass can be transformed into other forms. The general expression of the continuity equation can be written as follows [66]:

$$\frac{\partial \rho}{\partial t} = -\nabla(\rho.\vec{v}) + S \quad (2.26)$$

Rate of increase of mass	Rate of mass addition by convection	Rate of mass addition by source

The source S corresponds to the added mass to the continuous phase from a second phase or from a mass transformation by a reaction.

2.3.5.3 Energy equation

The energy equation states that the rate of change of energy inside a fluid element is equal to the rate of heat added to the fluid element and the work done on the fluid element. The energy equation can be written by [66]:

$$\underbrace{\frac{\partial}{\partial t}\left(\frac{1}{2}\rho v^2 + \rho\hat{U}\right)}_{\text{Rate of increase of energy}} = \underbrace{-\left(\boldsymbol{\nabla}\cdot\left(\frac{1}{2}\rho v^2 + \rho\hat{U}\right)\boldsymbol{v}\right)}_{\text{Rate of energy addition by convective transport}} \underbrace{-(\boldsymbol{\nabla}\cdot\boldsymbol{q})}_{\text{Rate of energy addition by heat conduction}}$$

$$\underbrace{-(\boldsymbol{\nabla}\cdot p\boldsymbol{v})}_{\text{Rate of work done on fluid by pressure forces}} \underbrace{-(\boldsymbol{\nabla}\cdot[\boldsymbol{\tau}\cdot\boldsymbol{v}])}_{\text{Rate of work done by viscous forces}} \underbrace{+W}_{\text{Rate of work done by external forces}} \underbrace{+S_E}_{\text{Rate of energy addition by external sources}} \quad (2.27)$$

The term $\frac{1}{2}\rho v^2$ corresponds to the kinetic energy associated to the motion of the fluid. The internal energy of the fluid is given by $\rho\hat{U}$ which is associated to the kinetic energy of the constituent molecules in motion with the velocity $\boldsymbol{v}$, plus the energy associated to the vibrational and rotational motions of the molecules. The term $\frac{1}{2}\rho v^2 + \rho\hat{U}$ corresponds to the convective heat transfer. The term $\boldsymbol{\nabla}\cdot\boldsymbol{q}$ corresponds to the conductive heat transfer. The term $-(\boldsymbol{\nabla}\cdot p\boldsymbol{v})$ corresponds to the work done on the fluid by pressure forces. The term $-(\boldsymbol{\nabla}\cdot[\boldsymbol{\tau}\cdot\boldsymbol{v}])$ corresponds to the work done on the fluid by viscous forces. The term W concerns the work done on the fluid by external forces (e.g. gravitational forces). Finally, the S_E term concerns the energy added to the fluid by chemical reactions.

2.3.6 Numerical methods

In the previous section, the relevant physical phenomena for the study of a fluidic system were described by governing equations. In this section numerical methods for solving these equations will be presented.

The fundamental principle of a numerical method is the concept of discretization. In mathematics, discretization is a process of converting continuous functions and equations into discrete values.

The analytical solution of a partial differential equation such as the governing equations presented in the previous section gives values of the equations as functions which are dependent on the variables x, y, z and t. The numerical solution provides values of the equations at a discrete number of points in the domain. These points are named grid points and can be nodes or centroid elements, depending on the discretization method.

The discrete values of governing equations are described by algebraic equations relating the values at grid points to each other. The numerical methods focus on the derivation of the algebraic equations and on a method to find their solution. The determination of the values of discrete governing equations requires a definition of profile assumptions between the grid points.

The conversion of the governing equation into discrete algebraic equations requires also the discretization of the domain. This discretization process corresponds to the division of the domain into discrete elements and to the association between the elements and discrete values of the

governing equations. This process domain discretization is usually called meshing or gridding. The choices made in the process of domain discretization influence the accuracy of the numerical solution.

Moreover, since the main goal is to obtain the solution given by the partial differential equations, the user must be critical when analyzing the results obtained via these methods. The number of discretization elements influences the approximation to the exact solution. A good numerical method will lean towards the exact solution as the number of the mesh elements increases. No matter which discretization method is employed, all good discretization methods should lean towards the same solution when the domain is discretized in a sufficiently large number of mesh elements.

2.3.6.1 Mesh terminology and types of mesh

The evaluated domain is discretized in elements by meshing or gridding it. The main unit of the mesh is the element. An element is surrounded by edges in two-dimensional domains and by edges and faces in three-dimensional domains.

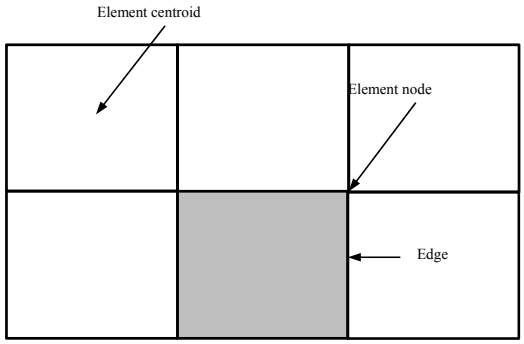

Figure 2.5 – Schematic representation of mesh elements and indication of their nodes, edges, faces and centroids

The edges of elements are delimited by nodes and the central coordinates of the element corresponds to the element centroid (See Figure 2.5).

In this project he software used for meshing is ICEM CFD® 14.5, which allows the meshing of the geometries via three possible methods: block-structured, unstructured and hybrid meshes.

In structured meshes, every interior vertex in the domain is connected to the same number of neighbor vertices. In contrast, in unstructured meshes a vertex is connected to an arbitrary number of neighbor vertices. The unstructured meshes have the advantage of imposing fewer topological

limitations which makes it easier to mesh very complex geometries. In block-structured meshes the mesh is divided in blocks and the mesh within each block is structured.

Meshes may be built using a variety of element shapes, where the most widely used ones are quadrilateral (Figure 2.6 a)) and hexahedral (Figure 2.6 d)) which are commonly used in structured meshes for two and three dimensions, respectively. However, there is also the possibility to set up unstructured meshes with triangular (Figure 2.6 c)) or tetrahedral elements (Figure 2.6 b)), for two- and three-dimensional meshes, respectively.

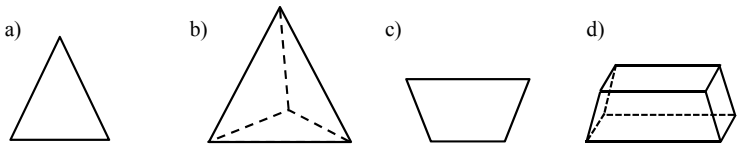

Figure 2.6 – Types of possible elements for meshes: a) triangular, b) tetrahedral, c) quadrilateral and d) hexahedral.

Structured meshes have been widely used, and the methods for generating them have existed for some time. Quadrilateral and hexahedral meshes are well-suited for flows with a dominant direction, such as boundary layer flows. However, in industry where the use of CFD has become more common, unstructured meshes have been extensively used due to their easy setup and consequently fast results. In contrast to the structured meshes, the unstructured meshes can be generated by automatic and general techniques, which means that the user does not need to spend extensive amounts of time working on the mesh.

Another possibility for creating a mesh that has been used recently is the use of hybrid meshes. Hybrid meshes consist of tetrahedral and hexahedral elements. For instance the hexahedral elements are placed in the boundary layers and the tetrahedral elements are placed in the core of the flow[67,68].

The user should take the advantages and disadvantages associated to each type of mesh into account, when choosing the type of mesh. Unstructured meshes give the opportunity of easy implementation on complex geometries using automatic approaches and as a result require low user time and effort. Moreover, an unstructured mesh has the capability of adapting itself to the geometry. As disadvantage, the unstructured mesh requires high computational time and memory usage and might result in low accuracy especially for gradient problems. On the one hand, structured meshes present high accuracy especially for systems with high gradients, better convergence, and a lower number of elements for a given geometry which results in reduced computation time and memory usage. On the other hand, structured meshes have the disadvantage that they can be complicated to set up and take extensive amounts of time and effort to fabricate.

Moreover, the set-up of structured meshes in complex structures might result in meshes with poor quality which consequently may not be usable for solving problems [67,68].

The hybrid meshes are a fusion of both unstructured and structured meshes, and therefore, they also present a mixture of the advantages and disadvantages from these two types of meshes [67,68].

A hybrid mesh has the advantage of improving the accuracy of unstructured meshes for problems with high gradients. This is very effective when it is applied to boundary layers that use structured mesh elements. Moreover, they might also be easier applied to complex geometries when compared to structured meshes. As disadvantages, the hybrid meshes might present long computational times which depends on the number of structured elements applied and requires user expertise in order to define the placement of structured elements in the geometry. A summary of the advantages and disadvantages of unstructured, structured and hybrid meshes can be found in Table 2.2.

Table 2.2– Summary of advantages and disadvantages of unstructured, structured and hybrid meshes [67,68].

Type of mesh	Advantages	Disadvantages
Unstructured	- Easy application to complex geometries - Adaptability of the mesh - Automatic generation, low investment of time and effort from the user	- High computational time and memory usage - Low accuracy
Structured	- High accuracy - Low computational time and memory usage - Better convergence	- Extensive time usage for creating the mesh - Complicated set-up for complex geometries
Hybrid	- Characteristics of structured meshes in boundary layers - Easy application to complex geometries - Results in memory and time savings	- Long computational time - Require user expertise in order to define the placement of the different types of elements

2.3.6.2 Node-based and element-based schemes

Numerical methods can be divided into two categories with respect to the calculation basis: node-based and element-based schemes. The node-based schemes store their primary unknowns at nodes or vertex locations and the element-based schemes at the element centroid. Finite element methods (FEM) are usually node-based schemes and finite volume methods (FVM) are usually based on element schemes [67]. For structured meshes, the application of both schemes generates similar results due to the fact that a number of elements and nodes in structured meshes are usually approximately the same. For other types of elements there might exist discrepancies

between the application of the two schemes due to the big difference in the number of nodes and elements. This fact must be taken into account when results are evaluated and a mesh should provide an adequate resolution for a given problem.

2.3.6.3 Discretization methods

The discretization methods have been mentioned in this section but they have not been characterized in terms of solving problems. There are several discretization methods for solving the governing equations in CFD such as Finite Difference Method, Finite Element Method and Finite Volume Method. This section describes the Finite Element Method and the Finite Volume Method.

2.3.6.4 Finite element method

The finite element method (FEM) is widely applied in engineering and is known in this field as finite element analysis (FEA). The FEM formulation has continuously changed along the years and nowadays there are several variational formulations (mathematical analyses which maximize or minimize functions in vector space that are maps from a set of functions into real numbers). In this description of FEM the variational formulation of Galerkin will be considered.

Considering the one-dimensional transport equation with constant diffusion coefficient and for a steady state system with no convection transport [67]:

$$D_f \frac{\partial^2 C}{\partial x^2} + S = 0 \tag{2.28}$$

where D_f is the diffusion coefficient, C is the concentration, x is the direction and S is the source.

The one-dimensional mesh representation can be found in Figure 2.7 (adapted from Murthy(1999)[67]):

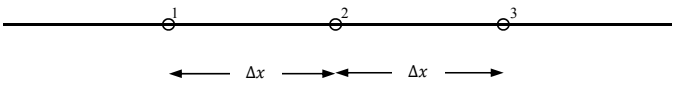

Figure 2.7 – Representation of one-dimensional mesh for application of numerical method which follows the node-based scheme. (adapted from Murthy(1999)[67])

Let us consider that $\bar{C}$ is an approximation to C. Since $\bar{C}$ is only an approximation, it does not satisfy equation (2.28) and therefore there is a residual, Res:

$$D_f \frac{\partial^2 \bar{C}}{\partial x^2} + S = Res \tag{2.29}$$

The goal of this method is to find a value of $\bar{C}$ such:

$$\int_{domain} WR\, dx = 0 \tag{2.30}$$

where W is a weight function. The method requires that the residual r becomes zero in a weighted way. A set of weight functions W_i, $i = 1,2 \ldots n$ is thus needed, where n corresponds to the number of grid points. The weight functions W_i are non-zero over the respective element i. The $\bar{C}$ value varies between nodes; this variation is typically local and can for example be assumed as a linear profile between points. This variation of the $\bar{C}$ value is designated by the shape function. The Galerkin method requires that the weight function and the shape function are the same. Performing the integration of the equation (2.30) results in a set of algebraic equations in the nodal values of C, which may be solved by a variety of methods.

2.3.6.5 Finite volume method

The finite volume method splits the domain in non-overlapping elements where conservation of C is enforced in a discrete manner [67]. The start of the discretization process may be done by integration of the differential equation and integration over the control volume. As an example of processing the discretization of a domain, a one-dimensional diffusional transport equation with a source term is considered:

$$\frac{\partial}{\partial x}\left(D_f \frac{\partial C}{\partial x}\right) + S_c = 0 \tag{2.31}$$

Let us also consider the two-dimensional mesh with cells represented in Figure 2.8 (adapted from Murthy (1999)[67]):

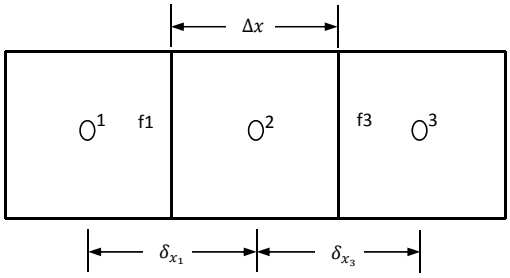

Figure 2.8 - Representation of a two-dimensional mesh for application of a numerical method which follows the element-based scheme (adapted from Murthy(1999) [67]).

Let us take into consideration the discrete values of C at the element centroids which are denoted by 1, 2 and 3. The element faces are denoted by f1 and f3. The integration of the equation (2.32) over the element 2 is given by:

$$\int_{f1}^{f3} \frac{d}{dx}\left(D_f \frac{dC}{dx}\right) + \int_{f1}^{f3} S_c \, dx = 0 \tag{2.32}$$

and results in

$$\left(D_f \frac{dC}{dx}\right)_{f3} - \left(D_f \frac{dC}{dx}\right)_{f1} + \int_{f1}^{f3} S_c \, dx = 0 \tag{2.33}$$

Assuming that C varies linearly between the element centroids, the equation (2.33) can be rewritten to the following form:

$$\left(D_f \frac{C_3 - C_2}{\delta_{x_3}}\right) - \left(D_f \frac{C_2 - C_1}{\delta_{x_1}}\right) + \bar{S_c}\Delta x = 0 \tag{2.34}$$

where $\bar{S}$ is an average value in the element 2. The equation is an approximation of the values of C since it was assumed that C varies linearly between the element centroids.
The reformulation of the equation (2.34) results in an algebraic equation:

$$\left(\frac{D_f}{\delta_{x_3}} + \frac{D_f}{\delta_{x_1}}\right) C_2 = \frac{D_f}{\delta_{x_3}} C_3 + \frac{D_f}{\delta_{x_1}} C_1 + \bar{S_c}\Delta x = 0 \tag{2.35}$$

Similar equations to equation (2.35) are generated for all elements of the domain, creating a set of algebraic equations which can be solved using an iterative method.

2.3.6.6 Solution methods for discrete equations

All discretized methods result in discrete algebraic equations which need to be solved in order to obtain the discrete values. These discrete equations can be linear or non-linear equations. The solution methods are independent from the discretization and may be classified in direct or iterative methods.
The direct methods use linear algebra methods to solve the set of discrete equations which can be given by:

$$\mathbf{A}C = \boldsymbol{B} \tag{2.36}$$

where $\mathbf{A}$ is the coefficient matrix, $C = [C_1, C_2 \ldots]^T$ is a vector consisting of all the discrete values C of all grid points and $\mathbf{B}$ corresponds to the results of the source terms. One direct method is inversion:

$$C = \mathbf{A}^{-1}\boldsymbol{B} \tag{2.37}$$

A solution for C is guaranteed if $\mathbf{A}^{-1}$ can be found. The inversion method accounts only for symmetric matrices and it is not possible to be applied in all case studies.

Direct methods are not widely applied in CFD problems due to their large computational and storage requirements. Nowadays, CFD problems involve hundreds of thousands or millions of elements with several unknown variables per element. Therefore, the matrix $\mathbf{A}$ would be very large and solving these large problems by direct methods becomes unfeasible.

In contrast, the iterative methods are the most commonly used methods for solving CFD problems. These methods start by guessing a value for all discrete values on the grid, and this is followed by generating a sequence of solutions which reduces the residual value, and consequently converges to the exact solution.

2.3.7 Remarks on ANSYS CFX®

In this project, the ANSYS CFX® 14.5 software is used to simulate and study flow coupled with mass transfer in the defined domain. ANSYS CFX® is a general purpose fluid dynamics commercial software for modelling fluid flow, heat and mass transfer in complex geometries.

The setup of a simulation using ANSYS CFX® is divided in 5 phases: design of the geometry (ICEM CFD®), establishment of mesh (ICEM CFD®), definition of problem and flow properties setup (ANSYS CFX-Pre®), solution of the problem (ANSYS CFX-Solver®) and evaluation of results by post-processing (ANSYS CFX-Post®).

The geometry design and meshing procedures can be set up using the software ICEM CFD®. The geometry is created by defining fixed points and lines, followed by connecting the lines to form surfaces and thereby forming the volume of the physical fluid flow domain. One should note that there are several other softwares available, which can be used for designing the geometry and some even for meshing such as AutoCAD® and Design Modeler®. Once the domain has been defined and finalized, its volume is discretized in subelements which form a meshed grid. ICEM CFD® has the possibility to set up three kinds of meshes: hexahedral elements, tetrahedral elements and hybrid meshes.

ANSYS CFX-Pre® is the interfacing software in which the user can define the fluidic properties of the discretized domain generated in ICEM CFD®. The fluidic properties include the type of fluid, diffusion coefficients of the compounds, the concentration of the compounds in the different parts of the domain (e.g. inlet, outlet, surfaces). In this software module it is also possible to define the regime of the flow: turbulence or laminar. In this project, microsystems were studied and their hydraulic diameters are in the range of micrometers, and therefore the flow is characterized by the laminar regime. As a consequence turbulence models will not be discussed in this thesis.

In terms of reaction systems, a reaction can be defined in this interface by establishing it as a source of mass. It is therefore necessary to define the rates of consumption and production of substrates/reagents and products, respectively.

The solver procedure, the convergence criteria (type and value of the residuals), and the conservation target which specifies the fractional imbalance are also defined in ANSYS CFX-Pre®.

The ANSYS CFX® software supports hexahedral, tetrahedral and hybrid element meshes [69]. This software uses a unique discretization method, namely the element based finite volume method [69]. The discrete algebraic equations determined by the discretization method are solved using an iterative solver named Multigrid Solver [69]. The convergence criteria can be defined using the residual values such as the maximum normalized value of the residuals or the root mean square (RMS) of the residuals.

Table 2.3 – Summary of the steps for setting up and running a simulation in ANSYS CFX, and the respective software modules used for establishing the simulation in this thesis.

Procedure	Software
Step 1 - Design the geometry	ICEM CFD®
Step 2 - Mesh generation	ICEM CFD®
Step 3 - Setup of all conditions and models for the system	ANSYS CFX-Pre®
Step 4 - Perform the simulation	ANSYS CFX-Solver®
Step 5 – Post-processing	ANSYS CFX-Post®

The solution of a simulation problem is analysed by using ANSYS CFX-Post. This software allows the user to analyse and quantify aspects of the analysed flow. Table 2.3 summarizes the steps for setting and running a simulation in ANSYS CFX® and the respective software modules used for establishing the simulation.

ANSYS CFX® is a commercial computational fluid dynamic program, which differs from other CFD software solutions by being a “black box” software. The expression “black box” refers to a software, which allow to set up and solve mathematical problems but the user is not able to access the governing equations, the modelling methods, the numerical methods or the solving methods. The fact that it is not possible to access the models and the presence of a well-defined user interface makes the automated manipulation of the simulation set-ups also difficult.

Although ANSYS CFX® is a “black box” software, it has a feature which allows batch manipulation of the set-up of simulations such as geometries, mesh configurations, fluidic properties and post-processing features. This software has a feature that enables the recording of the user steps for configuring a setup in a script file, in which code is written simultaneously when the user chooses a simulation operation e.g. flow regime, speed flow, concentration at the inlet. Afterwards, this script file is used to create the files used to run the simulation. One advantage of these script files is that the user does not need to learn how to program in CFX Command Language (CCL), the language used for programming the ANSYS CFX® user interfaces.

The user then has the possibility to manipulate the script files via MATLAB® or other programs, by converting these files into arrays, modifying the desired cells and converting the file again into a script file which can be read by ANSYS CFX® in batch mode. MATLAB® also gives the user the opportunity to execute the ANSYS CFX® in batch mode from MATLAB® by setting the executing commands. In this way, the user does not need to open the ANSYS CFX user interface in order to manipulate the files or to execute them.

The interface between MATLAB® and ANSYS CFX® also allows running cycles of simulations such as optimization problems. The simulation problems can be performed by setting the optimization cycle in MATLAB® and the system is then evaluated using computational fluid dynamics.

2.4 Microtechnology applied to process intensification

This project aims at applying topology optimization procedures to microbioreactors in order to find the best configuration computationally before testing it in the laboratory. Therefore, this section aims to give an introduction to the use of microtechnology in process intensification.

Microtechnology has been an area of great focus as a tool for studying and developing reaction systems. This technology has been characterized by innovative reactor designs since operation at the microscale presents considerable advantages compared with bench scale reactors commonly used for early stage process development. These advantages are efficient mixing which results in high mass and heat transfer, shorter reaction time, and small substrate quantities required per experiment. Moreover, microsystems allow easy regulation of reaction conditions such as temperature and flow rate and offer the possibility of adjusting these parameters in a simple and quick manner.

A microsystem is miniaturized system (e.g. channel or chamber) characterized by hydraulic diameters smaller than 1 mm. A microreactor is a microsystem in which chemical reactions take place.

Microsystems can be fabricated either as silicon and glass chips or as polymer chips. Lately, polymers have been more often chosen over silicon and glass chips due to their low material cost and fabrication cost, degradability and biocompatibility. The fabrication procedures for polymeric microsystems include hot embossing, injection molding, laser ablation and surface micromachining, just to name a few.

Process intensification is defined as the improvement of unit operations in order to reduce production costs by reducing energy consumption, ratio of equipment size to production capacity and production of waste [70].

The reduction of chemical reactor volumes and plants may induce the reduction of manufacturing costs and make the process more efficient. This approach for process intensification has been introduced in the 1980s by Colin Ramshaw [71,72]. Nowadays, there is no general method for achieving process intensification available. In this section, the characteristic time analysis for a unit operation will be presented. However, other strategies are available in the scientific literature such as: kinetic effects analysis [73], thermodynamics effects study [73], safety and hygiene effects strategy [74] and saturation effects analysis [75]. The reader can find more information regarding these strategies in the literature referred above.

The application of microsystems in process intensification has shown to be an innovative approach for reactor design in chemical engineering.

2.4.1 Characteristic time analysis for a unit operation

The application of microsystems as tools for process intensification requires the identification of parameters as analysis of characteristic times of physical and chemical processes [76].

By performing an analysis of the various phenomena involved in a system and comparing the individual phenomena with the global behaviour of the system, the limiting phenomenon will be identified. Further analysis of this phenomenon will allow the development of strategies for intensification of the process.

The evaluation of the characteristic time needs to take into account the purpose of the considered unit operation: heat transfer in heat exchangers, mass transfer in a mixing or separation units, reaction time in reactors.

Taking into account the unit operations stated above, characteristic times can be divided in three categories: the time of heat exchange, diffusion time or a characteristic of the reaction time. In this section, an overview of the characteristic times for reaction and mass transfer mechanisms will be presented. The heat exchange time will be excluded since it is not part of the scope of this thesis, because the case studies considered only include isothermal reactors and isothermal reaction mechanisms.

The scientific literature introduces characteristic time analysis as a relation between the characteristic times and their relations with the characteristic dimension of the unit operation (R) [76,77].

For homogeneous reactions the characteristic time depends only on the kinetic limitations and for heterogeneous reactions the characteristic time can depend on the kinetic limitation or on the diffusion limitation.

The characteristic times for homogeneous and heterogeneous reactions and for mass transfer are presented in Table 2.4[76].

Table 2.4– Characteristic times for heterogeneous and homogeneous reactions and dependence on the dimension ***R***.

Type of transfer	Characteristic time	Dependence of the dimension (R)
General homogeneous reaction	$\frac{1}{k \cdot C_0^{n-1}}$	1
General heterogeneous reaction	$\frac{C}{r}$	Varying
First-order homogeneous reaction	$\frac{1}{k_v}$	1
Apparent first-order heterogeneous reaction	$\frac{R}{2\,k_s}$	R
Diffusional mass transfer	$\frac{R^2}{D_f}$	R^2
Convective mass transfer	$\frac{R^2}{D_f\,Sh}$	R^2

The characteristic times for mass transfer phenomena are described by considering mass transfer analogies. The expression related to mass transfer describes the transfer of mass that diffuses in a specified medium. Thus, the characteristic time for mass transfer can be defined by:

$$t_{mass\ transfer} = \frac{R^2}{D\ Sh} \tag{2.38}$$

Where R is the characteristic dimension, D is the diffusion coefficient and Sh is the Sherwood number. The Sherwood number corresponds to the ratio of mass transfer by diffusion processes and mass transfer by convective processes. The Sherwood number is insignificant in cases for which mass transfer is purely diffusional as shown in Table 2.4.

Chemical reactions can be considered by using a very general expression of their characteristic times. The characteristic time relates the initial concentration of a reactant (C_0) to rate of its consumption (r_0) at the same initial conditions:

$$t_{reaction} = \frac{C_0}{r_0} \tag{2.39}$$

This general expression can be used for characterizing homogeneous reactions and some simplified cases of heterogeneous reactions, such as the apparent first-order heterogeneous reaction (See Table 2.4). However, many reactions present very complex kinetics which prevent

from using simplified equations and require numerical estimations for the characteristic times. For instance, heterogeneous, biological and enzymatic reactions can involve complex kinetics.

Moreover, the heterogeneous apparent reactions kinetic may vary as function of the operating conditions or reaction conversion. For example, the Langmuir-Hinshelwood kinetics has apparent first order kinetics under low partial pressures and apparent zero-order kinetics under high partial pressures. In fact, biological and enzymatic reactions may also present similar dependencies.

Another difficulty for determining the characteristic time is related to the knowledge about the intrinsic reaction mechanism. The choice of the used reaction kinetics for determination of the characteristic time must be made very carefully. The confusion between the intrinsic kinetics and apparent kinetics might have severe consequences on the analysis of intensification potentials. Intrinsic kinetics represents the reaction kinetics observed in the absence of mass transfer limitations of the reacting species. The apparent kinetics reflects the kinetics camouflaged by the heterogeneous nature of the system (e.g. including effects of substrate mass transfer limitations).

In microreactors, to eliminate mass transfer limitations, the characteristic transfer time should be one order of magnitude lower when compared with the characteristic reaction time.

A chemical reactor is also designed and dimensioned in order to obtain a desired yield and conversion of a determined raw material. The yield of a reaction is defined by the following equation:

$$\%yield = \frac{moles\ of\ desired\ Product\ formed}{initial\ moles\ of\ limiting\ substrate} \times 100 \qquad (2.40)$$

The limiting substrate is the substrate which limits the rate of product formation. This relation correlates to the selectivity of the reaction since the reaction yield is only related to the amount of desired product formed.

The conversion corresponds to the amount of substrate converted:

$$\%conversion = \frac{moles\ of\ substrate_{final} - moles\ of\ substrate_{initial}}{moles\ of\ substrate_{initial}} \times 100 \qquad (2.41)$$

The intensification of a unit operation is based on the relation between the reference time and the characteristic time. The reference time must be carefully chosen as a function of the unit operation. The reference time can also be denoted flow time, convection time or residence time, also known as fluid space time. The ratio of characteristic times represents the number of operation units (NOU) also known as number of transfer units (NTU) in heat transfer processes and the Damköhler number in a reactor. NOU is given by:

$$NOU = \frac{\tau}{t_{op}} \tag{2.42}$$

where τ denoted the reference time and t_{op} denotes the characteristic times.

An interesting study about using microsystems for process intensification using the characteristic times has been presented by Commenge and his co-workers[77]. They have presented an investigation which shows that the reduction of the characteristic dimensions of the channels allows the overall process intensification. The compared systems were a macro-channel and a system of micro-channels.

The miniaturization of systems becomes particularly interesting in cases of mass and heat transfer limitations. They concluded that intensification for scale-up is not possible for cases in which the characteristic time is independent of the characteristic dimension of the system such as the characteristic time for a homogeneous reaction (See Table 2.4).

The miniaturization of the macroscale system also revealed that simply reducing the characteristic dimension such as the radius would imply an increase of the pressure drop. Therefore, this challenge was overcome by increasing the number of channels. In this way, they have also investigated the miniaturization of the system by maintaining the pressure drop constant and evaluating the improvement with reduction of the radius and increasing the number of channels [77].

2.4.2 Mixing in microsystems

The general mixing mechanism is characterized by two principles, diffusion and convection. Diffusion is characterized by the migration of molecules from a region of high concentration to a region of low concentration. Convective mixing is characterized by the vertical transport of the fluid and its properties.

In microfluidics the flow is characterized by laminar flow, and the mixing in a simple straight microchannel is achieved by diffusional mass transfer.

Mixing by diffusion in a microsystem is an important principle to consider due to the small dimensions of the channels. The reduced dimensions of microsystems result in short distances for transfer phenomena (mass and heat) [78,79].

The short distances for transport phenomena also result in a fast and effective mass and heat transfer. The diffusive mass transfer with mean transport length can be expressed by the Einstein-Smoluchowski equation [80]:

$$x = \sqrt{2D_f t} \tag{2.43}$$

which gives the relation between the distance (x) that a molecule with diffusion coefficient (D_f) travels during time (t).

The diffusion coefficient of solutes in gases is typically in the range of 10^{-5}-10^{-6} m^2 s^{-1} [81] and in liquids with low viscosity the solutes present diffusion coefficients between 10^{-9} and 10^{-10} m^2 s^{-1} [81,82]. From the analysis of the equation (2.43) and Figure 2.9 it is possible to verify that for shorter diffusion lengths shorter times are required for the molecules to diffuse. Consequently, this results in better mixing and higher reaction yields in microreactors. However, the relation between the distances and the diffusional time is not linear, and for longer distances larger times are needed for the molecules to diffuse. As an example, the relation between the diffusion distance and the diffusion time of the species, whose diffusion coefficient is 10^{-9} $m^2 \cdot s^{-1}$, is represented in Figure 2.9. The time for the species to diffuse 100 µm is 5 seconds and the time for it to diffuse 1000 µm is 500 s (around 8 minutes). So, the interval time for the species to diffuse 1000 µm is a 100 times larger than for a distance 10 times smaller. Therefore, it is not advisable to work with large diameter microchannels.

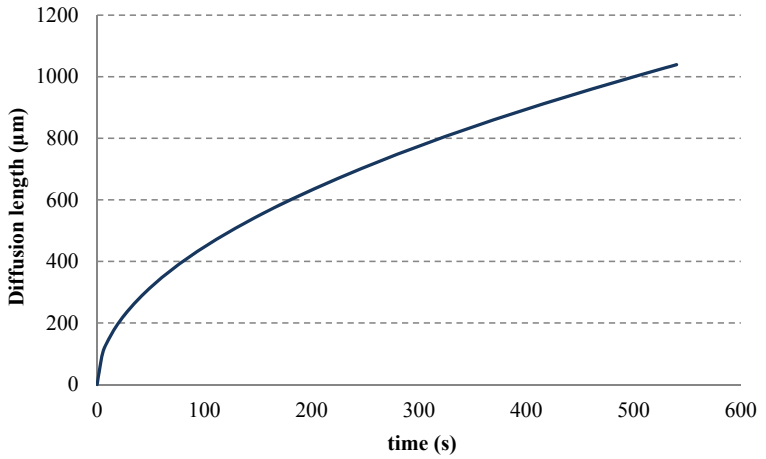

Figure 2.9 – Relation between diffusion length and time, considering a species diffusion coefficient of 10^{-9} $m^2 \cdot s^2$

Despite of the above-mentioned advantages, the diffusion mixing on its own is a challenge, since the size of the microchannels has to decrease greatly in order to ensure full mixing and uniform concentration in the cross section of the channel. The decrease of channel dimensions implies a large increase on fabrication costs [83]. Therefore, the introduction of convection mechanisms in microsystems demonstrated to be an important element for achieving enhanced mixing. Convective mixing is an effective mechanism for mixing since it enlarges the mixing interfaces between two fluids and reduces the diffusion distance [73].

In this respect, the designs of micromixers are relevant since they introduce mixing agents for promoting of uniform concentration profiles inside of a microsystem. Micromixers can be characterized in two categories: active mixers and passive mixers. In the past few years, several reviews have been written in this area in which the two types of mixers are revised in detail [73,84–86].

The mixing mechanism in passive mixers depends exclusively on the molecular diffusion or on the chaotic advection of the flow in the channel or chamber. This means that no external energy is used besides the driving forces of the flow. There are several types of passive mixers presented in the scientific literature. Nonetheless, in this thesis, the description of micromixers will focus particularly on passive mixing by lamination and chaotic advection due to the fact that these types of mixing are related to the shape of the channel. Therefore, these two types of passive mixing can be interesting for investigations of shape and topology optimization of microreactors.

In contrast, the active mixing systems rely on external disturbances to achieve mixing between the system's compounds. The source of these disturbances can be pressure [87,88], electrohydrodynamics, magnetic fields [90], [91], acoustics and thermal fields [91]. The active mixing microsystems require complex fabrication methods due to the difficult application of external disturbance fields and active agents. Therefore, the fabrication and integration of active mixing systems becomes challenging and expensive [73].

On the other hand, the passive mixers do not require the use of external power sources and their structures are simpler compared with the structure of active mixers. Moreover, the passive structures are robust and stable in operation and are easy to integrate into microsystems.

In the macroscale, mixing is usually associated to dimensionless numbers such as the Reynolds number which represents the ratio between the momentum and viscous friction, and the Peclet number which gives the ratio between the mass transfer due to diffusion and convective mass transfer. The Reynolds number (Re) is given by the following equation:

$$Re = \frac{\rho v D_h}{\mu} \tag{2.44}$$

where ρ is the density of the fluid, v corresponds to the velocity of the fluid, D_h corresponds to the hydraulic diameter and μ corresponds to the viscosity of the fluid. The Reynolds number characterizes also the regime of a fluid (laminar or turbulent). A turbulent regime (in tubes) is characterized by Re values above 2100. Since the dimensions of microsystems are very small, in general the Reynolds numbers in microsystems are expected to be in the range of laminar flow.

The Peclet number is expressed by the following equation:

$$Pe = \frac{Lv}{D_f} \tag{2.45}$$

where L is characteristic length, v corresponds to the fluid velocity and D_f corresponds to the diffusion coefficient. Large Peclet numbers indicate that convective mass transfer is more significant.

A relevant characteristic for evaluating homogeneities in a micromixer is the residence time distribution (RTD). This characteristic is highly important to consider since the parabolic velocity profile in laminar flow results in heterogeneities in the concentration profile and consequently into a wide residence time distribution. In passive micromixers, mixing can be enhanced by shortening the length of the diffusional path and increasing the surface between the two flows. Passive mixing systems by lamination are characterized by parallel and serial lamination mixers.

In parallel lamination, the inlet flows are split in substreams, where this number of substreams can be infinite. The basic design corresponds to the mixing of two streams. The two most well-known designs of this type of mixers are T-shape and Y-shape mixers.

The T- and the Y-shaped mixers have been commonly used and have been reported several times in the scientific literature (e.g. Esmaeelpanah *et al.* (2005), Kaminski and Uhlemann (2005), Andreussi *et al.* (2015) [92–94]). These types of channels allow the study of microfluidic phenomena such as the butterfly effect [95], the scaling law [96] and other non-linear effects.

Molecular diffusion is considered to be a slow process, and even in microsystems the mixing process by diffusion may take a long time. There are other solutions to reduce the mixing time, and several authors have presented splitting the inlet streams into multiple substreams [97,98], others introduced split-and-recombine micromixers [99,100] and others have presented mechanisms for inducing chaotic advection mixing.

The splitting into multiple substreams of two fluids results in several narrow streams alternating between the inlet fluids. This type of mixing mechanism results in the reduction of the thickness of fluidic streams and in an increase of the interfaces between the two different fluids. This effect develops faster and more efficient laminar mixing.

In microreactors, parallel lamination has been applied in order to achieve better mixing and consequently, better reaction yield. However, the splitting into multiple substreams in microreactors might not result in an improvement of the reaction yield comparable to the increase in the number of interfaces between substreams. In fact, Bodla *et al.*[101] have presented a comparison between two microreactors with mixing included for synthesis of *(S)*-1-phenylethylamine and acetone from acetophenone and isopropylamine catalysed by ω-transaminase. The first microreactor resembles a YY-microreactor in which the inlet was divided in two

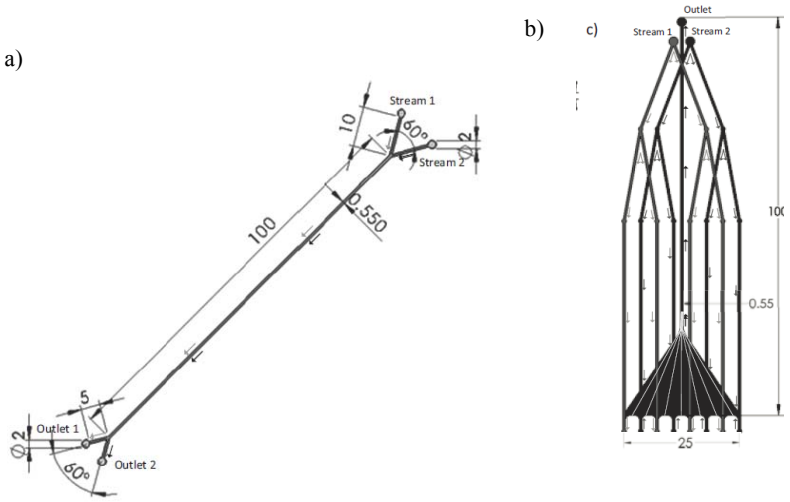

Figure 2.10 – Reactor configurations: a) YY-microreactor and b) 8-stream microreactor, top view (up) and side view (down) (adapted from Bodla *et al*. (2013)[101])

streams, one which carries the biocatalyst (enzyme) and the other one which carries the substrates (reagents) (Figure 2.10 a)). In the second reactor (8-stream microreactor), the two inlet streams were divided in four substreams each, generating seven interfaces between the enzyme streams and the substrate streams (Figure 2.10 b)) By analysing the results, it was possible to verify that the reaction yield in the 8-stream microreactor only increased by about 30% in relation to YY-microreactor. From these results it was possible to verify that in this particular case splitting of the inlet stream into multiple streams does not result in a yield improvement equal to the increase in the number of interfaces.

Aoki and his co-workers[102] have presented an extensive study on the effects of lamination width and reaction rate constant on the yield of the desired product.

The study was performed using two-dimensional computational fluid dynamics simulations of a microreactor. The total width of the microreactor channel was 200 μm and the length 1 cm. One of the reaction systems studied is a system of two reactions, a main reaction for formation of the desired product and a side reaction which depletes the product. The reaction system is given by the following reaction equation:

$$\begin{aligned} A + B &\rightarrow R & r_1 &= k_1 C_A C_B \\ B + R &\rightarrow S & r_2 &= k_2 C_B C_R \end{aligned} \qquad (2.46)$$

where R is the desired product, S and T are the co-products; r_i and k_i are the reaction rate and the rate constant of the *i*th step, respectively and C_j is the molar concentration of species j.

For this study, the authors considered three microreactor inlet configurations: well-mixed feed, 2 streams (lamination width of streams, *W*, is 100 μm) and 8 streams (lamination width of streams, *W*, is 25 μm). Figure 2.11 shows the lamination reactor configurations. Reactants A and B flow into the reactor in two parallel laminar flows, and then both species diffuse and react. The diffusion coefficient of both reactants was 10^{-9} $m^{-2} \cdot s^{-1}$.

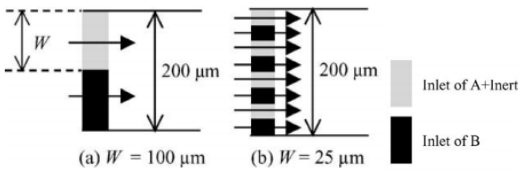

Figure 2.11 – Schematic representation of reactor inlet configurations (adapted from Aoki *et al*. (2004)[102]).

.

The microreactor performances were evaluated considering a low reaction rate ($k = k_1 = k_2 = 0.01\ m^3 \cdot kmol^{-1} \cdot s^{-1}$) and two fast reaction rates ($k = 1\ m^3 \cdot kmol^{-1} \cdot s^{-1}$ and $k = 100\ m^3 \cdot kmol^{-1} \cdot s^{-1}$). The reactants A and B were fed stoichiometrically according to the overall reaction $A + 2B \rightarrow S$.

The dimensionless number for nth order reactions, $\phi i = \frac{k_i C_{B0}^{n-1} W^2}{D}$, represents the ratio between the reaction rate and the diffusion rate. This number is a criterion to determine the rate controlling step. When $\phi i < 1$ the reaction is the controlling step, when $\phi i > 10^4$ the diffusion is the rate controlling step.

The results of this investigation were plotted as a relation between the yield of R and conversion of A and are presented in Figure 2.12:

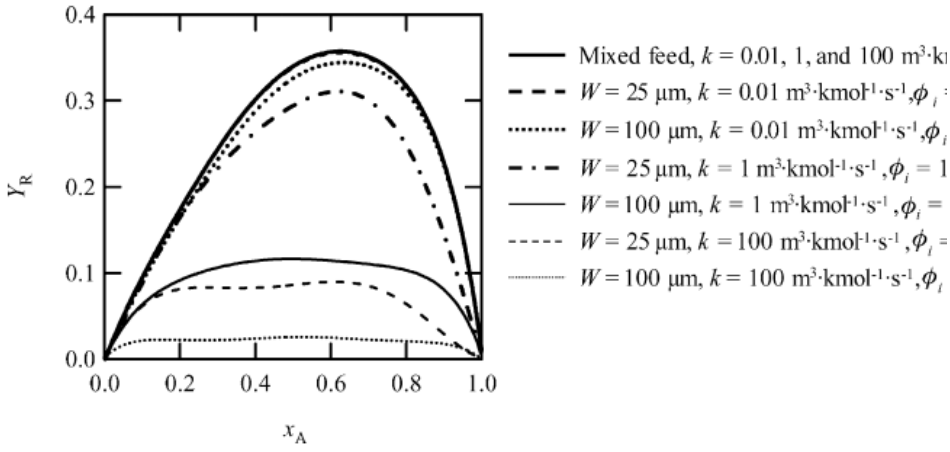

Figure 2.12 – Relation between the yield of R and conversion of A with different rate constants and lamination widths.

The results demonstrated that for a low reaction rate, the lamination width of 100 μm is narrow enough to achieve almost the same yield as would be the case for a well-mixed feed. The increase of the number of laminated streams did not improve product R yield significantly since the reaction is the rate controlling step in this case.

For greater rate constants, the diffusion of the reactants affects the reaction yield. In these cases, the microreactor performance is conditioned by mass transfer limitations. The yields of the desired product R at the same conversion of substrate A decrease with the increase of the lamination width and with the rate constants. Therefore, for faster reactions, a narrower lamination width is needed in order to improve product yield. The narrowing of the lamination width resulted in much larger yield improvements (up to 67%) when compared with the improvement achieved by narrowing lamination width for low reaction rate. From this study it is possible to verify that the improvement of the yield due to parallel lamination is dependent on the rate controlling step.

Chaotic advection is characterized by the folding and the expansion of the fluids and consequently, by expanding the fluid interfaces exponentially [73]. Passive chaotic mixing inducers are three dimensional structures which are part of the microchannels. These microstructures generate transverse flows and recirculation patterns which induce the growth of interfaces.

Several designs for chaotic advection structures in two dimensions can be found in the scientific literature. These structures can be characterized by narrowing and expanding the channel, modifying the straight channel into a zig-zag or meander shaped channel [103,104] (See Figure 2.13). Another possibility is modifying the channel so that it assumes deformations in three dimensions. The ascending and descending of fluid caused by the three dimensional twisted channel induces a more efficient mixing of the compounds. There are several types of shapes presented in the literature, C-shape [105], L-shape [106] and F-shape[107] are some examples (See Figure 2.13).

Lastly, a well-known mixing inducer is characterized by grooves on the channel wall. The most common shape of the grooves is the so-called herringbone structure which resembles the arrangement of the bones of a herring (See Figure 2.13). Usually, these grooves are introduced on the bottom wall of the channel but can also be introduced on the top wall. These mixing inducers are shown to have an impact even in slow velocity flows. These grooves modify the flow profile into a helix mass stream [108]. In the scientific literature, the influence of the length, width and the depth of the herringbone staggered structures on the mixing has been reported as well [109]. The shape of these structures has been optimized by some authors (e.g. Ansari (2007), Hossain *et al.* (2010) [110,111]). The shape optimization of these structures will not be reviewed since the scope of thesis is the application of shape optimization to microchannel geometries. Other variations of the grooves can also be found in the literature such as slanted ribs, slanted grooves or a combination of different groove shapes on the channel wall [108].

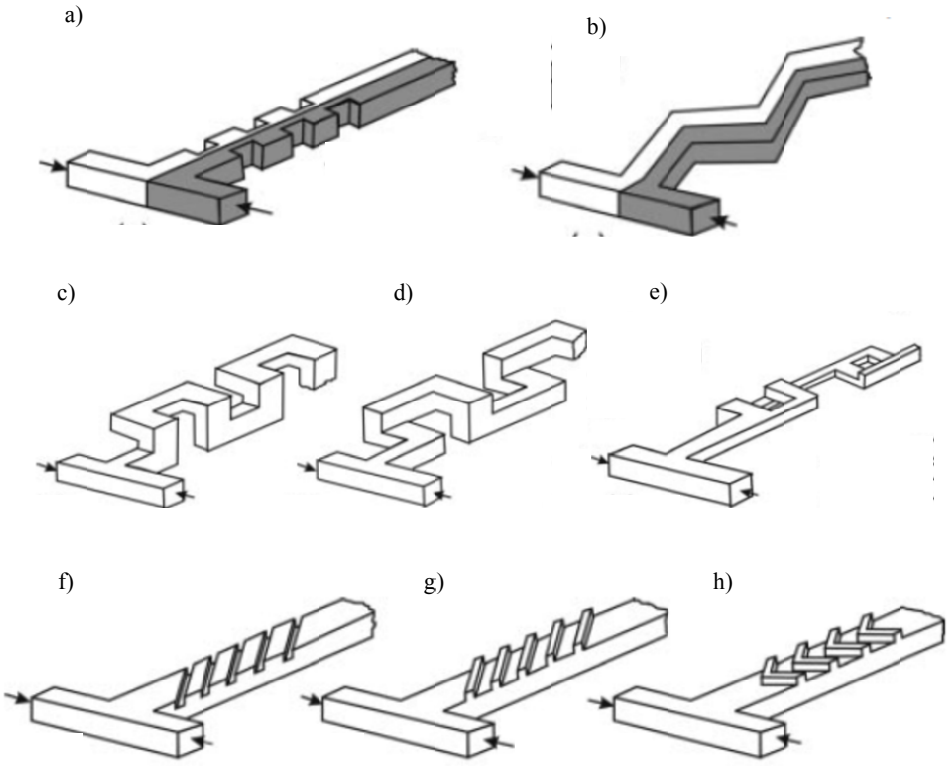

Figure 2.13 – Modification of the channel for passive mixing: Lamination – a) expansions and narrowing of the channel, b) zig-zag or meander shaped channel, c) C-shape, d) L-shape, e) F-shape. Chaotic advection – f) slated ribs, g) slated grooves, h) staggered herringbone grooves. (adapted from Hessel (2005) [83])

2.5 Shape and topology optimization applied to microfluidic devices

The application of topology and shape optimization to chemical engineering for modeling microreactors and microchannels has not been very often reported in scientific literature. Only few scientific groups have computationally investigated this application to microfluidic devices.

In this section, a brief review about the application of topology and shape optimization to microdevices will be given.

Hasebe and Tonomura performed studies on the influence of the shape of microchannels using Computational Fluid Dynamics [112–116]. They have investigated CFD as an alternative to design microchannels, a design which nowadays relies on trial and error.

In Tonomura and his co-workers[112], the shape optimization of a manifold was investigated. A manifold in this field is considered to be a wide pipe or channel which leads into smaller tubes. They proposed an automatic shape optimization by using the "Golden section" search method as the optimization method. This technique is used for finding the minimum/maximum of unimodal functions (i.e. functions with only one minimum/maximum) by narrowing the range of values which is known for containing the maximum/minimum[117]. The shape to be optimized was a plate-fin microdevice design in a two-dimensional plan. This microdevice has multi-microchannels, which are parallel to each other and have the same shape and size. The inlet and outlet are at opposite sides of the manifold and on opposite sides of the main channel (See Figure 2.14). The design variable corresponds to the length of the top borderline which defines the outlet manifold shape.

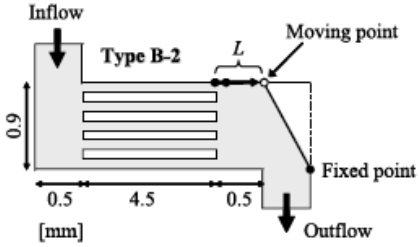

Figure 2.14 - Initial configuration of the manifold to be optimized. ***L*** corresponds to the design variable, length of the top borderline (adapted from Tonomura *et al*. (2004)[112]).

The optimization problem is formulated by minimizing the outlet manifold area for which they have encountered areas of dead volumes. In this way it was possible to minimize the accumulation of the flow and improve the distribution of the flow over the smaller channels. The objective function is given by:

$$\text{Minimize } A + P \times \sum_{i=1}^{5} \left| \frac{F(i) - \bar{F}}{\bar{F}} \right| \qquad \text{Subject to } \quad 11\ \mu m \leq L \leq 1000\ \mu m \tag{2.47}$$

Where i is the iteration number, A is the area of the manifold, L is the design variable, F is the flow, P is the weight factor. The second term of the objective function indicates the degree of flow maldistribution.

The weight factor is determined by comparing several optimization results using different P values so that the desired balance between the area of the manifold and the degree of the flow maldistribution is reached.

In this optimization problem the optimal length varies between 410 μm and 609 μm. It was concluded that this shape optimization results in considerable and useful information on the design of microdevices to engineers.

In another paper by the same authors (Tonomura *et al.* (2010)) [114] the shape optimization of a U-microchannel and a branched microchannel was presented. The purpose of the optimization was to minimize the pressure drop in the system. The chosen method to solve the optimization problem was the adjoint method which has been explained in the beginning of this chapter under the section entitled: *Shape optimization methods – gradient-based and gradient-free methods*. This method was adopted since the gradient functions are calculated in a more efficient manner due to their independency of the design variables.

The optimization procedure involves the following steps:

Step 1: Generate the initial shape

Step 2: Generate the computational mesh for the shape

Step 3: Solve the flow equations for deriving the flow velocity and pressure

Step 4: Solve the adjoint equations to obtain a set of Lagrange multipliers

Step 5: Calculate the shape gradient functions

Step 6: Obtain a new shape by moving each point according to the results of the optimization method

Step 7: Repeat Step 2 until Step 7 until the change of the cost function is smaller than a defined parameter.

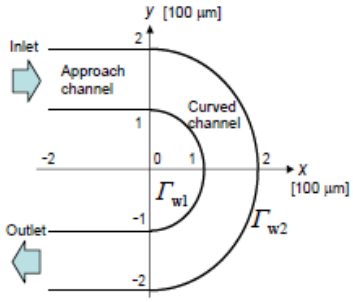

Figure 2.15 – Initial configuration of the U-microchannel (adapted from Tonomura *et al.* (2010) [114]).

In this investigation two case studies are presented: a U-microchannel and a branched microchannel for incompressible fluids.

The initial shape of the U-channel was a geometry of 100 µm width (See Figure 2.15). In this case only the channel curve is optimized and is delimited by two boundaries, the internal wall and the external wall in relation to the curve. The design variables are associated with the grid points, which intersect both boundaries. In this case study two solutions were presented considering no volume or constant volume constraints, respectively.

When considering no volume constraint, the width of the curve of the channel is larger and contributes to a reduced flow velocity. The shape has significantly changed and there is an expansion from the external wall (See Figure 2.16 (a-2)). On the other hand, when considering a volume constraint, both boundaries move towards the inner part of the U-curvature and there is not a drastic change of the curvature (See Figure 2.16 (a-3)). The pressure drops with shape optimization for no volume and constant volume constraints were reduced compared to the initial shape by 27.6% and 39.3%, respectively.

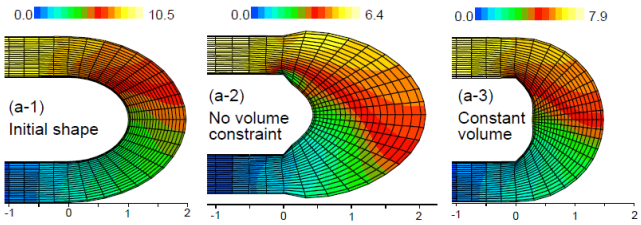

Figure 2.16 – Pressure distribution for the initial configuration (a-1), final configuration for optimization with no-volume constraint (a-2) and final configuration for optimization with constant volume (a-3) (adapted from Tonomura *et al.* (2010) [114]).

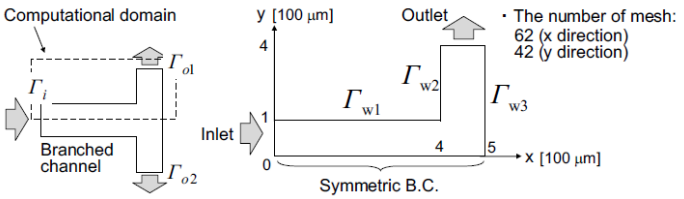

Figure 2.17 – Initial shape branched channel (adapted from Tonomura *et al.* (2010) [114]).

The same optimization procedure was applied to the branched channel and the cost function in this case study was to minimize the pressure drop as well. The initial shape of the branched channel resembles a T junction (See Figure 2.17) and it was optimized considering two case studies: the inlet Reynolds number 1 and the inlet Reynolds number 100.

The final configurations correspond to Y-branched channels with different angles for the case study Re=1 and the case study Re=100 (See Figure 2.18). The angle formed by the Y-channel is smoother and the fluid flows without collision with the wall. The pressure drop decreased by 33.1% and 38.1% for Reynolds number values at the inlet equal to 1 and 100, respectively.

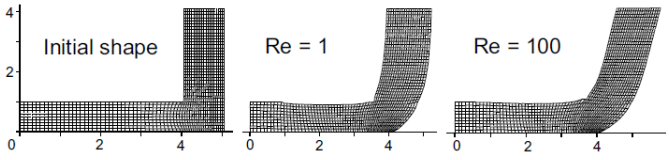

Figure 2.18 – Initial shape (left) and final shapes at Re=1 (middle) and 100 (right) (Tonomura *et al.* (2010) [114]).

These authors have also published similar shape optimization procedures to T-shaped microreactors (Tonomura *et al.* (2009)) [115] and to non-isothermal T-shaped microreactors with engulfment flow (Wang *et al.* (2012)) [116].

Topology optimization for designing microreactors has been introduced by Okkels and Bruus in 2007[118]. The main purpose of this work was to study how to optimize the design of bio-reactors for immobilized biological cultures. They have used a simplified kinetic reaction model for cell growth and have considered that the reaction mechanism is represented by a first order isothermal reaction which only depends on the local nutrient concentration and on the cell density. The cells were considered to be immobilized on a porous material, assuming that the structure has constant porosity (γ) which defines the local fluid density inside the structure. The porosity corresponds to the design variable and varies continuously between the values 0 and 1 where $\gamma = 0$ corresponds to solid material and $\gamma = 1$ corresponds to pure liquid. The microreactor design was considered to

be a two-dimensional square chamber with porous structures. From a first analysis of the problem, the solution seems to be quite simple: the cells should be densely distributed in order to maximize the metabolic reaction rate, and consequently the product formation. Nevertheless, a very dense cell distribution implies a reduction of the carrier porosity which slows down the pressure-driven feeding of the cells and subsequently, results in a low metabolic rate. Therefore, an optimization of the microreactor configuration is required in order to find the balance between the cell distribution and the metabolic rate and maximize the product formation.
The continuity equation for the nutrient A is given by:

$$(\mathbf{v}(\gamma)\cdot\boldsymbol{\nabla})C_A = D\boldsymbol{\nabla}^2 C_A - k_A(1-\gamma)C_A \tag{2.48}$$

where $\boldsymbol{v}$ is the velocity, C_A is the nutrient concentration, D is the diffusion coefficient, k_A is the first-order reaction constant. The reaction mechanism is given by $r_A = -k_A(1-\gamma)C_A$, where $(1-\gamma)$ is the carrier porosity.
The variation of γ characterizes the reactor configuration since it also affects the fluid flow. The effect of porous structures is assumed to increase the Darcy damping force given by:

$$\mathbf{F}_{Da} = -\alpha(\boldsymbol{\gamma})\mathbf{v} \tag{2.49}$$

where α corresponds to the local inverse permeability. The Navier-Stokes equation, governing the fluid flow, becomes:

$$\begin{gathered}\rho(\mathbf{v}\cdot\boldsymbol{\nabla})\mathbf{v} = -\boldsymbol{\nabla}p + \mu\nabla^2\mathbf{v} - \alpha(\boldsymbol{\gamma})\mathbf{v} \\ \boldsymbol{\nabla}\cdot\mathbf{v} = 0\end{gathered} \tag{2.50}$$

where μ and ρ correspond to the viscosity and the density of the fluid buffer and p the pressure. The inverse permeability is a function of the design variable γ and is defined by the following general form:

$$\alpha(\boldsymbol{\gamma}) = \alpha_{max} f(\gamma) \tag{2.51}$$

where $\alpha_{max} = \frac{\mu}{D_a L^2}$ represents the inverse permeability inside the cell immobilizing-structures and D_a is the Darcy number. The function $f(\gamma)$ in the limiting cases is $f(0) = 1$ for which no broth is present due to maximal occupancy of the carrier and $f(1) = 0$ for which only broth is present.

The aim of the topology optimization problem is to find the best particle porosity and the best configuration of the immobilization structures by optimizing the metabolic rate. The objective function $(J)$to minimize corresponds to the conversion of the nutrient A and is given by:

$$J = -k_A(1-\gamma)C_A \tag{2.52}$$

The design is characterized by an initial design where the whole domain-region is uniformly covered with a porous material. The microreactor shape corresponds to a square reaction chamber with an inlet and outlet positioned at the center of lateral walls. The walls of the squared reaction chamber were 6 mm wide and the inlet and the outlet width were 2 mm.

The optimization procedure was an iterative method starting with an initial porosity value (γ_0) and in this specific case it was considered that the initial design corresponded to an empty reactor, where no metabolism occurs. The optimization procedure started by solving the reactor model and then, it calculated the value of the objective function. Afterwards a sensitivity analysis was performed in order to achieve the values of the gradients $\frac{\partial J}{\partial \gamma}$. From this information, the Method of Moving Asymptotes (MMA) was used to obtain a new updated design variable (γ_{n+1}). The process continues until the algorithm has converged to an optimal design.

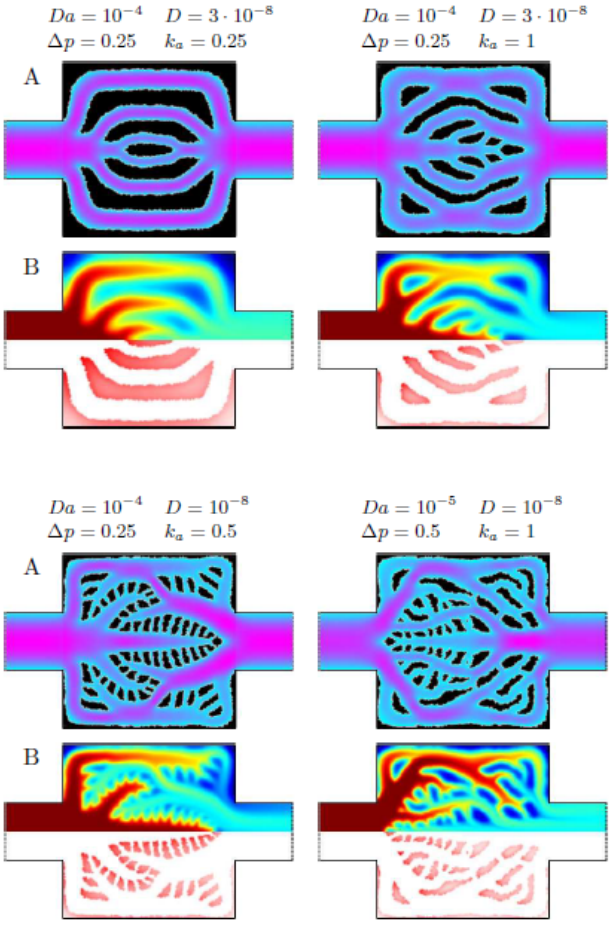

Figure 2.19 – Representation of the collection of optimized microreactors. The upper row (A) shows the distribution of the porous material in black together with a grey scale which indicates the flow speed. In row (B) the upper part of the figure shows the concentration profile of the substrate and the reaction profile [118].

Comparing the objective function of the empty design and the topologically optimized reactors shows a ten-fold improvement of reactant conversion. The topology optimized microreactor presents a cell immobilization structure that disperses small islands of carrier in the flow. Several configurations were studied according to changes in the reaction constant, pressure and Darcy number (See Figure 2.19).

A similar case study was presented by Schäpper and his co-workers[119]. This case study was also an investigation of a microreactor filled with a porous structure for immobilization of cells. The immobilized cells inside the reactor were brewer's yeast cells (*Saccharomyces cerevisae*).

The fluid dynamic model used was equal to the model used by Okkels and Bruus[118]. The local inverse permeability was also considered to be dependent on the porosity of the immobilization structure. The main difference between the two case studies is the used biological reaction model. Okkels and Bruus have used a simplified model for the reaction. Schäpper and his co-workers used a more complex reaction mechanism.

This reaction mechanism describes three metabolic events: glucose fermentation to ethanol, glucose oxidation and ethanol oxidation. The reaction kinetic model was based on the work from Brányik *et al.* (2004) [120] and Zhang *et al.* (1997) [121] and is given by the following form:

$$\mu_1 = \mu_{1,max} \frac{G}{K_{1'} + G} \frac{G}{k_{b'} + k_{a'} G} \tag{2.53}$$

$$\mu_2 = \mu_{2,max} \frac{G}{K_{2'} + G} \frac{1 + k_{c'} G}{1 + k_{c'} k_{d'} G} \tag{2.54}$$

$$\mu_3 = \mu_{3,max} \frac{E}{K_3 + E} (1 - \tanh(G)) \tag{2.55}$$

where $\mu_{1,max}$ is the maximum specific growth rate for a glucose fermentation, $\mu_{2,max}$ is the maximum specific growth rate for glucose oxidation, $\mu_{3,max}$ is the maximum specific growth rate for ethanol oxidation, $K_{1'}$ and $K_{2'}$ are the saturation constants, $k_{a'}$, $k_{b'}$, $k_{c'}$, $k_{d'}$ are enzyme pool regulation constants, E and G are concentrations for ethanol and glucose, respectively.

The product (recombinant protein) formation is connected to the growth and exclusively associated to the oxidative metabolism (ethanol and glucose oxidation, equations (2.54) and (2.55) in yeast cells, suspended and immobilized carrying the plasmid which encodes for the recombinant protein. The percentage of cells which carried the plasmid was maintained constant.

Moreover, this study has also included the immobilization kinetics, which considers the detachment of cells from the immobilization support. The release of the cells results from the flow of the culture broth, which was described according to the studies of Brányik *et al.* (2004) [120] and is mathematically described by:

$$k_{det}^{*} = k_{det}^{sst}\frac{G}{K_s + G} + C_3\frac{E}{K_s + E} \tag{2.56}$$

where k_{det}^{*} is the rate of detachment, k_{det}^{sst} is the maximum rate for growth on glucose, G is the concentration of glucose, C_3 reflects a switch to growth on ethanol, E is the concentration of ethanol and K_s is the saturation constant.

The complex model describes the effects of overflow metabolism, i.e. the production of co-product ethanol. The side reaction affects negatively the yield of the desired product, therefore this study allows the study of the cells positioning in the microreactor in order to maximize the formation of the product e reduction of the unwanted products.

The topology optimization routine was set up using COMSOL® and coupled with MATLAB®. The simulations were carried out for a square reaction chamber of length 1.2 mm and width 1.2 mm similar to the microreactor presented by Okkels and Bruus (2007). Similar to the previous case, the topology optimization was carried out in a two-dimensional domain. The objective function for this optimization problem is (minus) the total product formation rate which is the integral of the local product formation rate $r_P(t)$ [kg·s^{-1}] for every point of the domain Ω. The objective function ($J(\gamma)$) is given by:

$$\text{minimization} \qquad J(\gamma) = -\int_{\Omega} r_P\,(t)\,dV \tag{2.57}$$

The results of this study present a formation of islands of the porous structure with immobilized cells (See Figure 2.20). It was concluded that the distribution of immobilized cells on porous structures resembling islands allowed the best distribution of glucose and therefore the maximization of the production of the protein. The cell growth forms a similar pattern as the glucose distribution. However, the glucose oxidation was predominant in the areas of low concentration of glucose and therefore, the respiratory mechanism is not subject to overflow metabolism in these areas.

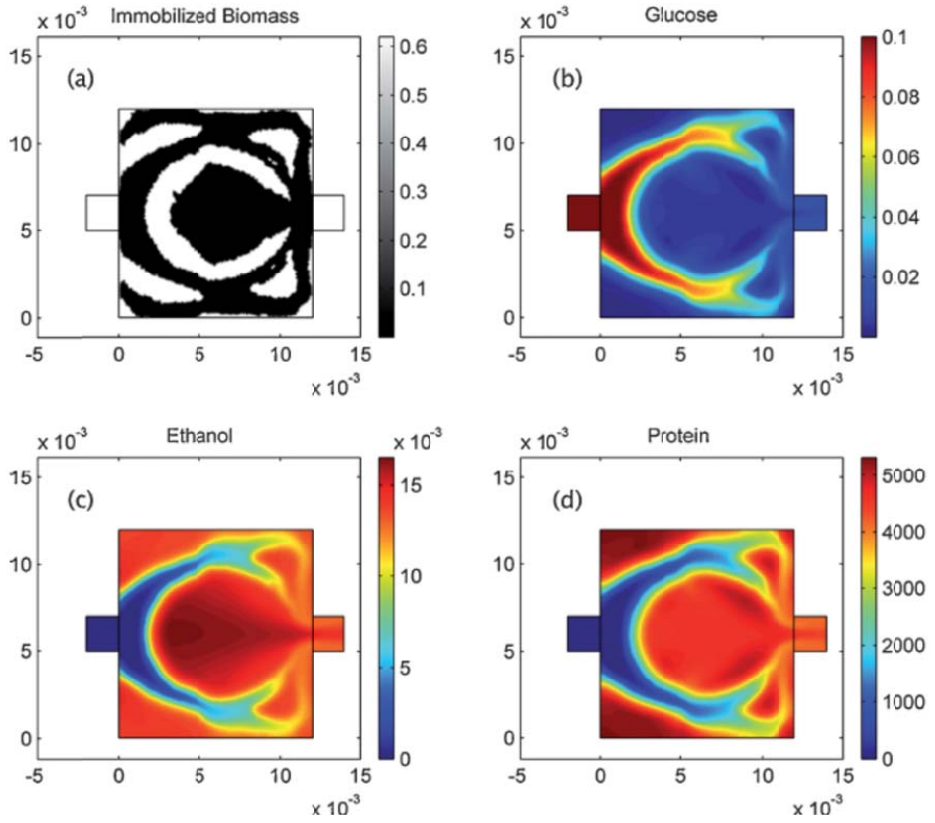

Figure 2.20 – Final configuration and concentration profiles for glucose concentration 0.1 g L^{-1}: a) Distribution of cells (white = cells and black = fluid), b) Glucose concentration profile in the microreactor (g L^{-1}), c) Ethanol concentration profile in the microreactor (g L^{-1}) and d) Protein (product) concentration profile (U L^{-1}) [119].

2.6 Theoretical background and literature review discussion

From the literature review, it can be concluded that topology optimization and shape optimization can be performed using different kinds of procedures such as deterministic or heuristic and gradient-based or gradient-free procedures. The gradient-based methods are the most commonly used in both types of structural optimization. These methods present as main advantage a fast convergence to the optimum; however they also present the disadvantage that the optimum might correspond to a local minimum. This drawback can be solved by applying a gradient-free method. Gradient-free methods have the advantage that it is possible to find the global minimum. Moreover, gradient-free methods allow the solution of problems with discrete variables and discontinuous functions and domains. Gradient-based methods have also shown to be potentially more efficient to solve optimization problems when the number of design variables is large which makes the use of gradient-based methods prohibitive due to their high computational costs for sensitivity analysis required to obtain a gradient. However, for gradient-free methods the high number of design variables might also have an influence on their efficiency and also contribute to high computational costs. The adjoint method has presented a solution to overcome this problem and it is formulated in order to be independent of the number of design variables. Nevertheless, the adjoint method – similar to the other gradient-based methods – can only be applied to continuous functions and domains and might converge to local minima.

In topology optimization, the most commonly used procedures are the Isotropic Solid and Empty methods and within these, the Solid Isotropic Microstructured with Penalization (SIMP) and the Evolutionary Structural Optimization methods are the most frequently found in the scientific literature. These gradient-based methods are frequently used in mechanical engineering and building structure problems.

The SIMP method evolves by using a penalization coefficient for the design variable which makes a minimization of intermediate values of the design variable on the domain and the optimal solution presents a discrete solution (0-1 values).

The ESO method is characterized for being a simple method and not requiring advanced mathematical approaches. Moreover, it can be used in discrete problems along with “black box” software. This method is characterized by the elimination of low efficient elements of the structure which is gradually done by considering an optimization criterion and a rejection criterion. The rejection criterion is updated when the process of removing elements reaches steady state.

Computational fluid dynamics (CFD) is a complement to experimental and theoretical approaches for studying fluid dynamics. In fact, this numerical method can be used to better understand phenomena which are not possible to fully investigate by means of experimental and theoretical studies. This tool has been continuously under development and it will not substitute any of the

other approaches for studying fluid dynamics. In process development, CFD has been used for equipment and reactor design. Although, CFD methods have been widely used they present several limitations when applied to multi-phase systems, turbulent flows and systems containing phase changes. The use of CFD demonstrated to be useful, reduces costs and time that experimental work requires for the development of processes. However, CFD is a complement to the experimental work and it does not substitute it.

There are several commercial CFD software packages available on the market, as well as open source solutions. Many of these tools present different discretization methods of the domain and also for solving the domain. In this project, ANSYS CFX® is the chosen CFD software to solve the fluidic problems. Although this software is a "black box" program for which is not possible to access and manipulate the underlying equations, it allows to setup the geometry and the domains and boundary conditions by using scripts. These scripts can be modified using other programs such as e.g. MATLAB®. Moreover, this CFD software can be executed in batch mode and this can be controlled from the MATLAB® environment. Therefore it is possible to couple CFD simulations in ANSYS CFX® with optimization procedures.

Microfluidic technology has been used over the years as experimental tool for process intensification especially for the development of processes. The main approach for application of microsystems as tools for process intensification is an analysis of characteristic times of physical and chemical processes. This approach helps with the identification of the limiting phenomenon of the process and further consequent analysis of these characteristic times will support the development of strategies for intensified processes.

The different phenomena existing in a specific unit operation each have a characteristic time such as heat transfer in a heat exchanger, mass transfer in a mixing or separation unit, reaction time in a reactor. The characteristic times are related to a characteristic dimension of the unit operation which can for example be the radius. The characteristic times for homogeneous reactions are independent of the dimension of the unit operation.

Complex reaction mechanisms such as heterogeneous or biological/enzymatic reactions might be dependent of external factors. Hence, the determination of the characteristic time may imply a complex procedure and might not account for intrinsic kinetics and instead rely only on apparent kinetics.

The yield of product and the conversion of substrates depend on the reactor dimensions. Therefore, the reactor dimensions which are required for achieving a certain reaction yield can be estimated by evaluating the ratio between the residence time in the reactor and the characteristic reaction time, the first Damköhler number.

The flow in a microfluidic device is characterized by a laminar flow regime and the mixing is often achieved or limited by diffusion. Since mixing by diffusion is a slow process it requires that the dimensions of the microchannels are small. Nonetheless, the fabrication of such small

channels results in high fabrication costs and therefore, it is necessary to introduce convective mixing in the microchannels. Convective mixing is frequently introduced by passive mixing, which can be performed by parallel lamination or by chaotic advection. The parallel lamination has been reported as a very efficient mixing method. However, it has been demonstrated that increasing the number of interfaces in a microreactor between two liquids does not result in equal improvement of the product yield. CFD studies have shown that reaction yield improvement due to increasing the number of interfaces depends on the rate controlling step of the reaction, i.e. the reaction itself or diffusion. The increase of lamination interfaces results in an improvement of the mass transfer limiting conditions (diffusion as rate controlling step).

Some examples of shape and topology optimization of microchannels/microreactors can be found in the literature. Hasebe, Tonomura and their co-workers have shown that shape optimization can be a useful tool for designing microchannels in order to minimize accumulation of material in dead zones in manifolds and to minimize the pressure drop in curved channels. They have also identified that shape optimization can be used as tool for understanding and gathering information about the relation between the flow and the microchannel shapes for posterior microdevice fabrication.

Topology optimization applied to microreactors has been introduced by Okkels and Bruus (2007). They optimized the distribution of cells immobilized on a carrying structure with a determined porosity inside a microreactor. The design variable for this problem corresponds to the porosity of the carrier. The system was evaluated by the amount of product formed inside the microreactor. A similar case has been presented by Schäpper *et al*. (2010) for which a more complex reaction mechanism has been considered that includes the growth of cells and the formation of product in a slightly different reactor.

Both cases, by considering the porosity as design variable, have resulted in final configurations with large void spaces within the carrier material and with placement of the carrier material as islands. These structures are mechanically unstable and, in a real microreactor it would not be possible to pack the material in fixed areas, i.e. the carrier material would change location due to the fluid flow. Therefore, it is not possible to validate these results experimentally.

Moreover, these studies change the porosity of the carriers which results in constantly changing the fluid profile at each iteration, which consequently modifies fluidic dynamic properties inside the microreactor. Thus, these studies do not allow an investigation of the flow profile influence on the formation of a product.

2.7 Concluding remarks

Topology and shape optimization have mostly been applied to structural design. Many mathematical methods are reported in the scientific literature for structural optimization. In fact the main focus of the experts in this field is to develop more efficient optimization methods.

Only few studies have been presented in the scientific literature with focus on shape and topology optimization of microchannels and microreactors.

Tonomura and Hasebe's numerical investigations about the use of shape optimizations applied to microchannels have revealed that this optimization technique is important for designing microdevices. These authors have presented computational studies for eliminating dead volumes and minimize pressure drop in microchannels. From the literature review, it is possible to conclude that this field can be used as a complement to the actual process intensification procedures. Moreover, the applications of shape optimization to microchannels can be further explored. For instance, shape optimization can be applied to microreactors in order to investigate the influence of the microreactor shape on the reaction yield or potentially also effects to improve the yield in the case of enzymatic reactions with unfavorable equilibrium or product and /or substrate inhibition.

Okkels and Bruus and Schäpper *et al.* have presented relevant studies on how to intensify a microreactor computationally by using a topology optimization procedure. However, the studies resulted in configurations which are very difficult to fabricate and test in the laboratory due to the unstable structures of the porous cell carrier material. The method used by these authors for application of topology optimization to microreactors prevents laboratory testing and involves constant change of the flow profile due to adjustment of the carrier porosity. In this field, a new method which allows laboratory testing and eliminates constant changes of the flow is necessary.

To conclude, the implementation of topology and shape optimization to microreactors as a process intensification technique requires further development and experimental validation.

Chapter 3

Shape optimization of a microbioreactor

3.1 Introduction

In the chemical industry, bioprocesses have been one of the main areas of expanding industrial development the past decades. Bioprocesses involve the use of microorganisms or their derivatives e.g. enzymes to produce valuable substances such as recombinant proteins, drugs (e.g. insulin, antibiotics) or other chemical substances (e.g. bioethanol) to name a few. Bioprocesses are usually applied to the pharmaceutical, the food and the chemical industry.

In the pharmaceutical industry, there are numerous enzymes which are used in pharmaceutical processes for production of drug products or intermediates [122].

At early stage development of bioprocesses the definition of the process conditions for optimizing the product formation is investigated. Often this optimization is done by adjusting process parameters such as temperature, feed flowrate and pH value. In addition, the reactor design is also an important aspect to consider in bioprocess implementation. Currently, chemical and biochemical reactor designs must facilitate the mixing between the substrate and the biocatalyst to overcome mass transfer limitations and improve the productivity.

Nowadays, the reactor design is chosen according to available configurations that have been reported in the scientific literature or that are available at the production sites. This includes stirred tank reactors, plug-flow reactors, packed bed reactors and fluidized bed reactors. After the reactor configuration has been chosen, the process conditions are optimized. However, although the process parameters are adjusted, the reactor configuration is not always optimal. In fact,

common phenomena that indicate non-ideal reactor behavior are frequently observed in reactors applied at industrial scale, such as poor mixing, channeling or dead zones, which can be the reason for unreacted substrate exiting the reactor. This might then have a severe impact on the product yield, on the downstream processing and on the respective operating costs. Furthermore, complex reactions related for example to enzymatic processes can also contribute to challenges in adapting the process to the reactor configuration.

The complexity of bioreactions on the one hand, and the difficulties in adapting the process to the reactor while simultaneously obtaining high reaction yields on the other hand, give a clear motivation to explore new strategies for improving a reactor configuration.

A new strategy for developing a reactor is suggested in this chapter. Instead of adapting the process to a well-known reactor shape, a shape optimization method is used to find the reactor shape with best performance regarding a specific reaction system.

Shape optimization is a mathematical method often used in mechanical and civil engineering. This method is characterized by finding the optimal geometry within a defined domain which minimizes or maximizes an objective function and fulfils specific constraints. The constraints can be defined for example by the amount of used material, the number of iterations and/or the improvement of the result of the objective function. As described in Chapter 2, shape optimization has been adapted to microfluidics and chemical engineering in order to minimize the pressure drop in microchannels and eliminate dead volumes in microscale manifolds.

This chapter will present a new implementation for shape optimization in chemical engineering which can be a new approach for intensifying equipment and complement the existing process intensification methods. Shape optimization can be an opportunity to improve equipment for bioprocesses such as reactors or static mixers.

A novel application in biochemical engineering of shape optimization using a stochastic evolutionary algorithm – random search – is presented. The purpose of this mathematical investigation is to introduce an innovative method for the design of a microreactor under laminar flow conditions and with an enzymatic reaction occurring inside.

Shape optimization is used in this chapter to improve the reaction yield occurring between two parallel laminar streams containing the enzyme and substrate respectively by modifying the shape of a microreactor channel. In this case, it is considered that the biocatalyst and one of the substrates are slowly diffusing compounds ($<10^{-10}$ m^2 s^{-1}). Therefore, the mixing of the compounds by diffusion is very slow and only a small amount of substrate is converted. This case study was chosen in order to verify that the shape optimization works by finding a better micromixing structure, which promotes the reaction inside the microreactor. In the theoretical background presented in Chapter 2, several passive mixing structures were presented which included alterations on the internal channel walls (e. g. by carving grooves out) to improve the mixing in micromixers.

These investigations will give the opportunity to identify the optimal process conditions, collect information regarding which flow characteristics influence the reaction yield or even obtain the final optimal shape before performing experimental work. This new implementation will potentially reduce extensive experimental work and waste of materials. Additionally, it will be possible to determine beforehand an optimal reactor design and to test it right away.

3.2 Shape optimization of a microbioreactor for enzymatic synthesis of optically pure chiral amines

The challenges concerning the biocatalytic process development are the high costs of the enzymes at an early stage of process development, as well as limited availability of enzyme candidates to be screened, preventing bench-scale process screening [123]. For this reason, microsystems are a good alternative, since they allow high throughput or high content screening of process parameters, reaction kinetics, solvents or materials, but are not yet broadly used in the field [124].

In this section, we will demonstrate the implementation of shape optimization via computational fluid dynamics studies of a microbioreactor for the production of optically pure chiral amines through an enzymatic reaction.

Chiral amines are crucial substances for the production of pharmaceutical drugs and agrochemicals [125]. Although chemical processes producing chiral amines already exist, the biocatalytic route has been considered as an alternative process due to its advantages. Biocatalytic processes using e.g. amine transaminase (ATA) as biocatalyst have several advantages when compared to chemical routes such as mild reaction conditions, high stereoselectivity and high enantioselectivity [126]. The reaction catalyzed by ATA is considered to be a very complex reaction with many downsides. One of the disadvantages of this biocatalytic reaction is the inhibition of amine transaminase by both the substrates and the products. Moreover, the biocatalysis by ATA is also characterized by an unfavorable thermodynamic equilibrium, which drives the reaction towards the substrates [127]. The complexity of this enzymatic reaction, combined with the versatility of microsystems fabrication, gives a clear motivation to explore the influence of the microreactor shape on the production yield.

The chosen model reaction corresponds to the synthesis of the chiral product (*S*)-1-phenylethylamine (PEA) and acetone (ACE) from acetophenone (APH) and isopropylamine (IPA) by using amine transaminase (ATA) as biocatalyst (See Figure 3.1).

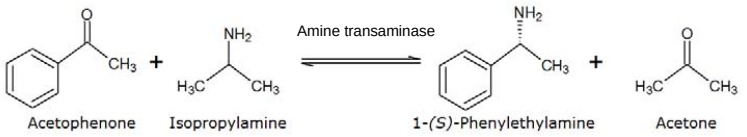

Figure 3.1- Reaction system for microreactor optimization.

ATA is known for following the ping pong bi bi kinetic mechanism in which one of the substrates (in this specific case, isopropylamine) binds first, the co-product (acetone) is released before the second substrate (acetophenone) binds and the final product ((*S*)-1-phenylethylamine) leave the enzyme site last [128]. The kinetic rate equation for this reaction mechanism is given by [129]:

$$r_{PEA} = \frac{d[PEA]}{dt} = \frac{[E_0]k_{cat}^f k_{cat}^r \left([APH][IPA] - \frac{[PEA][ACE]}{K_{eq}}\right)}{k_{cat}^f K_m^{APH}[IPA]\left(1 + \frac{[PEA]}{K_{Si}^{PEA}} + \frac{[IPA]}{K_{Si}^{IPA}}\right) + k_{cat}^r K_m^{IPA}[APH]\left(1 + \frac{[APH]}{K_{Si}^{APH}} + \frac{[ACE]}{K_{Si}^{ACE}}\right) + k_{cat}^f \frac{K_m^{PEA}[ACE]}{K_{eq}}\left(1 + \frac{[APH]}{K_{Si}^{APH}} + \frac{[ACE]}{K_{Si}^{ACE}}\right) + k_{cat}^f \frac{K_m^{ACE}[PEA]}{K_{eq}}\left(1 + \frac{[PEA]}{K_{Si}^{PEA}} + \frac{[IPA]}{K_{Si}^{IPA}}\right) + k_{cat}^r[APH][IPA] + k_{cat}^f \frac{K_m^{PEA}[IPA][ACE]}{K_{eq}K_i^{IPA}} + \frac{k_{cat}^f[ACE][PEA]}{K_{eq}} + k_{cat}^f \frac{K_m^{IPA}[APH][PEA]}{K_i^{PEA}}} \quad (3.1)$$

The specific kinetic parameters for this reaction system were determined and calibrated to the enzymatic mechanism by Al-Haque *et al.* (2012) [130]. The reaction mechanism is characterized by 14 parameters, which includes the reaction rate constants, the Michaelis-Menten constants, the product and substrate inhibition constants and the equilibrium constant of the reaction. The rate equation represents the mathematical equation which describes both the forward reaction towards the product formation (phenylethylamine and acetone) and the reverse reaction towards the substrate formation (acetophenone and isopropylamine). In the reaction rate equation, the turnover number of the forward reaction is represented by k_{cat}^f and the turnover number of the reverse reaction is denoted by k_{cat}^r. The rate equation includes also the Michaelis-Menten constant for each of the compounds participating in the reaction. The Michaelis-Menten constants for acetophenone, isopropylamine, (*S*)-1-phenylethylamine and acetone are denoted by K_M^{APH}, K_M^{IPA}, K_M^{PEA} and K_M^{ACE}, respectively.

This specific reaction is greatly influenced by competitive substrate inhibition of acetophenone and (*S*)-1-phenylethylamine. The substrate inhibition constants for both acetophenone and (*S*)-1-phenylethylamine are represented by $K_{Si}^{APH}$and K_{Si}^{PEA}, respectively. The significance of substrate inhibition by acetone (K_{Si}^{ACE}) and isopropylamine (K_{Si}^{IPA}) was found to be negligible. The core inhibition constants for acetophenone, isopropylamine, (*S*)-1-phenylethylamine and acetone are represented in the kinetic equation by (K_{Si}^{APH}), (K_{Si}^{IPA}), (K_{Si}^{PEA}) and (K_{Si}^{ACE}). The equilibrium constant is given by K_{eq}. The parameters γ and λ are the binary reaction direction indicators. The parameters, estimated by Al-Haque *et al.* (2012) [130] and used in these simulations, are summarized in Table 3.1.

In this case study, two compounds are considered as slowly diffusing compounds: acetophenone ($1 \cdot 10^{-12}$ $m^2 \cdot s^{-1}$) and ATA ($1 \cdot 10^{-11}$ $m^2 \cdot s^{-1}$).The slow diffusion of acetophenone has been documented in the scientific literature by Bodla *et al.* (2013) [101]. Although the acetophenone molecule is not a very large molecule it appears to be a slowly diffusing molecule. The low diffusion coefficient seems to be related to the low solubility of acetophenone in water.

Table 3.1 – Parameters of the kinetic model estimated by Al-Haque *et al.* (2012) [130].

Rate constants (min^{-1})		Substrate inhibition constants (mM)	
K^{f}_{cat}	0.0078	K_{Si}^{APH}	4.15
K^{r}_{cat}	0.013	K_{Si}^{PEA}	10.38
Michaelis-Menten constants (mM)		**Core inhibition constants (mM)**	
K_M^{APH}	1.85	K_i^{APH}	0.09
K_M^{IPA}	101.28	K_i^{IPA}	4281
K_M^{ACE}	148.99	K_i^{ACE}	0.11
K_M^{PEA}	0.12	K_i^{PEA}	105
Equilibrium constant			
K_{EQ}	0.033		

In the scientific literature [131], the acetophenone diffusion coefficient presents a value 766 times higher – $7.66 \cdot 10^{-10}$ $m^2 \cdot s^{-1}$ – for an organic-aqueous system containing 10% of methanol. Moreover, in the same article, the value of the diffusion coefficient improves slightly ($6.39 \cdot 10^{-10}$ $m^2 \cdot s^{-1}$) when the concentration of methanol increases to 30% in water. In another scientific article [132], the acetophenone diffusion coefficient was also determined in a microfluidic device for an organic-aqueous system which contains 10% of methanol. The diffusion coefficient has a similar value– $7.35 \cdot 10^{-10}$ $m^2 \cdot s^{-1}$ – to the one reported by Li *et al.*[131]. The results reported by Li *et al*.[131] demonstrate that there is non-significant difference of the diffusion coefficient value when the methanol concentration in solution decreases. Their results also showed that even in solutions with lower amount of methanol the diffusion coefficient is still much higher than the reported by Bodla and his co-workers.

From these reported results, it is possible to conclude that the diffusion coefficient value of acetophenone in water might not be much different from the values reported for solutions with low methanol concentrations. This indicates that the value reported by Bodla and his co-workers might not be the correct diffusion coefficient value for water solutions. However, we kept this value nevertheless in the optimization procedure. In this way it would also be possible to investigate the impact of the geometry on potential strategies for running the reactor such as *in situ* product removal conditions. *In situ* product removal is a strategy which can be used for shifting the unfavorable equilibrium towards the product formation and for removing an

inhibitory product [133]. In this way, it will be possible to evaluate the resulting reactor shape effects on the mixing and on *in situ* product removal. Therefore, conclusions regarding how to implement the process will be drawn from the analysis of the final design.

ATA, a protein, is considered to be a slowly diffusing molecule due to its large molecular structure. Therefore, its diffusion coefficient was considered to be similar to the values reported for enzymes, 10^{-11} $m^2 \cdot s^{-1}$ [134]. All the other compounds involved in this reaction system were considered to be fast diffusing substances and to have the same diffusion coefficient, $1 \cdot 10^{-9}$ $m^2 \cdot s^{-1}$.

3.2.1 Materials and methods

3.2.1.1 Initial configuration of the microreactor

The dimensions of the microreactor in this case study are in the range of micrometers, and therefore the flow regime corresponds to laminar flow conditions. Microreactors are characterized by very large surface-area-to-volume ratio, very effective heat and mass transfer and enhanced control of process conditions due to automation [78,124]. In microfluidics the flow is characterized by laminar flow and therefore the mixing is essentially characterized by diffusion. However, in this case study some of the compounds are characterized by slow diffusion, and therefore the mass transfer within the reaction chamber is not very effective. This phenomenon motivates the investigation of the impact of shape optimization on the slow mixing velocity of acetophenone and ATA.

The dependence of the reaction on the fluid mechanics of the system and the properties of the compounds will be evaluated by the governing equations of CFD i.e. the Navier-Stokes and the continuity equations which are presented below. These equations have been presented in detail in Chapter 2.

$$\text{Navier-Stokes equation:} \quad \frac{\partial}{\partial t}\rho \boldsymbol{v} = -(\boldsymbol{\nabla} \cdot \rho \boldsymbol{v}\boldsymbol{v}) - \boldsymbol{\nabla} \cdot p - (\boldsymbol{\nabla} \cdot \boldsymbol{\tau}) \tag{3.2}$$

$$\text{Continuity equation:} \quad \frac{\partial \rho}{\partial t} = -\nabla(\rho . \vec{v}) + S \tag{3.3}$$

The coupling with energy balances is not implemented since the reaction occurs under isothermal conditions.

The initial shape of the studied microreactor has the form of a YY-microchannel with a rectangular cross-section where the inlet and the outlet are located at the respective ends of the reactor. A YY-microreactor is characterized by a main long reaction channel and by two channels at each extremity which meet at the begin/end of the main channel forming an angle lower than 90°, forming a Y shape (See Figure 3.2).

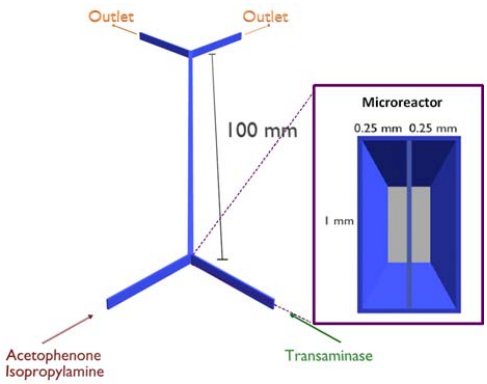

Figure 3.2 - YY-microreactor configuration with indication of the inlets and outlets and substances at each inlet with a detailed view of the inlet of the reaction channel.

The Y shapes at each end of the reaction chamber correspond to the inlet and the outlet where two streams meet at the entrance of the main channel and are split again into two streams at the exit of the channel. In one inlet of the microreactor a solution with ATA enters, and in the other inlet a solution of acetophenone and isopropylamine is introduced. The concentrations of the substrates and the enzyme at the inlet before mixing the flows are presented in Table 3.2.

Table 3.2– Concentration of substrates and enzyme at the inlet of the microreactor.

Substance	Concentration
Acetophenone	20 mM
Isopropylamine	2 M
Amine transaminase	0.15 mM

The choice of the substrate and enzyme concentrations considered in this study was made based on experimental work of Al-Haque *et al*[130]. and Bodla *et al.* [101]. The concentration of enzyme was calculated from information available in the scientific literature cited previously and considering that the molecular weight of the enzyme is 40 kDa.

The optimization routine focuses on the modification of the surface of the main channel of a microreactor. The main channel consists of a chamber without divisions. The initial configuration of the main channel has the following dimensions: 0.25 mm width for each inlet and outlet, 1 mm height and 100 mm length.

The shape optimization routine applies changes in small vertical sections of 1 mm. These vertical sections consist of a closed (mathematical) spline which connects a group of 14 points. These splines are connected to form the surface of the channel (See Figure 3.3 a)).

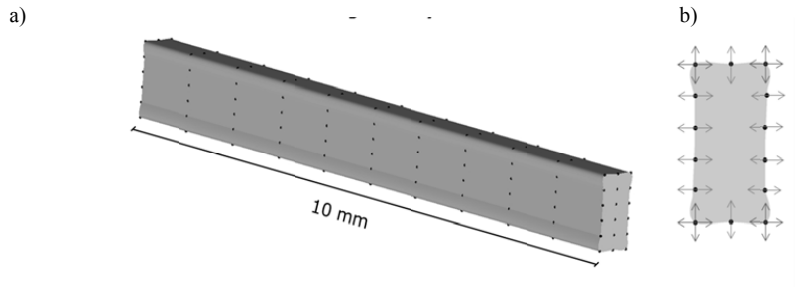

Figure 3.3 - a) Structure to be optimized with all surface points represented; b) channel cross section with the directions for modification of the points.

Since the spacing between the closed splines is very small if the whole channel was considered the problem would be excessively large in terms of computational efforts and thereby in terms of required solution time. This study focused therefore only on the optimization of the first section of the main channel (10 mm). The points on the surface of the considered section (140 points) are modified according to the random search procedure. The closed splines are modified due to the alteration of the position of the individual points, and consequently the shape of the channel is also modified. The points which are at the lateral parts of the channel can be moved horizontally, the points at the top and bottom of the channel can be moved vertically and the corner points can be moved in both vertical and horizontal directions (See Figure 3.3 b)). The residence time inside the microreactor is 30 minutes for all simulations. Since the volume of the microreactor varies from simulation to simulation, the flow rate has to be adjusted accordingly to the new volume in order to maintain the residence time constant.

3.2.1.2 Shape optimization procedure

The optimization routine consists of a finite volume analysis performed by ANSYS CFX® coupled with a MATLAB® routine which includes the optimization procedure. ANSYS CFX® is a commercial computational fluid dynamic (CFD) software, which differs from other open source CFD software solutions by being a "black box" software, meaning that the user has no access to the fluid governing equations such as the Navier-Stokes equation, continuity equation and energy equation. However, ANSYS CFX® differs from other commercial CFD software by offering the opportunity to the user to write mesh files (software ICEM CFD®), set up files for simulation (software CFX-Pre®) and also perform the post-processing of the files (software CFX-Post®) as script files. These script files are the basis for establishing geometry, mesh, setup and post-processing procedures. The executing files for mesh, setup and solving are then generated from

the script files. The change of these script files, the generation of the executing files and the execution of the simulation can be performed via batch mode processes. The batch mode is defined as an automated process for running files without opening a graphical program interface, which demands no user interaction. In the shape optimization procedure, it is possible with help of MATLAB® code to establish commands for defining a run of a simulation in batch mode; it is also possible to convert script files into arrays, modify the properties for definition of a geometry or the parameters of a simulation setup and command the start of a simulation. Therefore, there is a great opportunity to establish an optimization routine by coupling a "black-box" CFD commercial software – in this case ANSYS CFX® – and MATLAB®. In this way it is possible to link two commercial software packages through a self-programmed and fully automated optimization process. It is important to emphasize that the two software programs have distinct roles: ANSYS CFX® solves the fluidic problem with the integrated reaction system and evaluates the product concentration at the outlet and MATLAB® executes the optimization method. The routine and interaction between ANSYS CFX® and MATLAB® used for the shape optimization of the microreactor of this case study is represented in Figure 3.4.

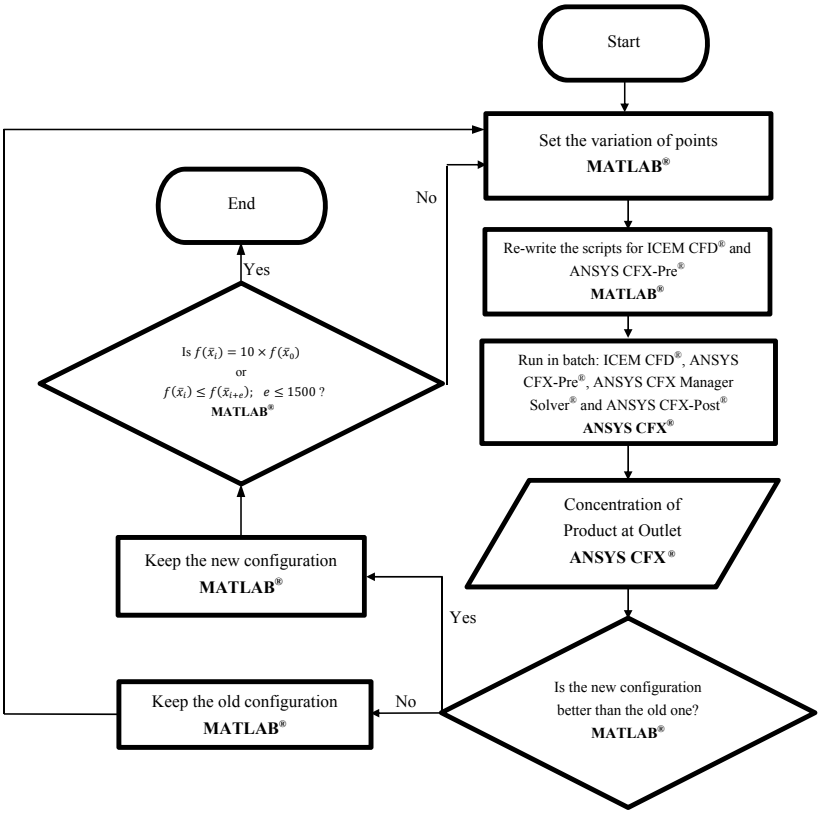

Figure 3.4 – Algorithm for the shape optimization of the enzymatic microreactor.

The optimization routine established in MATLAB® is characterized by five steps. The first step is to read information about the product concentration at the outlet of the reactor from the post processing file of ANSYS CFX®. The second step is the decision on keeping the new geometry according to results read from the post processing file. The third step is the generation of a new set of points according to the random search procedure. The two last steps, finally, are the update of the reactor geometry and the flowrate on the CFD scripts and the start of the new CFD simulation.

In shape optimization the alterations are directly made to the geometry and therefore the file that is being updated for every iteration is the script file which creates the geometry and mesh (ICEM CFD®). All the other set-up files are modified and generated automatically according to the changes of this new geometry/mesh file.

The microreactor geometry has been discretized in small volume elements creating a mesh. The mesh handles the division of the geometry domain into sub-elements. The generation of the mesh and discretization of the domain into elements allows the numerical solution of the governing equations of the CFD code which provides discrete values of the equations for each mesh node. The mesh is one important part of the CFD simulation since the quality of the mesh matters for the solution of the CFD analysis. Therefore, the mesh generation is usually a complicated and time consuming process.

The mesh generation method has been recorded into a script file when the mesh was generated for the initial shape. The method for generating the mesh is the same for all the shapes given by the random search method. The mesh adapts automatically to all the different geometries and it is ensured that the mesh covers the whole microreactor structure.

In this way it is possible to achieve consistency and automation in the mesh generation without user interference. In this case study, the geometry was discretized into a structured mesh. The choice of a structured mesh over an unstructured on was made based on the advantages of the structured mesh. The comparison of both types of meshes made in Chapter 2 highlighted that the solution of structured meshes requires lower computation time and memory usage and that it solves problems of high gradients more accurately than an unstructured mesh for the same geometry. By adopting a structured mesh discretization, the domain became discontinuous which means that not all the combinations of the points will be possible. The discontinuity of the domain is caused by the formation of sharp angles for some combinations of points and therefore the elements in that zone tend to be tetrahedral instead of hexahedral. Thus, the shape of tetrahedral elements will be difficult to use during the solver calculations.

The quality of the mesh is evaluated by the angles of the elements and it should be sufficient to fulfil the solver requirements. The ANSYS CFX® compatible mesh generator, ICEM CFD® has the option to verify the mesh quality. One of the methods available in ICEM CFD® to evaluate the quality is named Determinant.

This method computes the deformation of the elements in the mesh by calculating the Jacobian matrix of each hexahedron and then normalizes the determinant of the matrix. A value of 1 represents a perfect hexahedral cube, while a value of 0 corresponds to an inverted cube with a negative volume. In general, determinant values above 0.3 are acceptable for most of the solvers.
The created geometry does not correspond to an exact rectangular cross-section reactor. In fact, the corners of the cross-section are curved due to this specific design of the splines which was selected to minimize the domain discontinuity. A curvilinear mesh called O-grid in ICEM CFD®, which is usually applied to curved shapes, was applied to the faces of inlet and outlet as presented in Figure 3.5a) in order to also minimize the discontinuity of the domain.
The center points of the O-grid which correspond to the corners of the perfect hexahedral elements of the structure have been fixed to their position of the initial shape of the microreactor. In this way it was possible to minimize sharp angles inside the structure (see Figure 3.5b)).

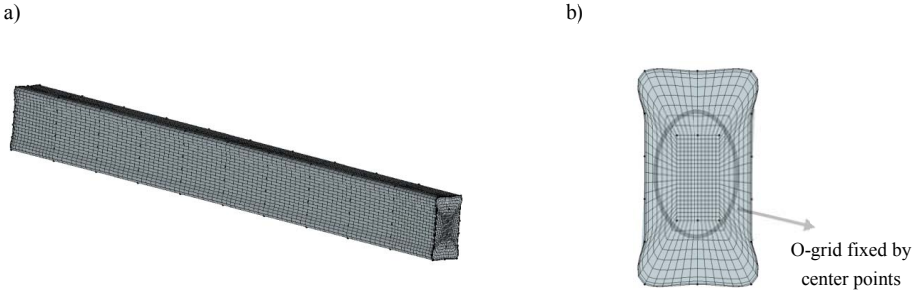

Figure 3.5 – a) Mesh strategy applied to microreactor for the shape optimization for the initial shape. b) O-grid application to the mesh of the microreactor

Despite all the efforts to avoid discontinuous domains, there were still several possible shapes for which it was not possible to solve the system due to a bad quality of the mesh. The implementation of an unstructured mesh could have avoided the domain discontinuation since it adapts easily to all geometries including shapes with sharp angles. Nevertheless, an unstructured mesh requires many more elements in order to achieve the same level of accuracy as a structured mesh especially in a case like this one in which the concentration gradient is a very important aspect to consider.
As reviewed in Chapter 2, shape optimization procedures can be performed by gradient-free or gradient-based methods. In this case study the choice of the optimization procedure relied on a gradient-free method. This decision was made by considering the possible discontinuity of the domain caused by the application of a structured mesh. Moreover, the choice also relied on the high number of design variables which would imply a high computational cost if a gradient-based

method was implemented. As stated above, the shape optimization procedure was based on a stochastic evolutionary procedure, the random search method.

For an optimization, it is necessary to define the objective function and restrictions. In this study, the objective function is the concentration of product at the outlet of the microreactor, which must be maximized (alternatively the substrate concentration can be minimized). The optimization routine stops either when one of the restrictions is satisfied or the system has converged. In this optimization problem, the routine can be stopped due to two restrictions, either when the amount of substrate produced is ten times higher than the initial one or the number of iterations between two local minima exceeds 1500. It was assumed that for such low reaction rate and low product formation, the minimum of improvement required to consider the fabrication of the optimized microreactor worthwhile is a factor 10 improvement. The restriction regarding the number of iterations between two local minima was set in order to prevent high computational costs due to the large number of design variables and the discontinuity of the domain.

The formulation of this optimization problem is given by the following notation:

$$\begin{aligned} &\text{Maximize} && f(\bar{p}_i) = \int_{\Omega} r_P(\bar{p}_i)dV \\ &\text{Subject to} && f(\bar{p}_i) = 10 \times f(\bar{p}_0) \\ & && f(p_i) \leq f(\bar{p}_{i+e}); \quad e \leq 1500 \end{aligned} \tag{3.4}$$

where f is the objective function, $\bar{p}_0$ is the vector which sets the points for the initial geometry positions, $\bar{p}_i$ is the vector with the points positions, i is the iteration number and e is the number which evaluates the interval of iterations between local optima.

Considering the notation above the optimization procedure is defined by the following algorithm:

Until either the concentration of substrate is ten times lower or the number of iterations between local optima is more than 1500, run the following cycle:

- Initialize the random search with initial vector $\bar{p}_i = \{p_1, p_2, \dots p_n\} \subset S$ which gives the shape presented in Figure 3.5.
- Sample a new position for each of the elements of the vector $\bar{q}_{i+1} = \{q_1, q_2 \dots q_n\} \subset S$ from the 0-sphere by the pair of points $\{p_n - 0.03p_n, p_n + 0.03p_n\}$ and by setting a random step size within the interval [0,1]. Thus, the changes made to each point will correspond to a relative change between -3% and +3%.
- If $f(\bar{q}_i) < f(\bar{p}_i)$ and a new local optimum set of points has been found. Set the vector $\bar{p}_i$ based on the optimum set of points $\bar{q}_{i+1}$.
- Interrupt the cycle when the concentration of product at the outlet is ten times higher or the number of iterations between local optima is more than 1500. Otherwise increase i and return to the second step.

3.2.2 Results and discussion

This optimization study included 9296 simulations in total, where each simulation took between 2 to 5 minutes to reach a solution. The achieved optimal shape has the properties of a wavy structure on all four walls of the channel. On the one hand, $4.4 \cdot 10^{-5}$ mM of substrate were converted with the initial configuration, on the other hand, $37.1 \cdot 10^{-5}$ mM of substrate were converted with the final shape. Finally, the yield in the final configuration corresponds to 8.4 times the yield in the initial shape which was very close to the pre-defined goal (10 times the yield of the initial shape). However, the number of iterations required to find the next local optimum increased exponentially which made the optimization procedure very expensive from a simulation point of view. Therefore, the restriction of maximum 1500 iterations between local optima was implemented.

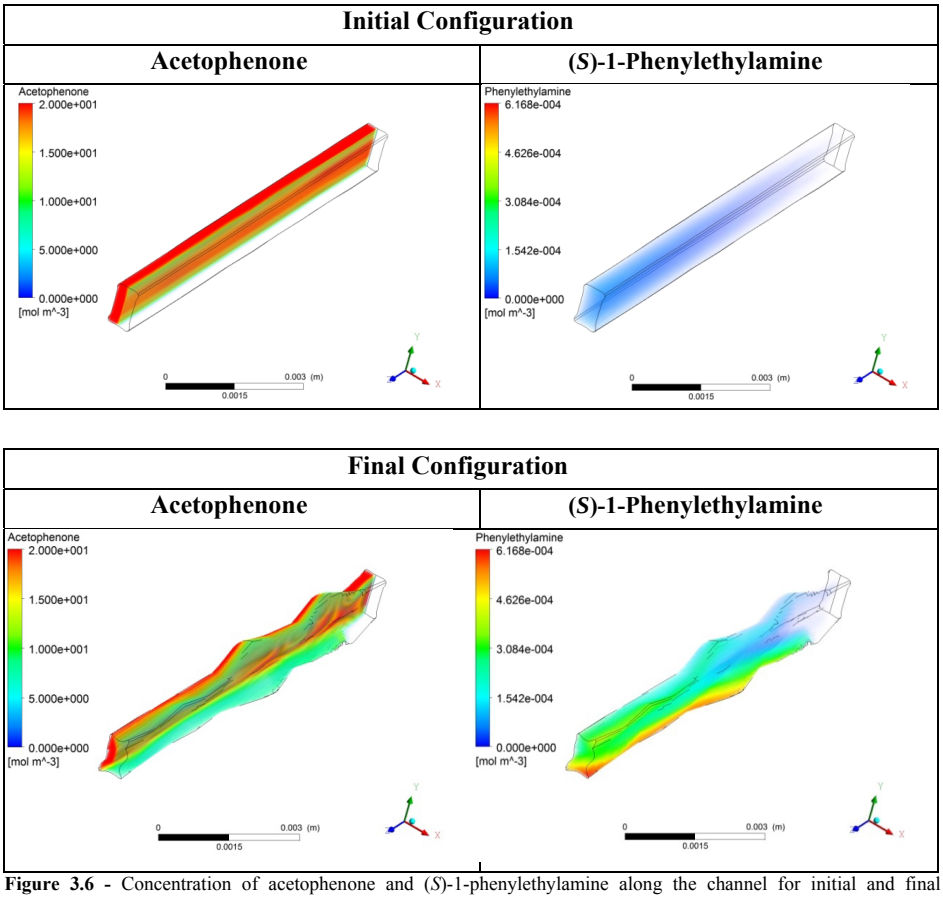

Figure 3.6 - Concentration of acetophenone and (*S*)-1-phenylethylamine along the channel for initial and final configurations.

Initial Configuration	
Left Side	**Right Side**
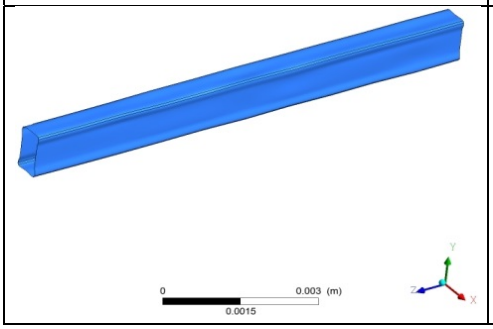	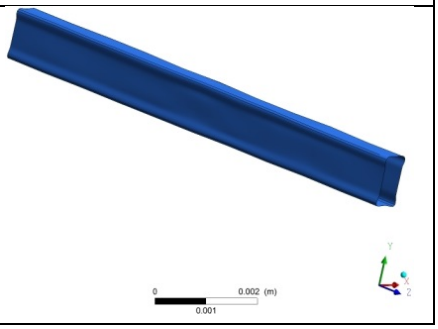

Final Configuration	
Left Side	**Right Side**
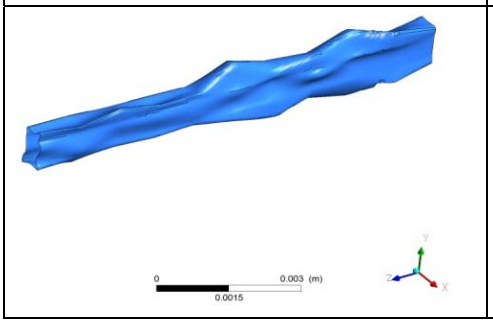	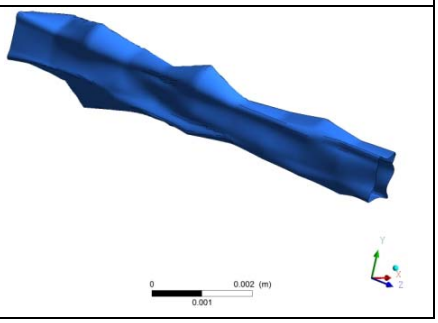

Initial Configuration		Final Configuration	
Bottom	**Top**	**Bottom**	**Top**
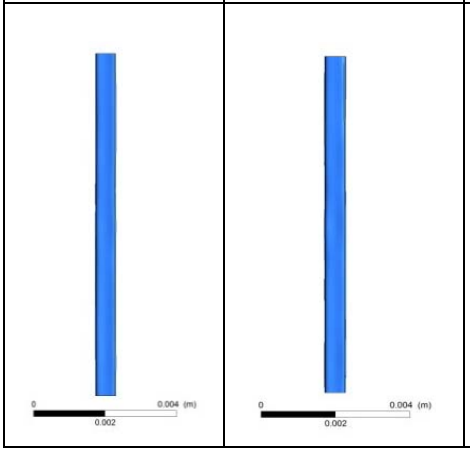			

Figure 3.7 - Views from the four directions of the initial and final configurations.

The comparison of the results between the initial configuration and the final configuration for the substrate consumption and the product formation can be found in Figure 3.6. The comparison between the initial and the final microreactor configurations can be seen in Figure 3.7. The final configuration is characterized by a series of expansions and shrinkages of the surface of the microreactor. From Figure 3.6 and Figure 3.7, it is possible to verify that the curvatures resulted from the optimization procedure have a significant impact on of the two parallel streams and consequently on the reaction yield.

It is also possible to verify that the bottom and the top surfaces suffered greater alterations compared with the lateral surfaces. The displacement of the points of the top and the bottom seem to have a higher importance than the movement of the points on the lateral surfaces.

From the bottom view, it is possible to see that a deep and narrow expansion contributes greatly to the mixing of the two streams and consequently to the product formation. The narrowing of the channel contributes to short diffusion distances of the compounds, and therefore it contributes to the mixing and consequently, to the reaction yield. In fact, the formation of product is higher in the region close to the bottom surface of the microreactor and seems to be related to this deep and narrow deformation of the channel. From the top view, the channel contributes to the mixing inside by introducing a passive mixing form similar to e.g. a staggered herringbone structure. The staggered herringbone and similar forms are structures which have been widely applied in micromixers and reported in the scientific literature. This kind of structures introduces helix shaped streamlines which have a considerable impact on the mixing of parallel streams [108].

From Figure 3.7, it is possible to observe that the first splines in the reaction channel present greater modifications than the splines closer to the outlet. It seems that the first part of the microchannel is more important for the mixing of the streams, and consequently for the reaction yield, since the modifications were more significant in the first part, and there were only minor changes in the last part of the channel. However, this is not completely certain and more investigations would be required to confirm this fact.

With respect to *in situ* product removal strategies and strategies for overcoming the unfavourable equilibrium referred in the beginning of this chapter, the results are inconclusive. The analysis of the results suggests that in this case the mixing plays a more important role for achieving higher yields.

The resulting structure of shape optimization of the YY-microreactor is very complex. The complexity of the shape makes the fabrication of the structure very difficult or impossible and therefore it will not be possible to investigate the final microreactor design experimentally. The achievement of this complex structure was caused by the high number of design variables (points distributed on the microreactor surface), by the various combinations for displacement of the points and by the discontinuous domain which withholds the solution of geometries which did not

fulfil the mesh solver requirements. However, this study allows gathering information which can be useful for the fabrication of microreactors with integrated mixing.

3.3 Concluding remarks

Shape optimization has been often applied in mechanical engineering and only few cases of applications of shape optimization to chemical engineering and microfluidics problems have been reported in the scientific literature. All the reported cases of shape optimization applications to microchannels are only two-dimensional cases. In this chapter, shape optimization is used for optimizing a three-dimensional geometry of a reactor. The presented case study in this chapter corresponds to the evaluation of the influence of the modification of a microreactor channel shape on the reaction yield. In order to achieve this, shape optimization was the technique used to perform this investigation.

The optimization cycle was relatively straightforward to implement in MATLAB® due to the ease of the optimization method. Nonetheless, the automatic mesh setup has been shown to be rather complex due to the implementation strategy to minimize the discontinuity of the domain. The setup of the O-grid was not a simple process and required several attempts to decide for the best strategy for automatic generation of the mesh.

The case study presented in this chapter differs from already presented cases in the literature due to its three-dimensional evaluation with application of a structured mesh with automatic adaption to all the different geometries. The initial configuration of the microreactor was a YY-microreactor which is described by a squared cross section reaction channel with two channels meeting at each end (inlet and outlet) of the reaction channel. The final configuration of the microreactor is a complex structure with many curvatures. The final configuration contributes greatly to the improvement of mixing of the two streams and consequently to the reaction yield improvement. The reaction yield is 8.4 times higher in the final microreactor configuration than in the initial configuration, which is a significant improvement.

The final configuration cannot be easily fabricated due to the complexity of the structure. However, the shape optimization of the microreactor allows the collection of information on how to build a microreactor with a shape that promotes the reaction. Upon the start of the implementation of the case study, there was no information on the impact of the complex kinetics on the reaction yield. From the results of shape optimization, it was possible to identify that the mixing is the most important phenomenon for the product formation in this specific case. The results of this case study are in fact a validation of this shape optimization method since the final configuration resembles a staggered herringbone structure which is a very well-known well-performing passive mixer.

In the scientific literature, it is stated that narrowing of microchannels improves the mixing of parallel streams by diffusion [135]. From this study, it is possible to conclude that although this fact is true, the diffusion process is slow and that mixing by convection is more important in large structures. It is also possible to conclude that the convection mixing stimulated by passive mixing structures inserted on the top and bottom wall contribute the most to the mixing and the product formation. These facts and the results of the case study indicate that shape optimization is a useful tool for optimizing large microchannels.

The final conclusion from this study is therefore that shape optimization allows the investigation of potential intensification strategies in order to build better designed reactors. Although in this case it is not possible to fabricate the final configuration due to the high number of design variables (surface points), nonetheless, this challenge can be overcome by simplifying the shape optimization method. This simplification can be achieved by implementing more restrictions in the optimization procedure which consider the feasibility of fabrication.

Chapter 4

Topology optimization of microreactors

4.1 Introduction

In Chapter 3, the implementation of shape optimization of the structure of a microreactor was presented. The results showed that it is possible to improve the yield of a microreactor by modifying its geometry, however they also demonstrated that the optimal configuration of the reactor was very complex to be fabricated. In this chapter, the investigation for optimization of the microreactor is directed to the phenomena inside the reactor. Therefore, topology optimization is used in order to investigate new modes of configuring the same reactor geometry such as the distribution of the enzyme inside. This method might potentially bring novel applications for designing a reactor.

Topology optimization has been used by mechanical and civil engineers to various mechanical structures and buildings. One of the main purposes behind the topology optimization application in mechanical engineering is related to the minimization of the amount of material that is required while maintaining the mechanical strength of a structure with the overall purpose of minimizing costs. It is a mathematical method, which optimizes the spatial distribution of the material within a domain, by fulfilling given constraints and minimizing/maximizing a predefined cost function.

In topology optimization there are several possibilities to apply the optimization method according to the characteristics of the material, e.g. isotropic or anisotropic material. This project focusses on isotropic material methods using the Isotropic Solid Empty concept. In an ISE method, the elements of the domain are either filled by a particular isotropic material or they are

empty. An isotropic solid is a material for which its physical properties are uniform in all orientations [17].

In the scientific literature, as reviewed in Chapter 2, there are two common techniques for Isotropic Solid and Empty (ISE) optimization: the Solid Isotropic Material with Penalization (SIMP) and the Evolutionary Structural Optimization (ESO).

The SIMP technique is based on the determination of the optimal structure by varying the density of the elements of the domain [2]. The predefined domain is discretized in a number of elements and a finite elements analysis is carried out to determine the structure performance. The cost function is penalized by adding an exponent to the design variable on the objective function. The penalization factor minimizes intermediate values of the design variable and approximates the solution to a discrete solution (0-1 values) [2,48].

The ESO method is based on the concept of progressively removing inefficient material from the studied structure [19]. The unneeded material is removed by using a rejection criterion (RR) [58], which identifies the ineffective material. The design variables are updated and a new finite element analysis is carried out to evaluate the structure performance. The rejection criterion is updated once it has reached the steady-state and the current rejection criterion does not remove more elements from the structure.

In this chapter, the method of the topology optimization of an enzyme distribution inside a microreactor will be established. This method will be an adaptation of the Evolutionary Structure Optimization (ESO). The method will here be used for two-dimensional and three-dimensional case studies. The two-dimensional case study corresponds to the optimization of the enzyme distribution immobilized on the walls of a microreactor. The three-dimensional case study corresponds to the optimization of the immobilized enzyme distribution in a packed bed microreactor.

The use of the topology optimization for microreactors is similar to the shape optimization and has as main goal to show that this method can be a tool for process intensification of microreactors. This tool will identify the bottlenecks of the reactor configurations and make alterations to the microreactor layout in order to improve the product concentration at the outlet. In this way, the optimal, or at least an improved microreactor configuration will be found before testing it in the laboratory. Moreover, it will be possible to gather information about the influence of the position of the enzyme in the microreactor which will be useful for its design.

4.2 The topology optimization method

Topology optimization has previously been applied to microreactors by Okkels and Bruus[118] and Schäpper and his co-workers[119]. They have optimized the immobilized cell distribution on a carrier by optimizing the porosity inside a microreactor.

In this approach the topology optimization will be implemented in a different way. Instead of considering the design variable as the porosity of the immobilization carrier, the design variable will be the concentration of enzyme inside the microreactor. The decision was taken in order to avoid solutions similar to the ones obtained by Okkels and Bruus and Schäpper *et al.* in which the immobilization carrier resulted in large void spaces within the carrier material. These carrier configurations are mechanically unstable and in a real reactor the packing of material at fixed locations would not be possible, since the material would change location due to the flow. Hence, it would not be possible to test these microreactor configurations experimentally. Furthermore, the modification of the carrier porosity results also in a change of the flow profile. As mentioned above, the purpose of applying topology optimization to a microreactor has as main goal to use it as a process intensification tool. Thus, the modification of the flow profile will make the conclusions about the relation between the flow profile and the product formation very difficult or impossible.

The topology optimization method used in this project is an adaptation of the Evolutionary Structural Optimization (ESO) method. As referred above, the design variable for all the case studies in this project is the enzyme concentration inside the microreactor. The cost function corresponds to maximizing the concentration of the product at the outlet of the microreactor. There is only one constraint in these topology optimization problems which is to maintain the amount of enzyme (number of moles) constant inside of the microreactor between iterations. This constraint makes this procedure different from the original ESO method. With the original ESO method the inefficient material is simply removed, but when the enzyme concentration is the design variable, the removal of elements influences the production negatively. When an element is removed the amount of enzyme will be less and the product concentration at the outlet will decrease. Thus, the ESO method has been modified. In this case, when an element is removed the amount of enzyme of that specific element will be distributed between all remaining elements which still contain immobilized enzyme. In this study a maximum concentration of enzyme on the surface is established and the initial concentration of enzyme is always lower than the maximum enzyme concentration.

The general formulation of the optimization problem in this thesis is given by:

$$\begin{aligned} \text{Maximize} \quad & J(C_E) = \dot{m}_{P\,outlet} = Q \times \overline{C_P}\left(C_E\,(x,\,y,z)\right)_{outlet} \\ \text{Subject to} \quad & C_E \leq C_{E\,max} \end{aligned} \tag{4.1}$$

where $\dot{m}_{P\,outlet}$ is the product mass flow rate at the outlet, $\overline{C_P}_{outlet}$ is the average product concentration at the outlet, C_E is the enzyme concentration and design variable which is

dependent of the position in the microreactor, $C_{E\,max}$ is the maximum enzyme concentration in the reactor, x, y, z are the space coordinates and J is the objective function.

In Chapter 2, the evaluation of the elements for a posterior decision of removal in the ESO method was done by evaluating the stress of the element. In this case, a sensitivity analysis is carried out for evaluating the influence of each element on the product concentration at the outlet. The enzyme concentration is varied equally for each element and a result is obtained by solving the system by computational fluid dynamics. A decision about the update of the design variable is made according to the sensitivity analysis results. In the description of the ESO method in Chapter 2, the update of the design variable was made according to an evaluation of stress ratio in relation to the rejection criterion. The stress ratio was defined by the ratio between the stress of the element and the stress of the overall structure. In this case, the ratio corresponds to the sensitivity number which is defined by the ratio between the sensitivity analysis result of the element removal (i.e. the product concentration at the outlet when the element is removed) and the result of the previous iteration (i.e. the product concentration at the outlet when no element is removed). This ratio will from now on be called the concentration ratio. The elements are removed if they satisfy the following condition:

$$\frac{[Product]_{\,element\ j}}{[Product]_{i-1}} > RR_k \tag{4.2}$$

where $[Product]_{\,element\ j}$ is the outlet product concentration when element j is removed, $[Product]_{i-1}$ is the product outlet concentration resulting from the previous iteration and RR_k is the current rejection criterion. An element with high influence is characterized by a larger decrease of outlet product concentration than an element of low influence.

This means that for the least influencing elements, the product concentration at the outlet will vary less and therefore, it will result in high concentration ratios, approximating $\frac{[Product]_{\,element\ j}}{[Product]_{i-1}}$ to 1. So, the elements with the highest concentration ratios will have to be eliminated. It should be emphasized that the concentration ratio has to be higher than the rejection criterion in order for the element j to be rejected.

The rejection criterion varies between 1 and 0 and is maintained constant until the process of removing the elements reaches a steady state, i.e. no more elements can be removed with that specific rejection criterion value. As similar to the original ESO method, when the steady-state is reached the value is updated according to the evolutionary rate. The evolutionary rate (ER) is added to the rejection criterion:

$$RR_{k+1} = RR_k + ER \tag{4.3}$$

The rejection criterion in the beginning of the optimization procedure is set equal to 1, but to eliminate the first elements it is adjusted with the evolutionary rate.

The implementation of the topology optimization method was done by linking two commercially available software modules, MATLAB® and ANSYS CFX®. As described in Chapter 2, ANSYS CFX® is a "black box" box" software and the user has no access to the governing equations, the modelling methods, the numeric methods or the solving methods. Nonetheless, this software has the possibility for writing the mesh files (software ICEM CFD®), the setup file for simulation (software ANSYS CFX-Pre®) and the post-processing files (software ANSYS CFX-Post®) as script files. These script files can be read and manipulated by other softwares such as MATLAB®. MATLAB® converts these script files into arrays and in this way it is possible to modify them. The array can be converted into a file again which can be read by ANSYS CFX®. ANSYS CFX® can then be executed in batch mode from MATLAB® by writing the executing commands. In this way, the user does not need to open the ANSYS CFX® user interface in order to manipulate the files or to execute them. The general procedure used in this project is presented in Figure 4.1. In the studies presented in this thesis, the topology optimization procedure is a routine which couples the simulations in ANSYS CFX® to MATLAB®.

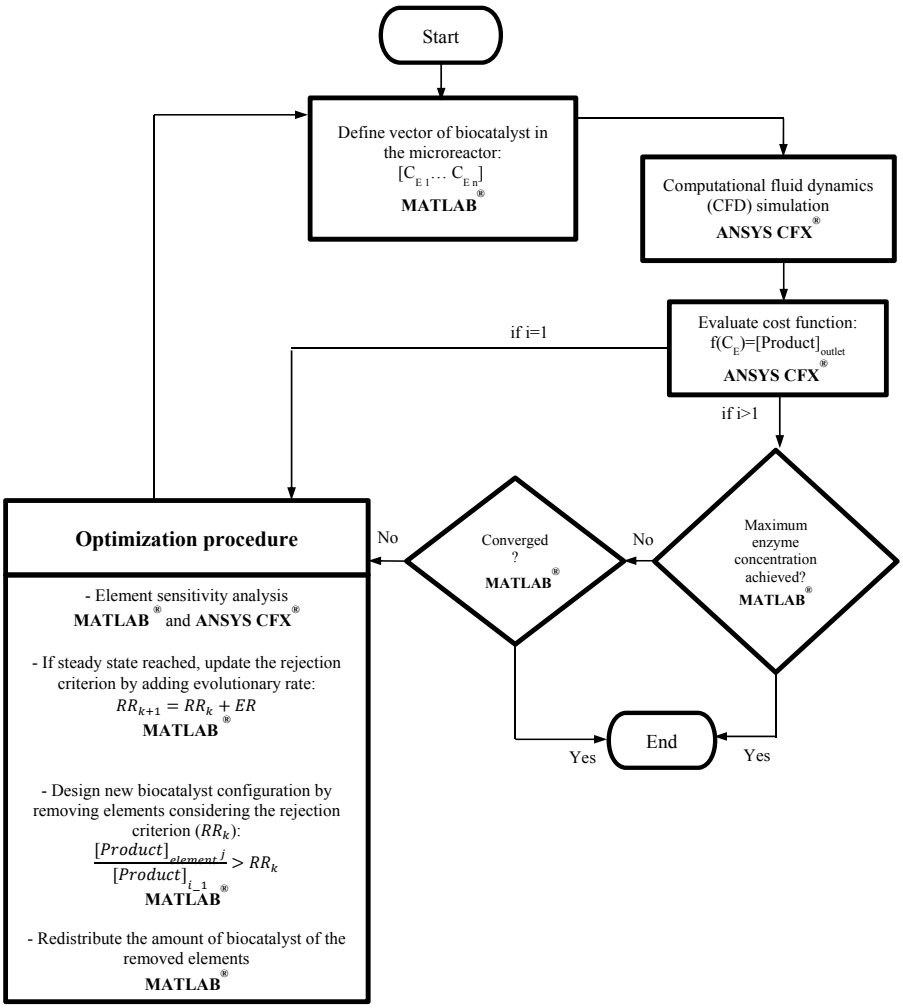

Figure 4.1 – General topology optimization procedure, adaptation of Evolutionary Structural Optimization.

The optimization loop starts by setting a vector in MATLAB® in which the enzyme concentration of the different locations in the microreactor ([C_{E1}…C_{En}]) is defined. The enzyme is initially uniformly distributed in the microreactor at half of the established maximum enzyme concentration. Afterwards, the ANSYS CFX-Pre® script is changed according to the defined vector, a computational fluid dynamics simulation is carried out by ANSYS CFX Solver® and the cost function is evaluated. The optimization procedure starts with a sensitivity analysis of each element in order to evaluate its influence on the product concentration at the outlet. One by one the enzyme concentration of each of the immobilization elements is varied equally. This is controlled by a self-programed routine in MATLAB® which makes the necessary modifications in

the ANSYS CFX-Pre® script while ANSYS CFX® carries out the computational fluid dynamics analysis using the new script.

The MATLAB® code removes the elements with the lowest sensitivity according to a predefined rejection criterion (RR_k). The amount of enzyme present in the removed elements is distributed within all other elements that have not been removed in order to keep the same amount of enzyme (mol) inside the microreactor. Subsequently the alterations of the enzyme configuration inside the microreactor and its new concentration are inserted in the ANSYS CFX® script through MATLAB® and a CFD simulation is repeated to evaluate the performance of the new enzyme distribution. The procedure is repeated until the maximum product concentration is achieved, the concentration of the enzyme has reached the maximum possible value or the optimization converges.

4.3 Case study 1 – Topology optimization for a microreactor with immobilized enzyme on the wall surface

An interesting case for investigating the potential of topology optimization inside an enzymatic microreactor is considering that the biocatalyst is immobilized on the surface of the internal walls. This case study is a two-dimensional investigation of the topology optimization of immobilized enzyme at the inner walls of a microreactor. The considered design variable is the enzyme concentration on the surface which will be spatially distributed during the optimization procedure in order to maintain the total amount (mol) of enzyme on the surface constant. In this way, the method will be used to evaluate the improvement of product concentration at the outlet per same amount of enzyme by modifying the spatial distribution of the immobilized enzyme.

The shape of the investigated microreactor is an extension of the two-dimensional shape presented by Okkels and Bruus[118] into a three-dimensional design. The choice of this microreactor shape was made in order to find similarities between on the enzyme placement in this case study and the cells placement presented in Okkels and Bruus. Moreover, this microreactor shape presents variations of the velocity profile inside the microreactor which will influence the product formation.

4.3.1 Materials and methods

4.3.1.1 Microreactor geometry

The view from the top of the microreactor shows that the microreactor consists of a parallelepiped measuring 30 mm of width and depth, combined with two channels for the inlet and outlet located at opposite sides of the square. The width of the inlet and outlet channels is 10 mm. The height of the microreactor corresponds to 0.25 mm. The microreactor shape is presented in Figure 4.2. The dimensions of this microreactor are much larger than the dimensions presented by Okkels and Bruus [118] who considered the following dimensions: 6 mm of width and 6 mm of depth. The large dimensions were defined in this investigation in order to guarantee that experimental validation would be possible. At very small microreactor dimensions the definition of immobilization areas would be much more complex to perform with an accurate precision.

In this case study, the enzyme is immobilized at the top and bottom surfaces of the reactor. Since the flow profile is symmetric for the central vertical and central horizontal planes, symmetry boundaries were created at half of the height and through the middle of the inlet and outlet as presented in Figure 4.3. In this way only a quarter of the whole microreactor geometry is simulated which provides an acceleration of the computational solution.

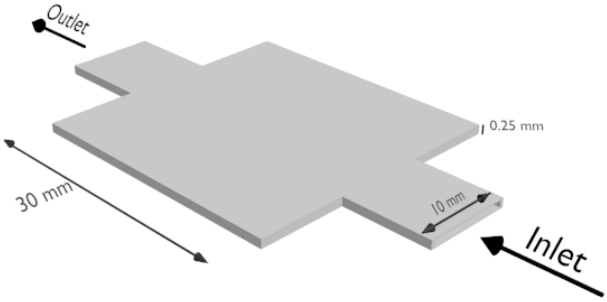

Figure 4.2 – Microreactor configuration with all the dimensions.

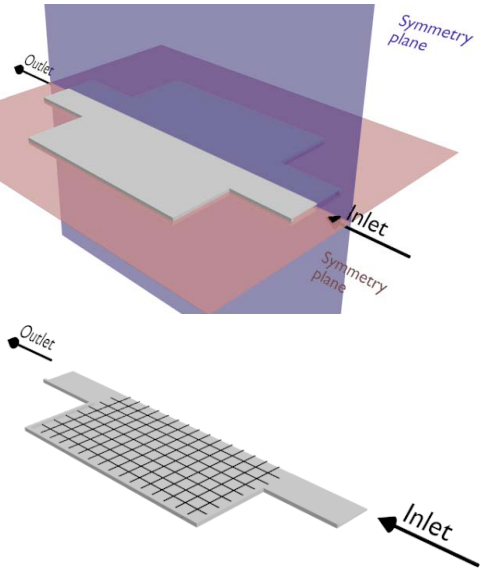

Figure 4.3 – Microreactor configuration: left – with indication of symmetry planes, right: quarter of the microreactor configuration, with all the symmetry planes defined, used in CFD simulations. View of the 128 immobilization elements

The microreactor was simulated considering steady-state mode. The flowrate was defined according to the residence time and the volume of the microreactor (225 µL). The decision for the residence was made such that the residence time of a fluid element would be in average 15 s inside the reaction chamber. The choice for such a low residence time was based on the minimization of the effect of the walls on the velocity profile.

The design of the microreactor was implemented in ANSYS CFX® and for this investigation the bottom surface of the simulated part of the microreactor was divided in small areas, in this case 128 immobilization elements as shown in Figure 4.3.

The surface is divided in 128 small areas which were defined when the geometry was designed and the mesh was set up. The definition of the 128 small areas implied specifying an individual part in the geometry for each of them. In this case, a part in the geometry design corresponds to an area with a specific role in the simulation such as an inlet, outlet, wall or symmetry plane. In this case it was necessary to establish a part for each of the small areas because each of them influences the product formation differently. Therefore, for each of them it was necessary to establish the reaction rate and the concentration of the enzyme on the surface.

This design was laborious since the same procedure for designing and setting up the properties in the small areas had to be repeated 128 times.

The studied reaction rate in this investigation follows the mechanism of an enzyme, which is characterized by Michaelis-Menten mechanism. The Michaelis-Menten reaction equation is described by Equation (4.4):

$$r_P = -r_S = k_{cat} \cdot C_E \frac{[S]}{[S] + K_M} \tag{4.4}$$

where k_{cat} is the turnover number, C_E the enzyme concentration, [S] the substrate concentration and K_M is the Michaelis-Menten constant.

The considered reaction parameter values for this case study are summarized in Table 4.1:

Table 4.1 – Summary of reaction parameters, $\boldsymbol{k_{cat}}$ and $\boldsymbol{K_M}$.

Parameter	Value
$\boldsymbol{k_{cat}}$	100 s^{-1}
$\boldsymbol{K_M}$	25 mM

The enzyme concentration on the surface was determined considering that the diameter of an enzyme molecule is 10 nm [136]. From the area of a molecule ($7.85 \cdot 10^{-17}$ m^2), the maximum concentration of enzyme that can be immobilized is $2.12 \cdot 10^{-8}$ $mol \cdot m^2$. The substrate concentration at the inlet is 10 mM. Both substrate and product were considered to be fast diffusers and their diffusion coefficients were considered to be $1 \cdot 10^{-9}$ $m^2 \cdot s^{-1}$.

4.3.1.2 Topology optimization procedure

The problem formulation of this two-dimensional topology optimization problem is given by:

$$\begin{aligned} \text{Maximize} \quad & J(C_E) = \dot{m}_{P\,outlet} = Q \times \overline{C_P}\left(C_E\,(x, y)\right)_{outlet} \\ \text{Subject to} \quad & C_E \leq C_{E\,max} \end{aligned} \tag{4.5}$$

where $\dot{m}_{P\,outlet}$ is the product mass flowrate at the outlet, $\overline{C_P}_{outlet}$ is the average product concentration at the outlet, C_E is the enzyme concentration and design variable which is dependent of the position in the microreactor, $C_{E\,max}$ is the maximum enzyme concentration on the surface, x, y are the space coordinates and J is the objective function.

The optimization procedure followed the layout of the method presented in the previous section. The optimization cycle starts by distributing uniformly the enzyme at half of the maximum concentration on the top and bottom surfaces of the microreactor, $1.06 \cdot 10^{-8}$ mol·m^{-2}. The enzyme concentration of the different locations on the microreactor ([$C_{E1} \ldots C_{E\,128}$]) is defined by a vector in MATLAB®. The optimization loop starts by modifying the ANSYS CFX-Pre® script according to the defined enzyme concentration vector. Afterwards, a computational fluid dynamics simulation is carried out by ANSYS CFX® and the cost function is evaluated. The optimization technique starts by performing a sensitivity analysis of each immobilization element according to the procedure described in the previous section of this chapter. The removal of the elements is performed according to the results from the sensitivity analysis. As stated in the previous section, the optimization cycle is repeated until the maximum enzyme concentration is achieved or the optimization converges.

4.3.2 Results and discussion

The optimization cycle ended when the maximum enzyme concentration ($2.12 \cdot 10^{-8}$ mol·m^2) was achieved. On the one hand, $2.92 \cdot 10^{-2}$ mM of product was formed with the initial enzyme configuration, on the other hand $3.06 \cdot 10^{-2}$ mM of product were formed with the final configuration. In the end, the topology optimization resulted in an improvement by 4.8% of the product formation per same amount (mol) of enzyme compared with the initial enzyme configuration. The reader should note that the amount of enzyme (mol) is the same inside the microreactor volume for both initial and final configurations. The concentration of the enzyme on the surface of the final configuration is twice more than in the initial configuration. However, the immobilization surface area is half in the final configuration than in the initial configuration and therefore the amount of enzyme (mol) is kept constant. A summary of the results is shown in Table 4.2.

Table 4.2 – Summary of results of two-dimensional topology optimization case study.

Configuration	Parameter	Value
Initial configuration	Enzyme concentration	$1.06 \cdot 10^{-8}$ mol·m^{-2}
	Product concentration	$2.92 \cdot 10^{-2}$ mol·m^{-3}
Final configuration	Enzyme concentration	$2.12 \cdot 10^{-8}$ mol·m^{-2}
	Product concentration	$3.06 \cdot 10^{-2}$ mol·m^{-3}
Improvement: 4.8%		

The enzyme distribution for the initial configuration and for the final configuration can be found in Figure 4.4. Moreover, an overview of the product formation for the initial and the final configurations can also be found in Figure 4.4.

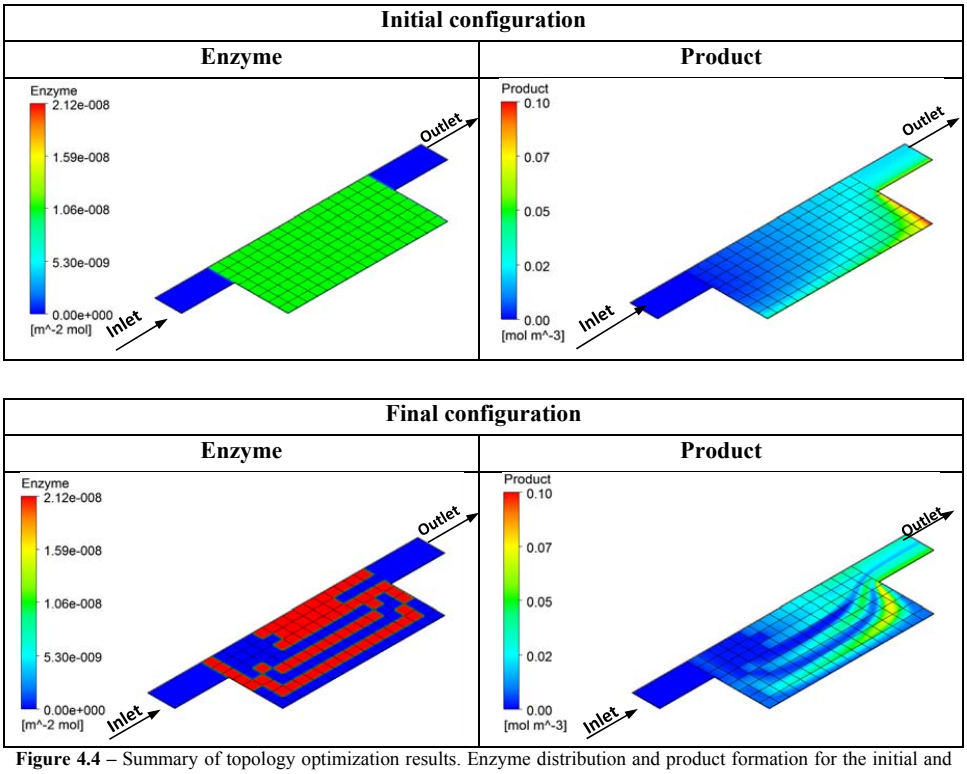

Figure 4.4 – Summary of topology optimization results. Enzyme distribution and product formation for the initial and final configurations.

The optimized distribution of the enzyme is characterized by the immobilization of enzyme at the areas close to the wall. In the final configuration, the enzyme is mostly immobilized at specific streams in the high residence time region, i.e. the area close to the side walls. From these results, it is possible to conclude that areas of higher residence time streams play a role in the product formation. This demonstrates that immobilized enzyme molecules at locations of higher residence time contribute more to the product formation. In these areas, the flow velocity is lower and therefore, the contact between the substrate and the enzyme is longer which contributes for higher product formation.

The final configuration of the enzyme distribution resembles the final configurations obtained by Okkels and Bruus [118] and Schäpper *et al.* [119]. These configurations can be found in Chapter 2 in the literature review on topology optimization of microreactors. Similarly to the configurations presented in the scientific literature, the distribution of the enzyme is made at concentric lines which are wider close to the side walls and decrease in diameter towards the reaction chamber center.

From the results of this optimization, it is possible to verify that areas situated in the corners of the reactor do not have a significant influence on the concentration of the product at the outlet. However, from the initial configuration it is possible to verify that high product concentration was present in the corner closer to the outlet. In fact, it seems that there is an accumulation of product in the corner close to the outlet due to convective mass transport limitations which are caused by the low flow velocity in those areas. Consequently, these elements do not contribute as much to the product at the outlet although the residence time of the compounds in these regions is high. This also shows that the analysis of the CFD results of a non-optimized configuration on its own does not give indications on the best way to immobilize the enzyme at the reactor surface. Furthermore, this also emphasizes the importance of topology optimization as a design tool for achieving process intensification of reactors.

In this specific case the improvement of the microreactor was minimal and it would not be worth it to fabricate it for validation purposes. Nonetheless, this method offers academic value and with this example it could still be proven that the topology optimization method can be used for intensification of microreactors.

4.4 Case study 2 – Topology optimization for a microreactor with immobilized enzyme in a packed bed

The microreactor in this investigation is considered to be a packed-bed reactor with immobilized enzyme on the surface of the packed bed.

After presenting the solution for a case of two-dimensional topology optimization, the next step is the investigation for the possible optimization of product formation in a three-dimensional domain. Moreover, this study will allow evaluating the influence of the flow profile on the product formation in the whole volume of the microreactor.

In this case study, the microreactor shape is different from the previous chosen case study A non-symmetric shape was selected in order to obtain a variation of velocities inside the reaction chamber and evaluate its influence on the reaction yield.

4.4.1 Materials and methods

4.4.1.1 Microreactor geometry

The shape of the studied microreactor is a square reaction chamber with an inlet and an outlet. The inlet is located in one of the corners of the reaction chamber. The outlet is located on the diagonally opposite corner of the inlet of the reaction chamber. The square reaction chamber is 5 mm wide at each side and the height of the chamber is 1 mm. The width of the inlet and outlet is 0.25 mm. The shape of the microreactor of this case study can be found in Figure 4.5. The choice of this reactor shape relied on the fact that this shape will create a non-uniform and asymmetric velocity profile with areas of high velocity (middle of the reactor) and areas of low velocity (corners and areas close to the walls).

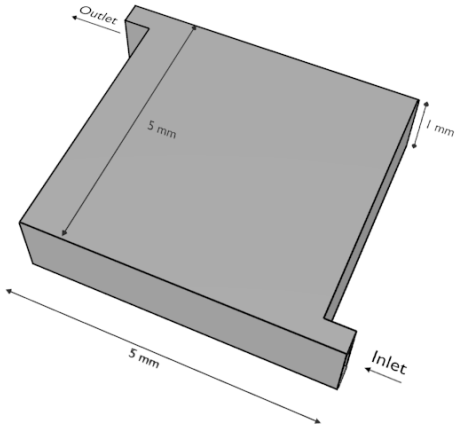

Figure 4.5 – Microreactor configuration with indication regarding dimensions.

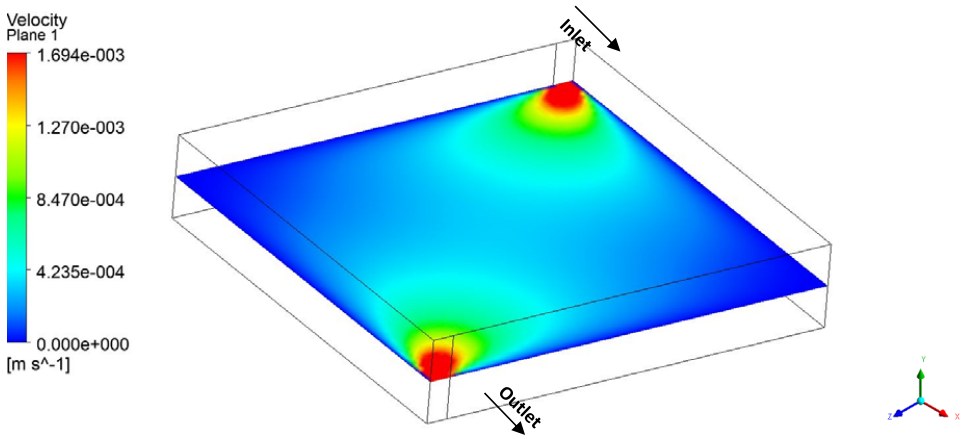

Figure 4.6 – Velocity profile on the mid height plane of the reaction chamber for average residence time of 100 s (average flowrate 15 μL·min^{-1}).

The velocity profile of the microreactor under steady-state operation on a plane at mid height of the reactor chamber can be found in Figure 4.6. The microreactor was in this case simulated as a whole and therefore, symmetry planes were not implemented.

In this case study the enzyme is immobilized on the surface of the packed bed reactor and it was assumed that the porosity of this packed bed reactor was 0.3. The porosity is defined by the ratio of void volume (fluid) and solid volume (packed bed) in the microreactor.

Similar to the two-dimensional case study, the flow rate was defined according to the residence time and the volume of the reaction chamber. The choice of the residence time/flow rate was made in order to create a gradient in the momentum inside the microreactor.

The studied reaction rate follows the same mechanism as the one used in the previous case study, i.e. Michaelis-Menten kinetics.

The enzyme concentration on the surface is calculated considering that the diameter of an enzyme molecule is 10 nm. The packed bed was constituted by non-porous spheres of 100 μm, so the enzyme is only immobilized at the external surface of the spheres. From the area of a molecule ($7.85 \cdot 10^{-17}$ m^2) and the specific area of one sphere (60000 m$^2 \cdot$m^{-3}), the maximum concentration of immobilized enzyme is calculated to be $1.27 \cdot 10^{-3}$ mol·m^3. Both substrate and product are considered to be diffusing fast and their diffusion coefficients are $1 \cdot 10^{-9}$ m$^2 \cdot$s^{-1}.

Two analyses are performed for this structure, Analysis 1 with a substrate concentration at the inlet of 10 mM and a residence time of 100 s and Analysis 2 with a substrate concentration at the inlet of 60 mM and a residence time of 1600 s. These settings will permit to analyze the distribution of enzyme as function of the reaction rate. In Analysis 2, the concentration of substrate is higher than the Michaelis-Menten constant

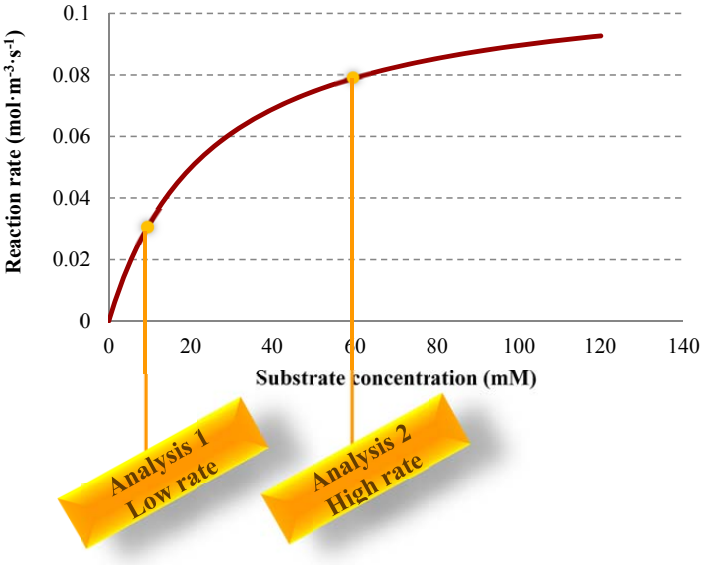

Figure 4.7 – Reaction rate as function of the substrate concentration.

(K_M=25 mM) and therefore the reaction rate will be much higher compared with Analysis 1, for which the substrate concentration is 10 mM (See Figure 4.7).

4.4.1.2 Topology optimization procedure

The problem formulation of this three-dimensional topology optimization problem is given by:

$$\begin{aligned} \text{Maximize} \quad & J(C_E) = \dot{m}_{P\,outlet} = Q \times \overline{C_P}\left(C_E\,(x,\,y,z)\right)_{outlet} \\ \text{Subject to} \quad & C_E \leq C_{E\,max} \end{aligned} \tag{4.6}$$

where $\dot{m}_{P\,outlet}$ is the product mass flow rate at the outlet, $\overline{C_P}_{outlet}$ is the average product concentration at the outlet, C_E is the enzyme concentration and design variable which is dependent of the position in the microreactor, $C_{E\,max}$ is the maximum enzyme concentration in the packed bed microreactor, x, y, z are the spatial coordinates and J is the objective function.

The design of the microreactor was implemented in ANSYS CFX® and for this investigation the volume of the reaction chamber was divided into small volumes. These volumes are entered in the setup of the simulation (ANSYS CFX-Pre®) by implementing a Matrix function. The Matrix function gives the opportunity for dividing the volume of the geometry in smaller volumes and defining parameters or properties in these volumes (enzyme concentration, reaction rates, velocities…). In this case, the Matrix function defines the coordinates of each immobilization volume center and the definition of the placement of the enzyme. The number of volumes defines

the size of the immobilization volumes, and thus the higher the number of center points is, the smaller the immobilization elements are. In the Matrix function the placement of the enzymes in the microreactor is established by the value 1 in case there is enzyme in the immobilization volume and by the value 0 in case there is no enzyme. In this way the Matrix function works as a discrete switch indicating the presence or absence of enzyme in the volume. This function is then afterwards multiplied by the enzyme concentration which in turn takes part in the reaction rate equation (4.4).

For demonstration purpose a microchannel with a squared cross section (5 mm width, 5 mm depth and 1 mm height) is considered. The inlet and outlet are at each end of the channel and have the same dimensions as the cross section of the microchannel. The microchannel is divided into 9 immobilization volumes; these volumes are distributed in the following manner 3 in the x direction, 3 in the z direction and 1 in the y direction. In Figure 4.8, three representations of the product formation in the same microreactor are presented considering different enzyme immobilization patterns.

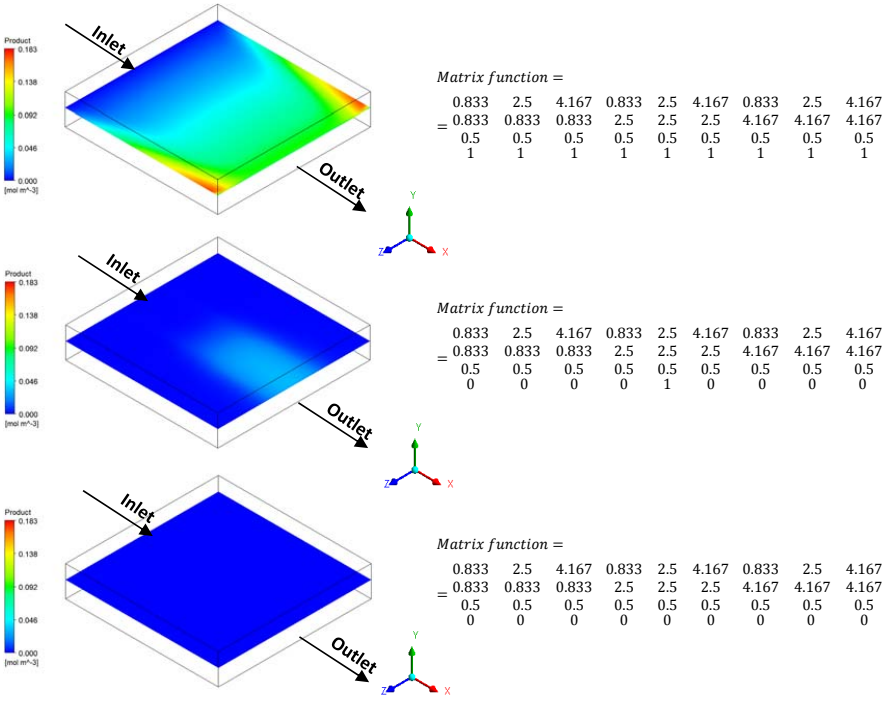

Figure 4.8 – Three configurations of immobilized enzyme in the microreactor with respective setup Matrix functions. Top figure: enzyme immobilized on all immobilization volumes, middle figure: microchannel with immobilized enzyme only on the middle immobilization volume (element 5) and bottom figure: no enzyme immobilized on the immobilization volumes.

The top figure corresponds to the product formation considering that enzyme is well-distributed in all immobilization volumes. The middle figure corresponds to the product formation in case there is only enzyme immobilized in the volume at the center of the microreactor. The bottom figure corresponds to the extreme situation where no enzyme is immobilized in any of the volumes. The Matrix function corresponding to each case is presented on the right side of the respective figure. The first three rows of the matrix are the coordinates (in mm) of the center of the immobilization elements and the fourth row corresponds to the discrete placement of enzyme which is defined by either the value 1 or 0.

The definition of the number of immobilization volumes, their placement and the definition of the coordinates of the immobilization volumes center are established in MATLAB® which transfers these data into the ANSYS CFX-Pre® script.

In this case study the microreactor volume was divided into 196 immobilization volumes, which were placed according to the following distribution: 7 volumes in the x direction, 7 volumes in the z direction and 4 volumes in the y direction.

The optimization procedure followed the layout of the method presented in the first section of this chapter – *4.1 Topology Optimization Method*. The optimization cycle starts with a uniform enzyme distribution at half of the maximum concentration at the packed bed surface, $6.34 \cdot 10^{-4}$ $mol \cdot m^{-2}$. Afterwards, the ANSYS CFX-Pre® script is changed according to the defined Matrix function, a computational fluid dynamic simulation is carried out by ANSYS CFX® and the cost function is evaluated. The optimization routine starts by performing a sensitivity analysis for each immobilization element and the decision of the removal of elements is made. Afterwards, the update for the locations of immobilized enzyme is made and the distribution of the removed enzyme over all the other elements is performed by MATLAB®. The CFD script files are updated and the new configuration is evaluated by ANSYS CFX®. The optimization cycle is repeated until the maximum enzyme concentration is achieved or the optimization converges.

4.4.2 Results and discussion

The topology optimization routine for the Analysis 1 (10 mM substrate at inlet) finished when the maximum enzyme concentration was achieved. The initial enzyme configuration in the microreactor resulted in the formation of 1.40 mM of product and the final enzyme configuration in the microreactor resulted in the formation of 1.57 mM of product. In the end the topology optimization resulted in an improvement of 12% of the amount of product at the outlet of the reactor per same amount (mol) of enzyme by modifying solely the spatial distribution of enzyme in the microreactor. Table 4.3 comprises a summary of these results.

Table 4.3 – Summary of results of three-dimensional topology optimization of Analysis 1: enzyme and product concentration at the outlet for the initial and final configurations.

Configuration	Parameter	Value
Initial configuration	Enzyme concentration	$6.34 \cdot 10^{-4}$ mol·m^{-3}
	Product concentration	1.40 mol·m^{-3}
Final configuration	Enzyme concentration	$1.27 \cdot 10^{-3}$ mol·m^{-3}
	Product concentration	1.57 mol·m^{-3}
Improvement: 12%		

The distribution of the enzyme for the initial and final configurations is presented in Figure 4.9 with the respective concentrations. Each point of the enzyme distribution representation corresponds to the position of the center of the immobilization volume.

An overview of the product formation for both initial and final enzyme distribution is presented in Figure 4.9. Analyzing the overview of the product formation in the initial configuration, it is possible to verify that the highest product concentration is observed in the corners of the reaction chamber. This fact suggests that the product formation occurs essentially in volumes of higher residence time, due to the lower flow velocity in these parts of the reactor which promotes the product formation. However, the results of topology optimization showed that the production in the corner of the reactor opposite to the inlet does not contribute significantly to the product concentration at the outlet; it was more the result of product accumulation and poor mixing.

Moreover, the overview also indicates that the low residence time streams across the middle of the reaction chamber do not contribute that much either to the production formation. Therefore, the outcome of the topology optimization shows that the enzyme should be rather placed in the corner in front of the outlet.

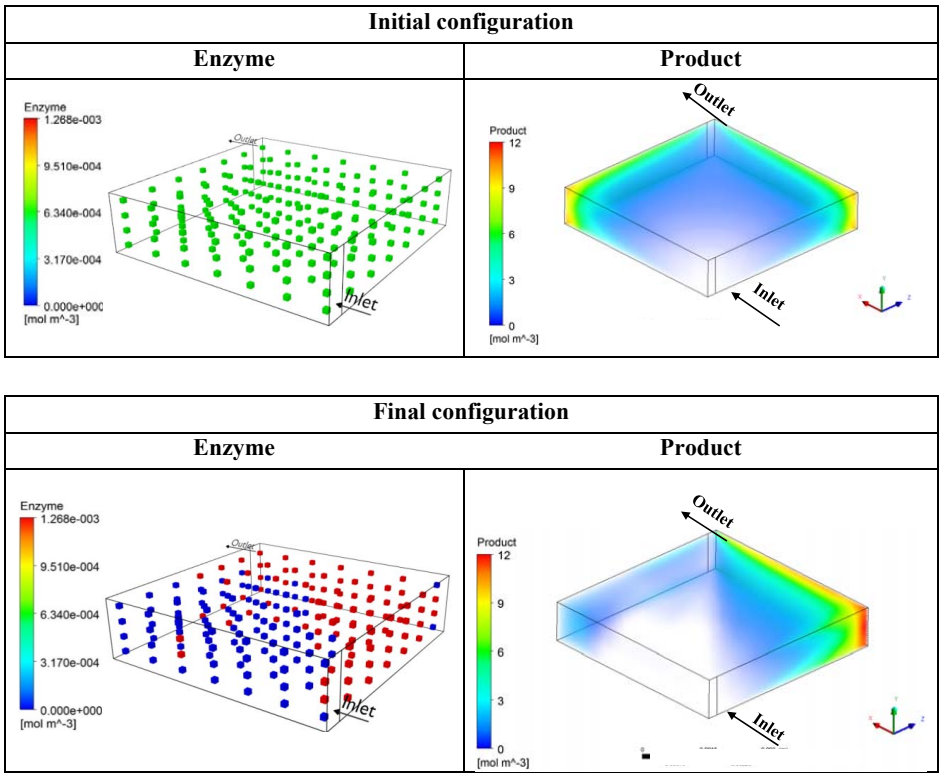

Figure 4.9 – Summary of topology optimization results for Analysis 1. Enzyme distribution and product formation for the initial and final configurations.

Moreover, the overview also indicates that the low residence time streams across the middle of the reaction chamber do not contribute that much either to the production formation. Therefore, the outcome of the topology optimization shows that the enzyme should be rather placed in the corner in front of the outlet.

The topology optimization routine for the Analysis 2 (60 mM substrate inlet) has finished when the maximum concentration of enzyme ($1.27 \cdot 10^{-3}$ mM) was achieved. The initial enzyme configuration in the microreactor resulted in the formation of 36.5 mM of product and the final enzyme configuration in the microreactor resulted in the formation of 39.2 mM. In the end the topology optimization resulted in an improvement of 7% in terms of the product concentration at the outlet by keeping the amount of enzyme constant. This can be achieved by modifying solely the distribution of the placement of the enzyme in the microreactor. These results are summarized in Table 4.4.

The improvement in the case with high substrate concentration was lower compared with the case with lower substrate at the inlet. A possible explanation for this is the lower flow rate that was used in this second case, relative to Analysis 1.

Table 4.4 – Summary of results of three-dimensional topology optimization of Analysis 2: enzyme and product concentration at the outlet for the initial and final configurations.

Configuration	Parameter	Value
Initial configuration	Enzyme concentration	$6.34 \cdot 10^{-4}$ mM
	Product concentration	36.5 mM
Final configuration	Enzyme concentration	$1.27 \cdot 10^{-3}$ mM
	Product concentration	39.2 mM
Improvement: 7.1%		

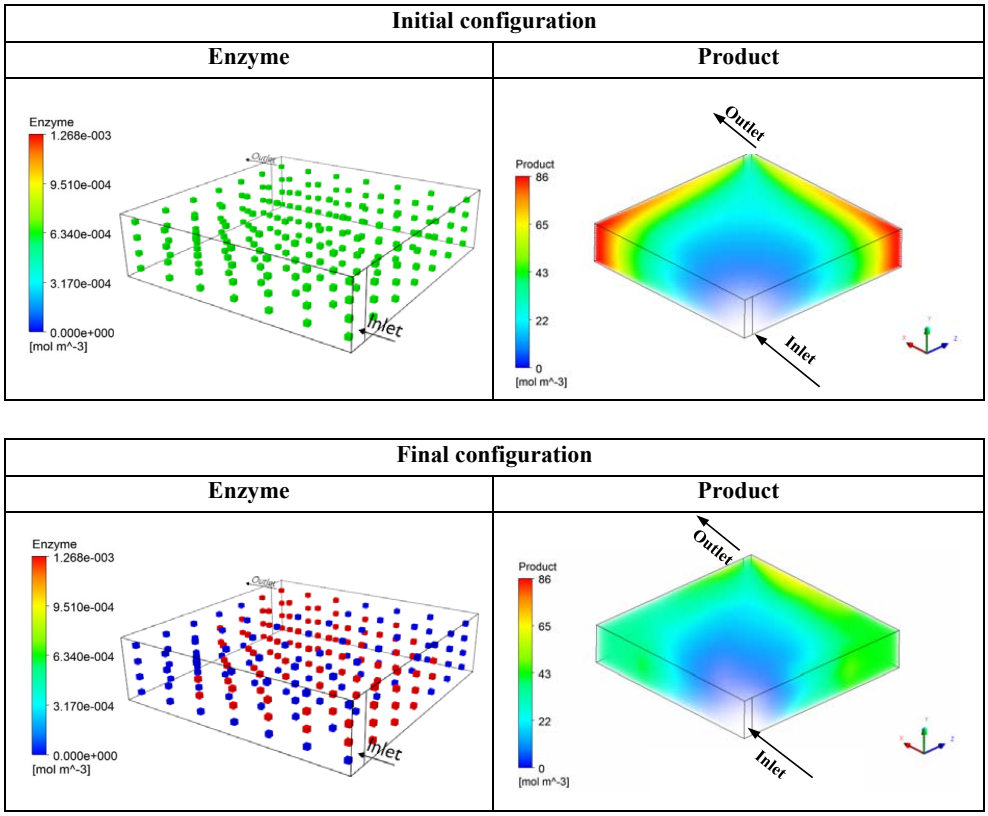

Figure 4.10 – Summary of topology optimization results for Analysis 2. Enzyme distribution and product formation for the initial and final configurations.

In this analysis, the velocity gradients inside the microreactor are lower due to the low flow rate. This has as consequence that the difference in the residence times between the streams is small. Therefore, the contact time of the enzyme and substrate is similar within streams and there is not much difference in the influence on product formation between the streams.

From the detailed view of the product formation in Figure 4.10, it also seems that the production is higher in the corners of the reaction chamber, but also that the product concentration is higher towards the chamber center compared with the case of Analysis 1.

According to the results of the topology optimization it seems that the enzyme should be preferably placed in the center of the reaction chamber. Moreover, it seems that the areas closer to the top and the bottom surfaces of the reactor chamber together with the corner in front of the inlet are the locations which contribute the least to the product concentration at the outlet.

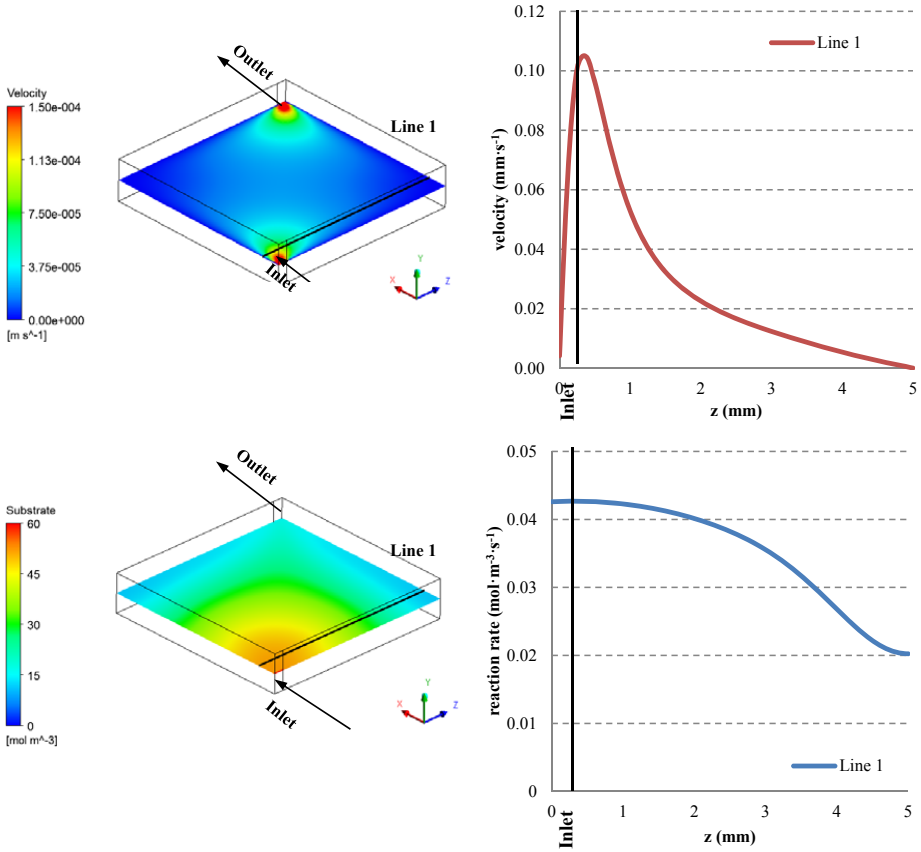

Figure 4.11 – Velocity profile and substrate concentration for the initial configuration at the plane y=0.5 mm. Top to the left: velocity profile; Top to the right: velocity in one line specified on the plane (Line 1: x=0.5 mm, y=0.5 mm, z between 0 and 5 mm); Bottom to the left: substrate concentration profile; Bottom to the right: substrate concentration for Line 1.

In this case, the low residence time streams seem to contribute more favorably to the product formation. The substrate mass transfer limitations seem to influence the placement of the enzyme at the low residence time volumes.

The concentration and the velocity profiles of the initial configuration in a plane at 0.5 mm height are presented respectively on the top left and bottom left figures in Figure 4.11.

Using ANSYS CFX-Post®, a line was traced along this streamline towards the outlet as presented in Figure 4.11. The Line 1 is located at the intersection of the height plane at 0.5 mm and the depth plane at 0.5 mm. The top right and bottom right figures correspond to the velocity and local reaction rate variations, respectively, along the microreactor width on Line 1. The local reaction rate was calculated from the local substrate concentration, the enzyme concentration and the kinetic parameters.

Analysing these figures it is possible to verify that for the high residence time volumes (z = 5 mm) a considerable part of the substrate is converted due to the combination of the fast reaction rate and low flow rate. Therefore, due to mass transfer limitations the concentration of substrate in these areas will be low, and consequently the local reaction rate will be slow and will not contribute considerably to the product formation. In contrast, at low residence time volumes (e. g. z=0 in Line 1) the substrate concentration is large and therefore the local reaction rate is high and consequently contributes greatly to the product formation.

4.5 Concluding remarks

In this chapter, a new setup of the topology optimization method is applied to microreactors using an adaptation of the Evolutionary Structural Optimization method. This method considers the design variable as the concentration of enzyme instead of the carrier porosity as presented by Okkels and Bruus and Schäpper *et al*.. The definition of enzyme concentration as the design variable offers the possibility to establish more realistic problems which can be tested in the laboratory whereas the cases reported in the literature resulted in structures which cannot be fabricated. Moreover, in this method, the flow profile is maintained constant which allows gathering the information regarding the influence of the flow profile on the product formation. This aspect will be further investigated and commented in Chapter 5 in the experimental validation of the topology optimization results.

This topology optimization procedure is an adaptation of the Evolutionary Structural Optimization (ESO) method established by Xie and Steven in 1993. The ESO method was modified such that when an element is eliminated the enzyme amount would be the same. Otherwise, the elimination of unneeded elements would also result in a removal of enzyme and therewith would reduce the product formation. Thus, upon the removal of elements, the enzyme of those elements is redistributed to those elements which still contain immobilized enzyme.

Comparing the implementation of the topology method with the application of the shape optimization method, the latter was easier to implement due to the simplicity of the gradient-free method. Nonetheless, the gradient-based method applied to topology optimization allowed faster achievement of results. Moreover, the topology optimization method did not need the modification of the reactor geometry and adaptation of the mesh. This fact is one of the great advantages of the topology optimization techniques and one of the reasons for the greater focus on topology optimization techniques among the structural optimization experts.

In this chapter, topology optimization was implemented for a two-dimensional case study and for a three-dimensional case study. Furthermore, the three-dimensional case study included two analyses of the same microreactor shape. In the first analysis, the substrate concentration at the inlet (10 mM) was considered to be lower than the Michaelis-Menten constant (25 mM) and the average residence time would be 100 s. In the second analysis, the substrate concentration at the inlet (60 mM) was considered to be higher than the Michaelis-Menten constant (25 mM) and the average residence time would be 1600 s.

The results for the two-dimensional study demonstrated that the more important elements in the systems are in the areas of high residence time streams in the microreactor. However, not all elements positioned at high residence time regions are equally important. The corners of the reaction chamber did not influence the product concentration at the outlet although the initial configuration suggested that they were important areas due to the product accumulation.

From the three-dimensional implementation it was possible to conclude that the ideal placement of the enzyme also depends on the reaction conditions such as high or low reaction rate and on flow conditions which might contribute to mass transfer limitations in the microreactor as could be seen in the Analysis 2.

The first analysis showed that the product formation overview it is not always possible to deduce the best placement of the enzyme in the reactor. In the initial configuration the corner opposite to the inlet demonstrated to be contributing to the product formation. However, in the final configuration this area was in fact inefficient since the product formation was not contributing to the concentration of product leaving the reactor.

The second analysis showed that the high residence time streams are not always the streams which influence the product formation. In this investigation, due to mass transfer limitations the enzyme should be placed in the areas with low residence time flow streams.

The results of the three-dimensional topology optimization analyses indicated to yield a higher improvement of the product formation than the two-dimensional topology optimization. From these results it is possible to conclude that the velocity profile and the effect of the walls play an important role in the improvement of the production. Therefore, it is important to consider this aspect when setting up a topology optimization problem.

The interaction between the reaction rate, the locally different residence times, the flow profile and the local substrate concentrations has a complex influence on the product formation. Thus, it is difficult to decide by simply looking at simulation results, where the best regions to place the enzyme are in the system. The optimization method was able to improve for all three case studies the product formation although each case needed a different immobilization configuration.

In Chapter 5, the experimental validation approach of the topology optimization will be presented. The experimental investigations will be presented for both a two-dimensional and a three-dimensional case study. The fabrication of the packed bed reactor and the placement of the particles with immobilized enzyme might be rather complex to implement and is therefore not further pursued. Further investigations will be performed in order to validate a topology optimization for a simpler case study in three dimensions.

From the implementation of the topology optimization into the above case studies it was possible to verify that the configuration of the enzyme inside plays an important role on the product yield. The evolution of the initial configuration to the final configuration showed the different bottlenecks of the initial configurations and the ideal areas in the microreactor to place the enzyme. In this way, it is possible to verify that topology optimization is a useful tool for intensification in microreactors. The method can serve as a tool which can be applied to design or retrofit existing reactors. The design is adapted according to the reaction and flow conditions instead of adapting a well-known design to the reaction system.

Chapter 5

Intensified microreactors – comparison of simulation and experimental results

5.1 Introduction

In Chapter 4, the topology optimization of microreactors has only been shown through computational fluid dynamic simulations. Although the computational topology optimization can be very helpful to find better performing reactors, only the experimental validation can really provide proof that this method can in fact have practical value when applied to seek for intensification of reactors.

The purpose of this chapter is to perform an experimental study on the influence of topology in microreactors on the performance. This investigation is performed through two case studies: first an investigation of the microreactor with immobilized enzyme on the wall surface presented in Chapter 4, second the analysis of a topology optimized square shaped cross-section channel with free enzyme in the solution. The first case study is more an investigation with academic value and serves for validation of the topology optimization method. The second case study focuses on how to use an existing microreactor platform and how to intensify the operation with the help of topology optimization.

This chapter is divided in three sections which give an overview of all the necessary steps that were taken in order to perform the computational fluid dynamic optimization and the experimental validation of the intensified microreactors. The first section is a characterization of the chosen reaction system, the oxidation of 2,2'-Azino-bis(3-Ethylbenzthiazoline-6-Sulfonic

Acid) (ABTS) to its radical form catalyzed by a peroxidase enzyme. In this section the kinetic parameters V_{max}, K_M and k_{cat} will be determined experimentally.

The following two sections present respectively the two case studies. Each case study description includes the presentation of the CFD setup with the implemented kinetic mechanism and the results of the topology optimization using simulations of the system. Moreover each case study includes also the experimental investigation for verification of the microreactor topology optimization results.

5.2 Characterization of the reaction system

As mentioned above the chosen reaction to validate the CFD topology optimization results is the reduction of hydrogen peroxide by oxidation of 2,2'-azino-bis(3-ethylbenzthiazoline-6-sulfonic acid) (ABTS) to its radical form catalyzed by horseradish peroxidase (E.C. 1.11.1.7). The radical form of ABTS presents a green color in solution and absorbs at a wavelength of 414 nm. The molar absorption coefficient for the radical form of ABTS at the wavelength 414 nm is reported in the scientific literature and corresponds to the value 31100 M^{-1} cm^{-1} [137].

The reaction system is presented in Figure 5.1:

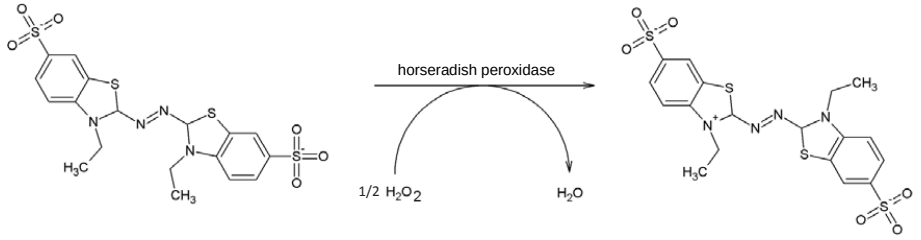

Figure 5.1 – Reaction system: peroxidase-catalyzed reduction of hydrogen peroxide by oxidation of 2,2'-azino-bis(3-ethylbenzthiazoline-6-sulfonic acid) (ABTS)

Enzymes are known to follow a Michaelis-Menten kinetic mechanism which represents the conversion of one substrate catalyzed by an enzyme. This reaction mechanism is given by:

$$v = \frac{d[P]}{dt} = -\frac{d[S]}{dt} = V_{max}\frac{[S]}{[S]+K_M} = k_{cat}[E]\frac{[S]}{[S]+K_M} \tag{5.1}$$

where $[P]$ is the product concentration, $[S]$ is the substrate concentration, V_{max} corresponds to the maximum reaction rate, K_M is the Michaelis-Menten constant which corresponds to the concentration at which the reaction rate is half of V_{max}, $[E]$ is the enzyme concentration and k_{cat} is the turnover number. Although, this mechanism is very well-known, there are only few reactions that follow it. Enzymatic reactions with two or more substrates do not follow the Michaelis-Menten mechanism.

According to the scientific literature, horseradish peroxidase follows the ping pong bi bi kinetic mechanism [138–140]. Thus, a reaction rate equation for the ping pong bi bi kinetic mechanism for the oxidation of ABTS catalyzed by horseradish peroxidase is given by:

$$v = k_{cat}[E]\frac{[H_2O_2][ABTS]}{K_M^{H_2O_2}[ABTS] + K_M^{ABTS}[H_2O_2] + [H_2O_2][ABTS]} \tag{5.2}$$

The relation between the reaction rate of an enzymatic reaction with two substrates (A and B) which follows the ping pong bi bi mechanism and the substrate concentrations is presented in Figure 5.2.

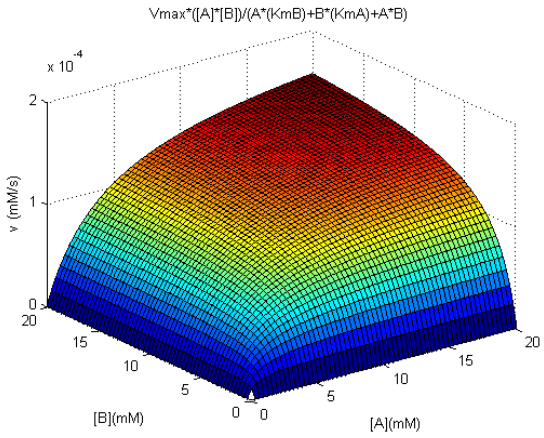

Figure 5.2 – Enzymatic reaction rate calculated according to the ping pong bi bi mechanism for different concentrations of the substrates ***A*** and ***B***.

From Figure 5.2 it is possible to verify that when the concentration of B is constant the reaction follows the Michaelis-Menten mechanism:

$$v = V_{max,app}\frac{[A]}{K_{M,app} + [A]} \tag{5.3}$$

So, if the concentration of H_2O_2 is maintained constant, the Equation (5.1) becomes:

$$v = \mathrm{V}_{\mathrm{max,app}}^{\mathrm{ABTS}}\frac{[ABTS]}{K_{M,app}^{ABTS} + [ABTS]} \tag{5.4}$$

where $\mathrm{V}_{\mathrm{max,app}}^{\mathrm{ABTS}} = \frac{V_{max}[H_2O_2]}{[H_2O_2]+K_M^{H_2O_2}}$ and $K_{M,app}^{ABTS} = \frac{K_M^{ABTS}[H_2O_2]}{[H_2O_2]+K_M^{H_2O_2}}$

In this study, it was decided to use a high hydrogen peroxide concentration in all experiments in order to keep the concentration constant. In this way, it is possible to simplify the reaction model

to the Michaelis-Menten model and to determine the apparent values of the maximum reaction rate ($V_{max,app}$) and the apparent Michaelis-Menten constant ($K_{M,app}$) for ABTS.

The simplified reaction model is adopted for the experimental study and therefore, the initial hydrogen peroxide concentration was 100 mM for all experiments. The kinetic parameters $K_{M,app}^{ABTS}$ and $V_{max,app}^{ABTS}$ will first be determined through the Hanes-Woolf method. Since the concentration of enzyme is used as design variable in the topology optimization, the $V_{max,app}^{ABTS}$ value cannot be used and it is necessary to calculate the apparent turnover number, $k_{cat,app}^{ABTS}$. The apparent turnover number is determined through the linear relation between the V_{max} values and the enzyme concentration.

The initial reaction rate is the parameter that is necessary for calculating the kinetic parameters and the enzyme activity. The initial reaction rate is determined from the slope of the linear relation between product concentration and time. The experimental protocol for the determination of the activity and kinetic parameters was based on the peroxidase assay with ABTS described by Sigma Aldrich [141].

The substrate solutions were pipetted into a microwell plate (Nunc MicroWell™ 96 well polystyrene plate, flat bottom [product number 260210], purchased at Thermo Scientific). The enzyme solution was introduced into the microwell by a syringe pump of the microtiter plate reader (POLARstar, Omega series from BMG LABTECH) just before starting the measurement. The microwell plate reader monitored the absorbance of the product over time at a wavelength 414 nm.

The activity of the enzyme was calculated by defining the conditions identical to one of the assays used for finding the kinetic parameters. The calculation of $K_{M,app}^{ABTS}$ and $V_{max,app}^{ABTS}$ through the Hanes-Woolf method requires the determination of the initial reaction rate for several substrate concentrations, and here the substrate concentration was varied in a range between 0.06 and 10 mM.

The $k_{cat,app}^{ABTS}$ value was determined through the calculation of the initial reaction rate for several enzyme concentrations for a substrate concentration in the saturated range (12 mM). In the saturated range the reaction rate is equal to the maximum reaction rate, $V_{max,app}^{ABTS}$. The substrate concentration was chosen according to the determined Michaelis-Menten constant, which was obtained from the previous experiment. This aspect will be further explained. The enzyme concentrations varied between 0.004 and 0.031 mg/mL.

The detailed protocols for the determination of the activity and the kinetic parameters can be found in Appendix B.

5.2.1 Determination of activity

The activity of the enzyme is defined for 1 mM ABTS and 100 mM H_2O_2, pH 5, 25°C. At these conditions there was one assay performed during the saturation experiments. The calculated initial reaction rate in absorbance units per second is 0.007±0.0004 ΔA/s. The calculations of the activity are presented afterwards. The data collected from the spectrophotometric measurements over time are presented in Appendix C.

The change of absorption with respect to time through the Lambert-Beer law is given by:

$$\frac{dA}{dt} = \frac{dC}{dt}\,\varepsilon\, l \tag{5.5}$$

A – Absorbance
C – concentration
ε – molar absorption coefficient = 31100 M^{-1} cm^{-1}
l – length of the light path = 1 cm
Calculation of the concentration:

$$\frac{\Delta C}{\Delta t} = \frac{\Delta A}{\Delta t\, l\, \varepsilon} = \frac{0.0070 s^{-1} \times \left|\frac{60\ s}{1\ min}\right| \times \left|\frac{10^6\ \mu mol}{1\ mol}\right|}{31100\ \frac{\mathrm{dm}^3}{mol} \times \mathrm{cm}^{-1} \times 1\ \mathrm{cm}} = \ 13.57\ \mu mol\ ABTS/(dm^3.\mathrm{min})$$

Calculation of the number of moles:

$$Number\ of\ moles\ = \ 13.57\ \mu mol/(dm^3.\mathrm{min}) \times 0.0002\ dm^3 = 0.0027\ \mu mol\ ABTS/\mathrm{min}$$

The associated standard deviation is:

$$\sigma\ = \frac{0.0004\ s^{-1} \times 0.0002\ dm^3 \times \left|\frac{60\ s}{1\ min}\right| \times \left|\frac{10^6\ \mu mol}{1\ mol}\right|}{31100\ \frac{\mathrm{dm}^3}{mol} \times \mathrm{cm}^{-1} \times 1\ \mathrm{cm}} = \ 0.000150\ \mu mol\ ABTS/min$$

The enzyme activity is expressed in units (U). One U of activity is the necessary enzyme amount to catalyse the conversion of 1 µmol substrate per minute. **At the conditions for which the activity is defined, the enzyme activity of peroxidase is 0.0027±0.0002 U.**

The enzyme activity concentration can be determined from the weighed mass of the enzyme preparation. In this case, 2 mg of the enzyme preparation were diluted in a 10 mL volumetric flask for preparing the stock solution. 510 µL of the stock solution were diluted in a 25 mL volumetric flask. Thereafter, 10 µL of the diluted solution were used in the activity assay.

So the volume of enzyme stock solution in the assay is:

$$volume\ of\ stock\ solution = \frac{510\mu L\ stock\ solution \times 10\mu L\ diluted\ solution}{25000\mu L\ diluted\ solution} = 0.2\ \mu L\ stock\ solution$$

The enzyme activity concentration per mL is:

$$Enzyme\ activity\ concentration = \frac{2.7 \cdot 10^{-3}\ U}{0.2\ \mu l} \times \left|\frac{1000 \mu l}{1 ml}\right| = 13.3\ U/mL$$

The standard deviation associated is:

$$\sigma = \frac{1.5 \cdot 10^{-4}\ U}{0.2\ \mu l} \times \left|\frac{1000 \mu l}{1 ml}\right| = 0.74\ U/mL$$

The enzyme activity concentration per mL is 13.3±0.7 U/mL.

The amount of protein in 0.2 µL of the stock solution is:

$$\frac{0.2\ \mu L \times 2\ mg}{10000 \mu L} = 4.08 \cdot 10^{-5}\ mg\ protein$$

Thus, the specific enzyme activity is:

$$Specific\ enzyme\ activity = \frac{2.7 \cdot 10^{-3}\ U}{4.08 \cdot 10^{-5} mg} = 66.2 \frac{U}{mg} protein$$

The associated standard deviation is:

$$\sigma = \frac{1.3 \cdot 10^{-4}\ U}{4.08 \cdot 10^{-5}\ \mu L} = 3.18 \frac{U}{mg} protein$$

The specific enzyme activity is 66±3 U/mg protein.

5.2.2 Determination of $K_{M,app}^{ABTS}$ and $V_{max,app}^{ABTS}$ for the saturation of ABTS at 100 mM H_2O_2

The determination of the parameters $K_{M,app}^{ABTS}$ and $V_{max,app}^{ABTS}$ is done through a Hanes-Woolf plot for the initial reaction rates obtained by the spectrophotometric assays at different ABTS concentrations and at 100 mM H_2O_2. The Hanes-Woolf plot is a graphical method for representation of enzyme kinetics. This method relates linearly the ratio of the initial substrate concentration, [S], to the reaction velocity, v and the substrate concentration by means of the following expression:

$$\frac{[S]}{v} = \frac{[S]}{V_{max}} + \frac{K_M}{V_{max}} \tag{5.6}$$

The initial rate, in units of mM/min, was calculated using the correlation between the concentration and the absorbance variation given by the Lambert-Beer law (Equation (5.5)). The procedure is similar to the procedure presented for the calculation of enzyme activity.

As an example, the conversion from absorbance to concentration units for the concentration of 1 mM of ABTS is presented below:

$$\frac{\Delta C}{\Delta t} = \frac{\Delta A}{\Delta t\ l\ \varepsilon} = \frac{0.0070\ s^{-1} \times \left|\frac{10^3\ mmol}{1\ mol}\right| \times 60s}{31100\ \frac{\mathrm{dm}^3}{mol} \times \mathrm{cm}^{-1} \times 1\ \mathrm{cm} \times 1\ min} = \ 0.0136\ mmol/(dm^3.\mathrm{min})$$

The procedure of the calculations was the same for all the other concentrations. The results are presented in Table 5.1

Table 5.1 - Data for determination the $K_{M,app}^{ABTS}$ and $V_{max,app}^{ABTS}$.

[ABTS]	Initial reaction rate	Standard deviation Σ	Initial reaction rate	Standard deviation σ	[ABTS]/v
mM	ΔA/s	ΔA/s	mM/min	mM/min	min^{-1}
0.06	0.0014	0.0002	0.0026	0.0003	23.03
0.1	0.0023	0.0001	0.0044	0.0002	22.89
0.2	0.0035	0.0002	0.0067	0.0003	29.78
0.6	0.0058	0.0002	0.0112	0.0003	53.67
1	0.0070	0.0004	0.0136	0.0006	73.70
2	0.0084	0.0007	0.0162	0.0011	123.58
6	0.0117	0.0009	0.0226	0.0014	264.91
10	0.0129	0.0006	0.0248	0.0010	402.61

The determination of the kinetic parameters was done by using the method of Hanes-Woolf. The Hanes-Woolf plot is presented in Figure 5.3.

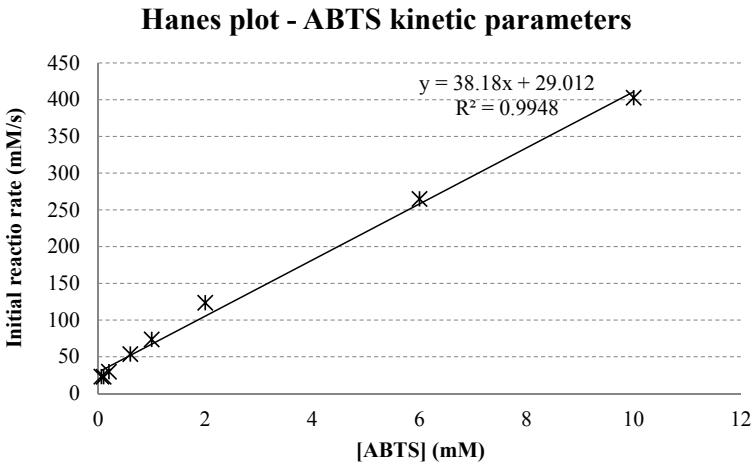

Figure 5.3 – Hanes-Woolf plot for determination of ABTS kinetic parameters.

The V_{max}^{ABTS} was determined from the slope of the linear regression and the K_M^{ABTS} was determined by the multiplication of the intercept value and the V_{max}^{ABTS}. The values for the kinetic parameters K_M^{ABTS} and V_{max}^{ABTS} are presented in Table 5.2.

Table 5.2 – Kinetic parameters $\boldsymbol{K_{M,app}^{ABTS}}$ and $\boldsymbol{V_{max,app}^{ABTS}}$ determined from the Hanes plot.

Hanes-Woolf plot data		**Kinetic parameters**		
Slope	38.18	V_{max}^{ABTS}	0.026	mM/min
Intercept	29.01	K_M^{ABTS}	0.760	mM

5.2.3 Determination of the kinetic parameter $k_{cat,app}^{ABTS}$

The kinetic parameter k_{cat}^{ABTS} corresponds to the turnover number and is defined as the number of molecules converted per second by one enzyme molecule under substrate saturation conditions. The determination of this parameter can be done by calculating the initial reaction rate for substrate concentrations in the saturated range. The saturated range corresponds to the substrate concentrations for which the reaction rate is constant and equal to the maximum reaction rate, V_{max}. The maximum reaction velocity is reached when all the enzyme sites are saturated with substrate. This phenomenon occurs when the concentration of substrate is much higher than the

Michaelis-Menten constant, K_M, $[S] \gg K_M$, so that $\frac{[S]}{[S]+K_M}$ approaches the value 1. Therefore, the Michaelis-Menten kinetic expression given by Equation (5.4) is reduced to:

$$v = \frac{dP}{dt} = V_{max,app}^{ABTS} = k_{cat,app}^{ABTS}[E]_0 \quad (5.7)$$

The turnover number was determined by keeping the initial substrate concentration constant at 12 mM and measuring the oxidation of ABTS in the presence of an excess of H_2O_2 (100 mM) with different concentrations of enzyme. The concentration of ABTS was chosen such as to guarantee that the reaction occurs at maximum reaction rate. When the concentration of ABTS is 12 mM the reaction rate corresponds to 94% of the maximum reaction rate and we considered that it is a value close to the maximum reaction rate. This value is calculated through the ratio $\frac{[S]}{[S]+K_M}$ and considering the determined value for the Michaelis-Menten, 0.76 mM. The maximum reaction rate varies, according to Equation (5.7), proportionally to the concentration of enzyme. Thus, it is possible to determine k_{cat}^{ABTS} by the slope of the Equation (5.7). Therefore, in this case enzyme solutions of different enzyme concentrations (U/mL) were used to perform these experiments.

Two mg were diluted in a 10 mL volumetric flask which corresponds to a concentration of 0.2 mg/ml. This solution was then diluted in order to obtain enzyme solutions with different concentrations. The enzyme concentration in molar units was calculated from the molecular weight. The molecular weight has been documented on the Sigma Aldrich website [142] as 44 kDa, which corresponds to 44000 g/mol.

However, the lyophilised enzyme preparation used in the experiments is not pure and only a percentage of its mass corresponds to pure enzyme. In this investigation, it is therefore necessary to calculate the concentration of enzyme in mol/L units in order to insert the data in the CFD simulations. We know, from personal communications with experts in the field, that the enzyme preparation is never 100% pure. Therefore, an assumption was made here and it was considered that 15% of the mass of the lyophilized protein preparation corresponds to enzyme molecules.

Therefore, the final concentration of peroxidase solution was adjusted to 15% of the mass of the initial protein solution and the final peroxidase concentrations in the microwell in mmol/mL are presented in Table 5.3.

Table 5.3 - Summary of the concentrations of peroxidase solutions used for determining the value of k_{cat}^{ABTS}.

Final concentration of protein in microwell plate (mg/mL)	Final concentration of peroxidase (15% of protein mass) in microwell plate (mmol/mL)
0.031	$5.2 \cdot 10^{-9}$
0.020	$3.5 \cdot 10^{-9}$
0.010	$1.7 \cdot 10^{-9}$
0.004	$6.9 \cdot 10^{-10}$

The determined values of absorbance over time for each enzyme solution together with the evaluation of the blanks can be found in Appendix C. The final results from the initial reaction rates for 12 mM of ABTS and 100 mM of H_2O_2 for the different concentrations of peroxidase were determined via the Lambert Beer law. A similar procedure for determining the initial reaction rates for calculating K_M^{ABTS} and V_{max}^{ABTS} was used.

The summary of the experimental results and the value of k_{cat}^{ABTS} is presented in Table 5.4:

Table 5.4 – Summary of initial reaction rates

Final concentration of peroxidase (15% of protein mass) in microwell plate mmol/mL	Initial reaction rate ΔAbsorbance/s	Initial reaction rate mmol/(mL.min)
0	0	0
$6.9 \cdot 10^{-10}$	0.0113	$2.19 \cdot 10^{-5}$
$1.7 \cdot 10^{-9}$	0.0351	$6.77 \cdot 10^{-5}$
$3.5 \cdot 10^{-9}$	0.0786	$1.52 \cdot 10^{-4}$
$5.2 \cdot 10^{-9}$	0.1209	$2.33 \cdot 10^{-4}$

The value of k_{cat}^{ABTS} was obtained from the slope of the linear regression fitted to the experimental data, as shown in Figure 5.4.

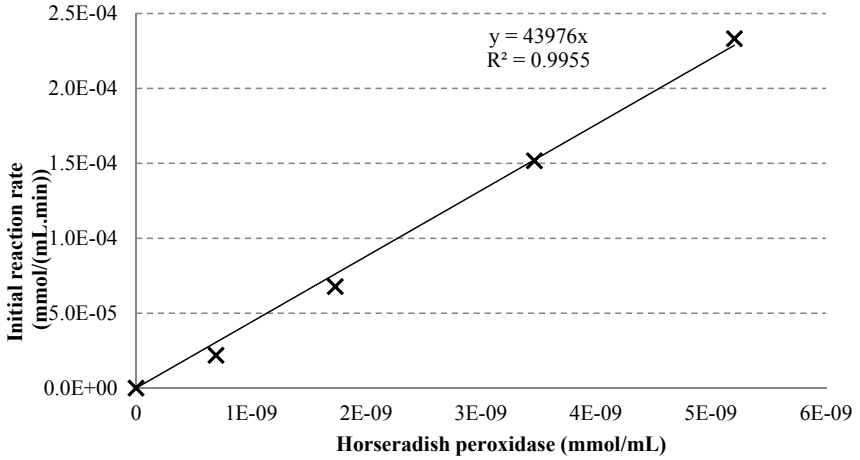

Figure 5.4 – Relation between the initial reaction rate for oxidation of ABTS and the horseradish peroxidase concentration.

The k_{cat}^{ABTS} value corresponds to the slope of this linear regression, 43976 min^{-1} which corresponds to 732 s^{-1}.

The kinetic parameters regarding the oxidation of ABTS catalyzed by peroxidase have been reported before in the scientific literature. Kamal and co-workers [143] have reported the kinetic parameter values corresponding to this enzymatic reaction and the substrate ABTS. The determined k_{cat} value was 810 s^{-1} and the determined K_M^{ABTS} value was 0.18 mM. Another article by Smith and co-workers [144] reported the kinetic parameters for this reaction. The value determined for k_{cat} was 736 s^{-1} and the determined value for K_M^{ABTS} was 0.27 mM.

Comparing values obtained in this study (k_{cat} = 732 s^{-1} and K_M^{ABTS}=0.76 mM) with the ones reported in the literature it is possible to conclude that the values of this investigation are in good agreement with the ones reported in the literature. Therefore, the implementation of this kinetic model into the CFD simulation can be done with confidence in the values for the kinetic parameters.

5.3 Case study 1 - Topology optimization applied to a microreactor with immobilized enzyme on the wall surface

5.3.1 Implementation of computational fluid dynamic simulations

The experimentally obtained reaction parameters for the oxidation of ABTS to its radical form catalyzed by peroxidase and reducing H_2O_2 to water allow the use of a more realistic and precise study with relation to the topology optimization of microreactors.

The experimental validation of the topology optimization can be performed in two stages, the first stage corresponds to the topology optimization using CFD simulations and the second one corresponds to the fabrication of the microreactor and the experimental validation.

The investigated microreactor shape corresponds to the same as presented in Case study 1 from Chapter 4. The reaction model previously described is applied to the topology optimization and the resulting reactor configurations result will subsequently be tested in the laboratory.

The presented experimental part in this section corresponds to the first studies towards experimental validation of a two-dimensional topology optimization of a microreactor with immobilized enzyme on the wall surfaces.

5.3.1.1 Materials and methods

As mentioned before, in this case study, the microreactor has the same shape as the microreactor of the two-dimensional case study reported in Chapter 4.

The microreactor shape is a parallelepiped measuring 30 mm in width and depth, combined with two channels for the inlet and outlet located at opposite sides of the square. The width of the inlet and outlet channels is 10 mm. The height of the microreactor corresponds to 0.25 mm.

Similar to the case study in Chapter 4, the enzyme is immobilized on the top and bottom surfaces of the reaction chamber. The symmetry planes will also be applied in this case study and therefore, only a quarter of the whole microreactor geometry is simulated as shown in Figure 5.5. Moreover, the bottom surface of the simulated part of the microreactor was divided in 128 immobilization elements as well (See Figure 5.5).

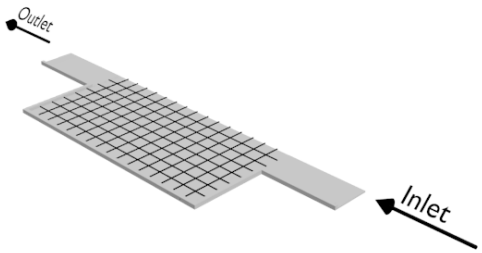

Figure 5.5 – View of a quarter of the microreactor configuration used in the CFD simulations. View of the 128 immobilization elements

The inlet flow rate was set according to the residence time and the volume of the microreactor (225 μL). The decision about the residence time was made such that the residence time of an average volume element would be 15 s inside the reaction chamber.

The geometry design and definition of the small areas procedure was the same as the one described in Chapter 4. The studied reaction rate is the Michaelis-Menten mechanism for the oxidation of ABTS by peroxidase considering that H_2O_2 is present in excess. The reaction rate equation is described by Equation (5.8):

$$r_P = -r_S = k_{cat,app}^{ABTS} \cdot [C_E] \frac{[S]}{[S] + K_{M,app}^{ABTS}} \tag{5.8}$$

where k_{cat}^{ABTS} is the turnover number, $[C_E]$ the enzyme concentration, $[S]$ the substrate concentration, P the product and K_M^{ABTS} is the Michaelis-Menten constant.

The reaction parameter values for this case study were previously derived experimentally and are $k_{cat,app}^{ABTS} = 732\ s^{-1}$ and $K_{M,app}^{ABTS} = 0.76\ mM$.

The enzyme concentration on the surface was determined considering that the diameter of an enzyme molecule is assumed to be roughly 10 nm [136]. From the area of a molecule ($7.85 \cdot 10^{-17}$ m^2), the maximum concentration of enzyme that can be immobilized in a monolayer is calculated as $2.12 \cdot 10^{-8}$ $mol \cdot m^2$. The substrate concentration at the inlet is 10 mM. In the scientific literature, the ABTS diffusion coefficient has been reported as $2.4 \cdot 10^{-10}$ $m^2 \cdot s^{-1}$ [145]. In this computational study this value was used as the diffusion coefficient for both ABTS (substrate) and its radical (product).

Topology optimization procedure

The problem formulation of this two-dimensional topology optimization problem is given by:

$$\begin{aligned} \text{Maximize} \quad & J(C_E) = \dot{m}_{P\ outlet} = Q \times \overline{C_P}\left(C_E\ (x,\ y)\right)_{outlet} \\ \text{Subject to} \quad & C_E \leq C_{E\,max} \end{aligned} \tag{5.9}$$

where $\dot{m}_{P\ outlet}$ is the product mass flow rate at the outlet, $\overline{C_P}_{outlet}$ is the average product concentration at the outlet, C_E is the enzyme concentration and design variable which is dependent of the position in the microreactor, $C_{E\,max}$ is the maximum enzyme concentration in the reactor, x, y are the space coordinates and J is the objective function.

The applied topology optimization procedure in this case study is the same as presented in Case study 1 in Chapter 4. At the starting point for this optimization problem, the immobilized enzyme concentration on the wall surface was set to half of the maximum concentration, $1.06 \cdot 10^{-8}$ mol·m^2.

5.3.1.2 Results and discussion

The optimization cycle ended when the maximum enzyme concentration ($2.12 \cdot 10^{-8}$ mol·m^2) was achieved. On the one hand, 0.861 mM of product was formed with the initial enzyme configuration. On the other hand 0.986 mM of product was converted with the final configuration. The reader should note that the enzyme concentration in the final configuration is double of the enzyme concentration in the initial configuration. However, the area where the enzyme is immobilized in the final configuration is half of the immobilization area of the initial configuration. Therefore, the number of enzyme molecules inside both microreactors is the same in both configurations.

Table 5.5 – Summary of results of the two-dimensional topology optimization case study.

Configuration	Parameter	Value
Initial configuration	Enzyme concentration	$1.06 \cdot 10^{-8}$ mol·m^{-2}
	Product concentration	0.861 mM
Final configuration	Enzyme concentration	$2.12 \cdot 10^{-8}$ mol·m^{-2}
	Product concentration	0.986 mM
Improvement: 14.5%		

In the end, the topology optimization resulted in an improvement of 14.5% of the product formation per same amount of enzyme (mol) compared with the initial enzyme configuration as presented in Table 5.5.

The enzyme distribution and an overview of the product formation for the initial and final configurations can be found in Figure 5.6.

The optimized microreactor configuration is characterized by enzyme immobilization mainly at the areas of low residence time streams and in the area close to the outlet. This demonstrates that the low residence time streams contribute more to the product formation. The low diffusion of the substrate and product ($2.4 \cdot 10^{-10}$ $m^2 \cdot s^{-1}$) and the high reaction rate results in mass transfer limitations inside the microreactor. The low concentration of substrate in the high residence time streams results in low reaction rates and consequently, in low product formation due to fast substrate conversion and low mass transfer to the surface.

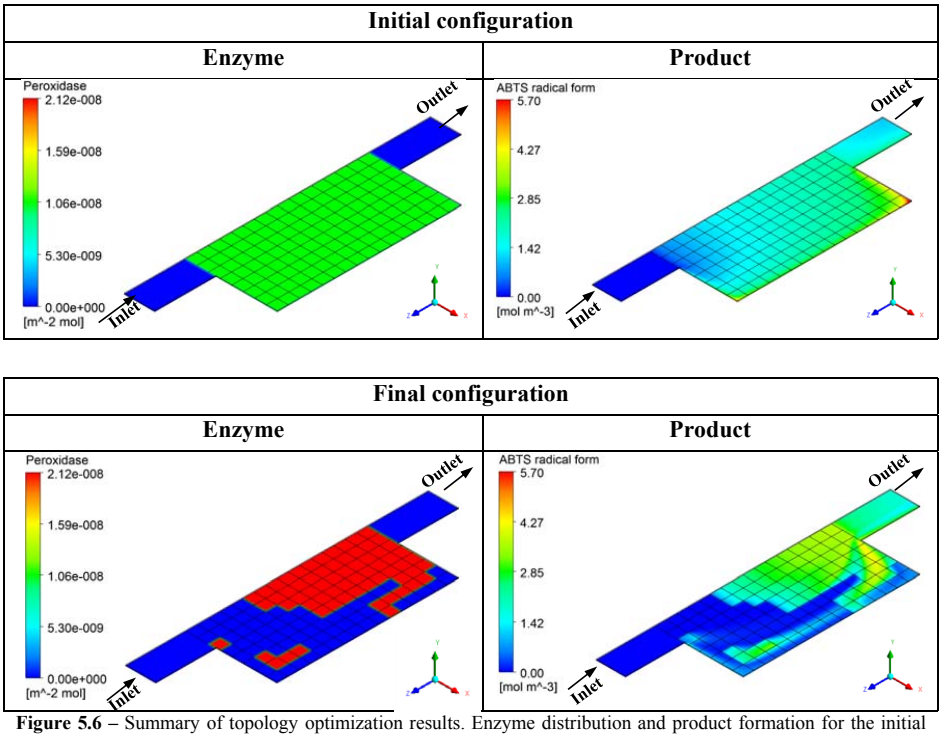

Figure 5.6 – Summary of topology optimization results. Enzyme distribution and product formation for the initial and final configurations.

Thus, in contrast to the case study from Chapter 4, the high residence time streams are not as important for the microreactor yield in this investigation.

Nonetheless in the final configuration, it is possible to see that there is a specific zone in the high residence time streamline for which the enzyme is immobilized on the wall surface. However, compared with the case study in Chapter 4 the enzyme immobilization in this streamline is

discontinuous which means that there is a large interval between areas with immobilized enzyme in the same streamline. Using ANSYS CFX-Post®, a line was traced along this streamline towards the outlet as presented in Figure 5.7.

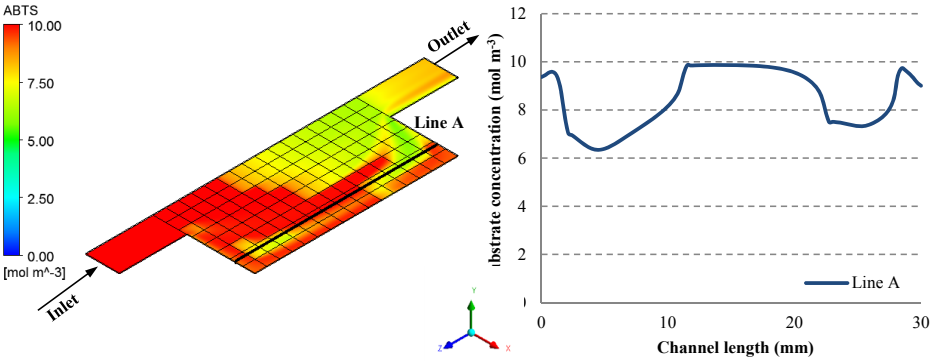

Figure 5.7– Left: **S**ubstrate concentration profile at the surface for the final enzyme configuration in the plane y = $1.5 \cdot 10^{-6}$ mm; Right: **S**ubstrate concentration in a specified line on the plane (Line A: x = 0.012 mm, y = $1.5 \cdot 10^{-6}$ mm, z from 0 to 30 mm)

The Line A in Figure 5.7 is located in a plane at a height (y-direction) of $1.5 \cdot 10^{-6}$ mm, at the width (x-direction) 0.012 mm and all along the length (z-direction) of the microreactor, i.e. from 0 to 30 mm. The graph on the right hand side of the figure with the microbioreactor corresponds to the substrate concentration variation along the line A. Following the concentration of substrate along the channel length towards the outlet it is possible to verify that the substrate concentration decreases in the areas where enzyme is immobilized due to fast substrate conversion. The substrate concentration at the surface decreases from 10 mM to 6 mM which results in a decrease of 27% of the reaction rate. Thus, the next elements are not efficient for the production and no enzyme is immobilized. This area allows then the diffusion of the substrate onto the surface. Since more substrate is present at the surface, the elements further to the outlet are more efficient since the reaction rate increases again in these areas.

In the final configuration, the preferential immobilization of enzyme on the areas close to the outlet instead of immobilizing at the inlet areas for the low residence time streams is difficult to explain. It can only be observed that the pattern in these specific areas is the result of the complex combination of mass transfer, reaction rate, substrate concentration and flow conditions.

Although the shape of the microreactor is equal and the flow conditions are the same as the case study presented in Chapter 4, the final immobilized enzyme configuration is substantially different due to the different values of the substrate and product diffusion rate that have been used here, and due to differences in the reaction rate. This fact emphasizes the importance of topology optimization for designing reactors and thereby intensifying processes.

5.3.2 Experimental work towards method validation

The experimental validation of the topology optimization procedure was attempted by comparing the final and initial configuration with immobilized enzyme on the surface of the top and bottom walls of the microbioreactor.

This experimental work is the result of a collaboration with the Danish Polymer Center (DPC). My co-supervisor Associate Professor Anders E. Daugaard and the Ph. D. student Christian Hoffmann have actively participated in this part of my Ph. D. project. The fabrication of the microreactor and the immobilization of the enzyme on the surfaces of the microreactor were performed at the DPC using methods which have been developed in the center and/or found in literature.

The quantification of the immobilized enzyme is not accurate at this point of the project. Thus, there is no certainty about the exact amount of enzyme that is immobilized on the surface. The exact amount of immobilized enzyme on the surface is a very important factor for the validation of the two-dimensional topology optimization, since the initial and the final configuration have different amounts immobilized on the surface. Therefore, the results with respect to the experimental validation will only include a proof of concept regarding the immobilization of enzyme on the wall surface. This work will be further developed and completed in the near future, when techniques for enzyme immobilization have been refined.

The microreactor fabrication and enzyme immobilization were performed by Ph.D. student Christian Hoffmann from the Danish Polymer Center. The microreactor chambers were fabricated using a polymer made of a crosslinked thiol-ene network. The crosslinked thiol-ene network was prepared with pentaerythritol tetrakis (3-mercaptopropionate) (PETMP), triallyl-1,3,5-triazine -2,4,6(1H,3H, 5H)-trione (TATATO) and bisphenol A diglycidyl ether (BADGE). The chemical formulas of the structural compounds used for preparing the crosslinked thiol-ene network are presented in Figure 5.8.

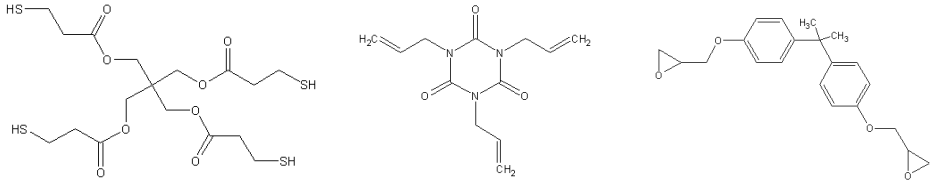

PETMP TATATO BADGE

Figure 5.8 – Structural formulas of the compounds used for preparing the crosslinked thiol-ene network.

The microsystems made of crosslinked thiol-ene network allow a great control of surface properties and have been shown to be good for flow systems by Mazurek and his co-workers [146,147]. They have included a detailed protocol for the preparation of the polymer network and the fabrication of microchambers. The thiol groups present on the surface were then utilized for further surface functionalization via a photo-initiated "thiol-ene" reaction. Using this strategy, the thiol groups can react with alkene functional compounds in order to introduce specific functionality on the surface. By using this technique, the surface was modified for immobilizing the enzyme through the photoreaction between the glycidyl methacrylate molecules and the thiol-ene groups on the surface. The microchamber was then afterwards covered by a polypropylene stencil mask with the desired immobilization pattern. The epoxide groups from glycidyl methacrylate are known to react with the amine groups of the enzyme molecules and can therefore be used for covalent enzyme immobilization [148,149]. Figure 5.9 is a schematic representation of the surface modification and enzyme immobilization procedures.

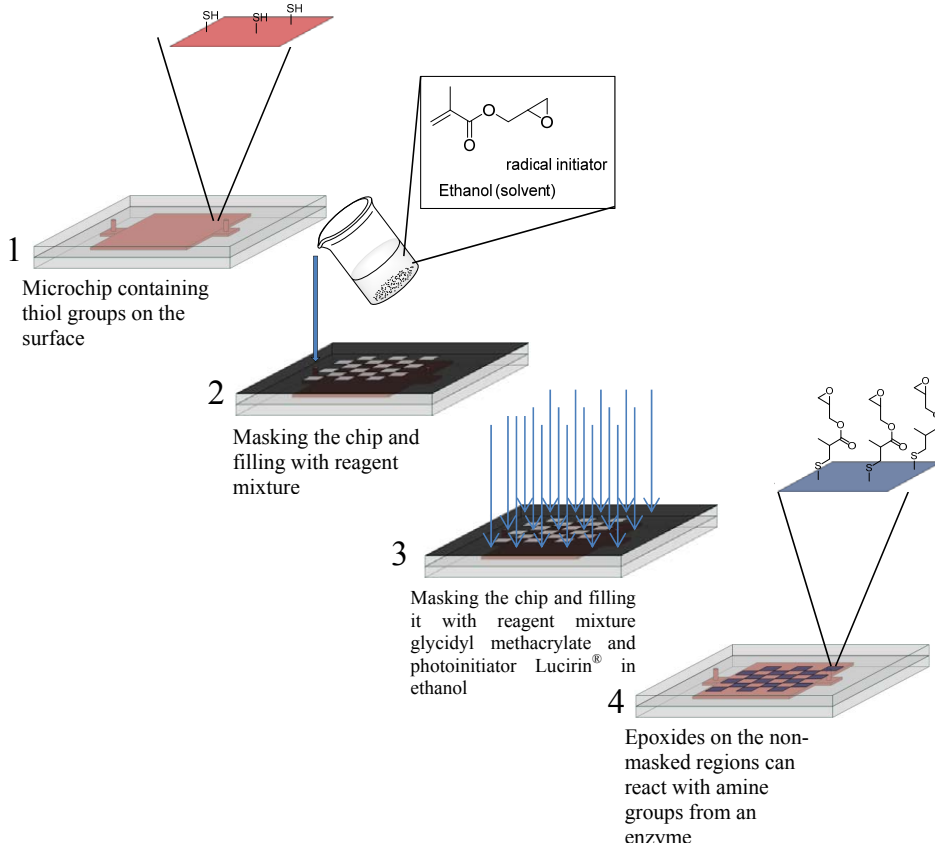

Figure 5.9 – Surface modification and photochemical reaction between the glycidyl methacrylate molecules and the thiol groups using a polypropylene stencil mask to establish enzyme immobilization patterns.

The investigated patterns for enzyme immobilization were the following: full immobilization surface, no masking (Figure 5.10 a)), half of the immobilization surface, with half of the surface covered by the mask (Figure 5.10 b)), coarse checkerboard immobilization surface (Figure 5.10 c)) and fine checkerboard immobilization surface (Figure 5.10 d)).

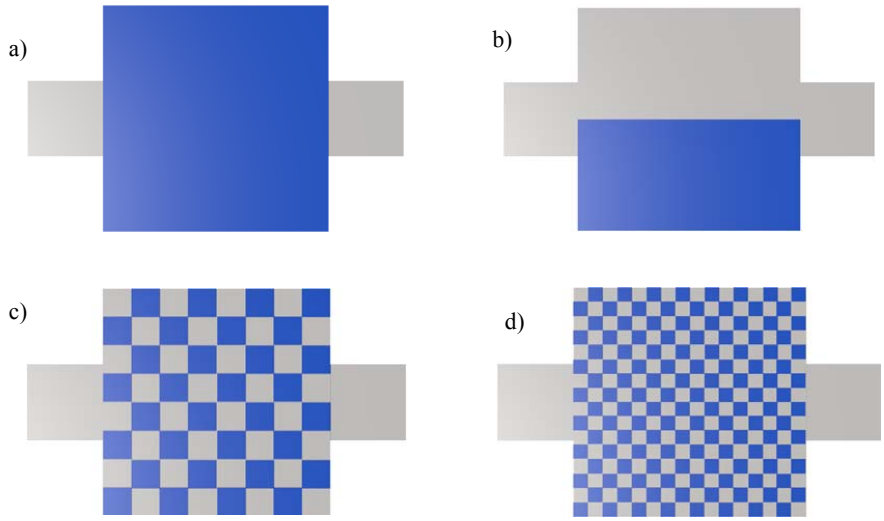

Figure 5.10 – Enzyme immobilization pattern configurations: a) full immobilization surface; b) half of the immobilization surface, c) coarse checkerboard immobilization surface and d) fine checkerboard immobilization surface.

The amount of immobilized enzyme was determined by analysing the absorbance of the horseradish peroxidase (HRP) solution. The correlation between the absorbance of the HRP solution and the concentration of the enzyme solution was performed through a calibration curve. The HRP solution was analysed using the spectrophotometer in order to obtain the initial enzyme concentration, before introducing the HRP solution in the microreactor. After the immobilization procedure, the HRP solution was removed from the internal volume of the microreactor with the help of a syringe. The solution was weighed and analysed using a spectrophotometer. Considering the solution density as 1 g/mL, the solution volume was determined from the weighed mass. The HRP immobilized mass was then calculated from the determined volume and the initial and final HRP solution concentrations. The microreactor inlet was connected to a syringe pump (500 µL) (model Cavro XLP6000, from Tecan) which contained the substrate solutions (1 mM ABTS, 100mM H_2O_2), respectively.

The flow rate was set to 225 µL/min in order to ensure that the residence time inside the microreactor was an average of 60 seconds. The performance of the microreactors was evaluated using an on-line UV-detection system. The microreactor outlet was connected to an 8-port

injection valve (model VICI E45-230 - CR2 head) which was programmed for collecting samples at a certain frequency. The UV-detector (model Agilent G1315AR) measured the absorbance of each sample at 414 nm. The experimental protocols for the surface treatment and enzyme immobilization and the operation of the on-line UV-detection system are described in more detail in Appendix B.

5.3.2.1 Results and discussion

The calibration curve which relates the concentration of HRP in solution is given by:

$$A = 0.5006 \times C + 0.3514$$

where A is absorbance and C is enzyme concentration. The results for the immobilized enzyme are summarized in Table 5.6.

Table 5.6 – Results of immobilized enzyme mass for all microreactor configurations.

	Initial solution	**Full immobilization surface**	**Fine checkerboard**	**Coarse checkerboard**	**Half immobilization surface**
Initial concentration (mg/mL)	1.067	-	-	-	-
Final concentration (mg/mL)	-	1.03	1.01	1.1	1.03
Solution mass (mg)	-	272.8	279.6	309.9	337.8
Final enzyme mass (mg)	**-**	**7.5**	**13.2**	**-21.5**	**9.3**

From these results it is possible to verify that the mass of enzyme immobilized in the microreactor with full immobilization surface is close to the amount immobilized at the microreactor half immobilization surface. However, the size of the surface for immobilization is double for the first configuration.

The immobilized enzyme mass for the coarse checkerboard configuration is a negative number. At this point of the experiments it was not certain if there was any enzyme immobilized and only the test of the microreactor for the oxidation of ABTS can verify that. In the fine checkerboard configuration it seems that there was more enzyme immobilized than in any of the other configurations.

All four microreactor configurations were tested by pumping the substrate solutions through each of them for 30 min in order to evaluate the performance of each microreactor. The results of the absorbance measurements by the on-line UV-detection system for each microreactor configuration are presented in Figure 5.11. The absorbance measurements can be found in Appendix C.

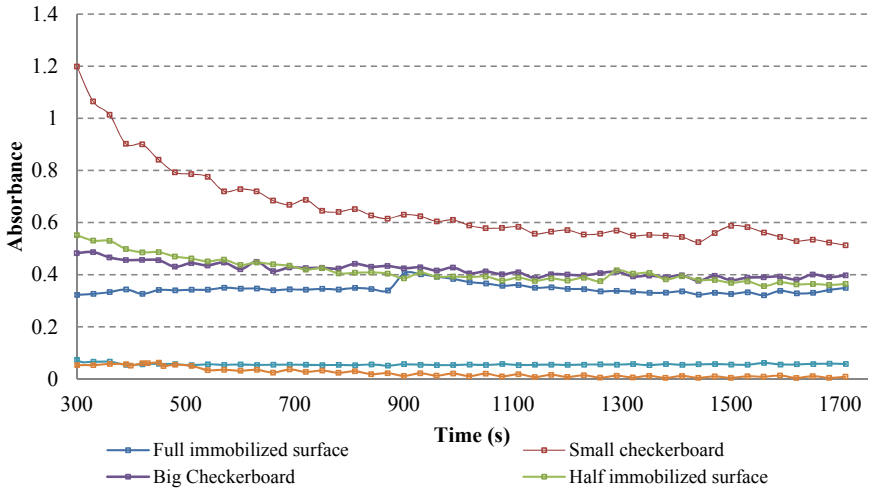

Figure 5.11 – Absorbance results for the four microreactor configurations with enzyme immobilization via covalent binding, one microreactor with enzyme immobilized by adsorption and the reference microreactor with no enzyme immobilized.

The reader should note that the microreactor was first operated by flowing the substrate solution in order to remove the air bubbles from inside the microchamber. Afterwards, the substrate solution flow was stopped and the microreactor was connected to the UV-detector. During the period of time required for connecting the microreactor to the detector system, the syringe pumps were switched off and the substrate molecules present in the microsystem reacted with the immobilized enzyme. As a consequence, some substrate has been converted at the start of each measurement in Figure 5.11, when the feed flow is started again, and therefore the absorbance signals for the microreactor configurations coarse checkerboard, half immobilization surface and the fine checkerboard decrease over time since the system is converging to steady state. The comparison of the microreactors performance must be done considering the steady state conditions (time larger than 1300 s).

The plotted results in Figure 5.11 are consistent with the results for the quantification of immobilized enzyme. For this experimental investigation, it is critical to ensure that the enzyme only immobilizes on the surface specifically onto the glycidyl methacrylate molecules since enzymes are known for adsorbing easily to polymeric surfaces.

Two reference assays were prepared for verifying possible spontaneous reactions or unspecific enzyme bonding. For the first reference, the microchamber had contact with enzyme solution inside the reaction chamber in order to investigate spontaneous product formation. For the second reference assay, a microchamber with no glycidyl methacrylate molecules was exposed to the enzyme solution in order to investigate if it was possible to prevent unspecific immobilization by adsorption.

The first reference system showed that the product concentration in these configurations is negligible (See Figure 5.11). These results demonstrate that there is no formation of product by a spontaneous reaction in the reference microreactor.

The negligible formation of product in the microreactor for the second reference assay (See Figure 5.11) demonstrates that the enzyme immobilized by adsorption is insignificant. Thus, this result shows that the immobilized amount on the surface on the treated surfaces is exclusively achieved by the covalent immobilization protocol.

The microreactor with the fine checkerboard configuration has a better performance compared with the other configurations. This fact can be explained by the high enzyme mass immobilized on the wall surface. The full immobilization surface and the half immobilization surface configurations present the same level of performance. The results are consistent with the determined amounts of immobilized enzyme mass, which are also very similar.

With respect to the performance of the coarse checkerboard pattern it seems that there was in fact immobilized enzyme inside the microreactor. The performance of the microreactor with coarse checkerboard configuration is also very similar to the full immobilization surface and the half immobilization surface configurations. Nonetheless, the determined amount of immobilized enzyme does not reflect these results. The negative value determined upon the qualification of the amount of enzyme immobilized (See Table 5.6) on the surface might be related to experimental errors. The large variations of the calculated values for the final mass and the negative value showed that it is very difficult to correlate the enzyme concentration to the amount of enzyme of the surfaces. These inconsistencies are believed to be due to the analytical detection limits when working with enzymes and proteins at such low concentration levels. Small inaccuracies in pipetting might be the source of large variations in the final results, since these errors might be amplified on the final measurement value.

During the process of surface treatment with the reaction of glycidyl methacrylate with the thiol groups on the surface, a formation of a milky colour in the solution was observed in the areas where the photochemical reaction occurs. Figure 5.12 shows the regions of immobilization for the coarse checkerboard and half immobilization surface configurations for both top and bottom surfaces.

These pictures were taken with the solution of glycidyl methacrylate inside the microreactors. In the microreactor with the coarse checkerboard configuration, a slight definition of the squares,

where the glycidyl methacrylate is being attached can be seen. A clearer view of these areas can be obtained closer to the side walls of the microreactor. The microreactor with half immobilized

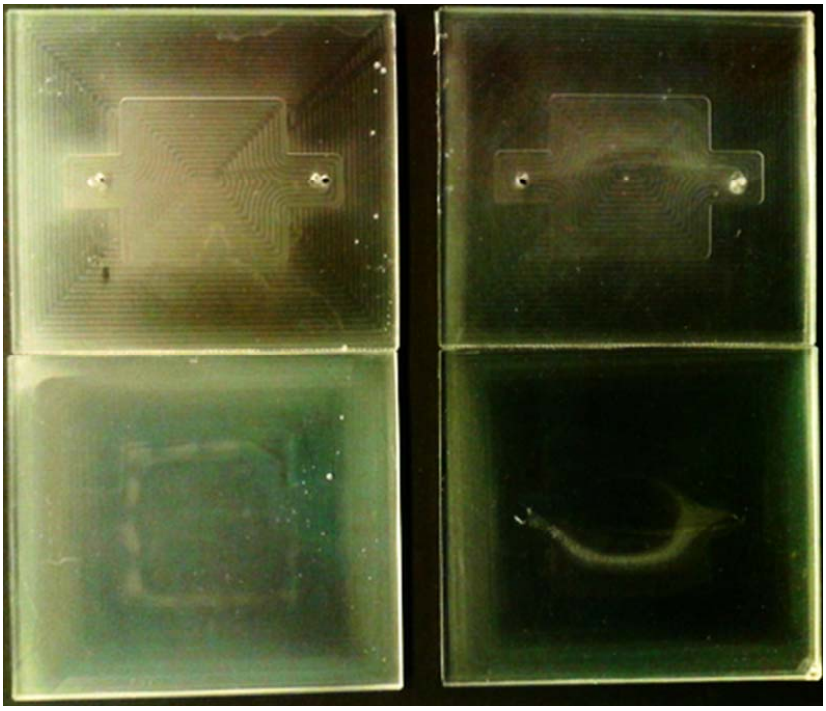

Figure 5.12 – Visualization of exposed immobilization areas to the photochemical reaction. Left: microreactor with coarse checkerboard configuration; Right: microreactor with half immobilization surface configuration.

surface configuration shows a relatively clear difference between the immobilization area and the non-immobilization area at the top surface. However, from the view of the bottom surface it seems that some glycidyl methacrylate molecules have immobilized outside the immobilization area. At this point of time we cannot explain the phenomena of the accumulation of glycidyl methacrylate molecules close to the walls and the attachment of the molecules outside the defined immobilization zone.

More experimental work is needed in order to improve the accuracy of the immobilization method and the determination of immobilized enzyme mass. The experimental validation of topology optimization of immobilized enzyme on the surface can only be performed when the determination of the immobilized enzyme mass is accurate enough. The amount of immobilized enzyme on the surface is extremely important since the concentration of immobilized enzyme on the surface of the initial configuration of the topology optimization is half the concentration of enzyme on the surface of the final configuration. Therefore, more experiments and studies need to be performed in order to successfully validate the two-dimensional topology optimization experimentally.

5.4 Case study 2 – Topology optimization of a microreactor with free enzyme in solution

This case study includes an experimental study of a topology optimized configuration of a microreactor with free enzyme in solution. In Chapter 4, the three-dimensional topology optimization was presented for a microreactor with immobilized enzyme on the surface of a packed bed. For experimental validation, the fabrication of this microreactor and the distribution of the enzyme would be a very complex procedure. Therefore, the experimental validation for a three-dimensional topology optimization can instead be performed with the help of a microreactor with free enzyme in solution.

The microreactor in this case study is a microreactor with a square shaped cross-section, with a well-mixed solution of enzyme and substrate at the inlet. The microreactor system was chosen in order to guarantee a mixed flow profile which deviates significantly from the plug-flow characteristics. In microfluidics, the plug-flow conditions can be achieved with a parabolic flow profile if the radial diffusion mass transfer is fast compared with the convective mass transfer along the flow direction[150]. This is mainly a function of the geometry, the flow rate and diffusion rate. In this case study, the mixed flow behavior is characterized by significant difference in residence times as a function of the radius, low radial transport by diffusion and large radial concentration profiles. The purpose of this case study is to investigate whether the product formation can be improved through the spatial optimization of the enzyme. With this optimization we want to see if there is a better way to use the microreactor which does not operate at perfect conditions. Hence, we want to investigate the placement of the enzyme streams at the inlet in order to find a new configuration which operates in a more efficient way and can be tested experimentally. Moreover, we want to demonstrate that the optimization method can contribute to the intensification of microreactors.

The applied reaction model in the topology optimization procedure corresponds to the reaction model in the previous section and corresponds to the oxidation of ABTS to its radical form catalyzed by peroxidase. The experimental study will be performed by using the same enzymatic reaction.

5.4.1 Implementation of Computational Fluid Dynamic simulation

The topology optimization is applied by introducing the reaction mechanism model of peroxidase as described above. The determined reaction parameters (k_{cat} and K_M) are then introduced in ANSYS CFX® and are applied to topology optimization studies.

5.4.1.1 Materials and methods

The shape optimized microreactor is a square shaped cross-section channel. The inlet and outlet are located at the ends of the microchannel. The square cross-section of the microchannel has the following dimensions: 0.5 mm width and 0.5 mm height. The microchannel length is 50 mm. the choice of this structure is based on the simple manufacturing process of the microreactor and the opportunity of testing it in the laboratory. The microreactor geometry with its dimensions is presented in Figure 5.13.

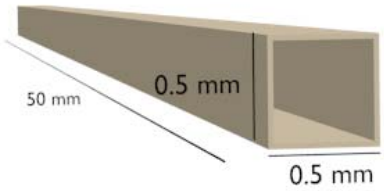

Figure 5.13 – Square shaped cross-section microreactor geometry with dimensions.

Similar to the Case Study 1 in Chapter 4, a horizontal and a vertical symmetry plane were applied to the geometry. Hence, only a quarter of the geometry was simulated using CFD. The simulated geometry with the symmetry planes is shown in Figure 5.14.

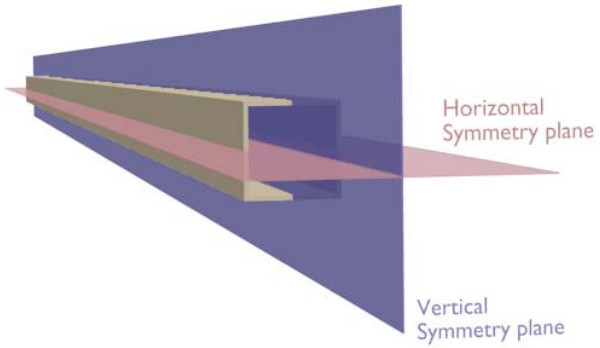

Figure 5.14 – Geometry of microreactor with horizontal and vertical symmetry planes.

The microreactor operates under steady-state conditions and the flowrate was set according to the chosen residence time of 20 s. The flow rate for the volume implemented in CFD simulation is 9.38 μL/min. This value was selected in order to obtain a sufficiently large difference between the radial residence times and diffusional mass transfer limitations and consequently create large radial concentration profiles.

Similar to the previous topology optimization case study it is necessary to establish a maximum allowed enzyme concentration in the microreactor. In this study, the maximum enzyme concentration was set to be $5 \cdot 10^{-5}$ mM. The maximum enzyme concentration was chosen in order

to guarantee that full conversion was not achieved and that there is an opportunity for improvement.

Enzyme (peroxidase) is simulated as a solute, the same way as the substrate (ABTS). Both enzyme and substrate enter the microreactor via the inlet. The concentrations at the inlet of ABTS and peroxidase are 10 mM and $2.5 \cdot 10^{-5}$ mM, respectively. The diffusion coefficient for both ABTS (substrate) and its radical (product) was fixed at $2.4 \cdot 10^{-10}$ $m^2 \cdot s^{-1}$. The diffusion coefficient of the peroxidase was considered to be similar to values reported for other enzymes. Therefore, it was adjusted to be the same value used for the case study in Chapter 3, i.e. $1 \cdot 10^{-11}$ $m^2 \cdot s^{-1}$ [134].

The reaction source term is applied in the whole reactor volume since the reaction occurs everywhere in the volume of the microchannel, where the reactants are present.

Topology optimization procedure

The problem formulation of this three-dimensional topology optimization problem is given by:

$$\begin{aligned} \text{Maximize} \quad & J(C_E) = \int_{\Omega} r_P(C_{E\ active}) dV\,; C_{E\ active}\ (x, y, z) \\ \text{Subject to} \quad & C_{E\ active} \leq C_{E\ active\ max} \end{aligned} \tag{5.10}$$

The design of the microreactor was implemented in ANSYS CFX® and for this investigation the volume of the reaction chamber was divided in small virtual volumes, in this case 160 virtual volumes. These volumes are set up in the simulation (ANSYS CFX-Pre®) by introducing the Matrix function explained in Chapter 4.

The Matrix function defines here the center of each virtual volume and the presence of active enzyme inside the reactor. So, when the Matrix function is 1 in a virtual volume, it means that enzyme is active and the reaction occurs and when it is 0, it corresponds to inactive enzyme and the reaction does not occur in that volume. Afterwards, this function is multiplied by the enzyme concentration. In this way the Matrix function works as a switch function indicating the presence or the absence of active enzyme in the volumes, and defines thus the areas where the reaction is occurring inside the reactor. When a virtual element is removed the amount of enzyme (mol) contributing to the reaction in that volume is distributed over all remaining active virtual volumes. The distribution of enzyme through all the other active elements will result in an increase of the enzyme concentration locally in these elements. However, since the volume with active enzyme decreases proportionally to the increase of enzyme concentration, the total amount of enzyme (mol) is guaranteed to be the same throughout the optimization routine for all the tested reactor configurations.

The 160 virtual volumes were placed according to the following distribution: 4 volumes in the x direction, 10 volumes in the z direction and 4 volumes in the y direction.

The optimization procedure followed the layout of the method presented in the first section of Chapter 4 – *4.1 The topology optimization method*. The optimization cycle starts by distributing uniformly the enzyme in the whole microreactor volume, at half of the maximum concentration, $2.5 \cdot 10^{-5}$ mM. The Matrix function is set to 1 for all the virtual volumes positions indicating that the enzyme present in the reactor is active. Afterwards, the ANSYS CFX-Pre® script is changed according to the defined Matrix function, a computational fluid dynamic simulation is carried out by ANSYS CFX® and the cost function is evaluated in MATLAB®. The optimization routine starts by performing a sensitivity analysis of each virtual volume and the decision on the removal of ineffective volumes is made. Afterwards, the update for the location of active enzyme is made and the total enzyme concentration in each volume containing active enzyme is increased by MATLAB® in order to maintain a constant amount (mol) of active enzyme inside the microreactor.

The script files are updated and the new configuration is evaluated by ANSYS CFX®. The optimization cycle is repeated until the maximum enzyme concentration is achieved or the optimization converges.

5.4.1.2 Results and discussion

Topology optimization of a microreactor with free enzyme in solution helped to find a new configuration for the inlet which contributes to a better efficiency and operation of the system. The initial configuration of the microreactor resulted in the formation of 0.433 mM of product and the final configuration resulted in formation of 0.566 mM product. This means that the topology optimized configuration has improved the product concentration at the outlet by 30.7% while keeping the active enzyme amount (mol) in the microreactor constant. The topology optimization cycle has finished when the maximum enzyme concentration was achieved.

Table 5.7 presents a summary of these results and Figure 5.15 presents an overview of the product formation for the initial and the final configurations. From the analysis of the final configuration, it is possible to verify that the areas with most influence on the product formation are located close to the corners of the channel cross section. This result suggests that the streams with high residence time contribute more to the product formation, which is also logical and expected. The wall of the microreactor causes a decrease in the velocity of the fluid due to the friction between the wall and the fluid. The reduction of the fluid velocity results in the higher residence time of the fluid elements in those locations.

Table 5.7 – Summary of results of the three-dimensional topology optimization case study.

Configuration	Parameter	Value
Initial configuration	Enzyme concentration	$2.5 \cdot 10^{-5}$ mM
	Product concentration	0.433 mM
Final configuration	Enzyme concentration	$5 \cdot 10^{-5}$ mM
	Product concentration	0.566 mM
Improvement: 30.7 %		

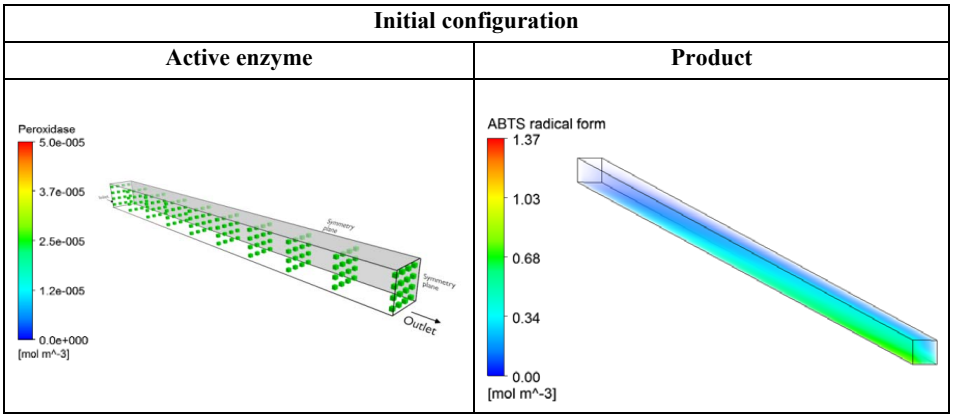

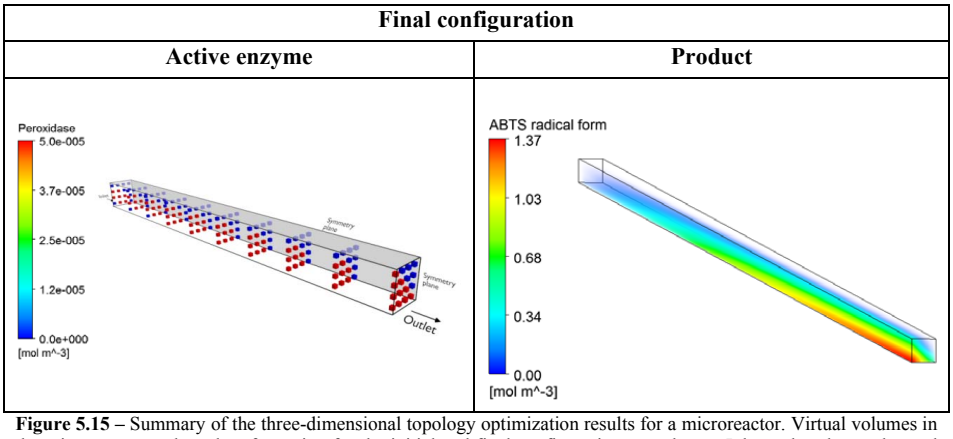

Figure 5.15 – Summary of the three-dimensional topology optimization results for a microreactor. Virtual volumes in the microreactor and product formation for the initial and final configurations are shown. Inlet and outlet are located on the right and left hand side of each figure, respectively. Both reaction volumes and product overview are presented in the microreactor with symmetry planes on the top and the right hand side of the presented channel.

Therefore, the contact between enzyme and substrates is longer in these locations compared with the regions in the core of the flow, where a high velocity is observed. The final configuration of the topology optimization indicates that if the enzyme flow is placed in the corners of the reactor with a maximum concentration it is possible to produce 30% more than if the enzyme at half of maximum concentration is well mixed with the substrate at the inlet. Thus, the outcome of the topology optimization suggests that the inlet of the microreactor should change from the configuration presented in Figure 5.16 a) to the configuration presented in Figure 5.16 b) for achieving the predicted improvement. The reader should notice that the sum of the inlet areas of all four streams at the corners should correspond to half of the inlet area. In this way it will be possible to maintain the average enzyme concentration at the channel cross section for both initial and final configurations.

Inlet of initial configuration Inlet of the final configuration

Figure 5.16 – Configurations for the microreactor inlet where S is the substrate concentration and E is the enzyme concentration: a) inlet configuration for the initial configuration before the topology optimization was applied; b) inlet corresponding to the final configuration results from the topology optimization.

The starting point of the topology optimization problem was a mixed flow microreactor with well-mixed streams of enzyme and substrate at the inlet. The flow inside the microreactor is characterized by a significant radial difference in residence times, diffusional transport and a large radial concentration gradient. Substrate conversion is influenced by the flow characteristics and therefore the reaction rate is not the same in the whole volume of the microreactor. Consequently, the product profile concentration in the cross-section is not uniform.

The studies reported by Bodla *et al.*[101] and Aoki *et al.*[102] demonstrated that the reaction yield improves by increasing the number of interfaces, i.e. reducing the lamination width of the parallel substrate and enzyme streams or reactant streams. These two case studies were described in detail in Chapter 2, section *2.4.2 - Mixing in microsystems*. These results indicate that increasing the number of interfaces improves the mixing between streams and thus, intensify the performance of the microreactor.

In contrast, the topology optimization results, which indicate that placing the enzyme flow close to the walls will produce more product per same amount (mol) of enzyme compared with a microreactor with a well-mixed stream containing enzyme and substrate at the inlet. This result

demonstrates that mixing is an important aspect to take into account for designing a reactor, but it might not be the only factor that should be considered. The improvement of the yield is a function of the flow conditions, local reactants concentration, reaction rate and diffusion properties. Therefore it is necessary to consider all these phenomena simultaneously in order to achieve reactor intensification.

5.4.1.3 Selection of the microreactor configuration for experimental testing

The configuration of the microreactor obtained through topology optimization is quite complex to be manufactured. However, the application of the optimization method to this case study allows gathering information regarding the flow influence on the reaction yield and evaluating options for alternative inlet configurations. The main outcome from the optimization is that the enzyme streams should enter close to the walls.

Further computational investigations on inlet configurations are needed in order to find a microreactor which is possible to be manufactured. Therefore, some configurations with enzyme streams entering close to the walls will be investigated.

In this section simulations of several microreactor inlet configurations are performed in order to investigate possible configurations which are simpler to fabricate and where the enzyme stream is placed next to the walls at the inlet. The eight different inlet configurations for the microreactor are compared by CFD simulations and are presented in Figure 5.17.

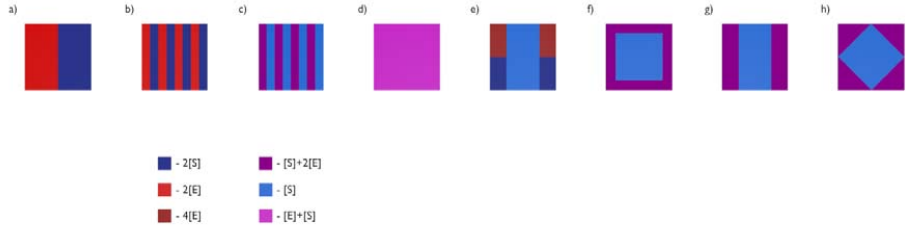

Figure 5.17 – Inlet configurations for the microchannel: a) T-microreactor; b) 8-stream microreactor with enzyme and substrate streams totally separated; c) 8-stream microreactor with 4 streams with double enzyme concentration and substrate mixed and 4 streams with only substrate; d) Mixed flow microreactor, substrate and enzyme well mixed; e) Five-stream microreactor with low substrate concentration at the center and separation of enzyme and substrate streams on the inlet sides; f)Square configuration with double enzyme concentration and substrate stream around the walls and pure substrate stream in the center; g) Three-stream microreactor, two double enzyme concentration and substrate streams on the sides of the channel with a pure substrate stream in the center; h) topology optimized microreactor, double enzyme concentration and substrate streams in the corners of the microchannel with a pure substrate stream in the center. Enzyme concentration [E]=$2.5 \cdot 10^{-5}$mM and substrate concentration [S]=10 mM.

Three new possible configurations which place the enzyme close to the walls are presented in Figure 5.17 e), f) and g). One of these configurations will afterwards be chosen for fabrication and laboratory testing as the better performing microreactor. The enzyme solution is considered to enter the microreactor well-mixed with substrate in both inlet configurations f) and g). However, the reader should note that these solutions enter separately in the configuration e). The configuration e) was chosen to be investigated due to its simple fabrication procedure. The microreactor can be fabricated using a series of layers of PMMA. The reaction microchannel can be placed in the middle layer, the enzyme and substrate side streams enter the microreactor at the bottom and the top layers, respectively, where they split into two streams. The split streams of the enzyme and the substrate join at the microreactor level and enter together as laminated streams in the reactor chamber. The substrate center stream enters directly in the microreactor channel layer.

The simulations of the configurations a), b), c) and d) in Figure 5.17 will allow a full understanding of the importance of the inlet configuration for the mixing of the streams. This aspect is important afterwards, for deciding whether one of these configurations will be chosen for laboratory testing as the poor performing microreactor.

All microreactor configurations are characterized by a squared shaped cross-section channel of 0.5 mm width, 0.5 mm height and 50 mm length identical with the microreactor used for the topology optimization study. The average flow rate inside the microreactor is the same as the flow rate considered for the topology optimization case study presented in the previous section. The reaction mechanism was also considered to be the same as applied to the optimization case study, i.e. the oxidation of ABTS using peroxidase. The difference between these different channels is the inlet configuration. The reader should note that although the placement of the substrate and the enzyme streams at the inlet is different, the average quantity of enzyme and substrate inside the microreactor per time unit are the same for all configurations in order to allow a fair comparison. Moreover, the flowrates of the streams were adjusted for all inlets in different inlet configurations such that the residence time (20 s) inside the microreactors and the flow profile are the same among the microreactors and it is possible to compare them.

The detailed description of the microreactor inlet of configurations a), b), c), e), f) and g) are presented in Appendix D. An overview of the product concentration at the outlet plane for all the configurations is given in Figure 5.18.

Microreactor configuration	Outlet product concentration	Microreactor configuration	Outlet product concentration
T-microreactor 	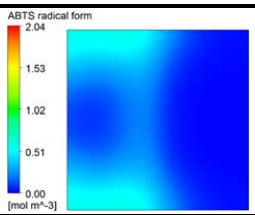	Five-stream microreactor 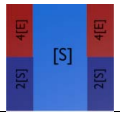	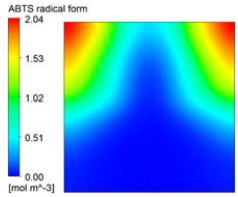
8-stream microreactor with separation of enzyme and substrate streams 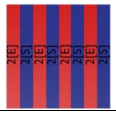	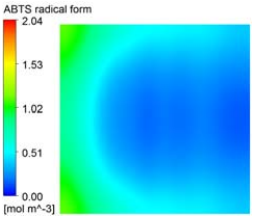	Square microreactor 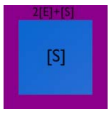	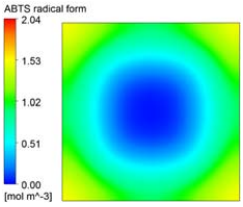
8-stream microreactor with uniform substrate concentration at inlet and separation of enzyme streams 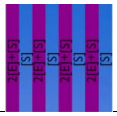	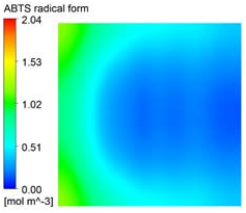	Three-stream microreactor 	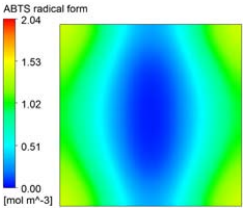
Mixed Flow microreactor 	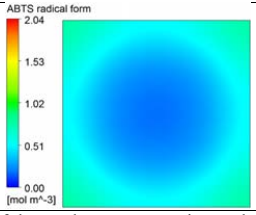	Topology optimized microreactor 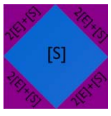	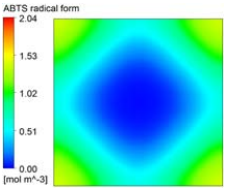

Figure 5.18 – Overview of the product concentration at the outlet plane for configurations a), b), c), d), e), f), g) and h). Enzyme concentration [E]=2.5·10^{-5}mM and substrate concentration [S]=10 mM

The average product concentration at the outlet for the different microreactor configurations is summarized in Figure 5.19.

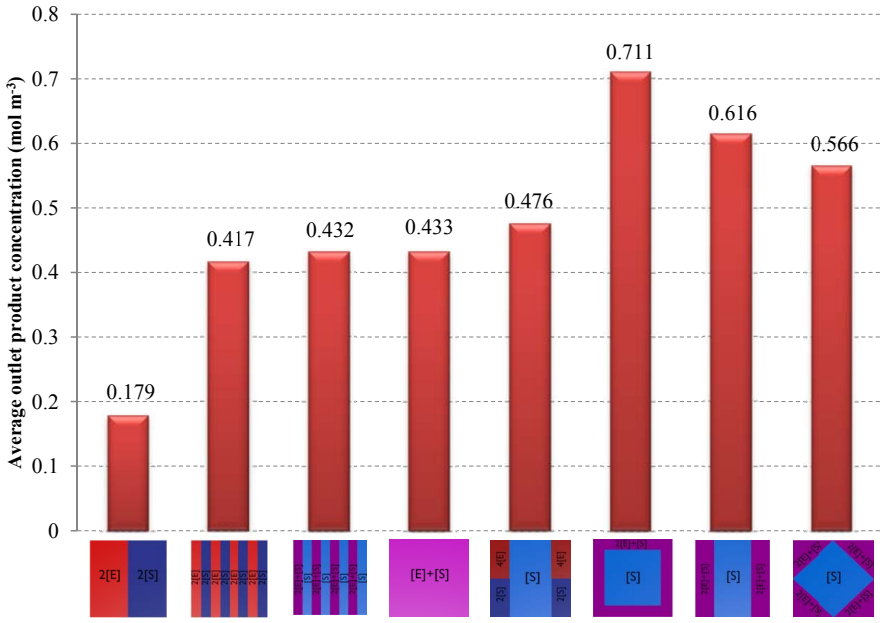

Figure 5.19 – Summary of results, product concentration at the outlet for all microreactor inlet configurations.

From the results presented above it is possible to verify that the T-microreactor is that configuration that performed worst. The enzyme molecules do not diffuse significantly in the microreactor due to its low diffusion coefficient (10^{-11} $m^2 \cdot s^{-1}$) and the enzyme is furthermore concentrated at the side where it enters. Therefore, the reaction only occurs particularly at the interface of the substrate and enzyme streams for this configuration. Moreover, the higher residence time streams close to the walls also contribute to the production. In the areas close to the top and bottom walls the compounds diffuse more due to the higher residence time of the substances and therefore, promote the diffusion of the different compounds and consequently the product formation.

Both 8-stream configurations show that the reduction of the lamination width of the streams results in smaller diffusion distances and consequently, contributes to a better mixing between the streams. The advanced diffusion conditions for the different compounds and the improvement of the mixing of the compounds inside the reactor result in a higher production compared with the T-microreactor. The improvement of the mixing between streams seems to improve the production yield such that it approximates the same value as achieved for the Mixed flow microreactor.

The Five-stream microreactor shows that the placement of the enzyme in the area close to the side walls results in a better performance than the Mixed flow microreactor. In fact, even though the

positioning of the enzyme streams is only at the top part of the reactor it seems that the production is very effective in these areas and improves the microreactor performance.

Both the Three-stream and the Square configurations have shown better yields than the optimized configuration resulting from the topology optimization. The performances of these configurations demonstrate that the outcome of the optimization does not correspond to the global optimum configuration. In Chapter 2, the gradient-based methods drawbacks were reviewed and one of them was indeed the great probability of the method converging to a local minimum instead of the global minimum.

Nevertheless the local optimal result of the topology optimization has given the needed information for manufacturing a microreactor design with better reaction yield.

From the investigation of the different inlet configurations, it is possible to conclude that the mixing inside a reactor is not the only factor to take into account when designing a reactor. The studies including the reduction of lamination width of the streams (from a) to b) and c)) improve the mixing and thereby their product yields converge only to reach the yield of the Mixed Flow configuration. The optimization method has demonstrated that the considered Mixed flow configuration, can be further improved by placing the enzyme streams in specific favorable inlet regions.

The main outcome of this study is that positioning of the catalyst plays an important role for the reactor performance. According to this computational study, the production can be improved up to 60% with the same reactor volume and the same amounts of catalyst and substrate by placing the enzyme stream close to the walls.

The T-microreactor and the Five-stream inlet were the microreactor configurations chosen for laboratory testing. For time reasons, the laboratory work had to be simplified and therefore, it was decided that the simplest configurations would be fabricated and tested. We are aware that these configurations are very different from the initial and the optimal structures.

The test of the Mixed flow configuration and one of the optimized structures (e.g. Three-stream and the Square microreactors) requires further investigation in order to guarantee well-mixed streams of enzyme and substrate at the inlet and low product formation during the mixing process. The laboratory testing of the simple configurations will still allow the verification of the improvement of the reaction yield by modifying the configuration of the substrate and the enzyme streams at the inlet. The results of the experimental verification are presented in the following section.

5.4.2 Experimental verification of the computational results

The experimental verification of the topology optimization will be achieved by comparing the T-microreactor configuration and the Five-stream microreactor.

According to the CFD simulation results, the experimental validation should show that the Five-stream microreactor is 166% better than the T-microreactor.

5.4.2.1 Microreactor fabrication

The microreactors were designed using the computer-aided design program SOLIDWORKS®. The microreactor configuration was fabricated using poly(methyl methacrylate) (PMMA) plates (1.5 mm) and double adhesive tape sheets (Medical Grade Tape -142 μm, PET foil, obtained from Microfluidic Chipshop). The PMMA plates and the double adhesive tape have the following dimensions: 4 cm width and 10 cm length.

The microreactor configuration consisted of 4 layers of PMMA plates and the reactor channel was made by attaching 4 sheets of double adhesive tape (height 0.568 mm). Since the height of a tape sheet is 142 μm and in order to maintain the height and the width the same dimensions, the microchannel design was changed in SOLIDWORKS® and the width was adjusted to 0.568 mm. The length of the microreactor is the same as in the CFD simulations, 50 mm.

The several layers of the microreactor (PMMA and double adhesive tape layers) were laser ablated using a CO_2 Laser Engraving Machine (model CMA-4030 from Hans' Yueming Laser).

T-microreactor

The T-microreactor was assembled by four plates of PMMA (1.5 mm) and four sheets of double adhesive tape. The layers of PMMA were used for defining the inlets and outlets of the microreactor and the channels which promote the division of the streams. The four sheets of double adhesive tape were glued together and cut to be compatible with the shape of the reaction chamber.

In the first layer of the reactor made of PMMA, three holes were drilled, two for the inlets for the enzyme solution ($5 \cdot 10^{-5}$ mM of peroxidase) and the substrates solution (20 mM ABTS, 200mM H_2O_2) and one outlet.

The second layer is also made of PMMA and is ablated in the form of a microchannel which carries the enzyme solution until the point the solution descends to the reaction microchannel layer to be combined with the substrate solution. In this layer, two other holes were drilled; one to carry the substrate solution to the fourth layer of the microreactor and one for carrying the outlet solution (See Figure 5.20).

The bottom and fourth layer which was made of PMMA was ablated in the shape of a microchannel to carry the substrate solution until the point it ascends to the reaction microchannel layer to be combined with the enzyme solution (See Figure 5.20).

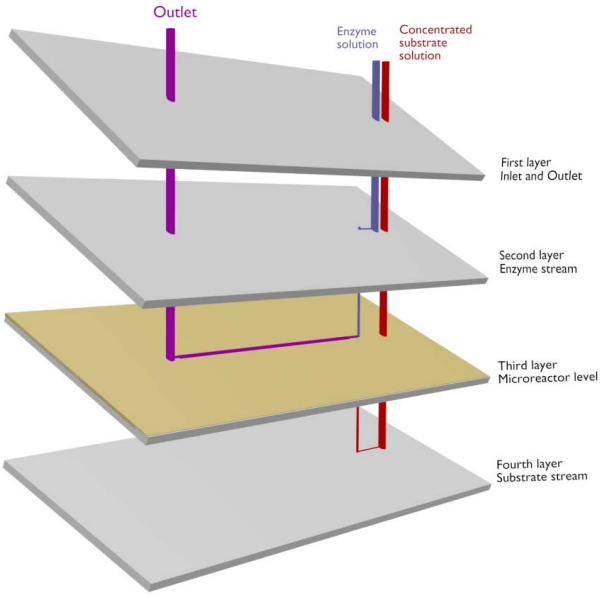

Figure 5.20 – View of the different layers of the T- microreactor and the different streams with details on the flows and the combination of streams.

The third reaction microchannel layer was made by four sheets of double adhesive tape with the dimensions stated above. The four sheets of double adhesive tape were glued to a plate of PMMA in order to guarantee physical separation from the channels carved in the bottom layer. A hole was also drilled in the reaction microchannel layer to carry the substrate solution to the fourth layer of the microreactor. The PMMA layers were glued to each other with a layer of double adhesive tape.

In the reaction microchannel layer, the enzyme and substrate solutions are combined before entering the microreactor (See Figure 5.20 and Figure 5.21). The combination of these two streams result in two laminated parallel streams of enzyme and substrate. The final configuration of this microreactor corresponds to the T-microreactor configuration but with the streams as fluidic layers instead of side-by-side streams. The final average concentrations at the inlet of the reaction chamber are 10 mM of ABTS, 100 mM of H_2O_2 and $2.5 \cdot 10^{-5}$ mM of peroxidase.

Figure 5.21 – Top view of the microchannel for the T-microreactor.

Five-stream microreactor

The Five-stream microreactor consisted also of four layers of PMMA (1.5 mm) and four sheets of double adhesive tape which are used for the reaction chamber. The complete microreactor design can be found in Figure 5.22.

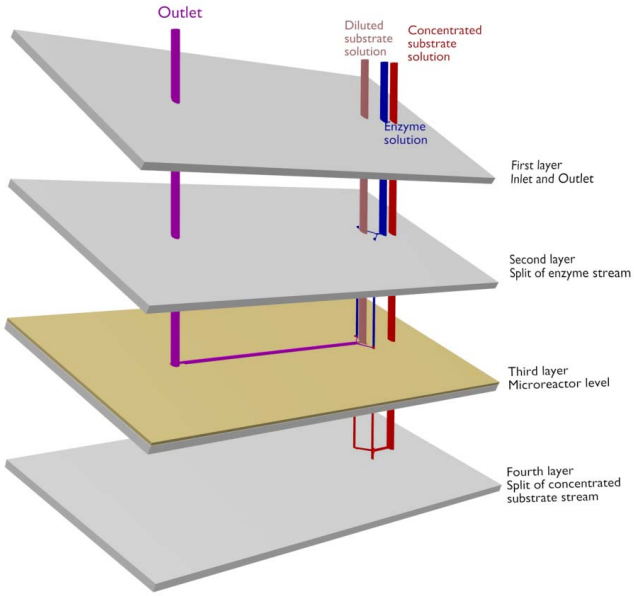

Figure 5.22 – View of the different layers of the Five-stream microreactor and the different streams with details of the flows and combination of streams.

The top layer of PMMA has four holes which are made for the concentrated substrate solution inlet (20 mM ABTS, 200 mM H_2O_2), the diluted substrate solution inlet (10 mM ABTS, 100 mM H_2O_2), the enzyme solution inlet ($1 \cdot 10^{-4}$ mM peroxidase) and the outlet. The second layer of PMMA was ablated in order to create microchannels for the splitting of the enzyme solution. The bottom and fourth layer of the microreactor is also made of PMMA and was ablated in order to create channels for the splitting of the concentrated solution of substrate.

The third layer of the microreactor holds the reaction chamber. The reaction chamber was fabricated in 4 sheets of double adhesive tape glued to each other. This layer is pasted to a plate of PMMA in order to guarantee physical separation from the channels ablated in the bottom layer. A hole was also drilled in this layer to carry the substrate solution to the fourth layer of the microreactor.

The PMMA layers were attached to each other with a layer of double adhesive tape.

The enzyme solution from the second layer and the concentrated substrate solution from the bottom layer are split into two streams. Afterwards each split enzyme stream is combined with one of the split substrate streams at the microreactor level before entering the reaction chamber (See Figure 5.22). The combination of these streams results in two parallel laminated streams of enzyme and substrate.

Three streams meet at the inlet of the microreactor: two streams containing the lamination of substrates and enzyme streams and entering close to each side wall of the channel and one stream containing the diluted substrate solution (10 mM ABTS, 100 mM H_2O_2) entering in the middle of the channel (See Figure 5.23). The final average concentrations at the inlet of the reaction chamber are: 10 mM of ABTS, 100 mM of H_2O_2 and $2.5 \cdot 10^{-5}$ mM of peroxidase.

Figure 5.23 –Top view of the microchannel for the Five-stream microreactor.

The T-microreactor inlets were connected to two syringe pumps (50 µL) (model Cavro XLP6000, from Tecan) which contained the peroxidase solution ($5 \cdot 10^{-5}$ mM) and the substrates solution (20 mM ABTS, 200 mM H_2O_2), respectively. The Five-stream microreactor inlets were connected to three syringe pumps (50 µL) (model Cavro XLP6000, from Tecan) which contained the concentrated substrates solution (20 mM ABTS, 200 mM H_2O_2), the diluted substrates solution (10 mM ABTS, 100 mM H_2O_2) and the enzyme solution ($1 \cdot 10^{-4}$ mM). The flow rate was set to ensure that the residence time inside the microreactor would be approximately 20, 10 and 5 seconds, respectively. The microreactor outlet was connected to the same UV-detection system used for the determination of the reactor performance in Case 1 of this chapter,

The experimental protocols and the operation of the on-line UV-detection system are described in detail in Appendix B.

5.4.2.2 Results and discussion

Both the T-microreactor and the Five-stream microreactor were tested at three different residence times (5, 10 and 20 s) using freshly prepared substrates and enzyme solutions. Figure 5.24 summarizes the average of the absorbance values obtained over time for both microreactor configurations and for the different residence times tested.

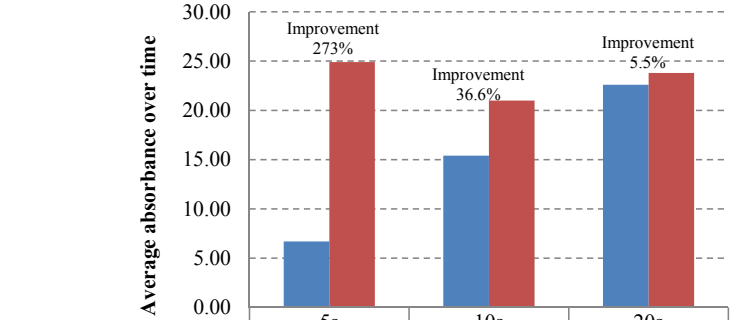

	5s	10s	20s
T-microreactor	6.7	15.4	22.6
Five-stream microreactor	24.9	21	23.8

Figure 5.24 – Comparison of average measured absorbance over time in the microreactor outlet, comparing the T-microreactor and the Five-stream microreactor for the residence times 5, 10 and 20 s. The improvement of the product formation when comparing the T-microreactor and the Five-stream microreactor is obvious, especially for low residence times.

The improvement of the product concentration in the Five-stream microreactor in relation to the T-microreactor for all residence times are also presented in Figure 5.24. The improvement was calculated using the average values of the absorbance registered over time for both microreactor configurations.

The absorbance measurements over time for the comparison between the T-microreactor and the Five-stream microreactor for the different residence times are presented in Figure 5.25. The Five-stream microreactor configuration showed for all residence times a better performance than the T-microreactor. The improvement was higher for the lowest residence time (5 s) compared with the residence times 20 s and 10 s.

For a residence time of 5 s, the improvement between the Five-stream microreactor and the T-microreactor was 273.4%. The production of the Five-stream microreactor for 5 s of residence time was as high as the production of the T-microreactor for a residence time of 20 s. For a residence time of 10 s, the improvement between the Five-stream microreactor and the T-microreactor was 36%. For the residence time of 20 s, the improvement between the Five-stream microreactor and the T-microreactor was only 5.5%.

Residence time (s)	Experimental results
5	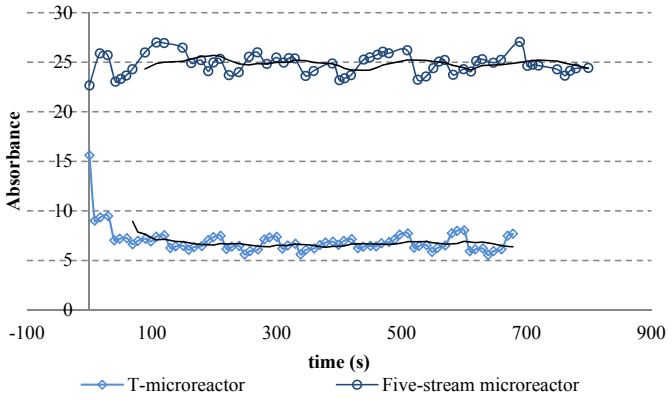
10	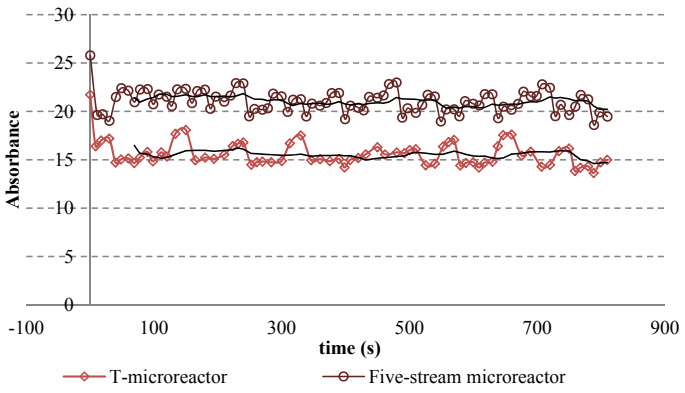
20	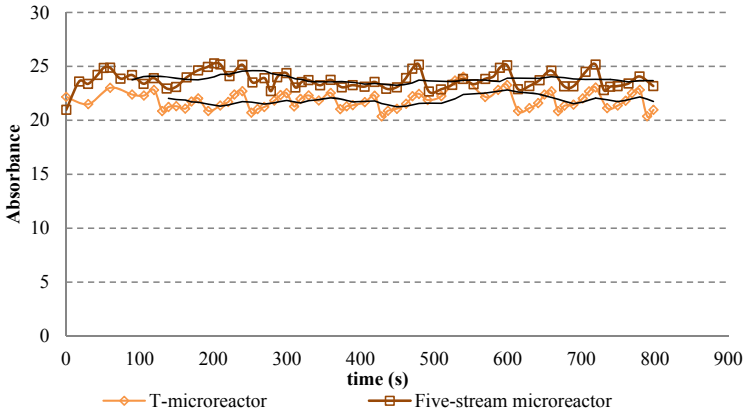

Figure 5.25 – Absorbance measurements over time for the comparison between the T-microreactor and the Five-stream microreactor for the different residence times.

The experimental work has verified the simulation results since the placement of enzyme in high residence time streams (close to the wall) resulted in a significant improvement of the reaction yield. Moreover, it was also experimentally shown that it is possible to increase the production per same amount (mol) of enzyme and substrates in the same reactor by modifying the placement of the enzyme in the inlet streams.

The experimental results show that the improvement tends to decrease when the residence time increases. More simulations were performed in order to verify this trend. The T-microreactor and the Five-stream microreactor configurations were simulated in order to include the results for residence times 5 s and 10 s. These simulations were performed in order to understand the trend with decreasing improvement of the performance in the Five-stream microreactor relative to the T-microreactor, when the residence time increases. The presented results in Figure 5.26 correspond to the substrate and product concentration profile along the channel width at the outlet and at a channel height of 0.45 mm.

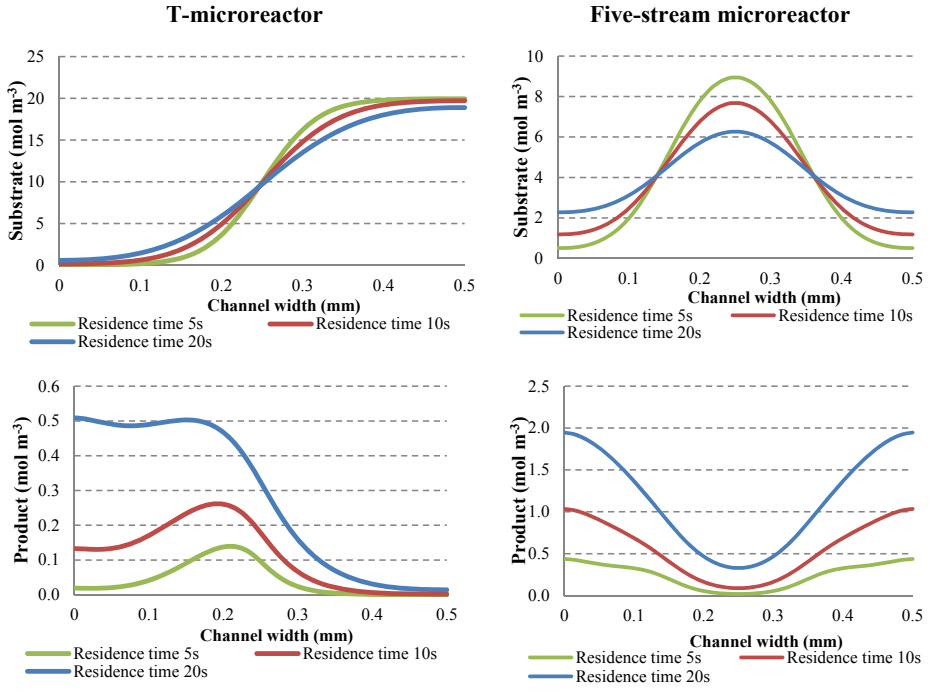

Figure 5.26 – Simulation results for T-microreactor and Five-stream microreactor for residence times 5s, 10s and 20s**.** Substrate and product concentration profile along the channel width at the outlet and at 0.45 mm of height.

It is possible to verify from the analysis of the simulated substrate concentration profile of the T-microreactor in Figure 5.26 (top left graph) that for high residence times the diffusion from the bulk to the walls is larger compared with low residence times. Thus, the level of substrate dispersion in the T-microreactor tends to approximate the dispersion level in the Five-stream microreactor when the residence time increases. This fact can explain the similar production achieved in both microreactors in the experimental results. Therefore, the achieved improvement at high residence times is lower than for cases with low residence time.

At low residence time, the dispersion between the streams in the T-microreactor is much lower due to the fast flow velocity close to the interface (See substrate concentration profile in Figure 5.26). When the enzyme streams are positioned next to the walls in the Five-stream microreactor the residence time of the molecules is higher and the diffusional mass transfer between the streams increases. Therefore, the improvement becomes much larger at low residence times. This trend of larger improvements at low residence times is also present in the simulations results (See Figure 5.27)

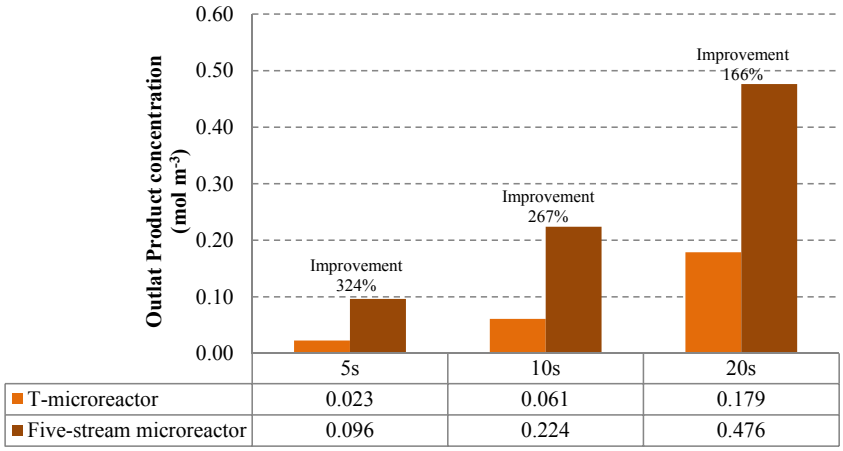

Figure 5.27 – Product concentration for simulations of the T-microreactor and the Five-stream microreactor for the residence times 5 s, 10 s and 20 s.

From the comparison between the simulation and the experimental results it is possible to verify that there is a considerable difference between the simulation values and the experimental values. This difference might be related to many factors and assumptions made along the project such as the diffusion coefficients collected from the scientific literature or the assumption of the percentage of enzyme present in the commercial preparation. Moreover, the enzyme and substrate streams have been combined before entering the microreactor and the compounds have already diffused to some extent between streams before reaching the microreactor chamber which might affect the yield results.

More experimental work is necessary to compare the Mixed flow microreactor (optimization initial configuration) with an optimized configuration such as the Three-stream or the Square microreactor. For this laboratory testing it is necessary to guarantee good mixing between the enzyme and the substrate streams. The streams should be mixed for a shorter period of time to avoid the formation of product before entering the reaction chamber. Currently, ensuring good mixing of these streams at the inlet and at the same time avoiding the product formation is the bottleneck which prevents the detailed laboratory comparison of the Mixed flow microreactor with one of the optimized microreactors.

5.5 Concluding remarks

This chapter included an experimental study for verification of the topology influence on microreactor performance. The experimental investigation procedure consisted of four stages: determination of the kinetic reaction mechanism associated with the chosen reaction, topology optimization of the chosen microreactor through numerical and computational methods, fabrication of the intensified and the reference configurations according to the information gathered from the topology optimization and experimental test of the manufactured microreactors.
The chosen reaction system for the topology optimization and further experimental work was the oxidation of ABTS to its radical by peroxidase by reducing H_2O_2. The concentration of H_2O_2 was maintained constant in order to guarantee that the reaction obeyed a Michaelis-Menten mechanism. The values of the determined reaction parameters are the following: $V_{max}^{ABTS} = 0.026\ \mathrm{mM/min}$, $K_M^{ABTS} = 0.76\ \mathrm{mM}$ and $k_{cat}^{ABTS}\ 732\ \mathrm{s^{-1}}$. The determined kinetic parameter values were found to be in good agreement with the reported values in the scientific literature.
The results of the two-dimensional topology optimization indicate that the enzyme should be mostly immobilized at the area where low residence time streams occur, and in the area close to the outlet. This demonstrates that the low residence time streams contribute more for the product formation. The low diffusion of the substrate and product and the high reaction rate result in an insignificant production in the high residence time areas. Thus, the low residence time streams are not important for the microreactor yield in this case.
Two-dimensional topology optimization experimental validation requires more work in order to improve the accuracy of the quantification of immobilized enzyme on the surface. Nonetheless, the covalent immobilization procedure using the photochemical reaction of glycidyl methacrylate with the thiol groups on the surface demonstrated promising results regarding the delineation of immobilization areas. Furthermore, the non-immobilization of peroxidase on the wall surface by adsorption contributes also to a precise definition of immobilization areas. Further work will be performed in order to quantify accurately the amount of enzyme on the surface and to validate experimentally the two-dimensional topology optimization results.

A three-dimensional topology optimization was applied to a squared channel considering free enzyme in solution. The computational study was performed by identifying the best areas to place the active enzyme at the inlet, and keeping the amount of active enzyme applied to the microreactor identical for all configurations. The final configuration of the microreactor structure obtained via topology optimization suggested that the enzyme streams should be placed next to the walls. From these results it was possible to conclude that good mixing might not be the only factor to consider for reactor design. In fact the placement of enzyme streams plays an important role in this specific case study. The placement of the enzyme solution stream close to the wall improves the production compared with a microreactor where the enzyme solution is well-distributed. In fact, the yield improvement depends on the flow conditions, the diffusion properties of the compounds involved in the reaction, the local reactant concentrations and reaction rate. Therefore the intensification of a reactor should be performed by considering all these phenomena.

Further computational investigations had to be performed since the fabrication of the optimal configuration would be rather complex. Therefore, eight different microreactors with different inlet configurations were simulated. It was observed that the obtained structure from topology optimization did not correspond to the global optimum. This fact is one of the known drawbacks of the gradient-based optimization methods such as the Evolutionary Structural Optimization method that has been used here. Nevertheless, the topology optimization allowed collecting information for designing a structure which could be fabricated.

The experimental verification of the optimization of the microreactor inlet configuration was performed by comparing the T-microreactor and the Five-stream microreactor configuration. The microreactors were chosen in order to simplify the fabrication process and to maintain the same conditions as used for the simulations. The fabrication of the initial configuration and structures such as the Three-stream and the Square microreactors requires further investigation in order to guarantee well-mixed streams of enzyme and substrate at the inlet.

The comparison between the two microreactor configurations was done by operating the reactors with the same amounts of substrates and enzyme inside the reaction channel. The obtained results in this experiment verify the simulation results of the microreactor configurations. For all experiments, it was possible to verify that the Five-stream microreactor always performed better than the T-microreactor. Furthermore, the experimental results demonstrate that it is possible to produce more with the same amount of enzyme by placing the biocatalyst in strategic locations at the inlet of the microreactor.

The simulation of the T- and the Five-stream microreactors for residence time 5 and 10 s show the same trend of improvement reduction. For low residence times the improvement between the two configurations is much higher than for high residence times. For high residence times the

substrate dispersion of the T-microreactor seems to approximate the dispersion values in the Five-stream microreactor, and therefore performance of both reactors is quite similar.

From the results obtained in this chapter, it is possible to confirm that topology optimization is a tool which can be applied to process intensification in microreactors. With this tool the design of the reactor is customized considering the reaction mechanism and the flow conditions. Although the studied microreactor has been very well described in the scientific literature, new and interesting aspects regarding the inlet configuration have been identified here with the help of topology optimization.

Chapter 6

Conclusions and future perspectives

6.1 General conclusions

The main goal of this Ph.D. project was to investigate the innovative application and development of shape and topology optimization for the intensification of microreactors and their validation. Both topology and shape optimization methods were successfully implemented by defining an interface between ANSYS CFX® and MATLAB®.

The shape optimization method was used for optimizing a three-dimensional microreactor geometry. The aim of this study was to evaluate the impact of the microreactor shape on the reaction yield. The random search method was chosen for performing this optimization. The optimization cycle was straightforward to implement due to the simplicity of this technique. The presented case study differed from cases presented in scientific literature due to the three dimensional evaluation and the usage of a structured mesh with automatic adaptation to all generated geometries. The automatic generation of the structured mesh was the foremost challenge in the setup of the optimization procedure due to the complex definition of the strategy for minimizing the discontinuity of the domain.

The starting point of the shape optimization was a YY-microreactor with a square shaped cross section along the z-axis of the reaction channel. The optimized microreactor shape is a very complex geometry with many curvatures. The expansions and shrinkages of the microreactor shell contributed greatly to the convective mixing of the parallel enzyme and substrates streams and consequently to the reaction yield improvement.

The topology optimization was implemented by adapting the Evolutionary Structural Optimization method commonly used by mechanical engineers for the optimization of the layout

of building or mechanic structures. This method considers that the structural elements contain a certain initial enzyme concentration. The adapted method differs from the original method in the process of removing inefficient structural elements. When an element is removed the amount of enzyme of that specific element has to be distributed over all the other elements which still contain immobilized or active enzyme. Otherwise the removal of elements would end up removing enzyme from the whole system and therewith would change the total amount of catalyst inside the reactor.

The subsequent investigated method, the topology optimization, was implemented differently from the case studies presented in the scientific literature since it considers the enzyme concentration as the design variable and provides the opportunity to study more realistic problems. Furthermore, this method is also different since the flow profile is maintained constant and allows the identification of possible effects of the flow conditions on the local reaction rate and the product formation.

A case study of topology optimization of a packed bed microreactor with asymmetric flow resulted in very different structures just considering different substrate concentrations and flow conditions between the two case studies. The chosen reaction mechanism of the enzyme followed the Michaelis-Menten equation and the kinetic parameters considered were: $k_{cat} = 100\ s^{-1}$ and $K_M = 25\ mM$. The case with lower substrate concentration (10 mM) resulted in positioning the enzyme in the streams with high residence time. However, not all high residence time streams had the same influence on the product concentration leaving the microreactor. Only the streams facing directly the outlet were the most important ones. The case with higher concentration (60mM) resulted in a configuration in which the enzyme should be placed in the low residence time streams instead. In fact, a study of the local conditions in the high residence time streams demonstrated that the concentration of substrate is low due to mass transfer limitations and therefore, do not contribute significantly to the outlet product concentration.

The two-dimensional topology was applied to a parallelepiped microreactor with an inlet and an outlet. The inlet and the outlet are located at opposite sides of the chamber. The enzyme was immobilized on the top and the bottom inner walls of the microchamber. This geometry was optimized with two different reactions following the Michaelis-Menten mechanism. The reactions were characterized by a slow reaction in Chapter 4 ($k_{cat} = 100\ s^{-1}, K_M = 25\ mM$) and a fast reaction in Chapter 5 ($k_{cat} = 732\ s^{-1}, K_M = 0.76\ mM$). In the case with the low reaction rate, the enzyme was immobilized mainly in the areas of high residence time streams. The flow velocity in these regions is low and thus the contact between the enzyme and the substrate is longer, contributing to the product formation. However, not all the high residence time streams contribute in the same way to the outlet product concentration. According to the optimization results, streams very close to the walls do not influence the reactor yield. The final enzyme

configuration resembles the spatial cell configurations documented previously in the scientific literature.

The optimized distribution is characterized by immobilized enzyme in the areas of high residence time. The low substrate and product diffusion associated to the fast reaction rate result in mass transfer limitations inside the reaction chamber.

As mentioned above, in Chapters 4 and 5 some geometries were investigated for different reaction systems and/or flow conditions such as the microreactor with immobilized enzyme on the wall surface and the packed-bed microreactor. The different conditions inside the microreactor for the several case studies demonstrated that even though the geometry was the same, the final configurations were very divergent. This indicates that every case is dependent on the residence times, the flow profile, local substrate concentration and the kinetics associated with the reaction. It was also shown that it is not always possible to identify a single cause for the optimal biocatalyst layout and the results might be a consequence of the combination of all factors stated above. Furthermore, it was confirmed that the optimized layout of the catalyst cannot be determined by simply looking at the initial configuration simulation results and making a decision based on those findings. From the analysis of the presented case studies it is possible to conclude that the CFD simulation results of the initial configurations do not give the information where to place the enzyme. This fact emphasizes the importance of topology optimization as a design tool and intensification of reactors. In Chapter 5 an experimental investigation of the influence of the microreactor topology on the product yield was presented. The used reaction for the experimental work was the oxidation of ABTS to its radical by peroxidase by reducing H_2O_2. The concentration of H_2O_2 was maintained constant in order to guarantee that the reaction was executed under a Michaelis-Menten kinetic mechanism. The values of the determined reaction parameters are: $V_{max}^{ABTS} = 0.026\text{mM/min}$, $K_M^{ABTS} = 0.76\ \text{mM}$ and $k_{cat}^{ABTS} = 732\ \text{s}^{-1}$.

Experimental work was performed towards the validation of the two-dimensional optimization with the parallelepiped microsystem with immobilized enzyme on the wall surface with the fast reaction mentioned above. A squared-shape cross section microchannel with free enzyme in solution was used for experimental studies for the verification of the three-dimensional microreactor optimization. Both systems were computationally optimized and were thereafter fabricated.

The computational results of the two-dimensional case study correspond to the case study with the fast reaction rate mentioned above. The covalent enzyme immobilization using the photochemical reaction of glycidyl methacrylate with the groups on the surface showed promising results regarding the delimitation of immobilization areas. However, the quantification procedure of the amount of immobilized enzyme on the surface has demonstrated to be quite erroneous. The quantification of immobilized enzyme is an important parameter in order to validate the topology optimization. The enzyme concentration on the wall surface duplicates along the optimization but

the immobilization surface in the final configuration is half than in the initial configuration. By adjusting the concentration to the immobilization surface area, the amount of enzyme (mol) in the microreactor is maintained constant between the designs. Therefore, more experimental work is necessary to accurately quantify the mass of immobilized enzyme.

The three-dimensional computational optimization results have shown that the enzyme streams should flow close to the microchannel walls. In the scientific literature, it is usually reported that the enzyme streams should be distributed along the width of the channel. In this way, the diffusion path between the enzyme and substrate streams is shorter and consequently, better mixing and product yields are achieved. However, the topology optimization has demonstrated that a well-mixed microreactor, considered by many microfluidics experts as an efficient system, has its limitations and can actually be further optimized. The main conclusion from the outcome of the computational optimization is that the yield improvement is also related to the flow conditions, substrates and enzyme diffusion rates, local concentrations and the reaction rate. Thus, the intensification of a reactor also requires an evaluation of the combination of all these phenomena and topology optimization is a suitable tool for the systems' development.

Since the fabrication of the optimal reactor configuration was very complex, further computational studies were performed in order to identify a feasible system. The investigated systems were designed considering the outcome of the optimization: the enzyme streams should flow close to the walls. These studies have shown that the optimal configuration was in fact not the global optimum. In fact one of the drawbacks of the ESO method is the high probability of converging towards a local optimum due to its gradient-based procedure. The experimental verification was performed by comparing a T-microreactor and a Five-stream microreactor. The T-microreactor has two laminar parallel streams entering, one with enzyme solution and one with substrate solution. The Five-stream microreactor inlet is characterized by five streams: a diluted substrate solution in the center stream and the lamination between a stream of enzyme solution and a stream of concentrated substrate solution at each side of the center stream. From the computational studies it was verified that the Five-stream microreactor has a better performance than the T-microreactor. And indeed, during experimental work, the Five-stream microreactor has performed better than the T-microreactor for all investigated residence times. It was verified that it is in fact possible to improve the reaction yield by placing the enzyme solution in the high residence time streams. Furthermore, it was also shown that it is possible to increase the production per same amount of enzyme and substrates in the same reactor volume by solely modifying the position of the enzyme and substrate streams at the inlet. With respect to the topology optimization validation, further experimental work has to be performed in order to decide whether the simulation predicts the performance correctly or not.

Comparing the topology and the shape optimization techniques, the first was simpler to implement due to the straightforwardness of the random search method. However, the

optimization cycle using the gradient free method was exponentially larger than the gradient-based cycle applied to topology optimization. Thus, the gradient-based method allowed faster achievement of results. Nonetheless, the gradient-based method presents a high probability of converging to a local minimum. One of the case studies for experimental validation has actually shown that the optimized geometry corresponded to a local optimum. In fact even better configurations were achieved through further computational investigation. Regarding the other presented optimal configurations in this thesis it is not possible to guarantee that they are a global optimum either. Despite the local optimum convergence, an optimal configuration can be obtained from gradient-based optimization methods which can be afterwards tested. Moreover, finding configurations through shape and topology optimization, even though they are at a local minima, avoid expensive experiments in order to find an improved configuration.

In conclusion, I showed successfully that shape optimization and topology optimization methods from mechanical engineering can be applied to the early stage development of microreactors design. It has also been demonstrated that a new strategy for designing reactors has been found. It was shown that it is possible to develop reactor configurations which can be customized according to the reaction mechanism, flow conditions and diffusion of the compounds.

6.2 Future work

The validation of topology optimization is still required and therefore more experimental work is necessary. The validation will be done by continuing the work presented in Chapter 5. The validation of the two-dimensional topology optimization will be performed by using the systems with immobilized enzyme on the wall surface. When the biocatalyst amount determination is accurate enough the optimal configuration obtained through the computational study will be tested and compared with the initial configuration. Regarding the three-dimensional topology optimization validation will be performed using the well-mixed microchannel. The main challenge at the moment is to guarantee the good mixing between the substrate and the enzyme streams at the inlet and avoiding the product formation at the same time.

The application of topology optimization to chemical processes is still in early development and for now it has mostly been implemented in microscale. The method used in this thesis is usually applied to mechanical engineering problems and therefore, it had to be adapted to chemical engineering problems. Although, it has successfully been applied in these case studies it might need to be adapted again to different investigations. Thus, the development of topology optimization methods applied to chemical engineering might be a requirement for further application of this methodology.

The case study for the application of shape optimization has shown that the mixing was the most important phenomenon for that specific reaction system and microreactor geometry. However, the

mixing might not be the dominant aspect in all systems and for other systems it might be possible to observe the microreactor shape impact on operation *in-situ* product removal strategies in order to overcome product inhibition or/and unfavorable equilibrium. Moreover, shape optimization can be applied to other structures in chemical processes such as impellers and static mixers.

Topology optimization was applied to the distribution of the enzyme inside the reactor. Nonetheless, this method could also be applied to other types of catalysts, such as cells and chemical catalysts. Looking at the long term, topology optimization could also be applied to multi-enzyme reaction systems such as cascade systems. Cascade systems are based on performing a sequence of two reactions: the first corresponds to the enzymatic synthesis of the desired product and the second enzymatic reaction has the function to remove the co-product inhibitory co-product or to shift the unfavorable equilibrium of the first reaction. Additionally, topology optimization can also be applied to more complex systems and be applied to both the catalyst and the substrate streams in a case with free catalyst in solution.

The presented case studies in this thesis were separate applications of shape and topology optimization. An interesting case to investigate would be to join the shape and topology optimization for intensification of reactors. In this way it would also be possible to optimize both the spatial distribution of enzyme and the flow conditions.

The implementation of these optimization methods for large scale reactor design should be investigated. These techniques have the potential to generate know-how for the industry and develop new strategies for developing reactors at higher scale.

Bibliography

1. Huang X, Xie YM. *Evolutionary Topology Optimization of Continuum Structures*. Chichester, UK: John Wiley & Sons, Ltd; 2010.

2. Bendsøe MP. *Topology Optimization : Theory, Methods and Applications*. Springer; 2003.

3. Schoofs AJG. Structural optimization history and state-of-the-art. *Top Appl Mech*. 1993:339-345.

4. Maxwell JC. On reciprocal figures, frames, and diagrams of force. *Sci Pap Univ Press*. 1890;2:161-207.

5. Michell AGM. The limits of economy of material in frame-structures. *Philos Mag*. 1904;47(8):589-597.

6. Schmit LA. Structural design by systematic synthesis. In: *Proc. Conf. Electronic Computation, ASCE*. ; 1960:105-122.

7. Vanderplaats GN. Structural optimization for statics, dynamics and beyond. *J Brazilian Soc Mech Sci Eng*. 2006;28(3):316-322.

8. Prager W. Optimality criteria in structural design. *Proc Natl Acad Sci U S A*. 1968;61(3).

9. Venkayya VB. Energy distribution in an optimum structural design. In: *Air Force Flight Dynamics Lab, Air Force Systems Command, Wright-Patterson Air Force Base, Ohio*. ; 1969.

10. Kirsch U. *Structural Optimization : Fundamentals and Applications*. Springer; 1993.

11. Munk DJ, Vio GA, Steven GP. Topology and shape optimization methods using evolutionary algorithms: a review. *Struct Multidiscip Optim*. May 2015.

12. Bendsoe MP. Generating optimal topologies in structural design using a homogenization method. *Comput Methods Appl Mech Eng*. 1988;71(2):197-224.

13. Rozvany GIN. Aims, scope, methods, history and unified terminology of computer-aided topology optimization in structural mechanics. *Structrural Multidiscip Optim*. 2001;21:90-108.

14. Hajela P, Lee E. Genetic algorithms in truss topological optimization. *Int J Solids Struct*. 1995;32(22):3341-3357.

15. Jain C. An Improved Material-Mask Overlay Strategy for Topology Optimization of Structures and Compliant Mechanisms. *J Mech Des*. 2010;132(6).

16. Madeira JFA, Pina HL, Rodrigues HC. GA topology optimization using random keys for tree encoding of structures. *Struct Multidiscip Optim*. 2009;40(1-6):227-240.

17. Rozvany GIN. A critical review of established methods of structural topology optimization. *Struct Multidiscip Optim*. 2008;37(3):217-237.

18. Bendsøe MP. Optimal shape design as a material distribution problem. *Struct Optim*. 1989;1(4):193-202.

19. Xie YM, Steven GP. A simple evolutionary procedure for structural optimisation. *Comput Struct*. 1993;49:885-896.

20. Jakobsson S, Amoignon O. Mesh deformation using radial basis functions for gradient-based aerodynamic shape optimization. *Comput Fluids*. 2007;36(6):1119-1136.

21. Mader CA, Martins JRRA. Computing Stability Derivatives and Their Gradients for Aerodynamic Shape Optimization. *AIAA J*. 2014;52(11):2533-2546.

22. Giannakoglou CK, Papadimitriou, DI, Papoutsis-Kiachagias EM, Othmer C. Adjoint methods in CFD-based optimization - Gradient computation & beyond. In: *ECCOMAS 2012 - European Congress on Computational Methods in Applied Sciences and Engineering, E-Book Full Papers*. ; 2012:8523-8539.

23. Allaire G, Toader A-M, Jouve F. A Level-Set Method for Shape Optimization. *Comptes Rendus Math*. 2009;334(12).

24. Osher S, Sethian JA. Fronts propagating with curvature-dependent speed: Algorithms based on Hamilton-Jacobi formulations. *J Comput Phys*. 1988;79(1):12-49.

25. Sethian JA. *Level Set Methods and Fast Marching Methods : Evolving Interfaces in Computational Geometry, Fluid Mechanics, Computer Vision, and Materials Science*. 1st Ed. Cambridge University Press; 1999.

26. Jameson A. Aerodynamic design via control theory. *J Sci Comput*. 1988;3(3):233-260.

27. Nadarajah SK, Jameson A, Alonso J. An adjoint method for the calculation of remote sensitivities in supersonic flow. *Int J Comut Fluid Dyn*. 2006;20(2):61-74.

28. Kuruvila G. Airfoil Design and Optimization by the One-Shot Method. *CASI*. 1995.

29. Giannakoglou KC, Papadimitrou KC. Adjoint Methods for Shape Optimization. In: Trévenin D, Janiga G, eds. *Optimization and Computational Fluid Dynamics*. 1st Editio. Berlin, Heidelberg: Springer-Verlag; 2008:79-108.

30. Stewart J. *Multivariable Calculus : Concepts and Contexts*. 4th Ed. Brooks/Cole; 2001.

31. Giles M. An introduction to the adjoint approach to design. *Fluct Noise Lett*. 2012;11(2):393-415.

32. Kita E. 2D shape optimization using genetic algorithm. *Comput Assist Mech Eng Sci*. 1998;5(3):311-321.

33. Pulliam TH. Aerodynamic Shape Optimization Using A Real-Number-Encoded Genetic Algorithm. *CASI*. 2001.

34. Oyama A. Aerodynamic Optimization of Transonic Wing Design Based on Evolutionary Algorithm. In: *Third International Conference on Nonlinear Problems in Aviation and Aerospace Proceedings*. ; 2002:537-546.

35. Tang Y-C, Zhou X-H, Chen J. Preform tool shape optimization and redesign based on neural network response surface methodology. *Finite Elem Anal Des*. 2008;44(8):462-471.

36. Haslinger J, Jedelský D, Kozuker T, Tvrdík J. Genetic and random search methods in optimal shape design problems. *J Glob Optim*. 2000;16(2):109-131.

37. Holst TL. Aerodynamic Shape Optimization Using A Real-Number-Encoded Genetic Algorithm. In: *19th Aiaa Applied Aerodynamics Conference*. ; 2001.

38. Mäkinen RAE, Periaux J, Toivanen J. Multidisciplinary Shape Optimization in Aerodynamics and Electromagnetics using Genetic Algorithms. *Int J Numer Methods Fluids*. 1999;30(2):149-159.

39. Rukolaine SA. Shape optimization of radiant enclosures with specular-diffuse surfaces by means of a random search and gradient minimization. *J Quant Spectrosc Radiat Transf*. 2015;151:174-191.

40. Zabinsky ZB. *Stochastic Adaptive Search for Global Optimization*. 1st Ed. Massachussets: Kluwer Academis Publishers; 2003.

41. Zabinsky ZB. Random Search Algorithms. In: *Wiley Encyclopedia of Operations Research and Management Science*. 2nd Ed. Kluwer Academic Publishers; 2010:1-13.

42. Marsaglia G. Choosing a Point from the Surface of a Sphere. *Ann Math Stat*. 1972;43(2):645-646.

43. Zingg DW, Nemec M, Pulliam TH. A comparative evaluation of genetic and gradient-based algorithms applied to aerodynamic optimization. *Rev Eur mécanique numérique*. 2008;17(1-2):103-126.

44. Conn AR, Scheinberg K, Vicente LN. *Introduction to Derivative-Free Optimization*. (Ed. 1st, ed.). Society for Industrial and Applied Mathematics; 2009.

45. Barros MFM. Analog circuits and systems optimization based on evolutionary computation techniques. In: *10th International Workshop on Symbolic and Numerical Methods, Modeling and Applications to Circuit Design*. Springer; 2010.

46. Aydın Z, Ayvaz Y. Optimum topology and shape design of prestressed concrete bridge girders using a genetic algorithm. *Struct Multidiscip Optim*. 2009;41(1):151-162.

47. Kane C, Schoenauer M. Topological optimum design using genetic algorithms. *Control Cybern*. 1996;25(5):1059-1087.

48. Bendsøe MP, Sigmund O. Material interpolation schemes in topology optimization. *Arch Appl Mech*. 1999;69(9-10):635-654.

49. Rietz A. Sufficiency of a finite exponent in SIMP (power law) methods. *Struct Multidiscip Optim*. 2001;21(2):159-163.

50. Sigmund O. A 99 line topology optimization code written in Matlab. *Struct Multidiscip Optim*. 2000;19(2):120-127.

51. Rozvany GIN. *Structural Design via Optimality Criteria : The Prager Approach to Structural Optimization*. Kluwer Academic Publishers; 1989.

52. Rozvany GIN, Sobieszczanski-Sobieski J. New optimality criteria methods: Forcing uniqueness of the adjoint strains by corner-rounding at constraint intersections. *Struct Optim*. 1992;4(3-4):244-246.

53. Kikuchi N, Nishiwaki S, Fonseca JSO, Silva ECN. Design optimization method for compliant mechanisms and material microstructure. *Comput Methods Appl Mech Eng*. 1998;151(3-4):401-417.

54. Nishiwaki S, Frecker MI, Min S, Kikuchi N. Topology optimization of compliant mechanisms using the homogenization method. *Int J Numer Methods Eng*. 1998;42(3):535-559.

55. Svanberg K. The method of moving asymptotes—a new method for structural optimization. *Int J Numer Methods Eng*. 1987;24(2):359-373.

56. Bendsoe MP. Topology and generalized layout optimization of elastic structures. *Nato Ad S E*. 1993;227:159-205.

57. Sigmund O. On the Design of Compliant Mechanisms Using Topology Optimization. *Mech Struct Mach*. 1997;25(4):493-524.

58. Xie YM, Steven GP. *Evolutionary Structural Optimization*. 1st Ed. Springer London; 1997.

59. Tu J, Yeoh GH, Liu C. *Computational Fluid Dynamics : A Practical Approach*. Butterworth-Heinemann; 2008.

60. Brenner G. *100 Volumes of "Notes on Numerical Fluid Mechanics."* Vol 100. (Hirschel EH, Krause E, eds.). Springer Berlin Heidelberg; 2009.

61. Walker R. CFD savings on process scale up. *Eur Semicond*. 1998;20(4):57-60.

62. Smith BL. Assessment of CFD codes used in nuclear reactor safety simulations. *Nucl Eng Technol*. 2010;42(4):339-364.

63. De La Quintana J, Aurtenetxe J, Morente F, Ugartetxe R. Computational Fluid Dynamic analysis of water mist system performance for fire safety of a nineteenth century cast-iron structured building. In: *COST ACTION C26: Urban Habitat Constructions Under Catastrophic Events - Proceedings of the Final Conference.* ; 2010:531-534.

64. Davidson D. The role of computational fluid dynamics in process industries. *Eighth Annu Symp Front Eng*. 2003:21-28.

65. Runchal AK. The future of CFD and the CFD of the future. *Comput Therm Sci*. 2012;4(6):517-524.

66. Bird RB. *Transport Phenomena*. 2nd Ed. J. Wiley; 2007.

67. Murthy JY. *Numerical Methods in Heat, Mass and Momentum Transfer*.; 1999.

68. Thompson JF, Soni BK, Weatherill NP. *Handbook of Grid Generation*. CRC Press; 1999.

69. CFX A. *ANSYS CFX-Solver Theory Guide*.; 2009.

70. Stankiewicz AI. Process intensification: Transforming chemical engineering. *Chem Eng Prog*. 2000;96(1):22-33.

71. Cross WT, Ramshaw C. Process intensification: laminar flow heat transfer. *Chem Eng Res Des*. 1986;64(4):293-301.

72. Ramshaw C. Process intensification: a game for n players. *Chem Eng*. 1985;(416).

73. Hessel V, Schouten JC, Renken A. *Micro Process Engineering: A Comprehensive Handbook*. Vol 1. (Hessel V, Renken A, Schouten JC, Yoshida J-I, eds.). Weinheim, Germany: Wiley-VCH Verlag GmbH & Co. KGaA; 2009.

74. Janicke MT, Kestenbaum H, Hagendorf U, Schüth F, Fichtner M, Schubert K. The Controlled Oxidation of Hydrogen from an Explosive Mixture of Gases Using a Microstructured Reactor/Heat Exchanger and Pt/Al2O3 Catalyst. *J Catal*. 2000;191(2):282-293.

75. Rouge A, Spoetzl B, Gebauer K, Schenk R, Renken A. Microchannel reactors for fast periodic operation: the catalytic dehydration of isopropanol. *Chem Eng Sci*. 2001;56(4):1419-1427.

76. Matlosz M, Falk L, Commenge J-M. Process Intensification. In: *Microchemical Engineering in Practice*. Hooken, New Jersey: John Wiley & Sons, Inc.; 2009.

77. Commenge J-M, Falk L, Corriou J-P, Matlosz M. Intensification des procédés par microstructuration. *Comptes Rendus Phys*. 2004;5(5):597-608.

78. Jensen KF. Microchemical systems: Status, challenges, and opportunities. *AIChE J*. 1999;45(10):2051-2054.

79. Kamper K-P, Ehrfeld W, Dopper J, Hessel V, Lehr H, Lowe H, Richter T, Wolf A. Microfluidic components for biological and chemical microreactors. In: *Proceedings IEEE The Tenth Annual International Workshop on Micro Electro Mechanical Systems. An Investigation of Micro Structures, Sensors, Actuators, Machines and Robots*. IEEE; 1997:338-343.

80. Atkins P. *Atkins' Physical Chemistry*. Oxford University Press; 2014.

81. Lide DR. *CRC Handbook of Chemistry and Physics*. 95th editi. CRC Press; 2014.

82. Cussler EL. *Diffusion : Mass Transfer in Fluid Systems*. Cambridge University Press; 1997.

83. Hessel V, Löwe H, Müller A, Kolb G. *Chemical Micro Process Engineering : Processing and Plants*. Wiley-VCH; 2005.

84. Kakuta M, Bessoth FG, Manz A. Microfabricated devices for fluid mixing and their application for chemical synthesis. *Chem Rev*. 2007;107(10):395-405.

85. Capretto L, Cheng W, Hill M, Zhang X. Micromixing within microfluidic devices. *Top Curr Chem*. 2011;304:27-68.

86. Meijer HEH, Singh MK, Kang TG, den Toonder JMJ, Anderson PD. Passive and Active Mixing in Microfluidic Devices. *Macromol Symp*. 2009;279(1):201-209.

87. Glasgow I, Aubry N. Enhancement of microfluidic mixing using time pulsing. *Lab Chip*. 2003;3(2).

88. Deshmukh AA, Liepmann D, Pisano AP. Characterization of a micro-mixing, pumping, and valving system. *Transucers '01 Eurosensors Xv, Dig Tech Pap Vols 1 2*. 2001:950-953.

89. West J, Karamata B, Lillis B, Gleeson JP, Alderman J, Collins JK, Lane W, Mathewson A, Berney H. Application of magnetohydrodynamic actuation to continuous flow chemistry. *Lab Chip*. 2002;2(4):224-230.

90. Oh D-W, Jin JS, Choi JH, Kim H-Y, Lee JS. A microfluidic chaotic mixer using ferrofluid. *J Micromechanics Microengineering*. 2007;17(10):2077-2083.

91. Kim S-J, Wang F, Burns MA, Kurabayashi K. Temperature-programmed natural convection for micromixing and biochemical reaction in a single microfluidic chamber. *Anal Chem*. 2009;81(11):4510-4516.

92. Andreussi T, Galletti C, Mauri R, Camarri S, Salvetti MV. Flow regimes in T-shaped micro-mixers. *Comput Chem Eng*. 2015;76:150-159.

93. Esmaeelpanah J, Kazemi SA, Passandideh-Fard M. Mixing Process in T-Shaped Micro-Mixers with Chaotic Advection: A Numerical Approach. *Proc 8th Jt Conf Inf Sci Vols 1-3*. 2005:1319-1326.

94. Kaminski S, Uhlemann J. Mixer with microchannels in LTCC technology. *Electron Technol*. 2005;37-38:1-3.

95. Kamholz AE, Weigl BH, Finlayson BA, Yager P. Quantitative Analysis of Molecular Interaction in a Microfluidic Channel: The T-Sensor. *Anal Chem*. 1999;71(23):5340-5347.

96. Ismagilov RF, Stroock AD, Kenis PJA. Experimental and theoretical scaling laws for transverse diffusive broadening in two-phase laminar flows in microchannels. *Appl Phys Lett*. 2000;76(17).

97. Löb P, Drese KS, Hessel V, Hardt S, Hofmann C, Löwe H, Schenk R, Schönfeld F, Werner B. Steering of Liquid Mixing Speed in Interdigital Micro Mixers– From Very Fast to Deliberately Slow Mixing. *Chem Eng Technol*. 2004;27(3):340-345.

98. Bessoth FG, DeMello AJ, Manz A. Microstructure for efficient continuous flow mixing. *Anal Commun*. 1999;36(6):213-215.

99. Lee SW, Kim DS, Lee SS, Kwon TH. A split and recombination micromixer fabricated in a PDMS three-dimensional structure. *J Micromechanics Microengineering*. 2006;16(5):1067-1072.

100. Hardt S, Pennemann H, Schönfeld F. Theoretical and experimental characterization of a low-Reynolds number split-and-recombine mixer. *Microfluid Nanofluidics*. 2005;2(3):237-248.

101. Bodla VK, Seerup R, Krühne U, Woodley JM, Gernaey K V. Microreactors and CFD as Tools for Biocatalysis Reactor Design: A case study. *Chem Eng Technol*. 2013;36(6):1017-1026.

102. Aoki N, Hasebe S, Mae K. Mixing in microreactors: effectiveness of lamination segments as a form of feed on product distribution for multiple reactions. *Chem Eng J*. 2004;101(1-3):323-331.

103. Nussbaum D, Knoll T, Velten T, Herrmann D. Micromixing structures for lab-on chip applications: fabrication and simulation of 90 degrees zigzag microchannels in dry film resist. *4m/icomm 2009 - Glob Conf Micro Manuf*. 2009:215-218.

104. Fries DM, Waelchli S, von Rohr PR. Gas-liquid two-phase flow in meandering microchannels. *Chem Eng J*. 2008;135(suppl.1).

105. Liu RH, Stremler MA, Sharp KV, Olsen MG, Santiago JG, Adrian RJ, Aref H, Beebe DJ. Passive mixing in a three-dimensional serpentine microchannel. *J Microelectromechanical Syst*. 2000;9(2):190-197.

106. Vijayendran RA, Motsegood KM, Beebe DJ, Leckband DE. Evaluation of a Three-Dimensional Micromixer in a Surface-Based Biosensor †. *Langmuir*. 2003;19(5):1824-1828.

107. Kim DS, Lee SH, Kwon TH, Ahn CH. A serpentine laminating micromixer combining splitting/recombination and advection. *Lab Chip*. 2005;5(7):739-747.

108. Stroock AD, Dertinger SKW, Ajdari A, Mezic I, Stone HA, Whitesides GM, Stroock AD. Chaotic mixer for microchannels. *Science (80-)*. 2002;295(5555):647-651.

109. Lim D, Kamotani Y, Cho B, Mazumder J, Takayama S. Fabrication of microfluidic mixers and artificial vasculatures using a high-brightness diode-pumped Nd:YAG laser direct write method. *Lab Chip*. 2003;3(4):318-323.

110. Ansari MA. Shape optimization of a micromixer with herringbone grooves using kriging model. *Trans Korean Soc Mech Eng B*. 2007;31(8):711-717.

111. Hossain S, Husain A, Kim K-Y. Shape optimization of a micromixer with staggered-herringbone grooves patterned on opposite walls. *Chem Eng J*. 2010;162(2):730-737.

112. Tonomura O, Tanaka S, Noda M, Kano M, Hasebe S, Hashimoto I. CFD-based optimal design of manifold in plate-fin microdevices. *Chem Eng J*. 2004;101(1-3):397-402.

113. Tonomura O. Optimal shape design of pressure-driven microchannels using adjoint variable method. *Proc 5th Int Conf Nanochannels, Microchannels Minichannels, ICNMM2007*. 2007:427-434.

114. Tonomura O. Shape Optimization of Microchannels Using CFD and Adjoint Method. *Comput Chem Eng*. 2010;28:37-42.

115. Tonomura O. Design of T-Shaped Microreactors by Reduced-Order Approach. *Comput Chem Eng*. 2009;27:891-896.

116. Wang L, Kawamura S, Tonomura O, Hasebe S. Design of Non-Isothermal T-Shaped Microreactors with Engulfment Flow by Using a Simplified Model. *Adv Mater Res*. 2011;396-398(396-398):1033-1038.

117. Arora JS. *Introduction to Optimum Design*. McGraw-Hill; 1989.

118. Okkels F, Bruus H. Design of micro-fluidic bio-reactors using topology optimization. *J Comput Theor Nanosci*. 2007;4(4):814-816.

119. Schäpper D, Lencastre Fernandes R, Lantz AE, Okkels F, Bruus H, Gernaey K V. Topology optimized microbioreactors. *Biotechnol Bioeng*. 2011;108(4):786-796.

120. Bányik T, Vicente AA, Kuncová G, Podrazky O, Dostálek P, Teixeira J. Growth model and metabolic activity of brewing yeast biofilm on the surface of spent grains: a biocatalyst for continuous beer fermentation. *Biotechnol Prog*. 2004;20(6).

121. Zhang Z, Scharer JM, Moo-Young M. Mathematical model for aerobic culture of a recombinant yeast. *Bioprocess Eng*. 1997;17(4):235-240.

122. Rasor JP, Voss E. Enzyme-catalyzed processes in pharmaceutical industry. *Appl Catal A Gen*. 2001;221(1-2):145-158.

123. Buchholz K, Kasche V, Bornscheuer UT. *Biocatalysts and Enzyme Technology*. Wiley-VCH Verlag; 2005.

124. Jensen KF. Silicon-Based Microchemical Systems: Characteristics and Applications. *MRS Bull*. 2006;109(02):101-107.

125. Turner NJ. *Chiral Amine Synthesis*. (Nugent TC, ed.). Weinheim, Germany: Wiley-VCH Verlag GmbH & Co. KGaA; 2010.

126. Koszelewski D, Lavandera I, Clay D, Rozzell D, Kroutil W. Asymmetric Synthesis of Optically Pure Pharmacologically Relevant Amines Employing ω-Transaminases. *Adv Synth Catal*. 2008;350(17):2761-2766.

127. Tufvesson P, Lima-Ramos J, Jensen JS, Al-Haque N, Neto W, Woodley JM. Process considerations for the asymmetric synthesis of chiral amines using transaminases. *Biotechnol Bioeng*. 2011;108(7):1479-1493.

128. Walsh C. *Enzymatic Reaction Mechanisms*. Freeman,1979; 1979.

129. Leskovac V. *Comprehensive Enzyme Kinetics*. Kluwer Academic; 2003.

130. Al-Haque N, Santacoloma PA, Neto W, Tufvesson P, Gani R, Woodley JM. A robust methodology for kinetic model parameter estimation for biocatalytic reactions. *Biotechnol Prog*. 2012;28(5):1186-1196.

131. Li J, Carr PW. Accuracy of empirical correlations for estimating diffusion coefficients in aqueous organic mixtures. *Anal Chem*. 1997;69(13).

132. Miložič N, Lubej M, Novak U, Žnidaršič-Plazl P, Plazl I. Evaluation of Diffusion Coefficient Determination using a Microfluidic Device. *Chem Biochem Eng Q J*. 2014;28(2):215-223.

133. Lima-Ramos J, Tufvesson P, Woodley JM. Application of environmental and economic metrics to guide the development of biocatalytic processes. *Green Process Synth*. 2014;3(3):195-213.

134. Kremzner LT, Wilson IB. A partial characterization of acetylcholinesterase. *Biochemistry*. 1964;3(12).

135. Veenstra TT, Lammerink TSJ, Elwenspoek MC, Berg A van den. Characterization method for a new diffusion mixer applicable in micro flow injection analysis systems. *J Micromechanics Microengineering*. 1999;9(2):199-202.

136. Chaplin MF. *Enzyme Technology*. Cambridge University Press; 1990.

137. Rodríguez-López JN, García-Cánovas F, Hiner ANP, Arnao MB, Acosta M, Lloyd Raven E. Kinetic study of the inactivation of ascorbate peroxidase by hydrogen peroxide. *Biochem J*. 2000;348(2):321.

138. Porstmann B, Porstmann T, Nugel E. Comparison of Chromogens for the Determination of Horseradish Peroxidase as a Marker in Enzyme Immunoassay. *Clin Chem Lab Med*. 1981;19(7).

139. Nicell JA. Kinetics of horseradish peroxidase-catalysed polymerization and precipitation of aqueous 4-chlorophenol. *J Chem Technol Biotechnol*. 1994;60(2):203-215.

140. Deyhimi F, Nami F. Peroxidase-catalyzed electrochemical assay of hydrogen peroxide: A ping-pong mechanism. *Int J Chem Kinet*. 2012;44(10):699-704.

141. Enzymatic Assay of Peroxidase (EC 1.11.1.7) 2,2'-Azino-bis(3-Ethylbenzthiazoline-6-Sulfonic Acid) as a Substrate. http://www.sigmaaldrich.com/technical-documents/protocols/biology/enzymatic-assay-of-peroxidase-abts-as-substrate.html. Accessed August 21, 2015.

142. Peroxidase from horseradish (product number P1825). http://www.sigmaaldrich.com/catalog/product/sigma/p8125?lang=en&region=DK. Accessed August 2, 2015.

143. Kamal JKA, Behere D V. Activity, stability and conformational flexibility of seed coat soybean peroxidase. *J Inorg Biochem*. 2003;94(3):236-242.

144. Smith AT, Sanders SA, Thorneley RNF, Burke JF, Bray RRC. Characterisation of a haem active-site mutant of horseradish peroxidase, Phe41 Val, with altered reactivity towards hydrogen peroxide and reducing substrates. *Eur J Biochem*. 1992;207(2):507-519.

145. Preedy VR, Patel V. *Biosensors and Environmental Health.*; 2012.

146. Mazurek P, Hvilsted S, Skov AL. Novel encapsulation technique for incorporation of high permittivity fillers into silicone elastomers. In: Bar-Cohen Y, ed. *Proceedings of Spie--the International Society for Optical Engineering*. Vol 9056. ; 2014:90562T.

147. Mazurek P, Daugaard AE, Skolimowski M, Hvilsted S, Skov AL. Preparing monodispersed liquid core PDMS microcapsules from thiol–ene–epoxy-tailored flow-focusing microfluidic devices. *RSC Adv*. 2015;5(20):15379-15386.

148. Oktay B, Demir S, Kayaman-Apohan N. Immobilization of α-amylase onto poly(glycidyl methacrylate) grafted electrospun fibers by ATRP. *Mater Sci Eng C (Materials Biol Appl*. 2015;50:386-393.

149. Xu FJ, Cai QJ, Li YL, Kang ET, Neoh KG. Covalent immobilization of glucose oxidase on well-defined poly(glycidyl methacrylate)-Si(111) hybrids from surface-initiated atom-transfer radical polymerization. *Biomacromolecules*. 2005;6(2):1012-1020.

150. Nagy KD, Shen B, Jamison TF, Jensen KF. Mixing and Dispersion in Small-Scale Flow Systems. *Org Process Res Dev*. 2012;16(5):976-981.

Appendix A

Included publication

Krist V. Gernaey, Jakob K. Huusom and Rafiqul Gani (Eds.), 12th International Symposium on Process Systems Engineering and 25th European Symposium on Computer Aided Process Engineering. 31 May – 4 June 2015, Copenhagen, Denmark.

Topology optimization for biocatalytic microreactor configurations

Inês P. Rosinha[a], Krist V. Gernaey[a], John M. Woodley[a] and Ulrich Krühne[a]

[a]*CAPEC-PROCESS Center, Department of Chemical and Biochemical Engineering, Technical University of Denmark (DTU), Building 229, DK-2800 Kgs. Lyngby, Denmark*
inros@kt.dtu.dk

Abstract

The aim of this study is to present an innovative strategy for selecting a reactor for a specific process. Instead of adapting the process to a well-known reactor shape, a topology optimization method is used to obtain the best reactor configuration, and is applied to a biocatalyic reaction system as a case study. The Evolutionary Structure Optimization (ESO) method is applied using an interface between Matlab® and the computational fluid dynamic simulation software ANSYS CFX®. In the case study, the ESO method is applied to optimize the spatial distribution of immobilized enzyme inside a microreactor. The results allow evaluating which regions in the microreactor have more importance for the product formation. In fact, it was possible to simulate the improvement of the outlet product concentration per same amount of enzyme by modifying the spatial distribution of the immobilized enzyme.

Keywords: topology optimization, biocatalysis, immobilized enzymes, CFD

1. Introduction

Topology optimization has been used by mechanical and civil engineers for many years, for example in order to minimize the amount of used material and the strain energy of structures while maintaining their mechanical strength (Bendsoe et al., 2003). Topology optimization is a mathematical method which spatially optimizes the distribution of material within a defined domain, by fulfilling given constraints previously established and minimizing a predefined cost function. For such an optimization procedure, the three main elements are design variables, the cost function and the constraints.

The traditional solutions for structural optimization problems in buildings were determined by the use of direct search methods on an Isotropic Solid and Empty (ISE) topology. In an ISE topology, the elements are either filled by a given isotropic material or do not contain any material. However, due to the large number of elements, the application of direct search methods on an ISE topology was found to be computationally extremely expensive. Therefore, since the 1980s, the main focus in this area has been to develop more efficient methods to obtain faster solutions. In the scientific literature, there are numerous techniques to perform a topology optimization; the two most popular methods are the Solid Isotropic Material with Penalization (SIMP) technique and the Evolutionary Structural Optimization (ESO) technique.

The SIMP technique is based on determining the optimum structure by varying the material density within the predefined domain. The predefined domain is discretized in elements and a finite element (FE) analysis is applied to determine the structure performance. Conceptually, the SIMP method comprises a FE analysis of the domain followed by an optimization of the density of each element of the domain. Afterwards, the configuration with the new element densities is analyzed and the optimization is

performed again. The optimization procedure continues until convergence (Bendsoe et al., 2003).
The ESO method was developed by Xie and Steven (1993) and it has been applied in various optimization research areas. The ESO method is based on the simple concept of progressively removing inefficient material from a structure. The unneeded material is removed by using a rejection criterion (RC) which identifies the ineffective material. This method has the advantage that it is easy to understand and to learn. Moreover, this method is also simple to program and to link with existing computer-aided engineering software e.g. ANSYS CFX®, ANSYS Fluent® or Nastran®.
This contribution presents a novel adaptation of the ESO method to optimize the catalyst spatial distribution inside microreactors considering a reaction carried out by a biological catalyst, an enzyme. The goal is to improve the product formation per same amount of enzyme by optimizing the immobilized enzyme spatial distribution. This contribution applies commercially available tools such as the computational fluid dynamics (CFD) software, ANSYS CFX®, and Matlab®, and will link them with a self-programmed topology optimization method.
Previously, selected studies dealing with topology optimization of catalyst inside microreactors have been reported by Okkels et al. (2007) and by Schäpper et al. (2010) where they used the porosity of the catalyst carrier as the design variable. This study changes the surface concentration of the enzyme instead of changing the porosity of the catalyst carrier, which consequently would modify the fluid dynamic properties inside the microreactor. The optimization procedures considering porosity as design variable have resulted in configurations with large void spaces within the carrier material. These configurations are mechanically unstable and, since in the real reactor such carrier material cannot be packed at fixed locations, the material might change the locations due to the fluid flow. Therefore it is not possible to validate these results experimentally.
The consideration of the enzyme concentration as a design variable, will allow new configurations by depositing the enzyme on favourable areas of the microreactor, either on a surface or on an immobilization carrier. Therefore, the presented topology optimization procedure will allow for the first time that future experimental validations of the simulated design can be performed.

2. Materials and Methods

The shape of the investigated microreactor is an extension of the two dimensional shape presented by Okkels et al. (2007) into a three dimensional design. The view from the top of the microreactor shows that the microreactor consists of a parallelepiped measuring 30 mm of width and depth, combined with two channels for the inlet and outlet located on opposite sides of the square. The width of the inlet and outlet channels is 10 mm. The height of the microreactor corresponds to 0.5 mm. The shape of the reactor is presented in Figure 1. In this investigation, the enzyme is immobilized at the top and bottom surfaces of the reactor. Since the flow profile is symmetric on the central vertical and central horizontal planes, symmetry boundaries were created at half of the height and through the middle of the inlet and outlet as presented in Figure 1b. In this way only a quarter of the whole reactor geometry is simulated which provides an acceleration of the computational solution. The flow velocity at the inlet is set to 0.01 m/s for all simulations. The choice of the residence time was made in order to ensure that the velocity close to the bottom wall is different from zero and varies between

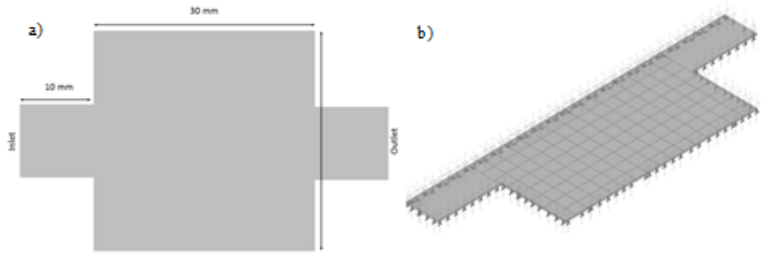

Figure 1- Microreactor configuration: a) full microreactor configuration; b) configuration with symmetry planes, horizontal and vertical planes

different locations on the bottom and top surfaces due to effects of the lateral walls and narrow inlet and outlet.The studied reaction rate (r) in this case study follows the mechanism of an enzyme, which is characterized by a Michaelis-Menten mechanism. The Michaelis-Menten reaction equation is described by Eq 1:

$$r = kcat \cdot [E]\frac{[S]}{[S] + K_M} \tag{1}$$

where $kcat$ is the turnover number, [E] the enzyme concentration, [S] the substrate concentration and K_M is the Michaelis-Menten constant. In this case, the values considered for the reaction are equivalent to the values determined experimentally for a catalase reaction, $kcat = 10^7$ mol·m^{-3}·s^{-1} and $K_M = 25$ mol·m^{-3} (Díaz et al., 2001). The reaction catalysed by catalase corresponds to the conversion of two molecules of hydrogen peroxide forming one molecule of oxygen and two molecules of water:

$$2H_2O_2 \xrightarrow{\text{catalase}} 2H_2O + O_2 \tag{2}$$

In this study, the maximum enzyme concentration was determined considering that the molecular weight of catalase is 315 kDa and assuming that the amount of enzyme that is possible to immobilize on the surface is 4 mg·m^{-2}. From here it is possible to calculate that the maximum enzyme concentration on the surface is $1.2 \cdot 10^{-11}$ mol·m^{-2}. At the inlet, the substrate concentration, hydrogen peroxide, is 1 mM.

The method applied to this study is an adaptation of the ESO method for the topology optimization of enzyme inside the microreactor. The procedure for the topology optimization is presented in Figure 2. In this case, the design variable is the enzyme concentration immobilized on the surface and the cost function to be maximized is the concentration of one of the products at the outlet. There is only one constraint to this problem which is to maintain the same amount of enzyme (number of moles) inside of the microreactor between iterations. This constraint makes the procedure different from the original ESO method. In the ESO method, the ineffective elements are simply eliminated, but in this case study it is not meaningful to simply remove an element. If an element is removed, the amount of enzyme inside of the microreactor will be less and consequently the product concentration at the outlet will decrease. Therefore the ESO method has been modified. When an element is removed the amount of enzyme corresponding to that element is distributed evenly between all the elements which still contain immobilized enzyme.

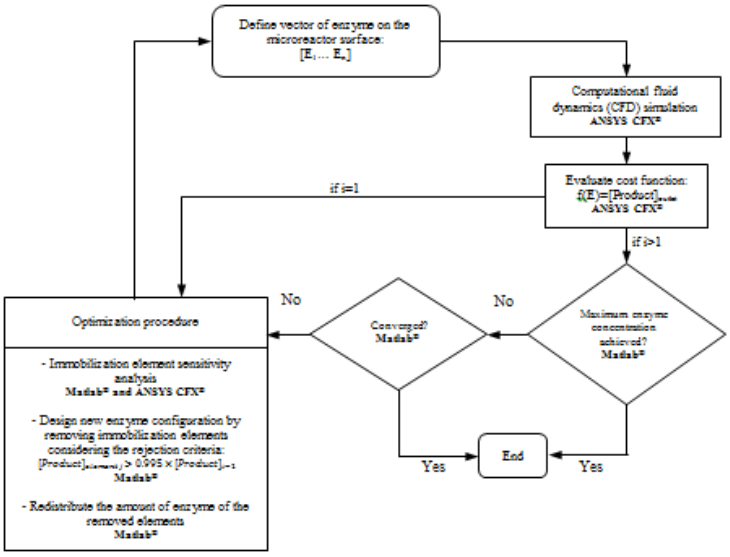

Figure 2 – Flowchart for topology optimization of enzyme in a microreactor using the ESO method through a routine coupling Matlab® and ANSYS CFX®.

The design of the microreactor is implemented into ANSYS CFX® and for this purpose the bottom surface of the microreactor was divided in small areas, in this case 128 immobilization elements as shown in Figure 1b. Then, the whole microreactor volume is discretized using a fine mesh of cells. The dynamics and the reaction parameters of the system are configured according to the conditions and the reaction system for the case study mentioned above.

The optimization procedure consists of a routine which couples the commercial computational fluid dynamics (CFD) software ANSYS CFX® to Matlab®. The optimization loop starts by setting a vector in Matlab® in which the enzyme concentration of the different locations on the surface ($[E_1 \ldots E_n]$) is defined. The enzyme was initially uniformly distributed at half of the maximum concentration on the surface of the microreactor $5.6 \cdot 10^{-12}$ mol·m^{-2}. Afterwards, the ANSYS CFX® script is changed according to the defined vector, a computational fluid dynamics simulation is carried out by ANSYS CFX® and the cost function is evaluated.

The optimization procedure starts with a sensitivity analysis of each immobilized element in order to evaluate its influence on the product concentration at the outlet. One by one the enzyme concentration of each of the immobilization elements is set to zero. This is controlled by a self-programed routine in Matlab® which makes the necessary modifications in the ANSYS CFX® script while ANSYS CFX® carries out the

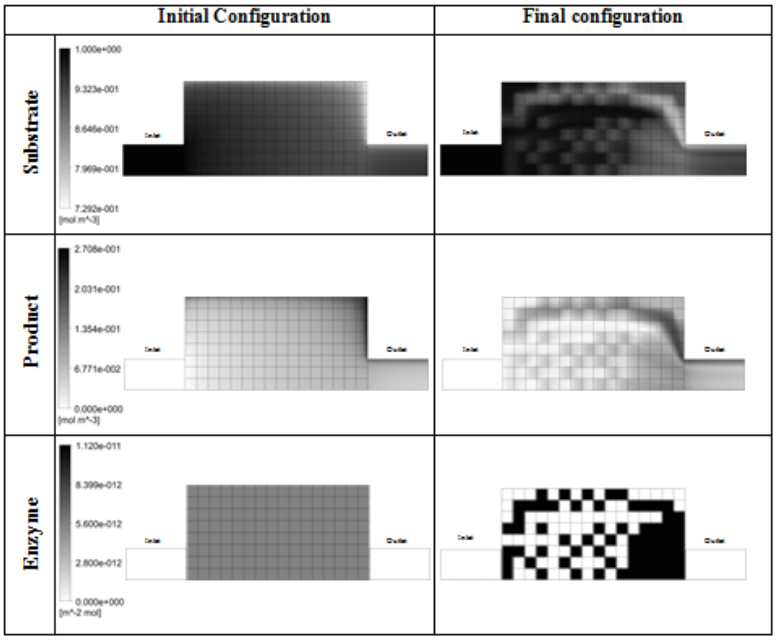

Figure 3 – Results from the topology optimization: Concentration of substrate (hydrogen peroxide) and product (water) inside the microreactor for initial and final configurations and immobilized enzyme (catalase) on the bottom surface of the microreactor.

computational fluid dynamics analysis using the new script. The Matlab® code removes the immobilized elements with the lowest sensitivity according to a predefined rejection criterion (RC). In this study the RC is defined for the immobilized element j which is removed if the product concentration at the outlet is:

$$[Product]_{element\,j} > 0.995 \times [Product]_{i-1} \qquad (3)$$

being *i* the iteration number and *j* is number of the element. That means if an element is not contributing substantially to the formation of the product it is removed. The amount of enzyme present in the removed elements is distributed within all other elements that have not been removed in order to keep the same amount of enzyme (mol) inside the microreactor. Subsequently the alterations of the enzyme configuration on the surface of the microreactor and its new concentration are inserted in the ANSYS CFX® script through Matlab® and a CFD simulation is repeated to evaluate the performance of the new enzyme configuration. The procedure is repeated until the maximum product concentration is achieved, the concentration of the enzyme has reached the maximum possible value or the optimization converges.

3. Results and Discussion

The optimization loop ends when the maximum enzyme concentration ($1.2 \cdot 10^{-12}$ mol·m^{-2}) was achieved. On the one hand, $6.75 \cdot 10^{-2}$ mM of substrate were converted with the initial configuration, on the other hand, $6.89 \cdot 10^{-2}$ mM of substrate were converted with the final shape. In the end, the topology optimization resulted in an improvement of 2% of conversion of the substrate per same amount of enzyme compared with the initial enzyme configuration. It is expected that the application of a topology optimization to a more complex reaction mechanism (with product or/and substrate inhibition) will result in larger improvements. The results of the topology optimization as well as the optimal enzyme configuration can be found in Figure 3. The final configuration of the enzyme is characterized by a higher concentration of enzyme close to the walls and in immobilization elements close to the outlet. This demonstrates that immobilized molecules at locations with higher residence time, due to low fluid velocity, contribute more to the product formation. In addition, within the immobilization elements with maximum velocity, the elements which are close to the outlet are the ones which seem to have more influence on the product formation.

4. Conclusion

The presented work demonstrates that it is possible to use existing methods and tools in an efficient way in order to use topology optimization for finding better reactor configurations for a particular reaction system. The application of the ESO method by combining a CFD software, ANSYS CFX®, with Matlab® revealed to be a feasible implementation to optimize the spatial distribution of immobilized enzyme in a microreactor. In this study, the product formation per same amount of enzyme was improved by optimizing the immobilized enzyme spatial distribution. This study contributes to the development of future innovative solutions for establishing a reactor with immobilized catalyst within a process. Currently, the studies are made in microreactors, because it will be easier to validate the results experimentally. Nevertheless, the topology optimization of catalysts can contribute to an improvement of production also at industrial scale, since the product formation is not uniform in full-scale reactors. The application of topology optimization will potentially change the development of reactors and contribute to the improvement of reaction yields.

Acknowledgments

The research leading to these results has received funding from the European Union FP7 (FP7/2007-2013) Project BIOINTENSE – Mastering Bioprocess integration and intensification across scales (Grant Agreement number 312148).

References

M. P. Bendsoe, O. Sigmund, 2002, Topology Optimization: Theory, Methods and Applications, 2nd. ed., Heidelberg: Springer, Berlin, Germany

A. Díaz, P. Rangel, Y, M Oca, F. Lledías, W. Hansberg, 2001, Molecular and kinetic study of catalase-1. A durable large catalase of *Neurospora crassa*, Free Radical Biology & Medicine, 31 (11), 1323-1333.

F. Okkels, H. Bruus, 2007, Design of micro-fluidic bio-reactors using topology optimization, Journal of Computational and Theoretical Nanoscience, 4 (4), 814-816.

D. Schäpper, R. L. Fernandes, A. E. Lantz, F. Okkels, H. Bruus, K. V. Gernaey, 2010, topology Optimized Microbioreactors, Biotechnology and Bioengineering, 108 (4), 786-796.

Y. M. Xie and G.P. Steven, 1993, A simple evolutionary procedure for structural optimization, Computers and Structures, 49 (5), 885-886.

Appendix B

Experimental protocols

Determination of the kinetic parameters $K_{M,app}^{ABTS}$ and $V_{max,app}$ Solutions

Preparation of potassium phosphate buffer (100 mM) at pH 5

1L in distilled water using Potassium Phosphate monobasic (purchased at Merck KGaA, product number 1.04877.1000). Adjust to pH 5 at 25°C by adding 1 M of KOH (purchased at Merck KGaA, product number 1.05033.0500).

Preparation of potassium phosphate buffer (40 mM) at pH 6.8

1L in distilled water using Potassium Phosphate monobasic (purchased at Merck KGaA, product number 1.04877.1000). Adjust to pH 6.8 at 25°C by adding 1 M of KOH (purchased at Merck KGaA, product number 1.05033.0500).

Preparation of hydrogen peroxide (100 mM) in potassium phosphate buffer (100 mM) at pH 5

100 mL solution of 100 mM of peroxide from 3% (w/w) Hydrogen Peroxide Solution (purchased at Sigma Aldrich, product number 88597) in potassium phosphate buffer (100 mM) at pH 5.

Preparation of 2,2'-azino-bis(3-ethylbenzthiazoline-6-sulfonic acid) Substrate Solution (ABTS) solutions (0.06, 0.1, 0.2, 0.6, 1, 2, 6 and 10 mM)

5 mL of the following solutions of 2,2'-azino-bis(3-ethylbenzthiazoline-6-sulfonic acid) 0.06, 0.1, 0.2, 0.6, 1, 2, 6 and 10 mM in the solution of 100 mM hydrogen peroxide and potassium phosphate buffer (100 mM) pH 5. The substrate used was 2,2'-azino-bis(3-ethylbenzthiazoline-6-sulfonic acid) diammonium salt (purchased at Sigma Aldrich, product number 11557).

Preparation of peroxidase from horseradish solution potassium phosphate buffer (40 mM) pH 6.8

25 mL of approximately 0.6 U/mL horseradish peroxidase according to the information on the flask. (Purchased at Sigma Aldrich, product number P8125)

Preparation of the microwell plate for analysis

Three types of solutions were pipetted into microwell plate before the insertion of the microplate in the reader. The used microwell plate was the Nunc MicroWell™ 96 well polystyrene plate, flat bottom (product number 260210), purchased at Thermo Scientific. The pipetted solutions were the reactants solution, and the base for the blanks. In this case two kinds of blanks were used: one containing enzyme solution and buffer solution and the other containing reactants and phosphate buffer solution. Table B-1 summarizes the volume of reactants solution in the well for the reaction and Blank 2 and the volume of the phosphate buffer solution for Blank 1. The addition of the other solutions is made automatically by the spectrophotometer just before the start of the absorbance measurements.

Table B-1– Summary of the phosphate buffer volume and reactants solutions pipetted into the microwells.

Solution	Reaction	Blank 1 with enzyme solution and without reactants	Blank 2 with reactants and without enzyme solution
Phosphate buffer solution 100 mM, pH 5	-	190	-
Reactants solution	190	-	190
Number of replicates	6*	3	3

*for each ABTS solutions

Measurements with microplate reader

The used microplate reader POLARstar, Omega series from BMG LABTECH has the possibility of inserting an enzyme solution and buffer solution in the well just before starting the measurement using a syringe pump located in the reactants compartment (See Figure B-1).

Figure B-1- a) Microwell plate reader POLARstar from BMG LABTECH, b) Reactants compartment with two syringe pumps.

After placing the reactants solution and placing the blanks in the microwell plate, the enzyme solution and the buffer solution were placed inside the syringe compartment. The syringe compartment features two syringe pumps with 500 µL capacity. One of the syringe pumps is filled with enzyme solution and the other syringe pump is filled with the buffer solution. Usually, the syringe pumps are filled with distilled water and therefore they are primed before performing

the kinetic measurements. The procedure to prime a syringe is a series of filling up and emptying the syringe pumps with the desired solution. A syringe pump is primed in order to ensure that the concentration inside the syringe, thesyringe pump valve and in the tubes connecting to the main solution and to the injection compartment is uniform and equal to the enzyme or buffer solution. The two syringe pumps were primed with 4.5 mL of the potassium phosphate buffer (40 mM) pH 6.8 and with 4.5 mL of horseradish peroxidase solution, respectively.

Before starting reading the absorbance of the solution in the wells, 10 μL of the enzyme solution or potassium phosphate buffer solution are added using the syringe pumps to the corresponding blank or reaction well. All this procedure is programmable using the software of the microplate reader. The absorbance at the wavelength of 414 nm is read for an experimental interval of 120 s all 5 s, corresponding to a total of 24 measurements points.

The path length corresponds to the height of the liquid inside the well. The microplate reader software has the option of adjusting the path length to 1 cm accordingly to the volume in the well by selecting the option *Path length correction*.

Determination of the kinetic parameter $k_{cat,app}^{ABTS}$

Solutions

Preparation of 2,2'-azino-bis(3-ethylbenzthiazoline-6-sulfonic acid) Substrate Solution (ABTS) solutions (12 mM)

Prepare 5 mL of the following solutions of 2,2'-azino-bis(3-ethylbenzthiazoline-6-sulfonic acid) 12 mM in the solution of 100 mM hydrogen peroxide and potassium phosphate buffer (100 mM) pH 5. The substrate used was 2,2'-azino-bis(3-ethylbenzthiazoline-6-sulfonic acid) diammonium salt, product from Sigma Aldrich, product number 11557.

Preparation of peroxidase from horseradish solutions with different concentrations potassium phosphate buffer (40 mM) pH 6.8

Prepare 10 mL solutions of concentrations approximately between 0.6 and 4.5 U/mL of peroxidase from horseradish. (Product from Sigma Aldrich, product number P8125)

Preparation of the microwell plate for analysis

Three types of solutions were pipetted in to microwell plate before the insertion of the microplate in the reader. The inserted solutions were the reactants solution, and the base for two blank. In this case two blanks were used: one containing enzyme solution and buffer solution and the other containing reactants and buffer solution. Table B-2 summarizes the volume of reactants solution in the well for the reaction and Blank 2 and the volume of the buffer solution for Blank 1. The

addition of the other solutions is made automatically by the spectrophotometer just before the start of the absorbance measurements.

Table B-2– Summary of volume phosphate buffer and reactants solutions pipetted into the microwells.

Solution	**Reaction**	**Blank 1** with enzyme solution and without reactants	**Blank 2** with reactants and without enzyme solution
Phosphate buffer solution 100 mM, pH 5	-	95	-
Reactants solution	95	-	95
Number of replicates	6*	3	3

*for each enzyme solution

Measurements with spectrophotometer

One of the syringe pumps was primed with 4.5 mL one of the enzyme solutions before being used for the kinetic parameters determination. The other syringe pump was primed with 4.5 mL of the potassium phosphate buffer (40 mM) pH 6.8 before being used for the kinetic parameters determination.

Before starting reading the absorbance of the well, 5 µL of the enzyme solution or potassium phosphate buffer solution are added using the syringe pumps to the corresponding blank or reaction well. All this procedure is programmable using the software of the microplate reader. The absorbance at the wavelength of 414 nm is read for an experimental interval of 120 s all 2 s, corresponding to a total of 60 measurements points.

The procedure was repeated for all the enzyme solutions.

Evaluation of two-dimensional topology optimization microreactors configurations performance

Solutions

Preparation of 2,2'-azino-bis(3-ethylbenzthiazoline-6-sulfonic acid) Substrate Solution (ABTS) solutions (1 mM)

Prepare 10 mL of 1 mM solution of 2,2'-azino-bis(3-ethylbenzthiazoline-6-sulfonic acid) and 100 mM hydrogen peroxide and potassium phosphate buffer solution (100 mM) pH 5. The substrate used was 2,2'-azino-bis(3-ethylbenzthiazoline-6-sulfonic acid) diammonium salt (product from Sigma Aldrich, product number 11557).

Microreactor molding

The microreactor chambers were fabricated using a polymer made of a crosslinked thiol-ene network. The crosslinked thiol-ene network was prepared with pentaerythritol tetrakis (3-mercaptopropionate) (PETMP) (purchased at Sigma Aldrich, product no. 381462), triallyl-1,3,5-triazine -2,4,6(1H,3H, 5H)-trione (TATATO) (purchased at Sigma Aldrich, product no.114235) and bisphenol A diglycidyl ether (BADGE) (purchased at Sigma Aldrich, product no. D3415).

The microreactor was prepared by molding each of the top and the bottom halves of the chip. The molding process involved the following steps. A master mold was micromilled with the shape of the microreactor on a plate of poly(methyl methacrylate) (PMMA). Polydimethylsiloxane (PDMS) was used to produce the mirrored-image mold of the master mold. The combination of the tetrathiol, triallyl and diepoxy monomers was mixed together with a Lucirin® (purchased at BASF GmbH Germany) as photoinitiator in order to form a stable network. The mixture was then degassed and transferred onto the PDMS mold. The mold with the crosslinked thiol-ene network was afterwards exposed to UV-irradiation to cross -link. After the two halves of the microreactor chamber were cured, they were assembled and placed for 2 hours in the oven at 80°C. In this step the excess of thiol and epoxy groups on the surfaces of both halves of the microchip react with each other assuring the covalent bonding of the two surfaces. This procedure is described in more detail by Mazurek and his co-workers [146,147].

Surface modification of the reaction microchamber and enzyme immobilization

The microchip was filled with glycidyl methacrylate (purchased at Sigma Aldrich, product no. 151238) (1.0 mL, 7.2 mmol) in ethanol (1.0 mL) containing Lucirin® (purchased at BASF GmbH Germany) (0.05 mol% to allyl component) as photoinitiator.

The microchip was then covered by a polypropylene stencil mask. The chamber was exposed to UV-radiation for 3 minutes in order to promote the photochemical reaction between the glycidyl methacrylate molecules and the thiol groups.

For immobilization of peroxidase, the microreactor was filled with enzyme (1 mg/mL) in phosphate-buffered saline (PBS) solution (pH 7) and was left for reaction during 16h at 4°C. After the immobilization procedure, the microreactor was flushed with PBS solution.

Control measurement - Preparation of a reference microreactor – no enzyme immobilized

The microreactor configuration to set the reference or blank experiment was prepared with a surface treatment with glycidyl methacrylate molecules. The microreactor was filled with phosphate-buffered saline (PBS) solution (pH 7) and it was left inside the refrigerator for 16h at 4°C.

Control measurement - Preparation of microreactor with enzyme immobilized by adsorption

The microreactor configuration to test possible immobilization of enzyme by adsorption to the microreactor surfaces was prepared without the surface treatment with glycidyl methacrylate molecules. The microreactor was filled with enzyme (1 mg/mL) in phosphate-buffered saline (PBS) solution (pH 7) and it was left reacting during 16h at 4°C. After the immobilization procedure, the microreactor was flushed with PBS solution.

Analysis of the microreactors performance

The microreactor inlet is connected to a syringe pump (500 µL) which was filled with the substrate solution. The flowrate was set to ensure that the residence time inside the microreactor would be an average of 60 seconds; therefore the flowrate was set to 225 µL/min. The outlet is connected to an 8-port injection valve of the model VICI E45-230 - CR2 head. The 8-port valve establishes the connection between the outlet of the microreactor and the UV-detector of the model Agilent G1315AR or the waste vessel. The valve also makes the connection between the eluent flow (***phosphate buffer solution (100 mM) pH 5***) and the UV-detector or the waste vessel. The eluent is pumped by an HPLC pump (model Knauer Smartline 100) at 0.6 mL/min into the UV-detector while there is no sample collection. For collecting a sample, the valve changes position from the eluent flow to the outlet of the microreactor flow. Then, the outlet of the microreactor flow is send into the tube that connects to the UV-detector. Immediately after, the valve returns to its initial position and the eluent carries the sample into the UV-detector. A sample of 5 µL (volume of the connecting tube) is collected every 15 s for 30 minutes for each

microreactor configuration. The absorbance at 414 nm was read for each sample. The absorbance peaks of each sample are evaluated by performing the integration of the peak area.

Evaluation of three-dimensional topology optimization microreactors configurations performance

Preparation of diluted substrates solution - 2,2'-azino-bis(3-ethylbenzthiazoline-6-sulfonic acid) Solution (ABTS) solutions (10 mM) and of hydrogen peroxide (100 mM)

Prepare 10 mL of solution composed of 10 mM of 2,2'-azino-bis(3-ethylbenzthiazoline-6-sulfonic acid) and 100 mM hydrogen peroxide and potassium phosphate buffer solution (100 mM) pH 5. The substrate used was 2,2'-azino-bis(3-ethylbenzthiazoline-6-sulfonic acid) diammonium salt (product from Sigma Aldrich, product number 11557).

Preparation of concentrated substrates solution - 2,2'-azino-bis(3-ethylbenzthiazoline-6-sulfonic acid) Solution (ABTS) solutions (20 mM) and of hydrogen peroxide (200 mM)

Prepare 10 mL of solution composed of 20 mM of 2,2'-azino-bis(3-ethylbenzthiazoline-6-sulfonic acid) and 200 mM hydrogen peroxide and potassium phosphate buffer solution (100 mM) pH 5. The substrate used was 2,2'-azino-bis(3-ethylbenzthiazoline-6-sulfonic acid) diammonium salt (product from Sigma Aldrich, product number 11557).

Preparation of horseradish peroxidase solutions

Prepare 10 mL of horseradish peroxidase solution with concentration of 0.1 mg/mL of lyophilized enzyme preparation from Sigma Aldrich, product number P8125. Prepare two solutions of horseradish peroxidase (15 mL) with the following concentrations 10^{-4} mmol/L and $5 \cdot 10^{-5}$ mmol/L considering that the molecular weight of the lyophilized preparation is 44000 g/mol and that the preparation contains 15% (w/w) of enzyme.

The enzyme solutions concentrations were determined considering that the molecular weight of the lyophilized preparation is 44000 g/mol and that the preparation contains 15% (w/w) of enzyme.

Analysis of the microreactors performance

The T-microreactor inlets were connected to two syringe pumps (50 μL) (model Cavro XLP6000, from Tecan) which contained the peroxidase solution ($5 \cdot 10^{-5}$ mM) and the substrates solution (20 mM ABTS, 200mM H_2O_2), respectively. The Five-stream microreactor inlets were connected to three syringe pumps (50 μL) (model Cavro XLP6000, from Tecan) which contained the concentrated substrates solution (20 mM ABTS, 200mM H_2O_2), the diluted substrates solution

(10 mM ABTS, 100mM H_2O_2) and the enzyme solution ($1 \cdot 10^{-4}$ mM). The flowrate was set to ensure that the residence time inside the microreactor would be approximately 20, 10 and 5 seconds. The flowrates were calculated considering the microreactor volume, 16 μL. The flowrates for the experiments with T-microreactor and Five-stream microreactor at the different residence times are summarized in Table B-3 and Table B-4, respectively.

Table B-3 – Flowrates for the experiments with the T-microreactor.

Residence time (s)	**Flowrate (μL/min)**	
	Substrates solution	**Enzyme solution**
5	96	96
10	48	48
20	24	24

Table B-4 – Flowrates for the experiments with the Five-stream microreactor.

Residence time (s)	**Flowrate (μL/min)**		
	Diluted substrates solution	Concentrated substrates solution	Enzyme solution (10^{-4} mM)
5	96	48	48
10	48	24	24
20	24	12	12

Appendix C

Experimental data

Experimental data for determination the kinetic parameters $K_{M,app}^{ABTS}$ and $V_{max,app}$

Time (s)	**Blank 1** with enzyme solution and without reactants			**Blank 2** with reactants and without enzyme solution			**Reaction** [ABTS]=0.06 mM				
	Absorbance			Absorbance			Absorbance				
6	0.1240	0.1786	0.1263	0.0631	0.0558	0.0600	0.0754	0.0652	0.0560	0.0602	0.0574
10.5	0.1240	0.1833	0.1251	0.0637	0.0555	0.0605	0.0844	0.0675	0.0579	0.0623	0.0579
15	0.1246	0.1808	0.1265	0.0622	0.0552	0.0607	0.0984	0.0723	0.0611	0.0645	0.0600
19.5	0.1251	0.1799	0.1259	0.0622	0.0559	0.0595	0.1190	0.0748	0.0624	0.0672	0.0627
24	0.1192	0.1800	0.1264	0.0617	0.0560	0.0593	0.1422	0.0787	0.0656	0.0702	0.0660
28.5	0.1252	0.1828	0.1234	0.0624	0.0566	0.0605	0.1654	0.0831	0.0688	0.0736	0.0695
33	0.1224	0.1828	0.1231	0.0614	0.0547	0.0604	0.1837	0.0872	0.0725	0.0797	0.0723
37.5	0.1222	0.1768	0.1242	0.0627	0.0552	0.0609	0.2031	0.0939	0.0774	0.0829	0.0757
42	0.1240	0.1803	0.1249	0.0615	0.0553	0.0604	0.2212	0.1010	0.0820	0.0878	0.0804
46.5	0.1257	0.1817	0.1244	0.0632	0.0551	0.0601	0.2377	0.1089	0.0869	0.0921	0.0861
51	0.1252	0.1795	0.1234	0.0621	0.0549	0.0601		0.1169	0.0910	0.0966	0.0901
55.5	0.1250	0.1819	0.1242	0.0624	0.0565	0.0603		0.1229	0.0968	0.1025	0.0974
60	0.1257	0.1792	0.1265	0.0626	0.0574	0.0604		0.1293	0.1040	0.1075	0.1040
64.5	0.1254	0.1796	0.1249	0.0621	0.0583	0.0609		0.1349	0.1113	0.1155	0.1112
69	0.1265	0.1812	0.1252	0.0621	0.0578	0.0600		0.1420	0.1181	0.1208	0.1182
73.5	0.1220	0.1789	0.1252	0.0616	0.0571	0.0603		0.1482	0.1255	0.1275	0.1259
78	0.1252	0.1847	0.1269	0.0624	0.0577	0.0604		0.1557	0.1331	0.1344	0.1335
82.5	0.1236	0.1815	0.1279	0.0615	0.0578	0.0605		0.1618	0.1393	0.1400	0.1412
87	0.1237	0.1786	0.1251	0.0613	0.0573	0.0594		0.1684	0.1463	0.1462	0.1480
91.5	0.1252	0.1815	0.1238	0.0610	0.0583	0.0600		0.1757	0.1537	0.1523	0.1567
96	0.1235	0.1795	0.1253	0.0622	0.0564	0.0610		0.1822	0.1616	0.1593	0.1630
100.5	0.1258	0.1812	0.126	0.0612	0.0582	0.0595		0.1882	0.1674	0.1643	0.1691
105	0.1251	0.1786	0.1256	0.0609	0.0570	0.0600		0.1949	0.1742	0.1712	0.1748
109.5	0.1244	0.1808	0.1232	0.0619	0.0564	0.0603		0.2022	0.1807	0.1777	0.1812
114	0.1245	0.1781	0.1268	0.0622	0.0559	0.0602		0.2077	0.1862	0.1831	0.1858

	6.037×10^{-06}	1.650×10^{-06}	5.869×10^{-06}	-1.137×10^{-05}	1.995×10^{-05}	-6.325×10^{-07}	1.596×10^{-03}	1.391×10^{-03}	1.281×10^{-03}	1.194×10^{-03}	1.294×10^{-03}
Average		4.51931×10^{-06}			2.650×10^{-06}				1.351×10^{-03}		
Standard Deviation		3.15662×10^{-06}			1.591×10^{-05}				1.533×10^{-04}		

Time (s)	Reaction [ABTS]= 0.1 mM					Reaction [ABTS]= 0.2 mM			
	Absorbance					Absorbance			
6	0.0653	0.0656	0.0662	0.0980	0.0887	0.0801	0.0727	0.0712	0.0684
10.5	0.0693	0.0699	0.0683	0.0685	0.0982	0.0893	0.0789	0.0804	0.0738
15	0.0742	0.0746	0.0734	0.0680	0.1091	0.1005	0.0931	0.0887	0.0801
19.5	0.0790	0.0787	0.0799	0.0718	0.1213	0.1166	0.1037	0.0973	0.0897
24	0.0880	0.0855	0.0883	0.0792	0.1397	0.1345	0.1158	0.1066	0.1015
28.5	0.0944	0.0964	0.1007	0.0859	0.1553	0.1513	0.1278	0.1199	0.1136
33	0.1013	0.1084	0.1130	0.0966	0.1717	0.1650	0.1469	0.1349	0.1282
37.5	0.1128	0.1183	0.1259	0.1056	0.1885	0.1798	0.1617	0.1519	0.1439
42	0.1239	0.1301	0.1358	0.1130	0.2059	0.1949	0.1746	0.1700	0.159
46.5	0.1309	0.1425	0.1468	0.1223	0.2217	0.2122	0.1892	0.1883	0.1754
51	0.1396	0.1528	0.1574	0.1329	0.2386	0.2299	0.2063	0.2084	0.1940
55.5	0.1492	0.1617	0.1681	0.1440	0.2558	0.2482	0.2255	0.2269	0.2130
60	0.1636	0.1704	0.1781	0.1554	0.2720	0.2658	0.2464	0.2461	0.2322
64.5	0.1791	0.1784	0.1872	0.1678	0.2865	0.2841	0.2685	0.2648	0.2501
69	0.1947	0.1885	0.1975	0.1824	0.3013	0.3023	0.2899	0.2829	0.2663
73.5	0.2109	0.1989	0.2074	0.1937	0.3151	0.3213	0.3101	0.2986	0.2826
78	0.2259	0.2102	0.2175	0.2050	0.3296	0.3396	0.3281	0.3166	0.2989
82.5	0.2403	0.2206	0.2274	0.2183	0.3425	0.3573	0.3454	0.3300	0.3135
87	0.2517	0.2315	0.2373	0.2287	0.3557	0.3751	0.3621	0.3443	0.3281
91.5	0.2616	0.2409	0.2475	0.2400	0.3675	0.3915	0.3745	0.3573	0.3421
96	0.2718	0.2518	0.2575	0.2502	0.3787	0.4068	0.3884	0.3701	0.3550
100.5	0.2809	0.2611	0.2666	0.2603	0.3880	0.4211	0.4001	0.3812	0.3676
105	0.2880	0.2714	0.2768	0.2704	0.3982	0.4374	0.4121	0.3937	0.3801
109.5	0.2950	0.2799	0.2850	0.2790	0.4062	0.4512	0.4231	0.4021	0.3906
114	0.3019	0.2896	0.2942	0.2876	0.4145	0.4624	0.4327	0.4131	0.4029
	2.435×10^{-03}	2.184×10^{-03}	2.235×10^{-03}	2.191×10^{-03}	3.212×10^{-03}	3.722×10^{-03}	3.636×10^{-03}	3.465×10^{-03}	3.374×10^{-03}
Average	2.261×10^{-03}					3.482×10^{-03}			
Standard Deviation	1.180×10^{-04}					2.036×10^{-04}			

Time (s)	Reaction [ABTS]= 0.6 mM						Reaction [ABTS]=1 mM					
	Absorbance						Absorbance					
6	0.1855	0.1701	0.1551	0.1397	0.1314	0.1167	0.2612	0.2375	0.2159	0.2128	0.1926	0.1848
10.5	0.218	0.1962	0.1775	0.1616	0.1547	0.1338	0.3009	0.2677	0.2526	0.2442	0.2254	0.2179
15	0.2437	0.2206	0.2002	0.208	0.1704	0.1595	0.3362	0.3064	0.2885	0.2853	0.2610	0.2540
19.5	0.2789	0.2456	0.2317	0.2395	0.2024	0.194	0.3748	0.3537	0.3313	0.3250	0.2952	0.2930
24	0.3112	0.2649	0.2572	0.2708	0.2388	0.2286	0.4245	0.3979	0.3748	0.3644	0.3333	0.3365
28.5	0.3396	0.2952	0.2866	0.306	0.2682	0.2491	0.4725	0.4418	0.4148	0.4074	0.3772	0.3803
33	0.3661	0.3255	0.3252	0.3362	0.2969	0.2771	0.5122	0.4808	0.4566	0.4496	0.4164	0.4228
37.5	0.3944	0.3482	0.3612	0.3583	0.3276	0.3067	0.5483	0.5181	0.5013	0.4884	0.4628	0.4650
42	0.4234	0.3711	0.391	0.3818	0.3605	0.335	0.5817	0.5570	0.5455	0.5230	0.5077	0.5062
46.5	0.4535	0.3987	0.4216	0.405	0.3910	0.3646	0.6154	0.5976	0.5853	0.5559	0.5431	0.5434
51	0.4852	0.4254	0.4526	0.4284	0.4207	0.3912	0.6482	0.6351	0.6233	0.5892	0.5704	0.5750
55.5	0.5153	0.4525	0.4822	0.452	0.4461	0.4173	0.6768	0.6698	0.6613	0.6220	0.5955	0.6077
60	0.5441	0.4782	0.5117	0.478	0.4734	0.4436	0.7067	0.7001	0.6977	0.6534	0.6226	0.6361
64.5	0.5724	0.5052	0.5398	0.5055	0.5010	0.4682	0.7333	0.7306	0.7325	0.6829	0.6532	0.6615
69	0.5999	0.5309	0.5665	0.5355	0.5266	0.4919	0.7604	0.7614	0.7669	0.7130	0.6835	0.6852
73.5	0.625	0.5563	0.5922	0.5655	0.5515	0.5166	0.7847	0.7900	0.7993	0.7409	0.7186	0.7083
78	0.6484	0.5806	0.6161	0.5949	0.5761	0.5396	0.8122	0.8194	0.8299	0.7680	0.7511	0.7324
82.5	0.6734	0.6038	0.6401	0.6233	0.5985	0.5647	0.8377	0.8470	0.8572	0.7940	0.7812	0.7541
87	0.6958	0.6247	0.6621	0.6511	0.6195	0.5889	0.8635	0.8742	0.8845	0.8196	0.8088	0.7740
91.5	0.7167	0.6466	0.6836	0.6761	0.6393	0.6137	0.8876	0.8988	0.9093	0.8438	0.8348	0.7934
96	0.7398	0.6676	0.7024	0.6995	0.6580	0.6359	0.9122	0.9222	0.9334	0.8686	0.8573	0.8113
100.5	0.7591	0.6881	0.7226	0.7212	0.6758	0.6600	0.9353	0.9454	0.9554	0.8929	0.8782	0.8295
105	0.7796	0.7047	0.7400	0.7420	0.6919	0.6805	0.9570	0.9683	0.976	0.9158	0.8963	0.8476
109.5	0.7978	0.7242	0.7587	0.7601	0.7077	0.7014	0.9806	0.9898	0.996	0.9391	0.9144	0.8632
114	0.8163	0.7413	0.7755	0.7778	0.7240	0.7224	0.9989	1.0098	1.0153	0.9621	0.9327	0.8799
	5.944×10^{-03}	5.438×10^{-03}	6.001×10^{-03}	5.941×10^{-03}	5.730×10^{-03}	5.712×10^{-03}	6.779×10^{-03}	7.264×10^{-03}	7.637×10^{-03}	6.963×10^{-03}	7.040×10^{-03}	6.516×10^{-03}
Average	5.794×10^{-03}						7.033×10^{-03}					
Standard Deviation	2.117×10^{-04}						3.886×10^{-04}					

Time (s)	Reaction [ABTS]= 2 mM						Reaction [ABTS]=6 mM			
	Absorbance						Absorbance			
6	0.3110	0.3111	0.2680	0.2655	0.2380	0.2441	0.4673	0.441	0.4616	0.4695
10.5	0.3550	0.3545	0.3051	0.3116	0.2783	0.2882	0.5410	0.4883	0.5222	0.5369
15	0.4022	0.3925	0.3587	0.3509	0.3284	0.3230	0.6136	0.5393	0.5838	0.6085
19.5	0.4477	0.4478	0.4142	0.3668	0.3819	0.3652	0.6861	0.5898	0.6443	0.679
24	0.4903	0.5178	0.4610	0.4312	0.4078	0.4043	0.7588	0.6440	0.7004	0.7476
28.5	0.5381	0.5963	0.5080	0.4662	0.4564	0.4344	0.8264	0.7095	0.7517	0.8144
33	0.5741	0.6446	0.5522	0.4884	0.5244	0.4600	0.8866	0.7849	0.7996	0.8722
37.5	0.6012	0.7009	0.5948	0.5087	0.5671	0.4885	0.9458	0.8643	0.8477	0.9259
42	0.6319	0.7462	0.6392	0.5470	0.5971	0.5194	1.0013	0.9386	0.9046	0.9736
46.5	0.6617	0.7719	0.6861	0.5956	0.6242	0.5540	1.0570	1.0071	0.9600	1.0215
51	0.6967	0.7857	0.7347	0.6462	0.6596	0.5919	1.1132	1.0698	1.0110	1.0668
55.5	0.7368	0.8029	0.7812	0.6915	0.7037	0.6300	1.1714	1.1271	1.0566	1.1143
60	0.7798	0.8325	0.8276	0.7308	0.7487	0.6665	1.2318	1.1813	1.0999	1.1622
64.5	0.8259	0.8668	0.8708	0.7693	0.7945	0.7033	1.2938	1.2272	1.1414	1.2106
69	0.8712	0.9007	0.9115	0.8091	0.8381	0.7396	1.3516	1.2710	1.18300	1.2634
73.5	0.9165	0.9282	0.9501	0.8471	0.8810	0.7740	1.4084	1.3087	1.2246	1.3126
78	0.9572	0.9500	0.9890	0.8879	0.9205	0.8078	1.4631	1.3423	1.2679	1.3650
82.5	0.9997	0.9736	1.0228	0.9284	0.9582	0.8394	1.5193	1.3756	1.3141	1.4166
87	1.0387	0.9984	1.0557	0.9676	0.9976	0.8713	1.5730	1.4088	1.3648	1.4704
91.5	1.0740	1.0275	1.0881	1.0054	1.0318	0.9019	1.6275	1.4441	1.4175	1.5199
96	1.1089	1.0572	1.1191	1.0414	1.0668	0.9312	1.6839	1.4817	1.4725	1.5712
100.5	1.1447	1.0899	1.1482	1.0754	1.0987	0.9613	1.7382	1.5229	1.5293	1.6220
105	1.1763	1.1243	1.1744	1.1068	1.1300	0.9894	1.7913	1.5669	1.5806	1.6701
109.5	1.2086	1.1588	1.2030	1.1348	1.1576	1.0169	1.8397	1.6135	1.6288	1.7179
114	1.2383	1.1902	1.2263	1.1631	1.1871	1.0444	1.8823	1.6625	1.6689	1.7609
	8.635×10^{-03}	7.674×10^{-03}	9.104×10^{-03}	8.532×10^{-03}	8.912×10^{-03}	7.443×10^{-03}	1.299×10^{-02}	1.143×10^{-02}	1.091×10^{-02}	1.164×10^{-02}
Average	8.383×10^{-03}						1.174×10^{-02}			

Standard Deviation	6.742×10^{-04}	8.872×10^{-04}

Time (s)	Reaction [ABTS]= 10 mM			
	Absorbance			
6	0.7171	0.6903	0.7128	0.7196
10.5	0.8009	0.7311	0.7911	0.7952
15	0.8891	0.7688	0.8700	0.8745
19.5	0.9718	0.8061	0.9424	0.9521
24	1.0577	0.8528	1.0141	1.0236
28.5	1.1400	0.9097	1.0771	1.0933
33	1.2254	0.9758	1.1388	1.1616
37.5	1.3081	1.0507	1.1988	1.2303
42	1.3801	1.130	1.2591	1.2990
46.5	1.4439	1.2130	1.3198	1.3658
51	1.5018	1.2929	1.3811	1.4316
55.5	1.5557	1.3692	1.4423	1.4938
60	1.6009	1.4378	1.5075	1.5506
64.5	1.6401	1.5059	1.5706	1.6043
69	1.6689	1.5656	1.6337	1.6541
73.5	1.6998	1.6193	1.6943	1.7014
78	1.7366	1.6706	1.7560	1.7517
82.5	1.7746	1.7167	1.8202	1.7982
87	1.8201	1.7594	1.8771	1.8453
91.5	1.8647	1.7999	1.9288	1.8919
96	1.9125	1.8382	1.9852	1.9353
100.5	1.9603	1.8743	2.0389	1.9841
105	2.0083	1.9052	2.0948	2.0308
109.5	2.0544	1.9336	2.1441	2.0751
114	2.1021	1.963	2.1922	2.1169
ΔA/s	1.212×10^{-02}	1.294×10^{-02}	1.363×10^{-02}	1.280×10^{-02}
Average	1.287×10-02			
Standard Deviation	6.196×10-04			

Experimental data for determination of the kinetic parameter $k_{cat,app}^{ABTS}$

Time (s)	**Blank 1** with enzyme solution and without reactants			**Blank 2** with reactants and without enzyme solution			**Reaction** concentration of protein in solution, 0.031 mg/mL			**Reaction** concentration of protein in solution, 0.02 mg/mL					
	Absorbance			Absorbance			Absorbance			Absorbance					
0	0.1263	0.1510	0.1173	0.3809	0.3954	0.3840	0.6615	0.8505	0.8155	0.7172	0.6712	0.6583	0.6796	0.6370	0.6565
2	0.1251	0.1508	0.1140	0.3798	0.3959	0.3861	0.8144	1.0881	1.0443	0.8715	0.8063	0.7775	0.8295	0.7428	0.7691
4	0.1265	0.1522	0.1138	0.3812	0.3969	0.3842	0.9778	1.3436	1.2783	1.0659	0.9393	0.9073	0.9982	0.8478	0.8911
6	0.1259	0.1514	0.1140	0.3822	0.3967	0.3879	1.1488	1.6184	1.526	1.2757	1.0837	1.0443	1.1638	0.9624	1.0135
8	0.1264	0.1500	0.1144	0.3809	0.3987	0.3834	1.3317	1.8944	1.7871	1.4718	1.2299	1.1876	1.3394	1.0794	1.1361
10	0.1234	0.1497	0.1140	0.3801	0.3949	0.3853	1.5243	2.1738	2.0597	1.6758	1.3884	1.3342	1.5230	1.1954	1.2633
12	0.1231	0.1478	0.1143	0.3827	0.3976	0.3831	1.7228	2.4524	2.3333	1.8649	1.5419	1.4886	1.7094	1.3182	1.3926
14	0.1242	0.1490	0.1142	0.3809	0.3980	0.3844	1.9358	2.7213	2.6084	2.0092	1.7067	1.6442	1.8998	1.4431	1.5192
16	0.1249	0.1513	0.1154	0.3820	0.3952	0.3858	2.1656	2.9893	2.8824	2.1486	1.866	1.8054	2.0923	1.5672	1.6484
18	0.1244	0.1521	0.1155	0.3815	0.3944	0.3835	2.4035	3.2406	3.1619	2.3136	2.0337	1.9658	2.2814	1.6929	1.7788
20	0.1234	0.1489	0.1160	0.3840	0.3958	0.3833	2.6640	3.4799	3.4474	2.5201	2.1973	2.1283	2.4747	1.8213	1.9071
22	0.1242	0.1518	0.1161	0.3841	0.3935	0.3867	2.9366	3.7140	3.7383	2.7523	2.3761	2.2908	2.6656	1.9482	2.0451
24	0.1265	0.1507	0.1154	0.3794	0.3956	0.3864	3.2316	3.9401	4.0276	2.984	2.5591	2.4535	2.8614	2.0796	2.1812
26	0.1249	0.1505	0.1145	0.3802	0.3949	0.3843	3.5402	4.1594	4.3410	3.1894	2.7416	2.6155	3.0508	2.2080	2.3151
28	0.1252	0.1486	0.1162	0.3794	0.3945	0.3825	3.8518	4.3887	4.6553	3.3664	2.9128	2.7771	3.2392	2.3394	2.4492
30	0.1252	0.1518	0.1169	0.3826	0.3922	0.3839	4.1775	4.5924	4.9918	3.5370	3.0841	2.9395	3.4267	2.4742	2.5897
32	0.1269	0.1521	0.1167	0.3835	0.3961	0.3836	4.5039	4.8194	5.3338	3.7038	3.2449	3.0949	3.6184	2.6021	2.7236
34	0.1279	0.1508	0.1145	0.3798	0.3970	0.3842	4.8244	5.0414	5.6992	3.8658	3.4043	3.2499	3.8036	2.7313	2.8654
36	0.1251	0.1504	0.1155	0.3797	0.3958	0.3856	5.1663	5.2592	6.0359	4.0301	3.557	3.4061	3.9726	2.8635	2.9997
38	0.1238	0.1487	0.1150	0.3815	0.3944	0.3830	5.4955	5.4918	6.4099	4.1989	3.7126	3.5573	4.1650	2.9950	3.1376
40	0.1253	0.1514	0.1151	0.3800	0.3942	0.3818	5.8332	5.7348	6.7414	4.3652	3.869	3.7074	4.3415	3.1266	3.2645
42	0.1260	0.1511	0.1179	0.3817	0.3942	0.3842	6.1321	5.9919	7.0778	4.5291	4.0197	3.8523	4.5150	3.2605	3.3951
44	0.1256	0.1487	0.1126	0.3832	0.3943	0.3855	6.5224	6.2332	7.4574	4.6847	4.1736	3.9956	4.6880	3.3928	3.5288
46	0.1232	0.1489	0.1158	0.3815	0.3945	0.3826	6.8509	6.4679	7.6003	4.8423	4.3370	4.1415	4.8613	3.5194	3.6515
48	0.1268	0.1521	0.1143	0.3804	0.3945	0.3827	7.1194	6.7163	7.9298	4.9901	4.4826	4.2790	5.0305	3.6569	3.7725
50	0.1260	0.1514	0.1153	0.3807	0.3957	0.3821	7.4830	6.9379	8.1326	5.1525	4.6288	4.4133	5.2025	3.7764	3.8962

52	0.1247	0.1500	0.1138	0.3807	0.3964	0.3842	7.8118	7.1752	8.4507	5.3057	4.7919	4.5528	5.3595	3.9063	4.0183
54	0.1248	0.1497	0.1145	0.3804	0.3946	0.3831	8.1219	7.4409	8.6105	5.4599	4.9341	4.6725	5.5432	4.0404	4.1357
56	0.1269	0.1524	0.1135	0.3840	0.3972	0.3832	8.4172	7.547	8.8188	5.6285	5.0935	4.8030	5.7075	4.1657	4.2540
58	0.1223	0.1512	0.1130	0.3804	0.3953	0.3801	8.7217	7.8593	9.0721	5.7636	5.2557	4.9315	5.8638	4.2999	4.3726
60	0.1242	0.1543	0.1141	0.3816	0.3964	0.3818	9.0542	8.1163	9.1636	5.9225	5.3813	5.0557	6.0143	4.4244	4.4772
62	0.1248	0.1497	0.1161	0.3830	0.3966	0.3816	9.1438	8.3993	9.5441	6.0979	5.553	5.1835	6.1749	4.5436	4.5997
64	0.1236	0.1534	0.1146	0.3801	0.3961	0.3840	9.5683	8.5061	9.5940	6.2661	5.6948	5.2919	6.3697	4.6647	4.7083
66	0.1266	0.1509	0.1158	0.3807	0.3930	0.3826	9.6343	8.8336	9.6577	6.3806	5.8255	5.4222	6.4983	4.7923	4.8202
68	0.1268	0.1520	0.1158	0.3827	0.3934	0.3832	9.8000	8.8679	9.8184	6.5363	5.9745	5.5223	6.6452	4.9175	4.9404
70	0.1249	0.1515	0.1137	0.3798	0.3958	0.3844	10.4532	9.2100	9.8420	6.7120	6.1331	5.6390	6.7862	5.0338	5.0551
72	0.1246	0.1498	0.1138	0.3824	0.3951	0.3834	10.1648	9.2731	10.2372	6.9037	6.2531	5.7550	6.9487	5.1558	5.1520
74	0.1256	0.1489	0.1150	0.3818	0.3967	0.3814	10.4535	9.6539	10.2496	7.0421	6.4067	5.8671	7.0722	5.2798	5.2678
76	0.1249	0.1513	0.1157	0.3804	0.3954	0.3842	10.4984	9.5985	10.3955	7.2328	6.5551	5.9924	7.1951	5.4129	5.3748
78	0.1260	0.1510	0.1184	0.3815	0.3951	0.3851	10.5262	9.7246	9.95010	7.2884	6.6981	6.1019	7.3804	5.5274	5.4803
80	0.1246	0.1533	0.1152	0.3818	0.3946	0.3817	10.5449	10.4712	10.5740	7.5357	6.8094	6.1946	7.4995	5.6636	5.5782
82	0.1259	0.1517	0.1140	0.3810	0.3941	0.3852	10.5740	10.1667	10.4981	7.6810	6.9439	6.3136	7.6802	5.7709	5.6884
84	0.1257	0.1502	0.1160	0.3823	0.3959	0.3847		10.1892	10.5436	7.7972	7.0868	6.4068	7.7379	5.8742	5.7764
86	0.1241	0.1537	0.1153	0.3813	0.3918	0.3810		10.2858	10.5740	7.9009	7.2192	6.5076	7.9351	6.0081	5.8899
88	0.1250	0.1522	0.1144	0.3828	0.3944	0.3830		10.574		8.0816	7.3609	6.6285	8.0756	6.1083	6.0010
90	0.1263	0.1511	0.1126	0.3824	0.3949	0.3852		10.574		8.2617	7.4769	6.7219	8.1976	6.2453	6.0958
92	0.1249	0.1475	0.1137	0.3827	0.3963	0.3807		10.3899		8.3003	7.6219	6.8145	8.4155	6.3465	6.1933
94	0.1254	0.1524	0.1150	0.3807	0.3942	0.3808				8.6435	7.7529	6.9011	8.4401	6.4778	6.2964
96	0.1238	0.1519	0.1144	0.3789	0.3916	0.3850				8.8512	7.914	7.0422	8.6832	6.5957	6.3984
98	0.1251	0.1516	0.1138	0.3807	0.3964	0.3827				9.0428	8.0519	7.0845	8.6942	6.6931	6.5038
100	0.1249	0.1514	0.1138	0.3811	0.3943	0.3831				8.8587	8.1457	7.2055	8.8625	6.8305	6.5807
102	0.1248	0.1528	0.1161	0.3797	0.3939	0.3829				9.2407	8.3366	7.2410	8.8507	6.8930	6.6826
104	0.1247	0.1506	0.1157	0.3784	0.3947	0.3842				9.2801	8.4903	7.3920	9.1473	7.0028	6.7712
106	0.1235	0.1512	0.1154	0.3808	0.3961	0.3821				9.4737	8.6526	7.5047	9.2178	7.1176	6.8474
108	0.1289	0.1520	0.1175	0.3801	0.3946	0.3833				9.8230	8.6827	7.5793	9.2231	7.2232	6.9361
110	0.1262	0.1508	0.1151	0.3795	0.3945	0.3805				9.8514	8.8501	7.6777	9.4240	7.3605	7.0270

112	0.1266	0.1487	0.1142	0.3790	0.3960	0.3842				9.9953	9.0445	7.7341	9.7657	7.4903	7.0990
114	0.1270	0.1514	0.1134	0.3793	0.3950	0.3813				10.0032	9.1061	7.8191	9.7577	7.5255	7.1892
116	0.1257	0.1514	0.1153	0.3776	0.3925	0.3827				10.3685	9.2463	7.9526	9.9798	7.6564	7.2883
118	0.1273	0.1502	0.1170	0.3791	0.3928	0.3835				10.4018	9.5726	8.0364	10.0531	7.8285	7.348
ΔA/s	5.870×10^{-6}	7.827×10^{-6}	-2.139×10^{-7}	-1.3115×10^{-5}	-1.515×10^{-5}	-1.985×10^{-5}	0.1386	0.1091	0.1148	0.0813	0.0746	0.0633	0.0798	0.0618	0.0579
Average		4.234×10^{-6}			-1.60415×10^{-5}			0.1209				0.0789			
Standard Deviation		3.457×10^{-6}			3.157×10^{-6}			0.0156				0.0035			

Time (s)	Reaction concentration of protein in solution, 0.01 mg/mL						Reaction concentration of protein in solution, 0.004 mg/mL					
	Absorbance						Absorbance					
0	0.6040	0.5889	0.5774	0.5643	0.6005	0.5793	0.5016	0.4916	0.5246	0.5119	0.5153	0.5308
2	0.6850	0.6533	0.6448	0.6203	0.6759	0.6387	0.541	0.5153	0.5494	0.5367	0.5403	0.5593
4	0.7727	0.7296	0.7174	0.6853	0.7523	0.6982	0.5823	0.5369	0.5715	0.5649	0.5646	0.5822
6	0.8626	0.8074	0.7851	0.7426	0.8342	0.7611	0.6268	0.5562	0.5921	0.5903	0.5878	0.6096
8	0.9584	0.8887	0.8619	0.8063	0.9162	0.829	0.6684	0.5782	0.617	0.6201	0.6146	0.6324
10	1.0569	0.9734	0.9367	0.8653	0.997	0.899	0.7113	0.5982	0.6409	0.6467	0.6398	0.6627
12	1.1538	1.0588	1.0152	0.9314	1.0796	0.9654	0.7527	0.6158	0.6635	0.6758	0.6681	0.6861
14	1.2549	1.1435	1.0952	0.9991	1.1649	1.0389	0.7972	0.6397	0.6868	0.7027	0.6927	0.7131
16	1.3642	1.2344	1.1734	1.0646	1.2483	1.1129	0.8417	0.6617	0.707	0.7315	0.7191	0.742
18	1.4707	1.3209	1.2533	1.1284	1.3275	1.1835	0.8812	0.6796	0.7316	0.7588	0.7462	0.7668
20	1.5765	1.4063	1.3348	1.1977	1.4105	1.2557	0.9173	0.7015	0.7524	0.783	0.7708	0.7954
22	1.6898	1.498	1.4149	1.2636	1.4948	1.3306	0.9596	0.7209	0.7737	0.8107	0.7982	0.8196
24	1.7996	1.585	1.4935	1.3331	1.5752	1.4073	0.9992	0.7443	0.7972	0.8367	0.829	0.8456
26	1.9081	1.6748	1.578	1.4026	1.6564	1.4773	1.0416	0.764	0.8194	0.8691	0.851	0.8728
28	2.0210	1.765	1.6575	1.4709	1.7386	1.5537	1.0845	0.7836	0.8377	0.8905	0.875	0.8961
30	2.1350	1.844	1.7387	1.5388	1.821	1.6248	1.1305	0.8059	0.8632	0.917	0.9039	0.9234
32	2.2447	1.9309	1.8203	1.6117	1.8998	1.6938	1.1781	0.8267	0.8848	0.9429	0.931	0.9516
34	2.3579	2.0164	1.8999	1.6816	1.978	1.7651	1.2263	0.8488	0.906	0.9681	0.9586	0.9777
36	2.4690	2.0989	1.9793	1.7496	2.0568	1.8325	1.2717	0.8689	0.928	0.9956	0.9825	1.0037
38	2.5760	2.1828	2.0561	1.8226	2.1334	1.9048	1.3212	0.8894	0.9456	1.0184	1.0124	1.0264
40	2.6867	2.2674	2.1398	1.8963	2.2158	1.9727	1.3645	0.9115	0.9692	1.0441	1.0354	1.0529
42	2.7905	2.3456	2.2152	1.9666	2.2872	2.0409	1.4107	0.93	0.9903	1.0685	1.0617	1.0769
44	2.8984	2.4219	2.299	2.0373	2.3648	2.1078	1.4532	0.9538	1.0121	1.0927	1.0892	1.1043
46	3.0030	2.5041	2.3725	2.1056	2.4391	2.1778	1.4958	0.9734	1.0302	1.1152	1.1131	1.1296
48	3.1041	2.5825	2.4531	2.1765	2.5157	2.2472	1.5342	0.9963	1.0515	1.1399	1.1405	1.1573
50	3.2106	2.6542	2.5245	2.2462	2.5899	2.3109	1.5784	1.0177	1.0687	1.1633	1.165	1.183
52	3.3127	2.7315	2.6044	2.3201	2.6604	2.3774	1.6164	1.0413	1.0925	1.1862	1.1911	1.2088
54	3.4133	2.8077	2.6818	2.3889	2.7334	2.4416	1.6574	1.0651	1.109	1.2095	1.2164	1.2344

56	3.5044	2.8768	2.7563	2.4622	2.8056	2.5103	1.699	1.0865	1.1356	1.2346	1.2432	1.2611
58	3.6050	2.9530	2.8309	2.5317	2.8786	2.5766	1.7389	1.1094	1.1497	1.2545	1.2664	1.2874
60	3.6994	3.0265	2.9097	2.5995	2.9521	2.6417	1.7808	1.1312	1.1725	1.2803	1.2924	1.3113
62	3.7946	3.0922	2.9833	2.6688	3.0204	2.7084	1.8229	1.1581	1.1916	1.3020	1.316	1.3357
64	3.8816	3.1636	3.0554	2.7373	3.0982	2.7732	1.8607	1.1804	1.2132	1.3209	1.3397	1.3611
66	3.9706	3.2339	3.1324	2.8076	3.1644	2.8378	1.9008	1.2026	1.2313	1.3447	1.3638	1.3837
68	4.0623	3.2964	3.2038	2.8731	3.2353	2.9084	1.9431	1.2286	1.2512	1.3621	1.3890	1.4056
70	4.1486	3.3645	3.2750	2.9395	3.3050	2.9751	1.9880	1.2488	1.2712	1.3840	1.4120	1.4314
72	4.2358	3.4306	3.3464	3.0076	3.3784	3.0392	2.0278	1.2718	1.2906	1.4050	1.4327	1.4560
74	4.3187	3.4909	3.4200	3.0731	3.4429	3.1069	2.0674	1.2978	1.3129	1.4264	1.4607	1.4778
76	4.4014	3.5565	3.4897	3.1435	3.5123	3.1690	2.1084	1.3230	1.3291	1.4467	1.4819	1.4991
78	4.4854	3.6189	3.5582	3.2042	3.5808	3.2381	2.1509	1.3488	1.3461	1.4684	1.5048	1.5267
80	4.5641	3.6856	3.6334	3.2686	3.6496	3.2994	2.1871	1.3733	1.3660	1.4897	1.5272	1.5481
82	4.6324	3.7476	3.7018	3.3332	3.7167	3.3681	2.2284	1.3966	1.3835	1.5055	1.5487	1.5656
84	4.7224	3.8088	3.7682	3.3964	3.7824	3.4341	2.2691	1.4182	1.4065	1.5285	1.5737	1.5875
86	4.7947	3.8710	3.8348	3.4575	3.8532	3.4939	2.3063	1.4441	1.4255	1.5439	1.5951	1.6103
88	4.8747	3.9325	3.9004	3.5184	3.9216	3.5620	2.3396	1.4696	1.4408	1.5648	1.6162	1.6307
90	4.9396	3.9916	3.9685	3.5844	3.9859	3.6256	2.3755	1.4935	1.4612	1.5830	1.6354	1.6507
92	5.0070	4.0505	4.0355	3.6425	4.0543	3.6913	2.4125	1.5181	1.4805	1.6028	1.6592	1.6722
94	5.0966	4.1090	4.0978	3.6986	4.1224	3.7519	2.4424	1.5465	1.4975	1.6222	1.6802	1.6951
96	5.1626	4.1645	4.1699	3.7531	4.1919	3.8183	2.4779	1.5697	1.5154	1.6369	1.7040	1.7147
98	5.2331	4.2210	4.2280	3.8143	4.2513	3.8793	2.5110	1.5908	1.5330	1.6570	1.7251	1.7365
100	5.2969	4.2799	4.2947	3.8718	4.3163	3.9403	2.5414	1.6171	1.5491	1.6751	1.7409	1.7578
102	5.3756	4.3332	4.3494	3.9253	4.3767	4.0007	2.5705	1.6428	1.5671	1.6894	1.7623	1.7738
104	5.4322	4.3962	4.4217	3.9855	4.4439	4.0610	2.5979	1.6658	1.5881	1.7117	1.7820	1.7959
106	5.4927	4.4464	4.4783	4.0391	4.5073	4.1259	2.6240	1.6904	1.6075	1.7248	1.8028	1.8175
108	5.5670	4.4931	4.5316	4.0948	4.5654	4.1852	2.6502	1.7111	1.6223	1.7451	1.8254	1.8360
110	5.6322	4.5492	4.5964	4.1414	4.6346	4.2445	2.6786	1.7401	1.6418	1.7599	1.8430	1.8584
112	5.7048	4.6067	4.6530	4.1979	4.6997	4.3071	2.7056	1.7598	1.6581	1.7793	1.8587	1.8791
114	5.7521	4.6479	4.7137	4.2527	4.7524	4.3622	2.7282	1.7828	1.6758	1.7921	1.8802	1.8995

116	5.8163	4.7178	4.7643	4.3013	4.8122	4.4224	2.7576	1.8049	1.6927	1.8102	1.8964	1.9148
118	5.8869	4.7681	4.8292	4.3557	4.8880	4.4824	2.7797	1.8265	1.7115	1.8263	1.9141	1.9350
ΔA/s	0.0461	0.0358	0.0367	0.0330	0.0363	0.0334	0.0199	0.01139	0.0100	0.0111	0.0120	0.01204
Average			0.0351						0.0113			
Standard Deviation			0.0017						0.0008			

Experimental data absorbance over time for the configurations: Full immobilization surface, Fine checkerboard, Half immobilization surface, Coarse checkerboard, Reference, Immobilization by adsorption

Full immobilization surface		Fine checkerboard		Half immobilization surface		Coarse checkerboard		Reference		Immobilization by adsorption	
Time (s)	Absorbance	Time (s)	Absorbance	Time (s)	Absorbance	Time (s)	Absorbance	Time (s)	Absorbance	Time (s)	Absorbance
0	0.0344	0	9.2108	0	1.1875	0	1.3467	0	0.0990	0	0.121713
30.2	0.2393	11.6	15.4226	30	3.4714	30	2.0990	11.2	0.0796	30	0.131546
60.4	0.2798	30	15.7625	39.4	2.9676	60	1.8159	30	0.0779	60.4	0.115346
90.6	0.2995	38.8	16.1594	60	3.0461	89.8	1.0780	42.4	0.0576	90.2	0.066775
120.8	0.3094	47.4	16.7032	90	1.8321	120	0.7703	60.6	0.0615	120.4	0.076453
150.6	0.3197	60	16.8257	120	1.1749	149.8	0.7066	69.4	0.0581	150.4	0.049403
180.4	0.3246	70.4	8.8410	150	0.8713	180	0.5761	90.4	0.0621	180.2	0.075493
210.8	0.3271	79	8.8775	180	0.7633	210	0.5597	120.6	0.0614	210.6	0.116813
240.6	0.3272	90	8.8928	210	0.6485	239.8	0.5382	150.6	0.0576	240.2	0.107678
270.4	0.3323	99.8	4.8795	240.2	0.6028	269.8	0.5085	158.8	0.0476	270.6	0.165107
300.6	0.3227	120.2	4.9352	270	0.5771	300	0.4827	180.6	0.0630	300.4	0.073186
330.6	0.3264	150	3.1585	300.2	0.5517	330	0.4868	191	0.0657	330.6	0.065877
360.4	0.3332	180.2	2.3041	330.2	0.5306	359.8	0.4664	210.6	0.0626	360.6	0.066141
390.6	0.3431	210.2	1.7567	360.2	0.5297	390	0.4563	240.6	0.0550	390.8	0.054015
420.6	0.3265	240.2	1.4944	390	0.4986	419.8	0.4569	270.4	0.0609	420.6	0.055976
450.4	0.3413	270	1.2817	420.2	0.4858	449.8	0.4557	280.2	0.0504	450.6	0.05782
480.6	0.3400	300.2	1.1989	450.2	0.4867	480	0.4307	300.6	0.0531	480.6	0.056721
510.6	0.3422	330	1.0651	480	0.4698	509.8	0.4442	330.4	0.0528	510.6	0.052777
540.4	0.3422	360	1.0138	510.2	0.4620	539.8	0.4354	360.8	0.0575	540.6	0.056061
570.6	0.3500	390	0.9022	540.2	0.4510	569.8	0.4466	390.6	0.0564	570.6	0.053774
600.8	0.3464	420	0.9002	570	0.4577	600	0.4211	399	0.0511	600.6	0.055324
630.4	0.3469	450	0.8411	600.2	0.4374	629.8	0.4494	420.6	0.0602	630.6	0.053394
660.4	0.3405	480	0.7929	630.2	0.4466	660	0.4139	430.2	0.0602	660.6	0.054445
690.6	0.3439	510	0.7861	660.2	0.4396	690	0.4278	450.6	0.0624	690.6	0.05438
720.4	0.3422	540	0.7756	690.2	0.4342	719.8	0.4254	459	0.0492	720.4	0.05422

750.4	0.3457	570	0.7201	720.2	0.4193	749.8	0.4262	480.4	0.0544	750.6	0.052644
780.6	0.3426	600	0.7285	750	0.4248	780	0.4235	510.6	0.0498	780.6	0.054042
810.4	0.3492	629.8	0.7197	780.2	0.4050	810	0.4419	540.2	0.0336	810.6	0.052548
840.4	0.3448	660	0.6846	810.2	0.4075	840	0.4304	570.4	0.0350	840.6	0.055444
870.8	0.3393	690	0.6679	840.2	0.4087	870	0.4334	600.2	0.0312	870.6	0.050621
901.2	0.4059	720	0.6872	870.2	0.4043	900	0.4245	630.4	0.0349	900.4	0.056581
931.2	0.4016	750	0.6454	900.2	0.3861	930	0.4285	660	0.0242	930.6	0.054056
960.8	0.3921	780.2	0.6408	930.2	0.4075	960.2	0.4157	690.4	0.0363	960.6	0.053002
990.6	0.3837	810	0.6517	960.2	0.3922	990	0.4272	720	0.0270	990.6	0.053156
1020.6	0.3714	840	0.6272	990.2	0.3930	1020	0.4050	750.4	0.0320	1020.6	0.055082
1050.8	0.3661	870.2	0.6149	1020.2	0.3908	1050	0.4123	780	0.0236	1050.6	0.053281
1080.8	0.3573	900	0.6303	1050	0.3933	1080	0.4013	810.2	0.0294	1080.6	0.057119
1110.4	0.3601	930	0.6244	1080.4	0.3777	1109.8	0.4088	840	0.0181	1110.6	0.053035
1140.6	0.3497	960.2	0.6045	1110.2	0.3888	1140.2	0.3870	870.2	0.0222	1140.6	0.054512
1170.8	0.3515	990	0.6103	1140.2	0.3762	1170	0.4017	900	0.0116	1170.6	0.054552
1200.4	0.3454	1020	0.5888	1170.4	0.3855	1200	0.4003	930.2	0.0216	1200.4	0.0536
1230.6	0.3443	1050	0.5785	1200.2	0.3779	1230	0.3975	959.8	0.0125	1230.6	0.054439
1260.8	0.3358	1080	0.5796	1230.2	0.3883	1260.2	0.4061	990.4	0.0206	1260.4	0.055944
1290.4	0.3378	1110	0.5834	1260.4	0.3752	1290	0.4113	1019.8	0.0106	1290.8	0.054409
1320.6	0.3348	1140	0.5570	1290.4	0.4169	1320.2	0.3935	1050.2	0.0200	1320.6	0.056761
1350.8	0.3302	1170	0.5649	1320.4	0.4039	1350	0.3966	1080	0.0095	1350.6	0.052744
1380.6	0.3311	1200	0.5711	1350.4	0.4067	1380	0.3902	1110.2	0.0179	1380.6	0.056869
1410.4	0.3357	1230	0.5543	1380.4	0.3819	1410	0.3975	1140	0.0073	1410.8	0.053889
1440.8	0.3234	1260.2	0.5573	1410.2	0.3940	1440.2	0.3767	1170.2	0.0158	1440.6	0.056208
1470.6	0.3305	1290	0.5690	1440.4	0.3796	1470	0.3957	1199.8	0.0074	1470.8	0.056711
1500.4	0.3261	1320.2	0.5501	1470.4	0.3795	1500	0.3792	1230.2	0.0138	1500.6	0.055035
1530.8	0.3325	1350.2	0.5526	1500.2	0.3687	1530	0.3885	1259.8	0.0050	1530.6	0.054291
1560.6	0.3210	1380.2	0.5499	1530.2	0.3741	1560	0.3903	1290.4	0.0121	1560.8	0.061208
1590.4	0.3377	1410	0.5450	1560.4	0.3562	1590	0.3924	1319.8	0.0056	1590.8	0.055083
1620.8	0.3282	1440.2	0.5249	1590.2	0.3706	1620.2	0.3811	1350	0.0117	1620.8	0.056118

1650.6	0.3303	1470.2	0.5597	1620.2	0.3626	1650	0.4008	1379.8	0.0039	1651	0.057028
1680.6	0.3412	1500.2	0.5876	1650.4	0.3641	1680	0.3906	1410.2	0.0113	1680.8	0.058477
1710.6	0.3495	1530.2	0.5823	1680.2	0.3607	1710.2	0.3974	1440	0.0041	1710.8	0.057254
		1560.4	0.5619	1710.2	0.3645			1470.2	0.0096		
		1590.2	0.5447					1499.8	0.0043		
		1620.2	0.5289					1530.2	0.0100		
		1650.2	0.5345					1559.8	0.0084		
		1680.2	0.5235					1590	0.0129		
		1710.2	0.5129					1620	0.0037		
								1650	0.0106		
								1680	0.0041		
								1710	0.0084		

Experimental data absorbance over time for the configurations T-microreactor and Five-stream microreactor for residence time 5 s, 10 s, and 20 s

5 s				10 s				20 s			
T-microreactor		Five-stream microreactor		T-microreactor		Five-stream microreactor		T-microreactor		Five-stream microreactor	
Time (s)	Absorbance	Time (s)	Absorbance	Time (s)	Absorbance	Time (s)	Absorbance	Time (s)	Absorbance	Time (s)	Absorbance
0.0	22.67	0.0	22.67	0.0	21.73	0.0	25.80	0.0	22.17	0.0	20.98
16.6	25.89	16.6	25.89	8.4	16.41	10.8	19.64	30.0	21.50	17.6	23.60
29.2	25.71	29.2	25.71	17.0	16.99	19.4	19.72	59.8	23.01	29.6	23.38
41.6	23.05	41.6	23.05	29.8	17.21	30.0	19.03	89.6	22.39	42.6	24.21
50.0	23.32	50.0	23.32	39.6	14.72	40.2	21.50	105.6	22.29	51.0	24.87
58.8	23.66	58.8	23.66	48.2	15.04	48.6	22.41	119.4	22.81	59.6	24.88
68.8	24.30	68.8	24.30	59.8	15.15	59.6	22.15	130.4	20.85	73.8	23.86
89.0	25.99	89.0	25.99	69.0	14.67	69.4	20.97	139.0	21.24	89.4	24.20
107.2	26.99	107.2	26.99	77.6	15.23	77.8	22.27	149.6	21.31	105.0	23.39
119.6	26.94	119.6	26.94	89.6	15.82	89.8	22.32	161.8	21.08	119.0	23.91
149.2	26.47	149.2	26.47	98.2	14.84	98.6	20.74	170.2	21.74	136.4	22.95
163.0	24.91	163.0	24.91	111.4	15.77	107.2	21.75	179.4	22.03	149.2	23.10
178.8	25.21	178.8	25.21	120.0	15.34	119.6	21.53	193.2	20.87	163.6	23.99
190.2	24.10	190.2	24.10	133.4	17.70	127.8	20.57	209.4	21.36	179.2	24.64
198.6	24.98	198.6	24.98	149.8	18.09	136.2	22.29	220.2	21.71	192.4	24.96
209.0	25.34	209.0	25.34	164.6	14.97	149.6	22.34	228.6	22.39	201.0	25.29
223.2	23.70	223.2	23.70	180.0	15.24	159.2	20.87	239.4	22.70	209.4	25.19
239.0	24.00	239.0	24.00	193.8	15.11	167.6	22.12	251.6	20.70	221.8	24.10
255.4	25.55	255.4	25.55	209.8	15.53	179.6	22.27	260.0	21.05	239.2	25.15
268.8	26.00	268.8	26.00	223.0	16.42	188.2	20.29	269.2	21.24	253.0	23.51
284.0	24.84	284.0	24.84	231.4	16.66	196.6	21.54	282.8	21.82	269.4	23.91
299.2	25.48	299.2	25.48	239.8	16.80	209.8	21.02	291.2	22.35	278.0	22.71
311.0	24.97	311.0	24.97	252.2	14.50	219.6	21.64	299.6	22.50	286.6	24.00
319.4	25.41	319.4	25.41	260.8	14.76	228.2	22.94	309.8	21.29	299.2	24.38

328.8	25.38	328.8	25.38	269.8	14.82	239.6	22.91	318.4	21.98	311.4	23.05
346.2	23.62	346.2	23.62	283.6	14.75	248.8	19.51	329.4	22.31	320.0	23.55
359.0	24.12	359.0	24.12	300.0	14.89	257.2	20.27	343.2	21.83	329.2	23.74
388.8	24.88	388.8	24.88	312.6	16.70	269.6	20.19	359.4	22.54	345.0	23.25
400.2	23.19	400.2	23.19	329.8	17.52	278.0	20.33	372.4	21.03	359.2	23.76
408.6	23.38	408.6	23.38	346.0	14.96	286.4	21.85	381.0	21.30	374.4	23.07
418.8	23.69	418.8	23.69	360.0	15.06	299.6	21.56	389.4	21.40	389.2	23.26
439.4	25.27	439.4	25.27	375.2	14.86	309.2	19.96	405.8	21.68	405.4	23.12
449.0	25.49	449.0	25.49	389.8	15.08	317.6	21.22	419.2	22.28	419.0	23.56
461.4	25.76	461.4	25.76	398.2	14.21	329.8	21.28	428.6	20.36	434.8	22.93
469.8	26.06	469.8	26.06	406.8	14.98	338.4	19.49	437.2	20.89	449.2	23.07
479.2	25.91	479.2	25.91	419.8	15.19	347.0	20.82	449.4	21.07	461.8	23.93
508.8	26.21	508.8	26.21	431.6	15.57	359.6	20.60	462.0	21.53	470.2	24.79
525.6	23.24	525.6	23.24	449.8	16.31	369.6	20.89	470.6	22.23	479.2	25.16
539.0	23.56	539.0	23.56	461.8	15.56	378.2	21.90	479.4	22.45	492.8	22.67
550.6	24.40	550.6	24.40	480.0	15.77	389.6	21.91	491.2	21.88	509.2	22.86
560.0	25.07	560.0	25.07	492.0	15.69	399.0	19.21	509.8	22.24	524.4	23.29
568.8	25.22	568.8	25.22	500.4	16.01	407.4	20.60	528.4	23.69	539.0	23.84
582.4	23.74	582.4	23.74	509.8	16.10	419.8	20.39	539.6	24.04	553.6	23.35
599.0	24.30	599.0	24.30	525.4	14.45	428.0	20.12	569.4	22.16	569.4	23.84
611.0	24.06	611.0	24.06	539.8	14.60	436.6	21.51	587.0	22.82	580.6	24.06
619.4	25.12	619.4	25.12	552.6	16.37	449.6	21.42	599.4	23.26	589.2	24.88
628.8	25.31	628.8	25.31	561.2	16.84	459.4	21.66	614.2	20.86	599.2	25.10
646.8	24.95	646.8	24.95	569.8	17.07	467.8	22.84	629.4	21.13	613.8	22.89
659.0	25.24	659.0	25.24	579.6	14.42	479.6	23.00	641.4	21.59	629.2	23.18
689.2	27.07	689.2	27.07	588.2	14.68	488.6	19.37	649.8	22.39	643.2	23.73
701.2	24.64	701.2	24.64	599.8	14.75	497.0	20.33	659.6	22.69	659.2	24.61
709.6	24.76	709.6	24.76	608.8	14.20	509.8	19.87	668.4	20.84	676.4	23.16
719.0	24.67	719.0	24.67	617.6	14.72	519.8	20.68	677.0	21.35	689.2	23.16
748.8	24.29	748.8	24.29	629.8	14.80	528.4	21.72	689.4	21.45	705.8	24.50

761.2	23.65	761.2	23.65	638.2	16.40	539.6	21.55	701.8	22.03	719.2	25.18
769.6	24.14	769.6	24.14	646.8	17.55	549.0	18.97	710.4	22.67	730.6	22.81
779.0	24.37	779.0	24.37	660.0	17.61	557.4	20.22	719.4	23.04	739.2	23.12
798.8	24.43	798.8	24.43	675.8	15.44	569.8	20.22	735.2	21.12	749.2	23.17
				689.8	15.85	578.2	19.51	749.4	21.36	764.0	23.42
				706.8	14.29	586.8	21.07	760.2	21.82	779.0	24.07
				720.0	14.49	599.6	20.80	768.8	22.51	797.6	23.18
				734.0	15.90	609.4	20.63	779.4	22.82		
				749.8	16.17	618.0	21.80	789.4	20.37		
				759.0	13.85	629.6	21.78	798.0	20.97		
				767.6	14.18	638.8	19.30				
				779.8	14.33	647.2	20.50				
				788.4	13.64	659.8	20.19				
				799.2	14.74	670.0	20.79				
				809.8	15.00	678.4	22.05				
						690.0	21.57				
						699.2	21.60				
						707.6	22.81				
						719.8	22.45				
						728.4	19.51				
						736.8	20.70				
						750.0	19.63				
						759.6	20.50				
						768.2	21.71				
						779.8	21.26				
						788.8	18.61				
						797.4	19.91				
						810.0	19.48				

Appendix D

Description of the microreactor configurations for posterior selection and experimental testing

Appendix D presents the description of the different microreactor configurations presented in section *5.4.1.3 - Selection of the microreactor configuration for experimental testing*. Moreover, the results of the CFD simulations are also presented in detail. The simulation results are presented only for the microreactors a), b), c), e), f) and g). The results for the microreactor configurations d) and h) correspond to the initial and the final configurations of the topology optimization of the microchannel with free enzyme in solution, respectively and the results are presented in section *5.4.1.2 – Results and discussion.*

The reader should note that although the concentration of the substrate and the enzyme streams at the inlet is different between configurations, the average amounts of enzyme and substrate (mol) inside the microreactor per time unit are the same for all configurations in order to allow a fair comparison.

T-microreactor (Figure 5.17 a))

The T-microreactor analyzed in this study is similar to the YY-microreactor presented in Chapter 3 for shape optimization and of the study presented by Bodla *et al.*[101] (which has been presented in Chapter 2). However the length is changed to 50 mm, and the inlet streams form 90° angles with reaction channel. The inlet is divided in two streams of equal width (0.25 mm) and one inlet the stream contains $5 \cdot 10^{-5}$ mM of peroxidase while the other inlet the stream contains 20 mM of ABTS (See Figure D-1).

Figure D-1– Inlet configuration. Enzyme concentration 2[E] = $5 \cdot 10^{-5}$ mM and substrate concentration 2[S] = 20 mM.

8-stream microreactor with separation of enzyme and substrate streams (Figure 5.17 b))

The 8-stream microreactor presented in this investigation is similar to the one presented by Bodla *et al.* [101] but its length corresponds to 50 mm. The inlet is divided into eight streams of equal width (0.0625 mm) and a stream containing $5 \cdot 10^{-5}$ mM of peroxidase enters in four of the inlets and a stream containing 20 mM of ABTS enters in the other four inlets. The different enzyme and substrate streams are dispositioned alternated and forming an interdigitation between them (See Figure D-2).

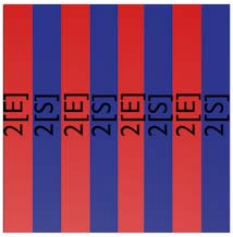

Figure D-2 – Inlet configuration. Enzyme concentration 2[E] = $5 \cdot 10^{-5}$ mM and substrate concentration 2[S] = 20 mM.

8-stream microreactor with substrate concentration uniform at inlet and separation of enzyme streams (Figure 5.17 c))

The 8-stream microreactor shape presented here is the similar to the as the one presented by Bodla *et al.*[101] but the substrate supply is different compared with the previous case. The inlet is divided into eight streams of equal width (0.0625 mm) (See Figure D-3). In this microreactor, the substrate enters in all streams of the inlet and therefore, its concentration is uniform for the inlet cross section of the microreactor (10 mM). The enzyme enters in every other inlet stream at a concentration of $5 \cdot 10^{-5}$ mM. This configuration will allow the investigation of the mixing by spreading the enzyme in different streams at the inlet. Moreover, the substrate concentration is uniform for the cross section of the microreactor and therefore the diffusion limitations will only be caused by the enzyme.

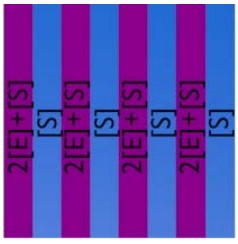

Figure D-3 – Inlet configuration. Enzyme concentration 2[E] = $5 \cdot 10^{-5}$ mM and substrate concentration [S] = 10 mM.

Five-stream microreactor with low substrate concentration at the center and separation of enzyme and substrate streams on the inlet sides (Figure 5.17 e))

The Five-stream microreactor configuration is characterized by a center stream with half of the width of the microreactor (width 0.25 mm) and by four streams located at the sides of the center stream (width 0.125 mm, height 0.25 mm) (See Figure D-4).

The substrate enters in three of the inlet streams: in the center stream (10 mM) and in the two bottom streams located on the side of the center stream (20 mM). The enzyme enters in the two top streams located on the side of the center stream at concentration of 10^{-4} mM. The enzyme concentration is four times the inlet enzyme concentration in the Mixed flow microreactor since the areas of the enzyme streams correspond to a total of a quarter of the entire inlet area.

Three streams meet at the inlet of the microreactor: two streams containing the lamination of substrates and enzyme streams, entering close to each side wall of the channel and one stream containing the standard substrate solution (10 mM ABTS) entering in the middle of the channel (See Figure D-4).

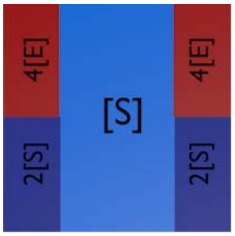

Figure D-4 - Inlet configuration. Enzyme concentration 4[E] = 10^{-4} mM, substrate concentration in concentrated solution and [S] = 20 mM and substrate concentration in diluted solution [S] = 10 mM.

Square microreactor, with uniform substrate concentration at inlet and placement of enzyme stream close to the walls of the microreactor (Figure 5.17 f))

The square microreactor configuration is characterized by a centered inner square of half of the cross sectional area of the microreactor (width and height 0.3536 mm) and by a rectangular ring inlet around the inner square (See Figure D-5).

The substrate enters in both streams of the inlet at the same concentration (in the ring and in the inner square) and therefore, its concentration is even across the inlet section of the microreactor (10 mM). The enzyme enters in the ring stream at a concentration of $5 \cdot 10^{-5}$ mM. This investigation might be a realistic option for fabrication since its configuration is close to the one obtained by topology optimization.

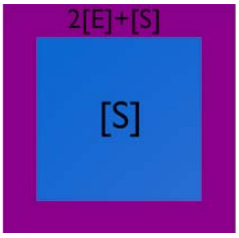

Figure D-5 – Inlet configuration. Enzyme concentration 2[E] = $5 \cdot 10^{-5}$ mM and substrate concentration [S] = 10 mM.

Three-stream microreactor, with substrate uniform concentration at the inlet and placement of enzyme streams on the sides of the microreactor (Figure 5.17 g))

The Three-stream microreactor configuration is characterized by a center stream with half of the width of the microreactor (width 0.25 mm) and by two streams located at the sides of the center stream (width 0.125 mm) (See Figure D-6).

The substrate enters in all streams of the inlet and therefore, its concentration is even at the inlet cross section of the microreactor (10 mM). The enzyme enters on side streams at concentration of $5 \cdot 10^{-5}$ mM.

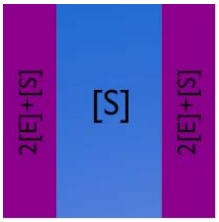

Figure D-6 – Inlet configuration. Enzyme concentration $2[E] = 5 \cdot 10^{-5}$ mM and substrate concentration [S] = 10 mM.

The overview of the enzyme, substrate and product concentrations inside the microchannel all the configurations described above are presented in Figure D-7.

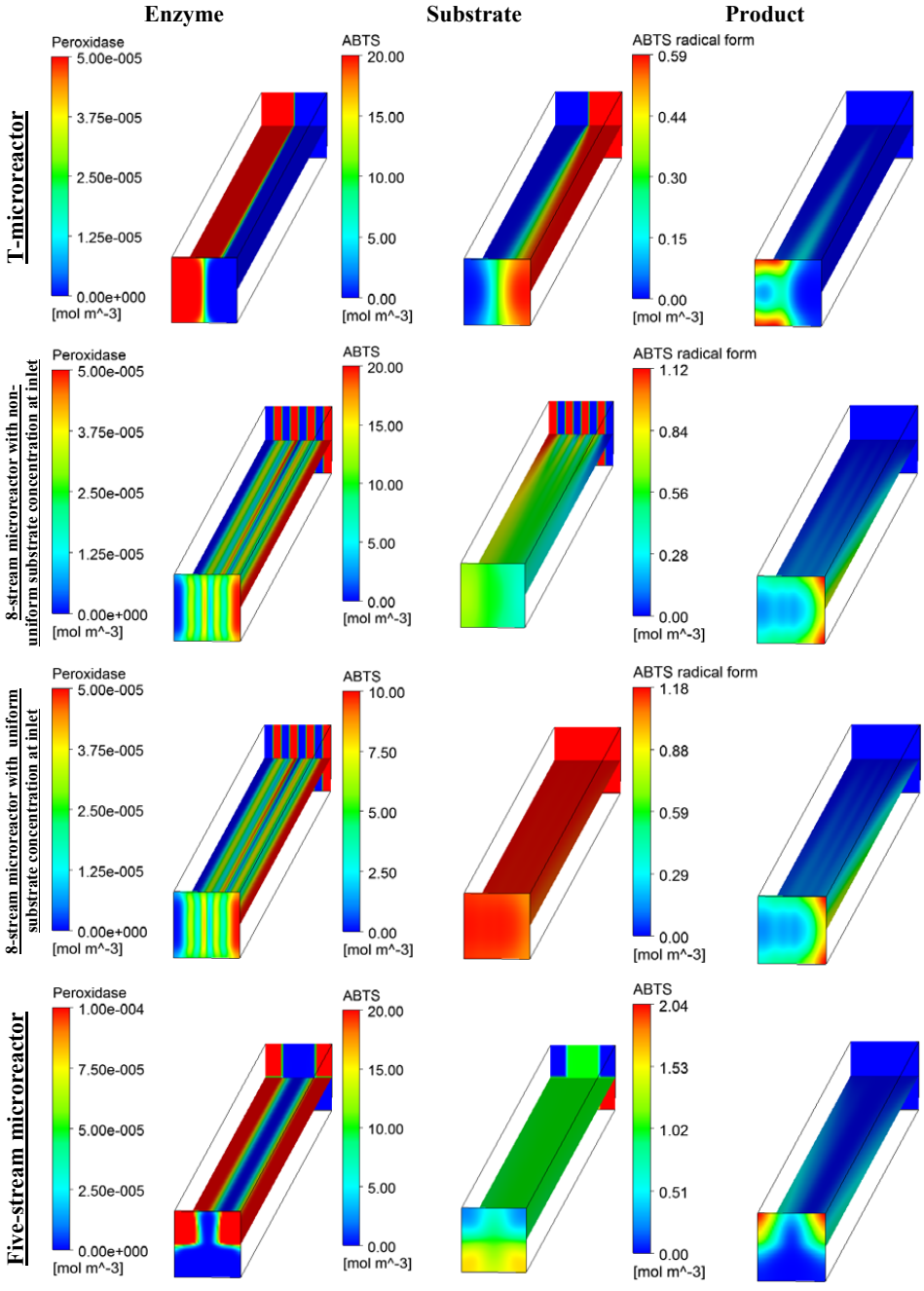
Enzyme
Substrate
Product
T-microreactor
8-stream microreactor with non-uniform substrate concentration at inlet
8-stream microreactor with uniform substrate concentration at inlet
Five-stream microreactor
Peroxidase
5.00e-005
3.75e-005
2.50e-005
1.25e-005
0.00e+000
[mol m^-3]
ABTS
20.00
15.00
10.00
5.00
0.00
[mol m^-3]
ABTS radical form
0.59
0.44
0.30
0.15
0.00
[mol m^-3]
1.12
0.84
0.56
0.28
0.00
[mol m^-3]
10.00
7.50
5.00
2.50
0.00
[mol m^-3]
1.18
0.88
0.59
0.29
0.00
[mol m^-3]
1.00e-004
7.50e-005
5.00e-005
2.50e-005
0.00e+000
[mol m^-3]
2.04
1.53
1.02
0.51
0.00
[mol m^-3]

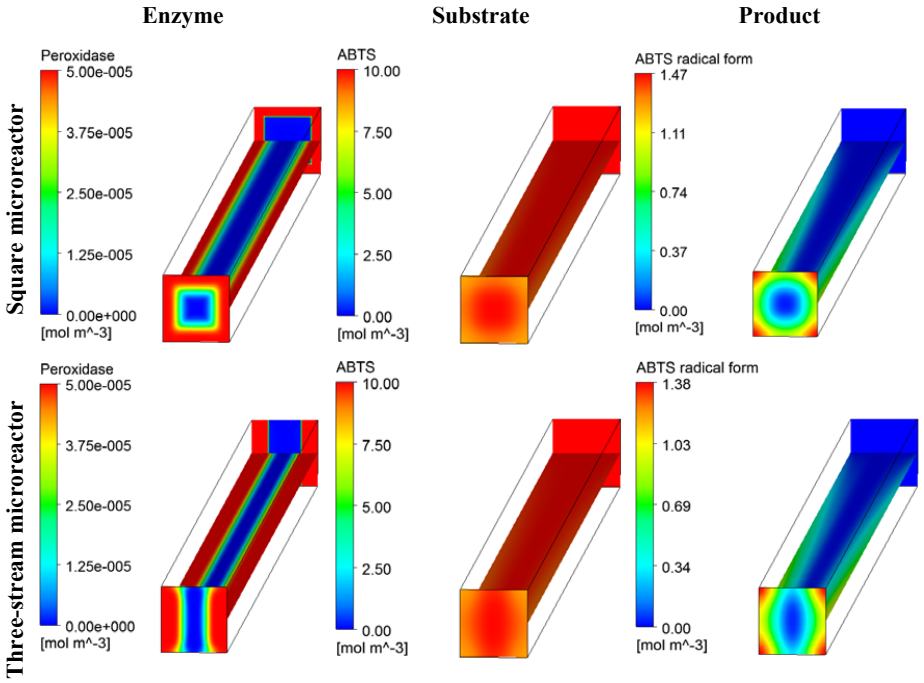

Figure D-7 – Overview of enzyme and substrate distribution and product formation in all microreactor configurations.

Process and Systems Engineering Center (PROSYS)
Department of Chemical and Biochemical Engineering
Technical University of Denmark
Søltofts Plads, Building 229
DK - 2800 Kgs. Lyngby
Denmark

Phone: +45 45 25 28 00
Web: www.kt.dtu.dk/forskning/prosys